Queen Mary
University of London

Electrochemistry of aluminium in room temperature A1C13-TMPAC molten salts.

Zhao, Yuguang

The copyright of this thesis rests with the author and no quotation from it or information derived from it may be published without the prior written consent of the author

For additional information about this publication click this link.
http://qmro.qmul.ac.uk/jspui/handle/123456789/1702

Information about this research object was correct at the time of download; we occasionally make corrections to records, please therefore check the published record when citing. For more information contact scholarlycommunications@qmul.ac.uk

ELECTROCHEMISTRY OF ALUMINIUM IN ROOM TEMPERATURE $AlCl_3$-TMPAC MOLTEN SALTS

BY

YUGUANG ZHAO

A Thesis Submitted to the University of London
for the Degree of Doctor of Philosophy

Department of Chemistry
Queen Mary and Westfield College

February 1997

BIBL.
LONDIN.
UNIV.

Dedicated to my father and mother

ABSTRACT

Aluminium can be electrodeposited on tungsten, aluminium, platinum, nickel and glassy carbon from 2:1 $AlCl_3$-TMPAC (trimethylphenylammonium chloride) molten salts at room temperature. The $AlCl_3$-TMPAC melts diluted with 1,2-dichlorobenzene of had a beneficial effect on increasing aluminium deposition and stripping currents by decreasing viscosity and increasing the conductivity of the melt.

The reductions of $Al_2Cl_7^-$ ions were quasi-reversible and diffusion controlled, The irreversibility of the reductions was due to the relatively low conductivity and high viscosity of the melts. The aluminium deposition was associated with the reduction of the resulting product $AlCl_4^-$ ions following the locally changing acidity of the melts, and a corrosion reaction between fresh aluminium deposits and the melt. The mechanism for aluminium electrodeposition from 2:1 $AlCl_3$-TMPAC was realised likely similar to that for the acidic $AlCl_3$-BPC melts.

The bulk depositions of aluminium on all electrode except platinum involved three-dimensional instantaneous nucleation process followed by hemispherical diffusion-controlled growth of the developing nuclei. On platinum the nucleation process was characteristic of instantaneous at short time and then tended to progressive.

The phenomena of aluminium UPD were found on all electrodes but not on aluminium itself, highly dependent upon substrates, and involved alloying effects on metal substrates. The UPD layers on the surface of the electrodes corresponded to about 2 ~ 10 aluminium monolayer equivalents. The UPD was surface constrained on tungsten, whereas were diffusion controlled on nickel and platinum. The processes on tungsten and platinum were under the limitation of kinetics. On nickel and platinum, the electrodes and the nickel and platinum components in fresh deposits were likely to react with $Al_2Cl_7^-$ and Cl^- ions in the melt to form corresponding metal complexes.

The passivation phenomena were observed to occur on all electrodes. These could resulted from a black layer formed by $AlCl_3$ precipitates. Particularly, on aluminium the stripping of aluminium was involved in an active dissolution-passivation process.

ACKNOWLEDGEMENTS

I would like to express my most heartfelt thanks to my research supervisor Dr. Ted J. VanderNoot, for his continuous encouragement and infectious enthusiasm throughout the course of this thesis. His excellent supervision in my project work, and his and his wife Christine's numerous thoughtful help and consideration in my overseas student life in London are far beyond a word of grateful appreciation.

It is impossible to fulfil this project without the financial support from Knopp Electronics Services, Ltd.. Particularly I am deeply indebted to Mr. J. Knopp for his generosity and kindness.

Dr. Yiping Zhang and Dr. Ian Harding have been an invaluable source of expertise and suggestion during the preparation of those room temperature molten salts sensitive to air and moisture.

I am most grateful to Mr. Trevor Pell, Mr. Brian Cook and Mr. Ralph Thompson for their technical support. In particular, Mr. John Cowley's excellent glass service is very much appreciated. Many thanks are also due to Mr. Alan Bradshaw's and Mr. Bernard Franks' effective supplement of chemicals and apparatus.

It is a great pleasure for acknowledging of indebtedness to my Chinese friends in QMW, especially San Yun, Luo Zhiyuan, Li Fan, Ou Duanli, Gao Yaiping, Mo Ning, Huang Jie, Zhang Guochang, Ren Qingchao, Xue Haibin, Guo Jianqing, Li Kueiwu, Miao Yi and Xu Ailing, and all my other friends who have made my time at QMW so enjoyable.

I can never thank my family and my relatives enough for their everlasting support and encouragement. Finally, I appreciate affectionately my wife for her patience, understanding and support.

CONTENTS

PART I. LITERATURE REVIEW

Chapter 1

ELECTRODEPOSITION OF ALUMINIUM

Part II. EXPERIMENTS, RESULTS AND DISCUSSION

Chapter 2

EXPERIMENTAL METHODS AND ELECTROCHEMICAL TECHNIQUES

Chapter 3

ALUMINIUM ELECTRODEPOSITION ON TUNGSTEN

Chapter 4

ALUMINIUM ELECTRODEPOSITION ON ALUMINIUM AND GLASSY CARBON

Chapter 5

ALUMINIUM ELECTRODEPOSITION ON NICKEL AND PLATINUM

Chapter 6

ALUMINIUM ELECTRODEPOSITIONS FROM MELTS WITH NICKEL IONS

Chapter 7

CONCLUSIONS AND A PROPOSED GENERAL REACTION SCHEME

Chapter 1

ELECTRODEPOSITION OF ALUMINIUM

1.1 INTRODUCTION

Aluminium coatings are well known to have several advantages for corrosion protection [1]. On exposure to air they become covered with an oxide layer which is very resistant to chemical and atmospheric attack. This oxide layer can be further thickened by anodisation. The oxide has good adherence, is silver coloured and has good thermal and electrical conductivity. In addition it can be well polished, shows good adhesion for varnish and has a very high reflectivity. The latter property is highly promising from the point of view of solar energy utilisation, the thermal insulation of buildings and the development of various optical devices. The oxide layer formed by anodisation provides an advantageous combination of good conductivity and inertness, which can be successfully used in electrical engineering and electronics. Aluminium coatings are also required in the protection of steel parts in aeroplanes and cars.

The recovery of aluminium metal is divided into two steps, the production of pure alumina (Bayer Process); and its molten salt electrolysis, using molten cryolites (Na_3AlF_6) in which aluminium oxide (Al_2O_3) has been dissolved [2]. The cryolite electrolysis process has been the most widely used and still accounts for about 95% of the total production of aluminium since 1886 [3]. However, it is not suitable for coating other metals with a layer of aluminium, since the electrolysis is performed at 1000 °C, a temperature at which cryolite and alumina

are in the liquid state. Today there are various methods available for low temperature plating of workpieces with aluminium, such as [4]:

a. thermal spray coating;
b. hot dipping;
c. roll binding;
d. PVD/CVD (physical or chemical vapour deposition);
e. electrolytic plating.

Except electrolytic plating, these techniques are rather expensive, as high temperatures are required for the preparation of the coating because of the high melting point of aluminium (660 °C) [5]. In addition, the above methods are often impractical as the specimens to be coated may be damaged by heating. Apart from uneven surfaces and the impossibility of controlling the thickness and quality of layer, the main disadvantage of these methods is an unnecessary waste of the metal and energy.

In contrast, electrolytically obtained aluminium coatings are of higher purity and lower porosity which results in good corrosion protection. The layer can be well controlled with savings in materials and energy. Thermal stress in the substrate material is also avoided since electrolytic coating can be carried out below 180 °C [5].

Because of the rather negative standard potential of Aluminium, the electrodeposition of aluminium from aqueous solutions is impossible due to hydrogen evolution at the cathode. The electrolytes must be aprotic, so, only molten salts and nonaqueous inorganic or organic electrolyte systems are eligible for electrolytic deposition of aluminium. Both types of electrolytes are sensitive to moisture and air, and their exclusion is essential for prolonging the bath life. This can be achieved in closed systems with an inert atmosphere.

In this review, aluminium electrodeposition from nonaqueous solvents and room temperature molten salts will be surveyed.

1.2 ALUMINIUM ELECTRODEPOSITION FROM ORGANIC ELECTROLYTIC SYSTEMS

Since the reduction of aluminium from organic solvents of aluminium halides was first attempted at the beginning of this century [6], numerous nonaqueous electrolytic systems for the electrodeposition of aluminium have been investigated. Basically, the choice of a suitable nonaqueous Al-electroplating bath is governed by the following conditions [5, 7]:

a. The electrolyte solution should consist of a solvent acting as a Lewis base and a solute (aluminium compound electrolyte) acting as a Lewis acid so that mutual co-ordination and dissolution of the solute can take place.
b. The co-ordination of the solute must not be so strong as to prevent release of aluminium during electrolysis. Weak co-ordination centres such as the oxygen atom in ethers or in aromatic hydrocarbons fulfil this requirement.
c. The solute, which is used as an aluminium source, should exhibit a high solubility in the solvent. A stable complex must be formed in the plating solution.
d. For some applications, it is desirable that the composition of the bath remains constant during operation. This implies that the electrode process has to be chemically reversible. This permits long-term operation of the bath without a change in the electrodeposition characteristics.
e. The medium must exhibit reducing and water-consuming properties.

A potentially suitable solvent for the preparation of Al-electroplating baths must also comply with the following criteria [8]:

a. The electrode reaction has to be kinetically feasible (low overpotential) and mass-transport phenomena have to be in favour of a controllable surface morphology. The free energy of the co-ordination complex of the solvent and aluminium solute, *e.g.*, aluminium halide, should be sufficiently low to ensure a good solubility of the salt.
b. The dissociated aluminium complex ion must allow plating of aluminium at a less negative potential than that of possible reduction reactions involving the solvent.

Based on an analysis of reported investigations, there are, only three classes of organic solvents which have been successfully used for Al-electroplating [9]:

i. ethers;
ii. aromatic hydrocarbons;
iii. dimethylsulfone.

1.2.1 Electrodeposition of Aluminium from Etheric Solvents

In etheric solvents such as diethyl ether and tetrahydrofuran (THF), $AlCl_3$ is used in combination with LiH or $LiAlH_4$ as the electroactive component. The resulting solutions are also called hydride baths, which can be classified as either the NBS bath or the THF bath.

A. The NBS bath

The first aluminium plating bath operated on an industrial scale was formulated by Brenner and his co-workers [10-13] at the NBS (National Bureau

Standards) in 1952. The first variant of the bath was composed of 2 ~ 3 mol dm^{-3} LiH in diethyl ether. In a subsequent paper [14] a modified composition was suggested, namely 3 mol dm^{-3} $AlCl_3$ and 0.13 ~ 0.4 mol dm^{-3} $LiAlH_4$, since the latter dissolved in diethyl ether more readily and the life-time of the bath was found to be longer. A cathodic current density of 2 ~ 5 A dm^{-2} was attained at ambient temperatures with a cathodic current efficiency of 90 ~ 100%.

The aluminium anodes were contained in a cellulose or paper cylinder in order to prevent the anode dissolution products from mixing with the plating solution since the anodic reaction products poisoned the bath. Consequently the aluminium content of the bath decreased during operation and aluminium chloride was added from time to time. The plating bath, which was sensitive to oxygen and carbon dioxide as well as water, was operated under an inert atmosphere.

Clay et al. [15] reported a prolonged life-time and a considerable improvement in the operation of the bath by using bare aluminium anodes and agitating the solution while employing relatively low current densities (up to 2 A dm^{-2}) at a somewhat higher temperature (40 °C). Under these circumstances the current efficiency of anodic dissolution was found to reach 100%. Adherent aluminium coatings were deposited on various aluminium alloys, titanium alloys and copper alloys well as steel [16]. The aluminium deposits were up to 0.3 mm thick. The crystalline structure of the coatings prepared in NBS bath was investigated [17].

The industrial application of the aluminium halide-ether bath was first reported by Schmidt et al. [18] at the General Electric Company. A plant equipped with a 760 dm^3 bath was built for electroforming 76 cm parabolic mirrors diameters. The bath was operated with continuous stirring and filtering without the use of any additives. The throwing power of the bath was found to be excellent under these conditions. In contrast to a previous report [19], the quality of the deposits was found to deteriorate in the presence of methyl borate

or amine additives. Another interesting practical application of the bath consisted of the production of high surface area deposits for the manufacture of electrolytic capacitors [20].

The NBS bath possessed several drawbacks such as flammability, limited life-time, variation of the composition, low current efficiency for the dissolution of aluminium anodes, and hydrogen embrittlement due to excessive hydrogen evolution [21, 22]. Nevertheless the process has been a commercial reality for a long time, and has been adopted by NASA [23].

Research work has continued in two directions: (i) to improve the quality of the coating and the bath performance with suitable additives and (ii) to reduce the fire hazards by substitution of the highly inflammable ether with other solvents. A review in Russian focusing on ether-containing baths was published by Levinskas [24].

B. The THF Baths

The use of THF alone or THF in combination with benzene instead of diethyl ether was proposed by Ishibashi and Yoshio [25, 26]. Not only was the THF bath less flammable and volatile but also showed better anode dissolution and therefore a longer bath life. They were able to use successfully current densities above 10 A dm^{-2} with agitation. The composition of the bath was roughly 60% benzene with 0.7 ~ 1.3 mol dm^{-3} $AlCl_3$ and $LiAiH_4$. Excellent deposits were obtained with an $AlCl_3$:$LiAlH_4$ mole ratio of 3:1. Other aromatic hydrocarbons were tried in addition to benzene, such as 1,2-dichloroethane and toluene and in these cases the deposit on the cathode was satisfactory but a white precipitate was observed on the anode. An unsuccessful attempt was made to improve the operation of the NBS electrolyte by adding aromatic hydrocarbons. A rather complicated pre-treatment of the cathode surface was suggested [25,26] prior to the electrolysis but Eckert and Kolling [27] have shown it to be

unnecessary. Kurata et al. [28-30] have also studied special pre-treatment of iron and steel surfaces in order to obtain more pure and adherent deposits.

THF electrolytes have been utilised by the Nisshin Steel Co. in Japan for the continuous aluminium coating of steel wires and strips (*e.g.*, in integrated circuits) [31]. Also, it has been used for the electroplating of carbon fibre [32]. A development of the THF bath, the REAL process (Room-temperature Electroplated Aluminium), took place in the laboratories of Philips Research [33]. The electroplating process could be carried out at ambient temperature. The current efficiency was 100%, and the deposited aluminium had a purity of 99.99%. Pilot plant arrangements for continuous aluminium electroplating on wire, metal tape, and small parts was developed. Aluminium layers with large surface areas targeted for electrolytic condensers could be deposited at a high current density. Al-Mg alloys containing up to 13% Mg could be obtained from the THF bath with $MgBr_2$ [34].

1.2.2 Electrodeposition of Aluminium from Aromatic Hydrocarbons

Having suitably weak co-ordination centres, aromatic hydrocarbons were found to be relatively good solvents for aluminium halides although the permitivity of the solutions was very low (ϵ <3) [35, 36]. All aluminium electrolytes in aromatic hydrocarbons may be classified into three characteristic groups according to their chemical and structural composition:

a. non-complexed $AlBr_3$ electrolytes;
b. $AlBr_3$ complexes with onium compounds;
c. organoaluminium compounds (aluminium trialkyls and their complexes with alkali metals or tetra-alkylammonium halides, especially fluorides, in aromatics or as melts).

A. Non-complexed $AlBr_3$ electrolytes

Aluminium halide solutions in aromatic hydrocarbons seem to be at first sight the simplest two-component electrolytes for the electrodeposition of aluminium [9]. Since AlF_3 is insoluble in aromatic hydrocarbons and $AlCl_3$ is slightly insoluble and forms a low conductivity solution, the most acceptable aluminium halide for the electrodeposition of aluminium is $AlBr_3$. The baths containing $AlBr_3$ are known as bromide baths. The solvents in these baths were usually aromatic hydrocarbons such as benzene, toluene, xylene and their mixtures and derivatives. In order to increase conductivity of the bromide baths and to improve the cathodic current efficiencies, the effects of various additives, mainly alkali halides (*e.g.*, KBr, HBr) were systematically studied [37].

a. $AlBr_3$ + MBr as the electroactive components

Attempts were made to increase the conductivity of $AlBr_3$ solutions by the addition of quaternary ammonium or pyridinium salts and the best deposits were obtained with quaternary pyridinium or dimethylaniline salts in toluene [38,39]. The anionic species was assumed to be $Al_2Br_7^-$ on the basis of conductivity measurements. In small amounts, the quaternary salts improved the brightness of the deposit but higher concentrations led to the incorporation of the quaternary salt into the deposit and thus to a decrease in its purity and corrosion resistance.

Better results were obtained by Peled and Gileadi [40] using alkali halides, mainly KBr, in combination with $AlBr_3$. They used an electrolyte consisting of 25 ~ 45% $AlBr_3$ and 1% aromatic hydrocarbons such as benzene, toluene, *m*-xylene, mesitylene, etc. $AlBr_3$ was the aluminium-containing component. The alkali bromide had two functions:

(i) to increase the solution conductivity to the minimum value required for electrolysis (1 ~ 6 mS cm^{-1});

(ii) to improve the throwing power of the solution by forming anions such as $Al_2Br_7^-$ or $AlBr_4^-$ ions.

The concentration of the alkali bromide was less than 1 mol dm^{-2} to avoid co-deposition of the alkali metal. Since the water in the baths could not be removed completely, the function of the aromatic hydrocarbons themselves, apart from their solution properties, consisted in their ability to bind the proton liberated during electrolysis. Thus the formation of ArH_2^+ ions, the σ complexes of aromatic hydrocarbons with protons, could be promoted and cathodic current efficiency increased. The stability of the σ complexes increased in the following sequence [37]: benzene < toluene < *m*-xylene < mesitylene. In general, the longer and more branched the chain or the higher the number of aromatic rings, the better the reactivity of the hydrocarbon towards protons.

The deposits obtained from such electrolytes were smooth, homogeneous and microcrystalline with good adherence [40]. Both the cathode and the anode efficiencies were 100% and the current density was 10 A dm^{-2}. The purity of the deposits was 99.5%. The metals coated were copper, brass and steel and the anode was 99.5% aluminium. Although there have been no reports concerning the industrial application of the bath, the results of laboratory experiments regarding plating quality and long-term performance appeared to be very promising. Its use would permit easier and more economical operation than the baths containing lithium aluminium hydride or aluminium organic compounds.

b. $AlBr_3$ + HBr as the electroactive component

This electrolyte [41-44] consisted of 36 - 45 vol.% $AlBr_3$ in a 1:1 mixture of ethylbenzene or diethylbenzene and toluene. The solution was prepared by the following method. An inert gas saturated with water vapour was passed through the solution to saturate the solvent with water, prior to dissolution of the $AlBr_3$, which would give rise to HBr. The solution thus prepared was carefully protected against moisture and oxygen by an inert atmosphere. The presence of

HBr in the solution ensured the required specific conductivity of 3 ~ 4 mS cm^{-1}. The coated surfaces were copper and steel and the anode was pure aluminium. At 1 A dm^{-2} the anode efficiency was 100% and the cathode efficiency 80%. Increasing the current density decreased the cathode efficiency. The low cathode efficiency compared with the anode efficiency led to an enrichment of the solution with aluminium, which successfully formed complexes with Br^- ions from the HBr. The quality of deposits up to 25 μ m thick was claimed to be very good with regard to mechanical strength and corrosion resistance. The bath life was also excellent: during one year of operation under optimum conditions the bath composition and function remained unchanged. Although Capuano et al. [43] regarded their electrolyte as highly suitable for application, no industrial use has been reported.

The system $AlBr_3$ + HBr in *o*-, *m*- and *p*-xylene has been investigated in detail [45-48]. Current efficiencies of 90% were attained. After the aluminium had been deposited completely on the cathode, hydrogen evolution and decomposition of the solvent were observed.

Some experiments have been performed to electroplate aluminium from an ethylbenzene solution of $AlBr_3$ without the addition of any further components [49-51]. The freshly prepared solution was light yellow and had a conductivity that was of the order of 10^{-8} S cm^{-1}. With time, the solution became dark brown and the conductivity increased to 10^{-3} S cm^{-1}. These changes, caused by traces of water in the electrolyte, have been ascribed to the formation of $Al_2Br_4OH \cdot C_8H_{10}^+$ complexes [51].

B. $AlBr_3$ Complexes with Onium Compounds

The continuous changes in $AlBr_3$ alkylbenzene solutions may be stabilised by introducing a third component — an alkali metal halide or a quaternary

ammonium compound. In the presence of a quaternary ammonium compound as well as an alkali halide, ionised complexes are formed:

$$R_4NBr + Al_2Br_6 \rightleftharpoons [R_4N]^+[Al_2Br_7]^- \rightleftharpoons R_4N^+ + Al_2Br_7^- \quad (1.2.1)$$

Among the examined compounds, aliphatic quaternary ammonium bromides were found to be more suitable for aluminium electrodeposition than iodides, which gradually decomposed evolving iodine [9]. At room temperature and current densities of 2 ~ 15 A dm^{-2}, optimal aluminium coatings were obtained from solutions of $AlBr_3$ complex with triethylisobutylammonium bromide. Some positive effect of tetramethyl-ammonium halides on aluminium deposition was reported when they were used not as the components of the electrolytes but only as additives [9]. A serious shortcoming of the aliphatic quaternary ammonium compounds were their hygroscopicity.

As in aromatic hydrocarbon solutions of "uncomplexed" $AlBr_3$, carbonium ions can be generated easily in electrolytes with aliphatic quaternary ammonium compounds, and therefore the first cathodic process in these solutions is hydrogen evolution. In contrast to $AlBr_3$ + xylene solutions, in solutions of aliphatic quaternary ammonium compound complexes, a distinct aluminium limiting current was observed and its value essentially depended on the chemical composition of the quaternary ammonium compound [9]. The analysis of voltammograms indicated that the rate of aluminium reduction was determined by both kinetic and diffusion limitations.

C. Organoaluminium Compounds

Of all nonaqueous electrolyte systems for the electrodeposition of aluminium, the solutions of complexes of organoaluminium compounds are the most accepted. This type of electrolyte was found by Ziegler and Lehmkuhl [52-53]. An industrial scale process (Sigal Process: Siemens galvanoaluminium) has

been developed. The electrolytes consist of alkylaluminium as well as alkali halides or quaternary onium salts, which are dissolved in aromatic solvents [54, 55]. Electrolysis is carried out at temperatures around 90 ~ 100°C. Electrolytes of this system have demonstrated their high productivity even in long term practical use. The high resistance of these electrodeposited aluminium layers to corrosion has been exploited especially in the automobile industry [56, 57]. The same type of electrolyte has been used for aluminium refinement for many years and purities of up to 99.9999% can be reached [58, 59].

The final performance limitation of alkyl electrolyte systems has not, so far, been reached. Substantially higher deposition rates than those realised today by electrodeposition technology with organoaluminium electrolytes, *i.e.* 1 ~ 1.5 A dm^{-2}, are probably attainable [60]. As a result, the industrial efficiency of both galvanic aluminium deposition and electrolytic aluminium refinement may be improved.

1.2.3 Electrodeposition of Aluminium from Dimethylsulfone

Dimethylsulfone ($DMSO_2$) has been considered a promising organic solvent for rechargeable cells [64], with a number of attractive features, such as: high conductivity; good thermal stability [61]; ability to dissolve numerous metallic salts; and weak co-ordination with metallic cations [62, 63]. Recent investigations [65, 66] have shown that aluminium can be reversibly plated and stripped in a mixture 2:1 mole ratio of $AlCl_3$-LiCl dissolved in $DMSO_2$ while no aluminium plating was observed in that of a 1:1 mole ratio. Analysis of chronoamperograms indicated that the aluminium deposition process on a tungsten electrode from the mixtures of $AlCl_3$-LiCl-$DMSO_2$ involved progressive nucleation with diffusion-controlled growth of the nuclei [65]. SEM observations showed that smooth and continuous aluminium deposits could be obtained from the $DMSO_2$ baths by potential step technique. A Raman study [67] revealed:

a. $AlCl_4^-$ ion was always the main Al(III) species even in a melt without LiCl;
b. $Al_2Cl_7^-$ was never found even in the more acidic baths , *i.e.* with $AlCl_3$-LiCl mole ratios greater than one;
c. A co-ordination complex, $Al[(CH_3)_2SO_2]_3^{3+}$, between $DMSO_2$ and Al(III) was formed in the acidic melts.

This complex was responsible for aluminium deposition on tungsten electrodes from $AlCl_3$/LiCl/$DMSO_2$ baths through the following reaction [65]:

$$Al[(CH_3)_2SO_2]_3^{3+} + 3e^- \rightleftharpoons Al + 3(CH_3)_2SO_2 \qquad (1.2.2)$$

No aluminium plating process occurred in mixtures with a 2:1 mole ratio of $AlCl_3$-LiCl, indicating that as a Lewis base, $DMSO_2$ was weaker than Cl^- ions but stronger than $AlCl_4^-$, leading to the following equilibrium for $DMSO_2$-based electrolytes:

$$AlCl_3 + Cl^- \rightleftharpoons AlCl_4^- \qquad (1.2.3)$$

$$4AlCl_3 + 3(CH_3)_2SO_2 \rightleftharpoons Al[(CH_3)_2SO_2]_3^{3+} + 3AlCl_4^- \qquad (1.2.4)$$

1.2.4 Assessments of Nonaqueous Al-electroplating Baths [5]

The best high purity (99.9999%) deposit was obtained from the organoaluminium bath. The disadvantage of this bath lies in the high cost of the organoaluminium compounds, their self-ignition in air, and their vigorous reaction with water. In solution, however, these compounds can be treated without any complication.

The hydride baths also give high purity (99.99%) deposits. However, they are inflammable, volatile, hygroscopic, and relatively complicated to handle.

The simple manipulation, low volatility, low inflammability and low cost are the advantages of the bromide baths. However, the purity of these deposits is only 99.5% and cathode current efficiency of 100% can be achieved only at low current densities of about 1 mA cm^{-2}.

To avoid the disadvantages mentioned above, the investigation of new nonaqueous electrolytic systems for the electrodeposition of aluminium has continued. Ambient temperature molten salts have been paid more attention as the most promising aluminium plating baths for industrial applications.

1.3 ALUMINIUM ELECTRODEPOSITION FROM AMBIENT TEMPERATURE MOLTEN SALTS

Generally, the molten salts used in aluminium-electroplating are AlX_3-MX melts, where X is either Cl^- or Br^-, and M^+ is an alkali ion (Li^+, Na^+ or K^+) or an organic cation. Normally, inorganic melts operate above 100 °C, while organic melts operate below 100 °C.

The molten salts reported have a very wide liquidus temperature range, from approximately -100 °C to >1000 °C, and specific conductivites in the range $<10^{-3}$ S cm^{-1} to <10 S cm^{-1}. The area of molten salt electrochemistry has been reviewed [**68-90**]. The high liquidus temperature (>100 °C) associated with most inorganic melts precludes their general application, whether practical or fundamental in nature [**90**]. For example, few organic compounds possess sufficient thermal stability to be dissolved in these melts, although some organic compounds might improve the features of the melts as either solvents or additives. Many potentially interesting inorganic solutes exhibit high vapour pressures at the elevated temperatures often encountered with inorganic melts. In addition, the high temperatures associated with inorganic melts frequently place exceptional requirements on either the design of apparatus used to study the neat melts or the extraneous solutes dissolved in melts and often add extraordinary amounts of non-essential experimental manipulation.

Thus, the development of low temperature molten salts for practical or fundamental applications including metal deposition has been an important field of investigation. Considerable interest has arisen concerning aprotic melts that are liquid close to room temperature. Theoretically, salts are characterised by high melting points due to the strong ionic bonds in the lattice, but the formation of low melting salts is favoured by the follow conditions [**91**]:

a. univalent cation and anion;

b. large cation and anion;

c. The charge which is delocalised or is well screened by ligands.

True ionic liquids that are molten at or below room temperature were first reported about forty years ago [92]. Since then, a large number of reports have appeared, detailing these unique materials which can be classified as:

i. haloaluminates [93];
ii. chlorocuprates[93];
iii. tetra-alkylborides[93];
iv. polyiodides [94];
v. nitrate amides [95].

1.3.1 Ambient Temperature Haloaluminate Molten Salt Systems

As ionic liquids, these nonaqueous, normally aprotic haloaluminate melts possess several attractive properties including low melting points (as low as -90°C in some cases), excellent chemical and thermal stabilities, negligible vapour pressure at elevated temperature, and high intrinsic electrical conductivities [96]. They are miscible in significant proportions with molecular solvents that exhibit a wide range of dielectric constants. Acetonitrile, benzene, propionitrile, toluene, and methylene chloride are some of the solvents that can be used [90]. In addition, a novel aspect of these ionic liquids is their adjustable Lewis acidity. Substantial variations in acidity can be effected simply by varying the molar ratio of the two components. These variations in acidity can be used to induce substantial changes in the co-ordination of complex solutes present in the melt.

When an aluminium halide, AlX_3, is combined with an organic salt, R^+X^-, the constituents of the resulting ionic liquid are determined by the mole ratio of these components, *q/p*, according to the following reactions, which proceed essentially to completion [96]:

$$pR^+X^- + qAlX_3 \rightleftharpoons qR^+AlX_4^- + (p\text{-}q)R^+X^-, \ (q/p < 1) \qquad (1.3.1)$$

$$pR^+X^- + qAlX_3 \rightleftharpoons (2p\text{-}q)R^+AlX_4^- + (q\text{-}p)R^+Al_2X_7^-, (1 < q/p < 2) \quad (1.3.2)$$

The dominant equilibrium describing the system is:

$$2AlX_4^- \rightleftharpoons Al_2X_7^- + X^- \quad (1.3.3)$$

The $Al_2X_7^-$ ions are a strong Lewis acid, while the X^- ions are the conjugate Lewis base. The q/p <1 melts in which X^- ions are in excess are termed basic. In the melts with $q/p > 1$ (acidic melts), $Al_2X_7^-$ ions, which are a halide ion acceptor, are the principle constituents of the system. Neutral melts are those where $q/p = 1$.

Among the reported Al-containing ambient temperature molten salts, haloaluminates can be generally classified as [1, 90]:

1) alkylpyridinium aluminates;
2) alkylimidazolium aluminates;
3) alkylfluoropyrazolium aluminates;
4) alkyltriazolium aluminates;
5) aralkylammonium aluminates;
6) alkylalkoxyammonium aluminates;
7) aralkylphosphonium aluminates;
8) aralkylsulfonium aluminates.

1.3.2 Alkylpyridinium Aluminates

A. Ethylpyridinium Bromide (EPB)-$AlCl_3$

The first experiments aimed at aluminium plating as a means of corrosion prevention were performed by Keyes et al. [97-99] using a low-melting mixture of aluminium bromide and tetraethyl ammonium bromide at 100 °C.

Aluminium electrolytes using pyridinium quaternary compounds were the first to have been used for practical aluminium electroplating. Hurley and Wier **[100-102]** found that a 2:1 mole ratio mixture of $AlCl_3$-EPB formed ambient temperature molten salts, which were useful as an aluminium plating electrolyte. A current density of 2 A dm^{-2} and 90% current efficiency were attained when the eutectic melt was saturated with an aromatic hydrocarbon (*e.g.*, benzene, toluene, etc.) which formed a supernatant layer on the bath. The superimposition of an alternating current on the direct current improved the adherence and the thickness of the deposit **[103].** To reduce the working temperature and simultaneously protect the solution against the influence of oxidation and moisture, Safranek et al. **[104-107]** employed a co-solvent for electroforming aluminium melt, which consisted of 32% of a 2:1 mole ratio mixture of $AlCl_3$ and EPB and 67% toluene and 1% methyl-*t*-butyl ether. Deposits of 0.6 ~ 1 mm thick were obtained at ambient temperature. A levelling effect similar to that observed in the presence of methyl-*t*-butyl ether was also obtained when dimethylaniline, phenylamines and aromatic or aliphatic ethers were used **[108].**

Simanavicius et al. **[109, 110]** studied the electrode reactions taking place in an $AlBr_3$-EPB bath. The reduction of carbonium ions and hydrogen evolution were found to precede aluminium deposition. The reduction of the ethyl pyridinium ion was also observed to occur. Cathodic polarisation curves indicated that aluminium deposition was diffusion controlled.

An aluminium plating bath consisting of a solution of aluminium bromide and EPB at a 1:1 molar ratio in an aromatic hydrocarbon permitted formation of adherent deposits at a current density of 2 A dm^{-2} with the superimposition of a.c. on the electrolysing current **[111, 112].**

Independently, Silvestroni and Rallo **[113]** also studied solutions of aluminium bromide and pyridinium bromide in toluene. An aluminium deposit having 50 μm thickness was obtained at 2 A dm^{-2}. The use of higher current

densities resulted in the occlusion of pyridinium salts in the coatings. This phenomenon was also observed by Peled and Gileadi [**114**].

Various ethers (*t*-butyl ether, iso-amyl ether, phenyl ether) were used as additives in order to avoid dendrite formation [**108, 109**]. When used as levelling additives, N, N-dimethylaniline and methyl-*t*-butyl ether were found to have only a temporary effect [**109**]. Bokor [**115**] attained 95% current efficiency in these types of baths.

However, $AlCl_3$-EPB melts suffer from several serious limitations: they readily undergo photo-decomposition and the melting points of the melts increase dramatically if the $AlCl_3$ content is less than or greater than about 66.7% by volume [**100**]. In addition, the presence of bromide, which is easily oxidised, leads to an electrochemical window (*i.e.*, the potential range over which an electrochemical reactions can be observed) of about 1.7 ~ 1.8 V.

B. N-(1-butyl)-pyridinium Chloride (BPC) -$AlCl_3$

Osteryoung et al. [**116-120**] found that a mixture of BPC and $AlCl_3$ formed low temperature melts, which were transparent viscous liquids at or near room temperature. Their acid-base properties were very similar to the higher-temperature alkali-metal chloroaluminates, although exhibiting somewhat more extreme conditions (*i.e.* the *pCl* range was much greater) and they had an electrochemical window of more than 2 V. As a consequence of their high viscosity, these melts had a relatively low conductivity for molten salts, although the value was significantly higher than for typical non-aqueous solvent/electrode systems. The viscosity could be reduced, and the conductivity increased with very little change in the properties, by the addition of up to 50 volume percent of benzene or toluene. As with other chloroaluminates, the most commonly used reference electrode was an aluminium wire, immersed in a 2:1 $AlCl_3$-BPC melt.

Robinson and Osteryoung [**121**] used potentiometric techniques to confirm that the addition of benzene to $AlCl_3$-BPC had no chemical effect other than

dilution. They showed that the equilibrium constant for the acid-base reaction in the 50 vol % benzene described by **Reaction 1.3.4** was above 2.2×10^{-13}, which was similar to that obtained for the pure melt:

$$2AlCl_4^- \rightleftharpoons Al_2Cl_7^- + Cl^- \qquad (1.3.4)$$

Robinson and Osteryoung also went on to consider the electrodeposition of aluminium, both from the pure melt and from benzene-melt mixtures, on tungsten, platinum, and glassy carbon electrodes. From chronoamperometry, the deposition on all three electrodes was shown to involve instantaneous nucleation, followed by diffusion-controlled three-dimensional growth. The deposition overpotential was greatest on carbon and smallest on tungsten. Cyclic voltammetric studies indicated the formation of an underpotential deposit on both tungsten and platinum, although not on glassy carbon. In all melts, the freshly deposited aluminium was shown to corrode slowly, reacting with the BP^+ cation.

In acidic melts, the negative limit on tungsten, platinum and carbon electrodes was always found to be the deposition of aluminium, but in basic melts this was not the case, since the BP^+ cation was reduced more readily than $AlCl_4^-$ ions [122]. This obviously limits use of basic $AlCl_3$-BPC melts for aluminium electrodeposition, and it would be necessary to use a cation that was less easily reduced.

1.3.3 Alkylimidazolium Aluminates

Using Molecular Orbital theory, Hussey et al. [123] calculated the electron affinities of a number of organic cations that might be reduced less easily than the alkylpyridinium ions. They found that alkylimidazolium cations gave acceptable molten salts. In particular, the most favourable was 1-methyl-3-ethylimidazolium chloride (MEIC). When mixed in excess with $AlCl_3$, it formed

a very low melting point system with an electrochemical window larger than that of the BPC system. In addition, the liquidus temperatures were sufficiently low to permit a much larger mole ratio of MEIC to $AlCl_3$ (a more basic melt) than with the BPC melts. Of the chloroaluminates, $AlCl_3$-MEIC melts were the most widely studied and understood. Recently, a family of ambient temperature ionic liquids formulated from MEIC and anhydrous metal chloride salts have been reported [124]: AgCl, CuCl, LiCl, $CdCl_2$, $CuCl_2$, $SnCl_2$, $ZnCl_2$, $LaCl_3$, YCl_3, $SnCl_4$ and $TiCl_4$. Nearly all of these mixtures, in most cases, produced ionic liquids at or near room temperature for at least some compositions, according to the reaction [124]:

$$MCl_n + mCl^- \rightleftharpoons MCl_{n+m}^{m-} \qquad (1.3.5)$$

Generally, the metal chloro complexes formed were of the lowest stoichiometry.

Compared with the BPC-$AlCl_3$ melt, the MEIC-$AlCl_3$ melt was a more promising electrolyte bath for industrial aluminium electroplating [125], and some continuous plating processes have been recently reported [126-128]. The rates of deposition and stripping of aluminium were high (25 A dm^{-2}), and the deposited aluminium was quantitatively cycled in large amounts (>25 C cm^{-2}) at high efficiency (>99%) [127]. Thin, continuous aluminium coatings could be electrodeposited onto a tungsten substrate from acidic $AlCl_3$-MEIC melts at ambient temperature using controlled potential deposition [127]. At deposition potentials negative of -0.2 V vs. an Al(III)/Al reference electrode, the resulting coating consisted of nuclei (or cluster) sizes smaller than optical resolution (< 0.5 μm). At more positive potentials, the microscopic structure consisted of larger (>0.5 μm) observable nuclei. Evidence for underpotential deposition of aluminium on tungsten electrodes was also presented [128]. The morphology of aluminium deposits produced using a 2:1 $AlCl_3$-MEIC melt was reported to be dense, smooth, and corrosion resistant [126, 129]. In addition, aluminium may be

deposited on amalgamated aluminium electrodes where no passivation behaviour was observed [131].

1.3.4 Tetraalkylammonium Aluminates

A. Trimethylphenylammonium chloride (TMPAC) -$AlCl_3$

Although the MEI^+ cation was not as easily reduced as the BP^+ cation, difficulty in the preparation of these melts has been encountered [123]. In particular, MEIC has only recently become commercially available and is expensive. Furthermore, the highly exothermic reaction between MEIC and $AlCl_3$ during melt preparation caused decomposition of the MEIC, leading to highly coloured electroactive decomposition products, unless special precautions were taken to control the reaction rate [127].

Since quaternary ammonium species were expected to have superior electrochemical stability, *i.e.*, they were less reducible compared to BP^+ or MEI^+ cations [122], molten salt electrolytes made from a quaternary ammonium halide and $AlCl_3$ would be expected to have increased stability. Jones and Blomgren [132] found a family of commercially available, fully substituted quaternary ammonium salts suitable for forming low-temperature melts. The key chemical feature of the group was that at least one of the substituents was an aromatic radical like phenyl or benzyl. The other substituents were preferably small aliphatic groups like methyl or ethyl. The central atom of the onium ion could be nitrogen, phosphorous, or sulphur.

Of them the $AlCl_3$-TMPAC (trimethylphenylammonium chloride) melt [132] was found to have electrochemical stability equal to $AlCl_3$-MEIC. The conductivity of the melt was comparable to that of BPC-$AlCl_3$ but lower than that of MEIC-$AlCl_3$. Aluminium was cycled reversibly in the melt (67% by volume $AlCl_3$), which melted at -75 °C. $AlCl_3$-TMPAC melts were easy and inexpensive to prepare in a relative high state of purity since TMPAC is commercially available in high purity.

Emmenegger et al. [133,134] used some small Gutmann donor number solvents such as 1,2-dichlorobenzene, anisole and diphenylether as co-solvents of $AlCl_3$-TMPAC melts with a view to possible use of these systems in batteries. The anodic passivation characteristics were observed in the neat and diluted melts on aluminium and amalgamated aluminium electrodes. With anisole as a cosolvent, aluminium deposition was faster on a pure aluminium electrode than on an amalgamated aluminium one [134]. However, the anisole-diluted melts had very low conductivities

B. Dimethylethylphenylammonium bromide (DMEPAB) - $AlBr_3$

Simanavicius [9] reviewed dimethylethylphenylammonium bromide (DMEPAB)-$AlBr_3$ melts as aluminium plating baths. The room temperature molten salts had a sufficiently high conductivity (about 10^{-3} S cm^{-1}), which could be increased nearly tenfold after their dilution by toluene. Some additives such as triethylammonium halide were used to remove moisture in the melts.

1.3.5 Mechanism of Aluminium-electroplating from Room Temperature Melts

Generally, the following equilibrium exists in an $AlCl_3$:MCl system, where M represents alkali metal ions or organic onium ions:

$$2AlCl_4^- \rightleftharpoons Al_2Cl_7^- + Cl^- \qquad (1.3.4)$$

In basic melts, the Al-containing ion is mainly present as $AlCl_4^-$, whereas in acidic melts the $Al_2Cl_7^-$ ion becomes predominant.

In the inorganic melts, aluminium deposition is possible by the discharge of either the $AlCl_4^-$ or $Al_2Cl_7^-$ ions. In basic melts, the deposition reaction involves the discharge of the $AlCl_4^-$ ion:

$$AlCl_4^- + 3e^- \rightleftharpoons Al + 4Cl^- \qquad (1.3.6)$$

In acidic melts, $Al_2Cl^-_7$ ion is the species reduced to give the aluminium deposit:

$$4Al_2Cl_7^- + 3e^- \rightleftharpoons Al + 7AlCl_4^- \qquad (1.3.7)$$

However, in all organic melts, organic cations are reduced at less negative potentials than that required for $AlCl_4^-$ [135]. Potentiometric titrations of the MEIC-$AlCl_3$ system and gravimetric analysis of electrodes in acidic melts indicated that the cathodic reaction was given by **Reaction 1.3.7**. Aluminium can only electroplated from the acidic melts. In MEIC-$AlCl_3$ and BPC-$AlCl_3$ systems, aluminium deposition reactions were found to be quasi-reversible processes with preceding chemical reactions [122,127]. A current-reversal chronopotentiometric study showed that the deposited aluminium underwent a slow corrosion reaction. The proposed the mechanism for aluminium electrodeposition from these acidic melts [136] was:

$$Al_2Cl_7^- \rightleftharpoons [AlCl_3 ... AlCl_4^-] \qquad (1.3.8)$$

$$4[AlCl_3 ... AlCl_4^-] + 3e^- \rightleftharpoons Al + 7AlCl_4^- \qquad (1.3.9)$$

$$Al + X \longrightarrow \text{Products (corrosion)} \qquad (1.3.10)$$

where X represents organic cations or impurities.

1.4 THE PURPOSE AND PLANS OF THIS PROJECT

It should be noted that aluminium electrodeposition processes are much more complicated than those of any metal from aqueous solutions. The electrolyte system for aluminium plating operates properly only when using reliably sealed fully automatic electroplating baths equipped with air-locks. At the moment, the process should be suitable particularly for coating high-value products that can benefit from the specific properties of aluminium and aluminium oxide. Therefore, it is understandable that although aluminium was electrodeposited from non-aqueous solvents for the first time at the beginning of this century [137], only one attempt to use it in practice was made in 1948 [138], and it was introduced into production only in 1981 [139]. Nevertheless, plating baths for electroplating aluminium may still become a broad commercial reality [140]. Among them, low and ambient temperature molten salts will play a very important role.

1.4.1 The Aim and the Requirements

The aim of this project was to recover aluminium from pure alumina slurries with electrochemical techniques. The processes were required to be environmentally friendly.

1.4.2 The Selection of Al-plating Baths

As the literature review indicated, organic electrolytic Al-plating baths possess the disadvantages of low conductivity, high inflammability, volatility and toxicity. Inorganic melts required high temperatures, with consequent high vapour pressures and energy consumption. Few organic compounds can be dissolved in these melts as either solvents or additives to improve the features of the melts. Therefore, the novel room temperature organic molten salts were

reasonably chosen as the Al-plating bath in this project. For the consideration of the environment and the production cost, the non-toxic, inexpensive and commercially available trimethylphenylammonium chloride (TMPAC) was used to make the room temperature Al-plating melt with aluminium chloride.

1.4.3 The Production of Anhydrous Aluminium Chloride

Since the room temperature molten salts are very sensitive to air and moisture, aluminium chloride, as a component of the melts, must be anhydrous. According to the available processes, anhydrous aluminium chloride can be obtained from the dehydration of alumina and the following chlorinating process [141]:

$$Al_2O_3(s) + CO(g) + Cl_2(g) \xrightarrow{400\text{–}700^\circ C} AlCl_3(s) + CO_2(g) \qquad (1.4.1)$$

Therefore, in this project, research focused on the electrodeposition of aluminium from room temperature molten salts $AlCl_3$-TMPAC.

Basically, information of the electrodeposition of metals in room temperature molten salts is of critical importance to the technological development for applications in electrodeopsition, electropolishing, electrorefining and electroetching. However, little information about the electrodeposition of aluminium in room temperature molten salts has been reported, although these melts, especially $AlCl_3$-TMPAC melt possess several attractive properties. Therefore, in this project the electrochemical behaviour of aluminium in room temperature molten salts $AlCl_3$-TMPAC on several foreign substrates were examined:

a. To reach a better understanding of electrochemical reactions occurring at very negative potentials in these melts. This was necessary since some of the electrochemical reactions involving lower oxidation states of

refractory metals, such as zirconium [142], niobium [143], and tungsten [144] occur at potentials near the deposition of aluminium.

b. To learn whether the deposition of aluminium on foreign substrates involved nucleation phenomena of the type previous observed in some melts [145,146]. It was pointed out that it was unlikely that similar nucleation effects would be observed in molten halides where predeposition reaction to form monolayers frequently occurred [147].

In addition, electrochemical behaviour of some metal ions such as nickel, gallium and iron in $AlCl_3$-TMPAC melts were investigated.

Chapter 2

EXPERIMENTAL METHODS AND ELECTROCHEMICAL TECHNIQUES

2.1 EXPERIMENTAL METHODS

2.1.1 Chemicals

Trimethylphenylammonium chloride, (Merck, >99%, m.p. 237 °C) was dried under vacuum at 100°C. $AlCl_3$ and $NiCl_2$ (Aldrich, anhydrous, > 99%) were used as received. 1,2-dichlorobenzene 1,2-DCB (Aldrich anhydrous 99%) was dried over activated 4 Å molecular sieves which were treated under vacuum at 150°C for 1 hour prior to use.

2.1.2 Preparation and Pre-treatment of the Melt

$AlCl_3$-TMPAC molten salts, which are liquid at room temperature, are obtained for compositions between 61 ~ 67% $AlCl_3$ [132]. A 2:1 mole ratio melt was prepared by adding TMPAC to $AlCl_3$ with continuous stirring under a purified helium atmosphere in a Schlenk system, instead of a vacuum atmosphere dry box. The melts began to form spontaneously upon mixing the two solids. Since this mixing process was rather exothermic, a room temperature water bath was used to ensure that the temperature did not rise above 100°C, where decomposition might occur. Decomposition of the melt was indicated by

the melt becoming a deep brown colour. When the mixing was completed, the melt was clear, faint yellow and honey-like, but it turned yellow and then slightly brown within a week. It became brown and finally dark brown within the Schlenk line within a few weeks, or in a few days off the line. When exposed to the air, the melt was hydrolysed and oxidised within hours, resulting in white precipitates on the wall of the cell and a dark brown solution. Therefore, any impurities in fresh, clear melts were from the chemicals. This discoloration has also been observed in some inorganic and organic chloroaluminate melts, and were attributed to carbonaceous impurities and to the presence of $FeCl_3$ impurities in the $AlCl_3$.

The melt was further purified by pre-electrolysis between two high purity Al electrodes at approximately 0.5 mA cm^{-2} for 48 h.

The formation reaction for 2:1 $AlCl_3$-TMPAC molten salts can be represented by:

$$2AlCl_3(s) + TMPA^+ Cl^-(s) \rightleftharpoons Al_2Cl_7^-(l) + TMPA^+(l) \qquad (2.1.1)$$

The concentration of Al(III) species in the 2:1 $AlCl_3$:TMPAC neat melt was estimated at 3.09 M [**134**]. According to deposition reaction of aluminium in the melt:

$$4Al_2Cl_7^- + 3e^- \rightleftharpoons Al + 7AlCl_4^- \qquad (1.3.7)$$

the concentration of $Al_2Cl_7^-$ ions can be taken as either 3.09 M with n = 3/4 or 0.77 M with n = 3 [**148**].

The diluted melts were prepared by adding 50% by volume of 1,2-dichlorobenzene (assuming no partial molar volume change with mixing).

2.1.3 Electrochemical Cell

A home-made electrochemical cell with an air-lock and a water/oil bath jacket (**Fig. 2.1.1**) was constructed with a four-neck flask and standard ground glass joints in which three electrodes and a thermometer were sealed.

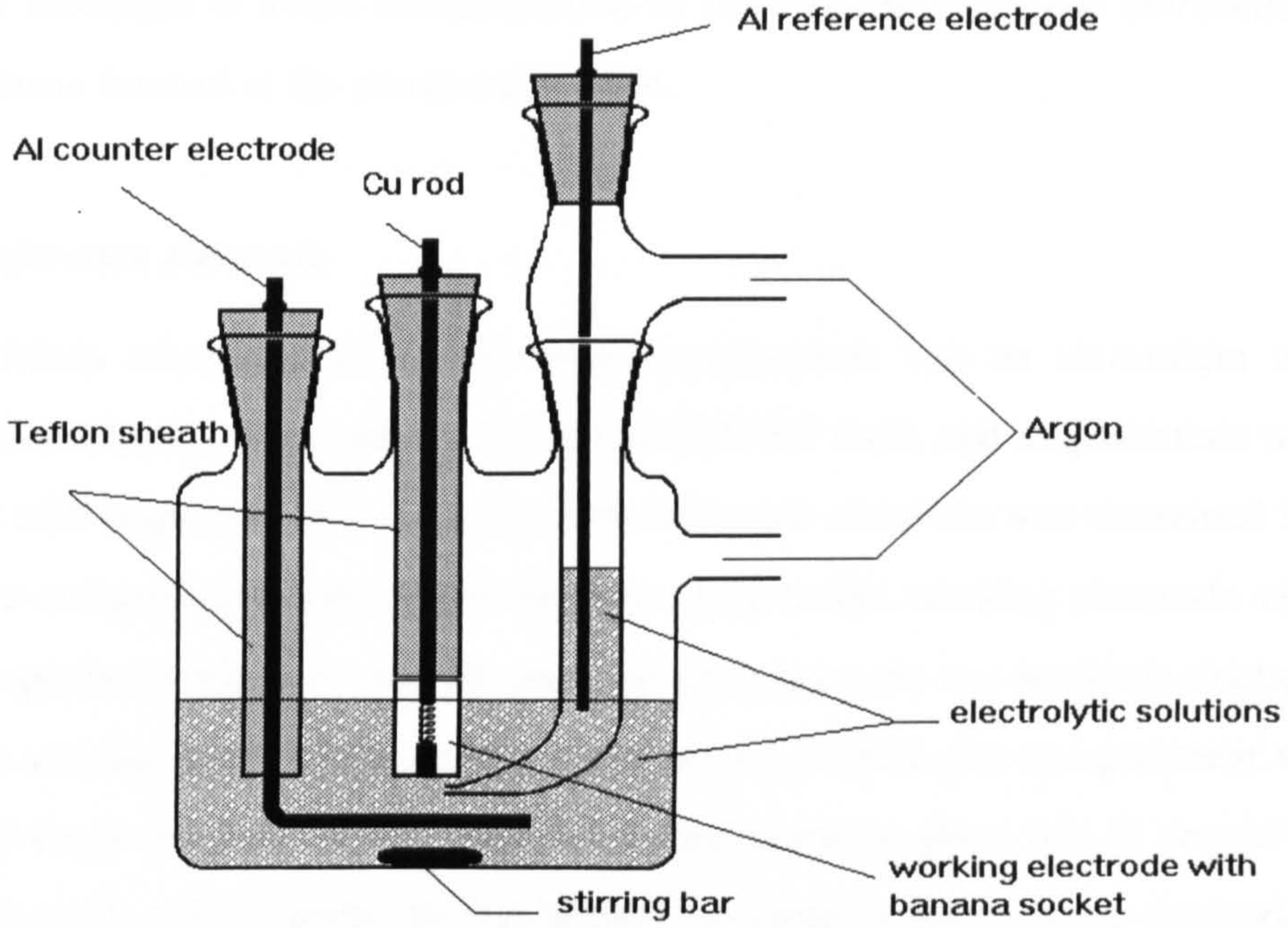

Fig. 2.2.1. Electrochemical cell for aluminium deposition from room temperature 2:1 $AlCl_3$-TMPAC melts.

A. Working and counter electrodes

To establish a symmetrical electric field at the working electrode, a concentric cylindrical arrangement of the working and counter electrodes were used. The resistance of the cell was reduced by placing the working and counter electrodes as close as possible. The working electrode consisted of a banana socket in which the working electrode was sealed inside a length of 2 ~ 3 cm Teflon tubing. The electrode surface was exposed from the end of the Teflon. The other end of the electrode was connected by a copper spring with a copper or tungsten rod plugged in the banana socket. The conducting rod was fitted into a Teflon stopper and the exposed part in the cell was covered with several layers

of heat-shrinkable tubing. The working electrodes were made of several materials: tungsten wire (ϕ =2 mm), aluminium rod (ϕ =2 mm), glassy carbon rod (ϕ =3 mm), platinum wire (ϕ =1 mm) and nickel wire (ϕ =2 mm), respectively. High purity aluminium wire (5N, Goodfellow) served as the counter electrode to avoid contamination of the working electrode environment by products formed at the counter electrode.

B. Reference electrode

Unless otherwise stated, the reference electrode was an aluminium wire (5N, Goodfellow) immersed in a 2:1 $AlCl_3$:TMPAC melt, and all potentials were quoted with respect to this electrode. The reference electrode was contained in a separate compartment, which was brought close to the working electrode via a Luggin probe to minimise the IR potential drop between the working electrode and the sensing point. In the melts diluted with 1,2-DCB, the compartment was isolated from the bulk of the melt by a fine porosity glass frit. It should be pointed out that if the probe tip was placed too close to the working electrode it might have shielded the surface thereby producing local inhomogeneity in the potential and current distribution. Following a general rule, the probe was placed no closer than twice the diameter of the probe tip [149].

C. IR compensation

Although the Luggin probe was effective in reducing the uncompensated resistance, the residual component could be sizeable causing serious distortion of current-potential, potential-time, and current-time curves. The effect of uncompensated resistance is particularly important in transient studies, since the current-voltage curves are further distorted by alteration of the perturbation function. For example, in potential step studies the actual potential drop across the interface may vary with time, even though the applied potential is constant, since the product IR_u is also a function of time. This problem was avoided by use

of a home made potentiostat with positive feedback, whereby the potential drop across the uncompensated resistance between the working electrode and the Luggin probe was eliminated. The potential difference between the working and reference electrodes was therefore independent of the current (and hence time) for a constant input voltage.

D. Preparation of electrode surfaces

In order to achieve reproducible electrochemical results, great care had to be taken in preparing the electrode surfaces. All working electrodes were polished successively to a mirror-like finish with increasingly finer grades of emery paper, given a final polishing with an aqueous slurry of 0.05 μm alumina prior to use and then rinsed with distilled water and acetone. The aluminium electrodes were chemically polished by immersion in a solution of H_2SO_4 (*98%wt*) : H_3PO_4 (*85%wt*) : HNO_3 (*52.5%wt*) (25:70:5 by volume) for 25 min [**150**]. Since the nucleation phenomena on the electrodes were highly dependent upon the electrochemical pre-treatment of the electrode, a pre-treatment consisting of scanning the potential from 1.0 to 3.0 V and back to 1.0 V was performed prior to each chronoamperometric transient [**128**]. At 2.7 V the oxidation of $AlCl_4^-$ ions occurs according to **Reaction 2.1.2**, so substantial quantities of chlorine gas were generated by scanning to 3.0 V.

$$4AlCl_4^- \rightleftharpoons 2Al_2Cl_7^- + Cl_2 + 2e^- \qquad (2.1.2)$$

This pre-treatment may clean the working electrode surface by removing oxide impurities adsorbed from the melt. For sets of successive cyclic voltammetric sweeps, the electrode was not removed and polished between sweeps. Instead the potential was held at 3.0 V for 5 min to strip any deposits on the electrode.

To assess the reproducibility of the experiments freshly polished tungsten electrodes were run under identical conditions in separate freshly prepared melts. The results are shown in **Table 2.1.1**. The variability in the parameters for sweeps or potential steps was approximately 3-4%.

To determine the reproducibility of the stripping procedure (5 min at 3.0 V) on sets of successive voltammograms or potential steps, a tungsten electrode was polished once and then a series of successive transients were run in a fresh melt. Between each transient the electrode was held for 5min at 3.0 V to strip the deposit, however it was not removed and repolished. **Table 2.1.2** shows the results of a series of successive sweeps or potential steps. The variability in the parameters in the sweeps or potential steps was approximately 3-4%.

Table 2.1.1 Reproducibility of voltammograms and potential step transients of freshly polished tungsten electrode in different fresh 2:1 $AlCl_3$-TMPAC melts*

	Cyclic Voltammetry		Potential Step	
	I_p, c	E_p, c	I_m	t_m
	(mA cm^{-2})	(mV)	(mA cm^{-2})	(s)
	-25.75	-15.24	-18.05	0.170
	-26.48	-14.86	-16.32	0.182
	-26.15	-15.15	-17.35	0.175
	-24.95	-15.44	-16.25	0.176
	-25.98	-15.58	-17.62	0.186
	-24.24	-16.40	-18.15	0.172
s**	**0.839**	**0.412**	**0.871**	**0.0046**
s_{rel} %	**3.28**	**3.64**	**4.81**	**3.44**

* All experiments were carried out at 25°C, with 0.10 V s^{-1} sweep rate for voltammograms and –0.26 V overpotential for potential step transients.

** **s** and s_{rel} are standard derivation and relative standard derivation.

Since the fresh melts turned slightly brown and finally dark brown within a couple of weeks, no long term repetitive results could be observed (see **Fig. 3.1.8**).

Table 2.1.2 Reproducibility of voltammograms and potential step transients of a single tungsten electrode in the fresh 2:1 $AlCl_3$-TMPAC melts.* The electrode was not repolished between transients.

	Cyclic Voltammetry		Potential Step	
	I_p, c	E_p, c	I_m	t_m
	(mA cm^{-2})	(mV)	(mA cm^{-2})	(s)
1	-24.64	-0.162	-17.25	0.165
2	-25.25	-0.154	-18.4	0.176
3	-24.28	-0.158	-18.65	0.185
4	-26.75	-0.164	-17.46	0.182
5	-26.35	-0.160	-16.82	0.168
6	-25.80	-0.144	-17.75	0.172
s**	**0.966**	**0.0072**	**0.697**	**0.0078**
s_{rel} %	**3.79**	**4.61**	**3.93**	**4.49**

* All experiments were carried out at 25°C, with 0.10 V s^{-1} sweep rate for voltammograms and –0.26 V overpotential for potential step transients.

** **s** and s_{rel} are standard derivation and relative standard derivation.

2.1.4 Apparatus

Transfer and weighing of all solid chemicals were conducted in a dry glove box full of nitrogen. The cell containing 15 ml of the melt was connected by a Young's joint with a Schlenk vacuum line for the air and moisture sensitive melt systems. Staircase cyclic voltammetric and chronoamperometric measurements were performed using an 286IBM compatible computer controlled Keithley 575-2 Data Acquisition System with AMM2 16-bit Analog Master Measurement model. The system featured an output range of ±5 V, an A/D range of ±10 V, ×1 ~ ×100 programmable gains and noise < 0.005% of full scale rms on all ranges and gains. Staircase cyclic voltammograms and potential step plots were collected with 5 mV step increments. All experimental data and graphs were further processed with *Easyplot II* and *Microsoft Excel.*

The conversion of the analogue current response transient into a digital form for analysis of convolution or chronocoloumetry was achieved with a IBM computer, in conjunction with programs written by Dr. VanderNoot. Reduction and oxidation charges were calculated by graphical integration.

Since the reduction product of $Al_2Cl_7^-$ ions was insoluble aluminium, the equilibrium potential of the electrode, E_{eq} (vs. Al), was obtained to within 3 mV, by the following equation [151], when the current density $I = 0$:

$$E = E_{eq} = E^{\circ'} + (\frac{RT}{nF}) \ln c \qquad (2.1.3)$$

where $E^{\circ'}$ is the formal potential of the electrode and c is the bulk concentration of $Al_2Cl_7^-$ ions. In fact, the value of E_{eq} was so small as to be ignored. Therefore, measured potentials were considered as overpotentials.

All electrochemical experiments were carried out with the Schlenk system at room temperature (approx. 25±2 °C).

2.2 ELECTROCHEMICAL TECHNIQUES

2.2.1 Transient Electrochemical Techniques

It is well known that many important electrochemical reactions involve the formation of a solid phase, either as the result of the reduction of ions in solution, as in the case of metal electrodeposition, or by oxidation of the electrode and subsequent reaction with anions to form an anodic film. Basically, the electrodeposition processes of metals that involve the transfer of charge at an electrode/solution interface are examples of a general class of electrochemical reactions referred to as heterogeneous processes. The kinetics of heterogeneous reactions is normally determined by a sequence of steps involving both transport through the solution (and sometimes the electrode) phase and transfer of charge at the interface. Generally, an electrodeposition process involves a number of distinct steps [152]:

1) diffusion of ions in solution to the electrode surface;
2) electron transfer;
3) partial or complete loss of the solvation sheath, resulting in the formation of ad-atoms;
4) surface diffusion of ad-atoms;
5) clustering of ad-atoms to form critical nuclei on a perfectly smooth surface or on a foreign substrate;
6) incorporation of ad-atoms at lattice sites;
7) development of crystallographic and morphological characteristics of the deposit.

Although, in practice, the last of these steps is of most interest, it is necessary to look more closely at the earlier steps in order to gain a fundamental understanding of the electrodeposition process. Since these steps occur sequentially, then the rate of the overall reaction depends upon the rates of the individual steps. Furthermore, under non-steady-state or transient conditions the rates of the individual processes are also time dependent. Therefore, the analysis of this time dependence can be carried out by transient electrochemical techniques.

In any transient technique, it is necessary to disturb the reaction from equilibrium or the steady state by applying a perturbing impulse to the system. The system is then allowed to relax to a new equilibrium or steady state, and the transient (*i.e.*, the response as a function of time) is analysed to extract the desired electrochemical information. In electrochemical studies the rate of the reaction is related to the current by Faraday's law, and is dependent upon the potential difference across the electrode/solution interface. So, transient techniques can be classified as potential perturbations including potentiostatic and potential sweep methods, and current perturbations including galvanostatic techniques.

In general, it is necessary to use a combination of techniques in order to characterise and explain the involved processes satisfactorily. With the apparatus

available, in this project, several potential perturbation transient techniques such as potential sweep (*staircase cyclic voltammetry*) and potential step (*chronoamperometry* and *chronocoulometry*) were applied. Also, *convolution* techniques were used in the analysis of the experimental data.

2.2.2 Potential Sweep Techniques

It is in the area of preliminary mechanistic investigations that potential sweep techniques, in particular *cyclic voltammetry* (CV), are probably most useful. A CV can be rapidly obtained and indicates the potentials where processes occur. From the sweep rate dependence the involvement of coupled homogeneous reactions is readily identified, and other complications such as adsorption can be recognised. In view of these capabilities, cyclic voltammetry is nearly always the technique of choice when studying a system for the first time, though better techniques probably exist for determining precise kinetic data.

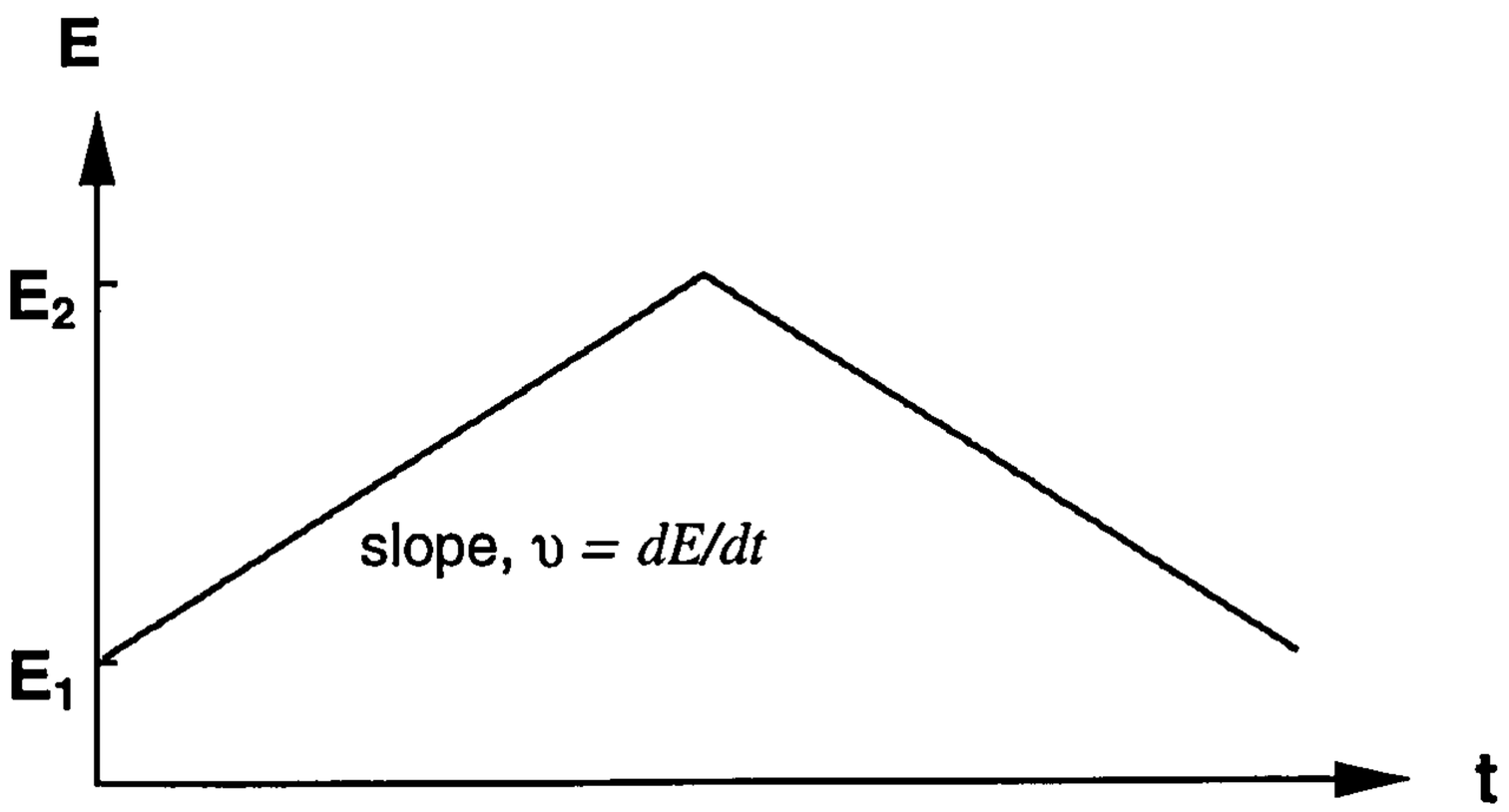

Fig. 2.2.1. Potential-time profiles for cyclic voltammetry

The potential-time waveforms used for sweep measurements are shown in **Fig. 2.2.1.** As a generally more useful (and consequently more widely applied) technique, cyclic voltammetry involves sweeping the electrode potential between

limits E_1 and E_2 at a known sweep rate. Upon reaching the potential E_2 the sweep is reversed (usually at the same scan rate).

In this project, a variant of cyclic voltammetry, *staircase cyclic voltammetry* (SCV), which is particularly appropriate for computer control, was used. The potential in SCV is advanced in steps of δE volts every $\delta\theta$ seconds. This corresponds to a voltage ramp of $\delta E/\delta\theta$, the equivalent of the quantity υ . Any desired value of the ratio $\delta E/\delta\theta$ can be implemented by various combinations of the two variables [153]. The sensitivity is good (10^{-7} M) due to the elimination of the charging current [153]. In SCV experiments the cell current is recorded as a function of the applied potential (it should be noted, however, that the potential axis is also a time axis). The sweep rates used here ranged from 0.01 V s^{-1} to 1.0 V s^{-1} and δE was 5 mV.

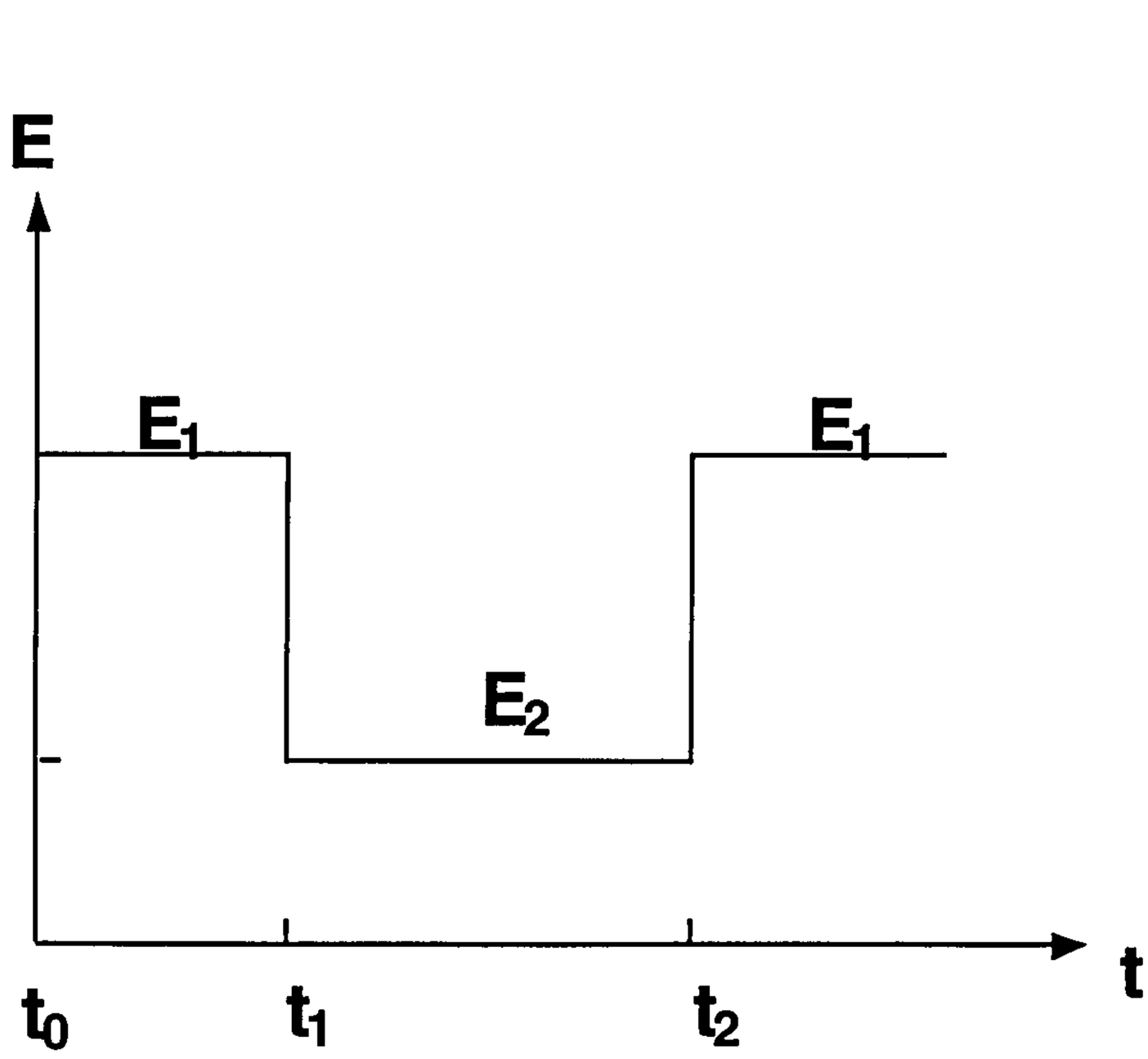

Fig. 2.2.2. Potential-time profiles for chronoamperometry

2.2.3 Potential Step Techniques

In potential step experiments the potential of the working electrode is changed instantaneously, and either the current-time response (*chronoamperometry*) or the charge-time response (*chronocoulometry*) is recorded.

A. Chronoamperometry

A potential-time profile of chronoamperometry applied to a working electrode is shown in **Fig. 2.2.2.** E_1 was chosen such that reduction of the reactants, or indeed any other electrode reaction, did not occur. Then at the time $t = 0$ the potential was instantaneously changed to E_2, where the reduction of the reactants took place. Finally, the potential was jumped back to E_1, where the products were reoxidised. For an unstirred solution, under conditions of purely semi-infinite diffusion to a planar electrode, the current-time response is described by the Cottrell equation [**148**]:

$$I = nFAc(D/\pi\ )^{1/2}t^{-1/2} \qquad (2.2.1)$$

Based on experimentally evaluated *I-t* curves for a fixed concentration of electroactive species, and according to **Eqn. 2.2.1**, a plot of I versus $t^{-1/2}$ should be linear. Similarly, a plot of $It^{1/2}$ versus t for longer times should be constant. From such plots, it is possible to determine the diffusion coefficient of electroactive species if concentration values, *c,* are known. Moreover, chronoamperometry can be also used to analyse nucleation processes and the calculation of the rate constants of the reactions (see **Section 3.1.7**).

B. Chronocoulometry

In chronoamperometry, kinetic constants are obtained by analysis of current time data. It is often advantageous if the comparable chronocoulometric experiment is performed, *i.e.* the cumulative charge Q (determined by the electronic integration of the current) is recorded as a function of time. If Q is plotted as function of $t^{1/2}$, at long times the data approaches the straight line defined by [**154**]:

$$Q = n\,k^{\circ}\,FAc(t_l^{1/2}t^{1/2} - t_l)/\pi \qquad (2.2.2)$$

where $t_l^{1/2}$ is the intercept on the $t^{1/2}$ axis of the Q *vs.* $t^{1/2}$ plot. The value of k° is obtained from the slope and the value of t_l. As the value of k° increases, the value of t_l decreases until under the conditions of diffusion control no intercept is seen on the $t^{1/2}$ axis. Integration of the Cottrell equation (**Eqn. 2.2.1**) then shows that Q will vary with $t^{1/2}$ according to the expression:

$$Q = 2nFAc(D/\pi)^{1/2}t^{1/2} \qquad (2.2.3)$$

and the value of D may be obtained from the gradient.

The advantage of chronocoulometry over chronoamperometry is that, since the charge is the integral of the current it retains at long time information about the value of the current at short times even at longer time. The charge at very short times is still distorted by the double layer charging process, but its influence on the total charge rapidly becomes negligible. Hence, **Eqn. 2.2.3** is applicable over a very wide time range (perhaps 2000 times as long as the range for *I vs.* $t^{1/2}$ plots*)* and only breaks down when natural convection begins to influence data, *i.e.* after several seconds. The value of k can therefore be found from data at quite long times. This permits k values perhaps an order of

magnitude greater to be determined from charge, rather than current measurements [155, 156].

2.2.4 Convolution Techniques

In all potential sweep techniques, the interpretation of the mechanism and the estimation of kinetic parameters is based upon the analysis of peak currents and peak potentials and their variation with sweep rate and concentration. Such approaches discard much of the information contained within the voltammogram, in particular the shape of the peak. An alternative approach, which has become possible with the increased availability of microcomputers capable of rapid data acquisition and treatment, is to transform the whole curve prior to analysis. One such transform which has proved very successful is the convolution [157,158,159,160] or semi-integral transform [161].

The essential feature of convolution potential sweep voltammetry (CPSV) in non-convective systems stems from the ability to determine the surface concentration of a reacting species directly from a convolution transformation of the current response transient, when the electrode potential is changed with time in a predetermined manner. The convolution procedure serves as a mathematical means for eliminating the mass transport polarization effects that are often inherent in experimental CV current-potential data.

The principal advantage of using a convolution analysis in treating CV data is an increase in the accuracy of mechanistic diagnosis and kinetic parameter determination. This is a direct consequence of using information from the entire current-potential curve, instead of only the peak current and peak potential values. Furthermore, it is not necessary, in the study of potential-dependent phenomena to assume an *a priori* knowledge of a kinetic model in order to compare it with experimental data [162].

The application of convolution voltammetry requires a semi-infinite system, where the reaction at the electrode surface is eventually diffusion-

limited, and mass transport is by diffusion and described by Fick's laws [157,163,164]. By proper treatment of the potential sweep data, the voltammetric *I vs. E* curves can be transformed into forms, closely resembling the steady-state voltammetric curves, which are frequently more convenient for further data processing. This transformation makes use of the convolution principle and has been facilitated by the availability of digital computers for the processing and acquisition of data. The solution of the diffusion equation for semi-infinite linear diffusion conditions, and for species **O** initially present at a concentration c_o yields for any electrochemical technique, the expression [164]:

$$c_O(0,t) = c_O - \frac{1}{nFA\,D_O^{1/2}}\left(\frac{1}{\pi^{1/2}}\int_0^t \frac{i(u)}{(t-u)^{1/2}}du\right) \qquad (2.2.4)$$

where n, F, A and c_o are the number of electrons transferred, Faraday's constant, the electrode area, and the bulk concentration, respectively. If the term in brackets, which represents a particular transformation of the experimental I_t data, is defined as m_t, then **Eqn. 2.2.4** becomes [157]:

$$c_O(0,t) = c_O - \frac{m_t}{nFAD_O^{1/2}} \qquad (2.2.5)$$

where:

$$m_t = \frac{1}{\pi^{1/2}}\int_0^t \frac{i(u)}{(t-u)}du \qquad (2.2.6)$$

This integral can be considered as the semi-integral of I_t, generated by the operator $d^{-1/2}/dt^{-1/2}$ so that [165,166]:

$$\frac{d^{-1/2}}{dt^{-1/2}}i(t) = m_t = I_t \qquad (2.2.7)$$

Clearly the convolutive [167] and semi-integral [162,168] approaches are equivalent. Thus the transformed current data can be used directly, by **Eqn. 2.2.5**, to obtain $c_o(0,t)$. Once the current becomes diffusion limited, $c_o(0,t) = 0$, m_t reaches its limiting or maximum value, m_l, where:

$$m_l = nFAD_O^{1/2} C_O \tag{2.2.8}$$

or

$$C_O(0,t) = \frac{(m_l - m_t)}{nFAD_O^{1/2}} \tag{2.2.9}$$

Similarly for species **R**, assumed absent initially, the expression that results is:

$$C_R(0,t) = \frac{m_t}{nFAD_R^{1/2}} \tag{2.2.10}$$

It should be stressed that these equations hold for any form of signal excitation in any electrochemical technique applied under the above conditions (semi-infinite diffusion, absence of migration, convection, soluble **O** and **R**, etc.), and no assumptions have been made concerning the reversibility of the charge transfer reaction or even the form of the dependence of $c_o(0,t)$ and $C_R(0,t)$ on E. Thus, with the application of any excitation signal that eventually drives $C_O(0,t)$ to zero, the transformed current m_t will attain a limiting value, m_l, that can be used to determine C_O by **Eqn. 2.2.8** [169]. If the electron transfer reaction is Nernstian, the application of **Eqns. 2.2.9** and **2.2.10** immediately yields:

$$E = E_{1/2} + \frac{RT}{nF} \ln \frac{m_l - m_t}{m_t} \tag{2.2.11}$$

where

$$E_{1/2} = E^{\circ'} + \frac{RT}{2nF} \ln \frac{D_R}{D_O} \tag{2.2.12}$$

where $E^{\circ\prime}$ is the formal potential. Note that this expression is identical in form to those for the steady-state or sampled-current *I vs. E* curves [170].

For irreversible processes and those involving coupled chemical reactions **Eqn 2.2.11** will no longer hold. However, Saveant et al. [157,159,160,171] have derived similar linear plots of logarithmic functions of m_t as a function of E to enable kinetic parameters to be determined.

For a totally irreversible or a quasi-reversible reaction the convolution forms are given, respectively:

$$E = \frac{RT}{\alpha nF}\ln\frac{k^{\circ}}{D^{1/2}} + \frac{RT}{\alpha nF}\ln\frac{m_l - m_t}{m_t} \qquad (2.2.13)$$

and

$$E = \frac{RT}{\alpha nF}\ln\frac{k^{\circ}}{D^{1/2}} + \frac{RT}{\alpha nF}\ln\frac{m_l - m_t(1+e^{(nF/RT)(E-E_{1/2})})}{i} \qquad (2.2.14)$$

The reversible $E_{1/2}$ value for such a system can be determined from:

$$E_{1/2} = E_{i=0} - \frac{RT}{F}\ln\frac{m_l - m_{i=0}}{m_{i=0}} \qquad (2.2.15)$$

where $E_{i=0}$ and $m_{i=0}$ are the potential and the convoluted current when the current, *i(t)*, passes through zero on the reverse scan.

Significantly, the convolution analysis can be extended to mechanisms of electrochemical processes. In all cases where the charge transfer reaction is reversible, the slope of the logarithmic analysis (**Eqn. 2.2.11**) is equal to *RT/nF*. Irrespective of the kinetic character of the charge transfer reaction, the location of the logarithmic plot along the potential axis is independent of both the sweep rate υ and the initial concentration C_o. This property is a useful diagnostic criterion, because if the proper mechanism has been chosen then the logarithmic

plots for different sweep rates and initial concentration must be superimposable. Furthermore, in the cases where the charge transfer reaction is not completely reversible α and k° may be determined from the slope and intercept.

It is to be noted that in the case of chronoamperometric experiments, application of the semi-integral operator to **Eqn. 2.2.1**, or in the case of chronocoulometric experiments application of the semi-differential operator on **Eqn. 2.2.2**, leads to:

$$\frac{d^{-1/2}}{dt^{-1/2}} I = \frac{d^{1/2}}{dt^{1/2}} Q = nFAD_O^{1/2} C_O \qquad (2.2.16)$$

which is exactly the same as **Eqn. 2.2.8**. **Eqns. 2.2.15** and **2.2.16** are very useful for analytical purposes because they indicate a direct proportionality of the semi-integral function of current or semi-differential function of charge on concentration.

It should be pointed out that the electrodeposition processes involve the formation of insoluble products. This particular case has not received theoretical analysis in terms of convolution. Hence, the application of the convolution methods to the case of electrodeposition is informative but at best approximative.

PAGE NUMBERING AS ORIGINAL

Chapter 3

ALUMINIUM ELECTRODEPOSITION ON TUNGSTEN

3.1 ELECTROCHEMICAL STUDIES IN PURE MELTS

3.1.1 Cyclic Voltammetric Characterisation of 2:1 $AlCl_3$-TMPAC Melts

A typical cyclic voltammogram of the 2:1 mole ratio $AlCl_3$-TMPAC melt is shown in **Fig. 3.1.1**. Similar to that of the 2:1 $AlCl_3$-MEIC melt [172], an electrochemical window of about 2.5 V vs. Al reference electrode was observed. The residual current density in the window was found to be less than 1 mA cm^{-2}, showing that the melt was virtually pure. The negative and positive limits were the deposition of aluminium and the evolution of chlorine, respectively. Chlorine gas corresponding to the decomposition of the melt was observed evolving on the electrodes at 2.5 V. The cathodic peak **A** started at roughly -0.18 V and it was attributed to the deposition of aluminium. The anodic peak **A′** at 0.02 V corresponded to the stripping of the aluminium deposit. This behaviour was essentially the same as that observed by Robinson and Osteryoung in the $AlCl_3$-BPC system [173]. As can be seen, there was a small prepeak, **B**, positive of the main deposition process and a corresponding stripping peak **B′**. The nature of these peaks will be discussed later.

A characteristic "current loop" or "nucleation loop" [121, 174] (a region where the current on the reverse sweep is higher than on the forward sweep) was observed. This loop occurred because the deposition of aluminium on the tungsten electrode during the negative scan required a considerable overpotential in order to

initiate the nucleation and subsequent growth of an aluminium deposit. When the scan was reversed, the reduction current continued to flow because the deposition of aluminium continued on existing aluminium nuclei rather than on a bare tungsten electrode. This was evidence of phase formation by a nucleation and growth mechanism.

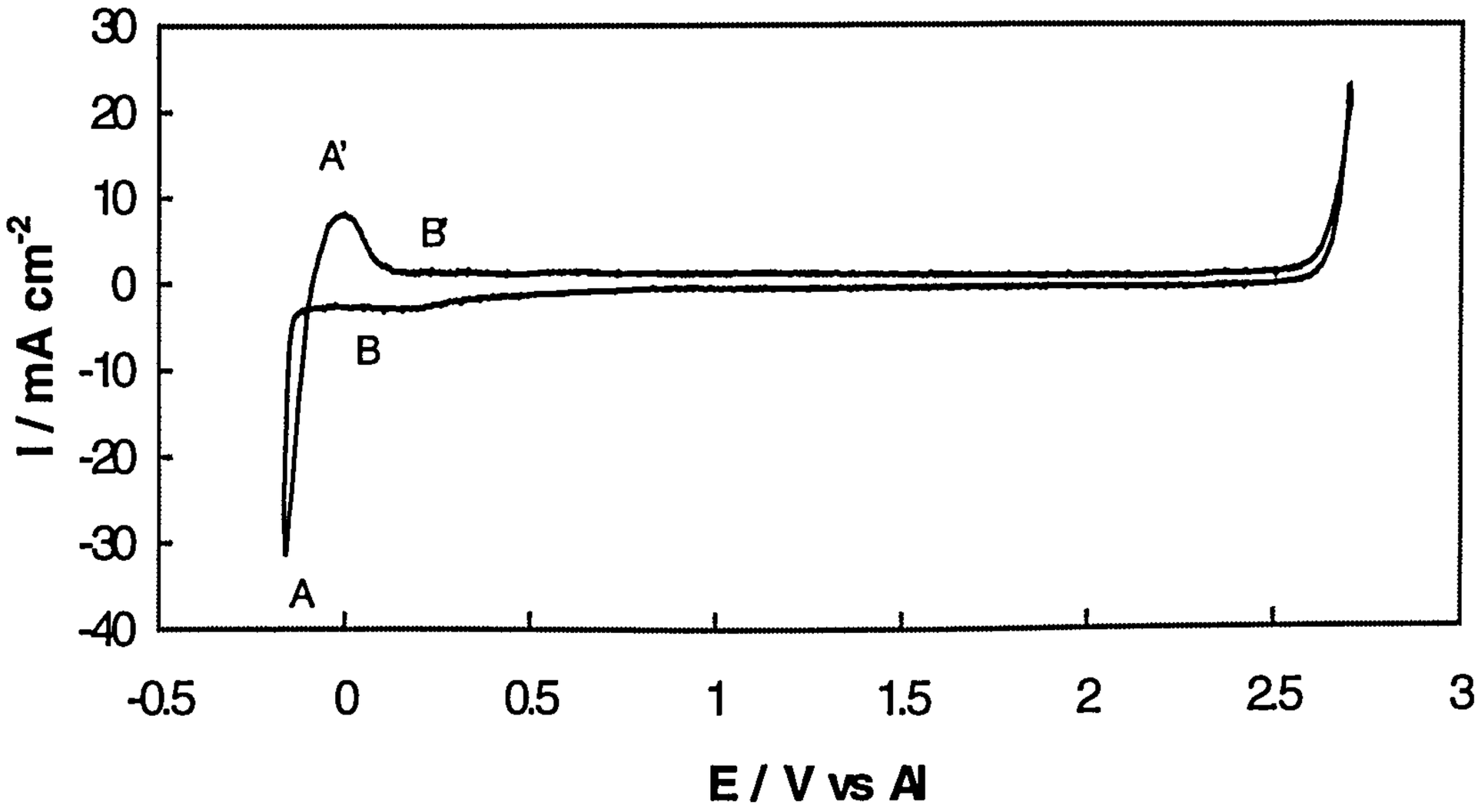

Fig. 3.1.1. Cyclic voltammogram of 2:1 $AlCl_3$-TMPAC melt on tungsten at 25°C. Sweep rate: 0.10 V s^{-1}.

3.1.2 Bulk Electrodeposition of Aluminium

Voltammograms at various scan rates for deposition and stripping of aluminium on the tungsten electrode are shown in **Fig. 3.1.2**. The analysis of the voltammograms is summarised in **Table 3.1.1**. The differences $|E_{p,c} - E_{p,a}|$ ($E_{p,c}$ and $E_{p,a}$ are the cathodic and the anodic peak potentials, respectively) were considerably larger than expected (0.02 V) for reversible processes, and $E_{p,c}$ shifted negatively with increasing scan rates. This suggested that the process was quasi-reversible. The dependence of I_p *vs.* $\upsilon^{1/2}$ was linear ($I_p \upsilon^{-1/2}$ was independent of υ) at low scan rates (< 0.5 V s^{-1}), indicating that deposition and stripping

processes were diffusion controlled. The deviation from the linearity at higher scan rates was attributed to kinetic limitations brought about by the nucleation phenomena in the deposition process.

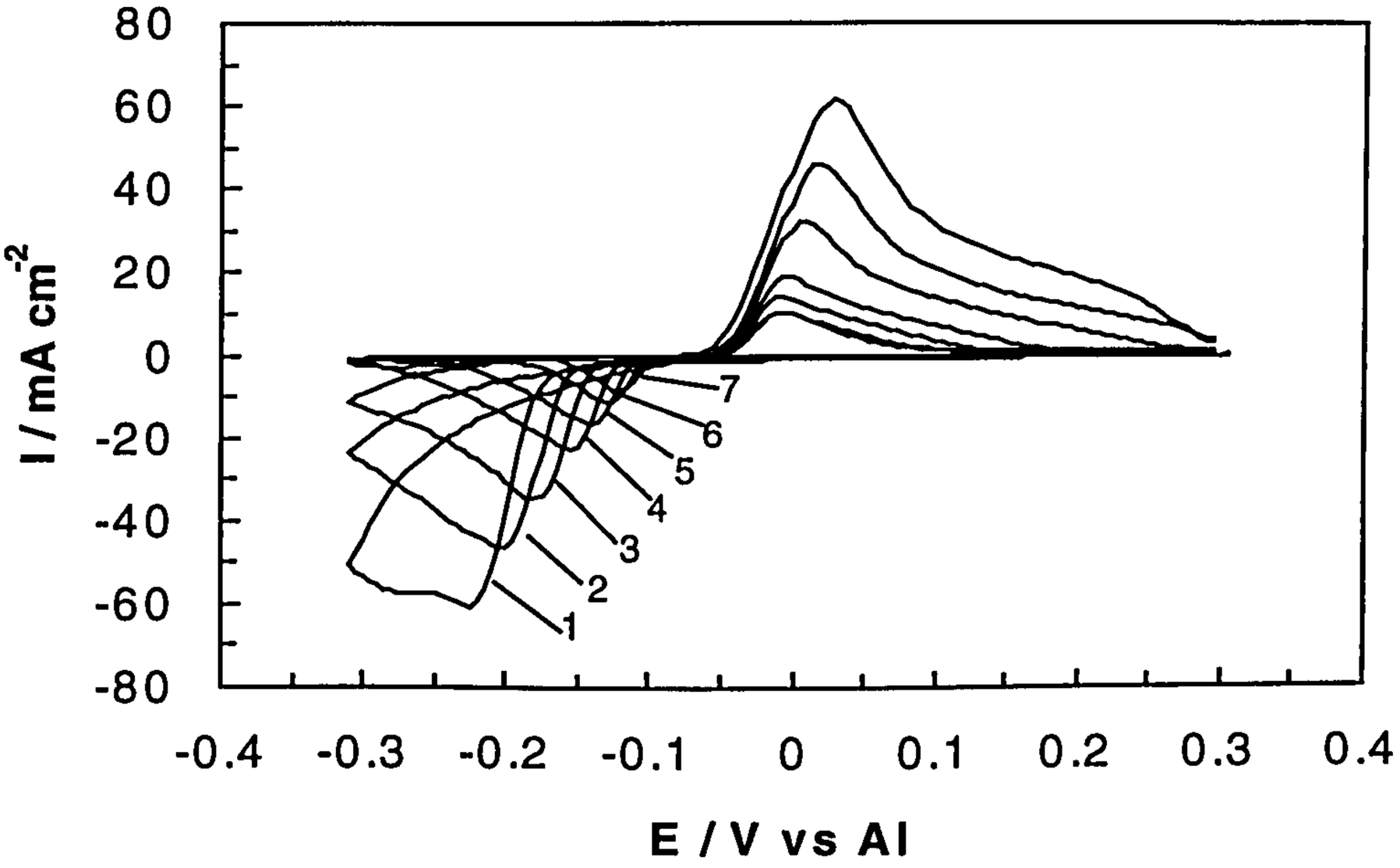

Fig. 3.1.2. Voltammograms for deposition and stripping of aluminium on tungsten from 2:1 $AlCl_3$-TMPAC melt at 25°C. Sweep rates: (V s^{-1}): (1) 1.0; (2) 0.5; (3) 0.25; (4) 0.10; (5) 0.05; (6) 0.02.

Table 3.1.1 Voltammetric data for aluminium deposition on tungsten from 2:1 $AlCl_3$-TMPAC melts

υ (V s^{-1})	$I_{p,c}$ (mA cm^{-2})	$I_{p,c}\,\upsilon^{-1/2}$ (mA cm^{-2} $V^{-1/2}$ $s^{1/2}$)	$I_{p,a}/I_{p,c}$	$E_{p,c}$ (V)	$\lvert E_{p,c} - E_{p,a}\rvert$ (V)	$\lvert E_{p/2,c} - E_{p,c}\rvert$ (V)
0.01	-7.80	77.96	1.23	-0.120	0.114	0.015
0.02	-11.24	79.48	0.90	-0.130	0.125	0.020
0.05	-16.49	73.75	0.85	-0.140	0.135	0.020
0.10	-22.98	72.68	0.81	-0.155	0.155	0.020
0.20	-34.95	78.16	0.92	-0.180	0.190	0.025
0.50	-46.15	65.27	0.99	-0.205	0.220	0.030
1.00	-60.58	60.58	1.01	-0.225	0.255	0.030

Considering the quasi-reversibility of the processes, the average value of the cathodic transfer coefficient α was estimated as 0.45, by the following formula [175]:

$$|E_p - E_{p/2}| = \frac{47.7}{\alpha n_a} \text{ mV} \quad (25°) \qquad (3.1.1)$$

where, n_a is the charge number for the reaction and $E_{p/2}$ is the half peak potential. An estimate of the diffusion coefficient of $Al_2Cl_7^-$ ions was obtained using a simplified treatment for reversible deposition of a metal/metal ion electrode [176]:

$$I_p = 6.33 \times 10^5 T^{1/2} n^{3/2} \upsilon^{1/2} D^{1/2} c \qquad (3.1.2)$$

where c and D the concentration and the diffusion coefficient of $Al_2Cl_7^-$ ions, respectively.

Table 3.1.2 Stokes-Einstein values for $Al_2Cl_7^-$ in ambient temperature $AlCl_3$ + MCl molten salts

MCl	$[Al_2Cl_7^-]$ (M)	T (°C)	η (cp)	$10^7 D$ $cm^2\ s^{-1}$	$10^{10} D\eta/T$ (g cm s^{-2} K^{-1})	Ref.
TMPAC	3.09	25	36.2**	2.17	2.6	this work
TMPAC*	0.16	25	-	10.30	~	[133]
MEIC	0.445	40	11.7	3.95	1.5	[123]
BPC	0.27	40	20.9	2.10	1.4	[121]
BPC	0.156	60	13.0	4.26	1.7	[122]

* $AlCl_3$ + TMPAC diluted with 80% volume of 1,2-DCB.

** Ref. [133].

Based upon **Eqn. 3.1.2** and the slope of $I_p \sim \upsilon^{1/2}$ plots, the average value of the diffusion coefficient, D, of $Al_2Cl_7^-$ ions was calculated assuming that the deposition peak corresponded to the reversible formation of an insoluble product

and that the tru surface area of the electrodes corresponded to their geometric areas [176,177]. **Table 3.1.2** shows viscosities, D coefficients, and the Stokes-Einstein products, $D\eta/T$, of several ambient temperature molten salts with different temperatures and compositions. $D\eta/T$ here is related to the Stokes-Einstein equation [178]:

$$D = \frac{kT}{6\pi\eta r} \tag{3.1.3}$$

where k is Boltzmann's constant and r is the radius of the diffusing species. Since the viscosities of these melts vary with temperature and melt composition [128,132,134,179], the comparison of D values for $Al_2Cl_7^-$ ions in melts under different conditions was replaced by the comparison of $D\eta/T$ values. The $D\eta/T$ value of 2.6×10^{-10} g cm s^{-2} K^{-1} in the present melt was close to the $D\eta/T$ values in $AlCl_3$-BPC and $AlCl_3$-MEIC melts, although the viscosity of the 2:1 $AlCl_3$-TMPAC melt was much higher than those of $AlCl_3$-BPC and $AlCl_3$-MEIC melts.

3.1.3 Coulombic Efficiencies

The coulombic efficiency (ratio of the stripping charge Q_a to the deposition charge Q_c) was investigated by integrating the current corresponding to the reduction and oxidation portions of the sequential cyclic voltammograms shown in **Fig. 3.1.2**. These results, whose average value was 93.5%, showed good reversibility of deposition and stripping of aluminium (**Fig. 3.1.3**).

However, the fact that the coulombic efficiencies were less than 100% suggested a loss of charge. **Fig. 3.1.4** shows the dependence of the coulombic efficiency with the cathodic peak current density at different scan rates. The coulombic efficiency initially increased with current density but decreased slightly at higher current densities. The fact that the coulombic efficiency decreased when the current density was lower could be due to several possibilities.

BIBL. LONDIN. UNIV.

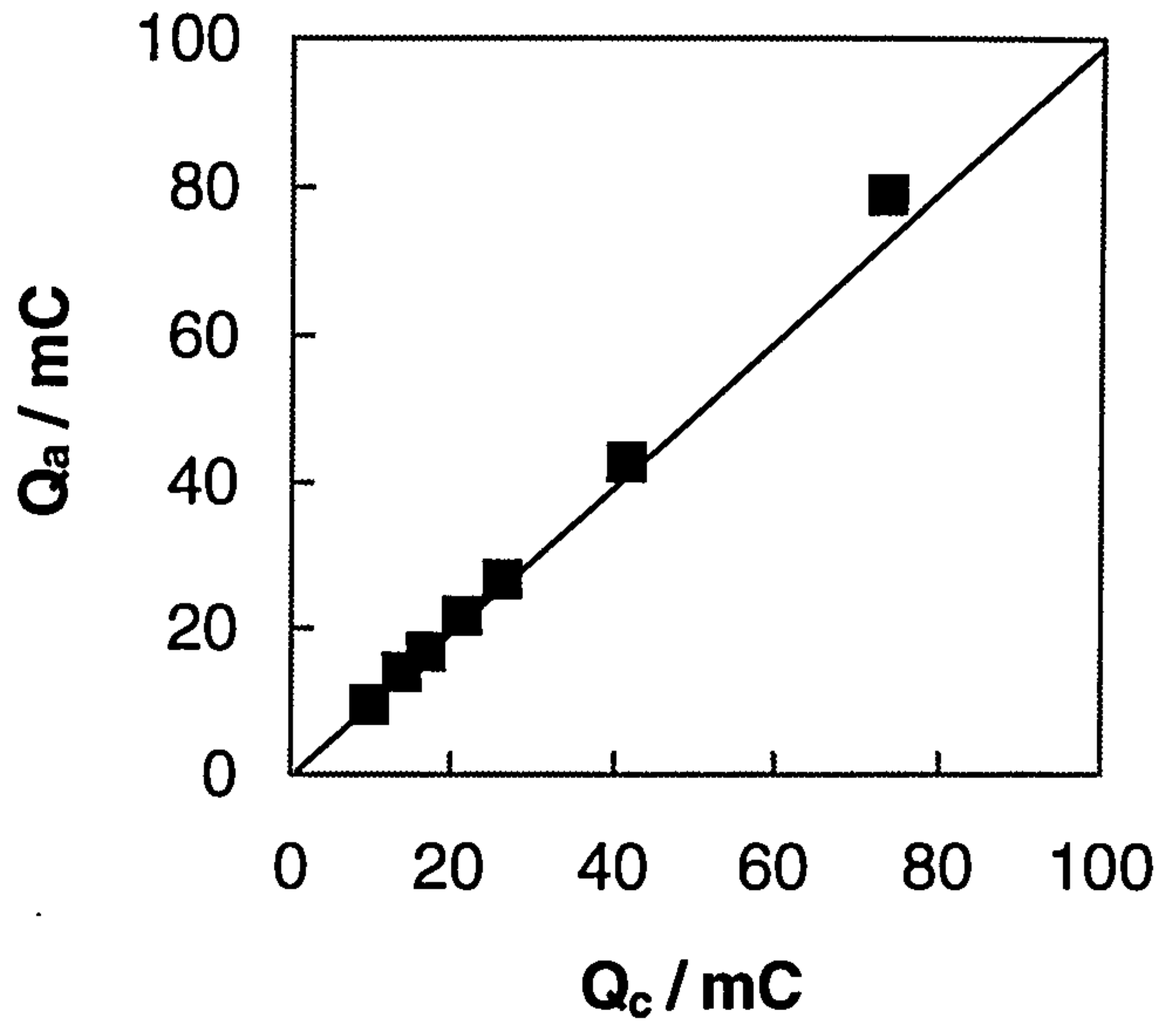

Fig. 3.1.3. Plot of aluminium deposition charge *vs.* stripping charge constructed from voltammograms shown in **Fig. 3.1.2.** The solid line denotes a coulombic efficiency of 100%.

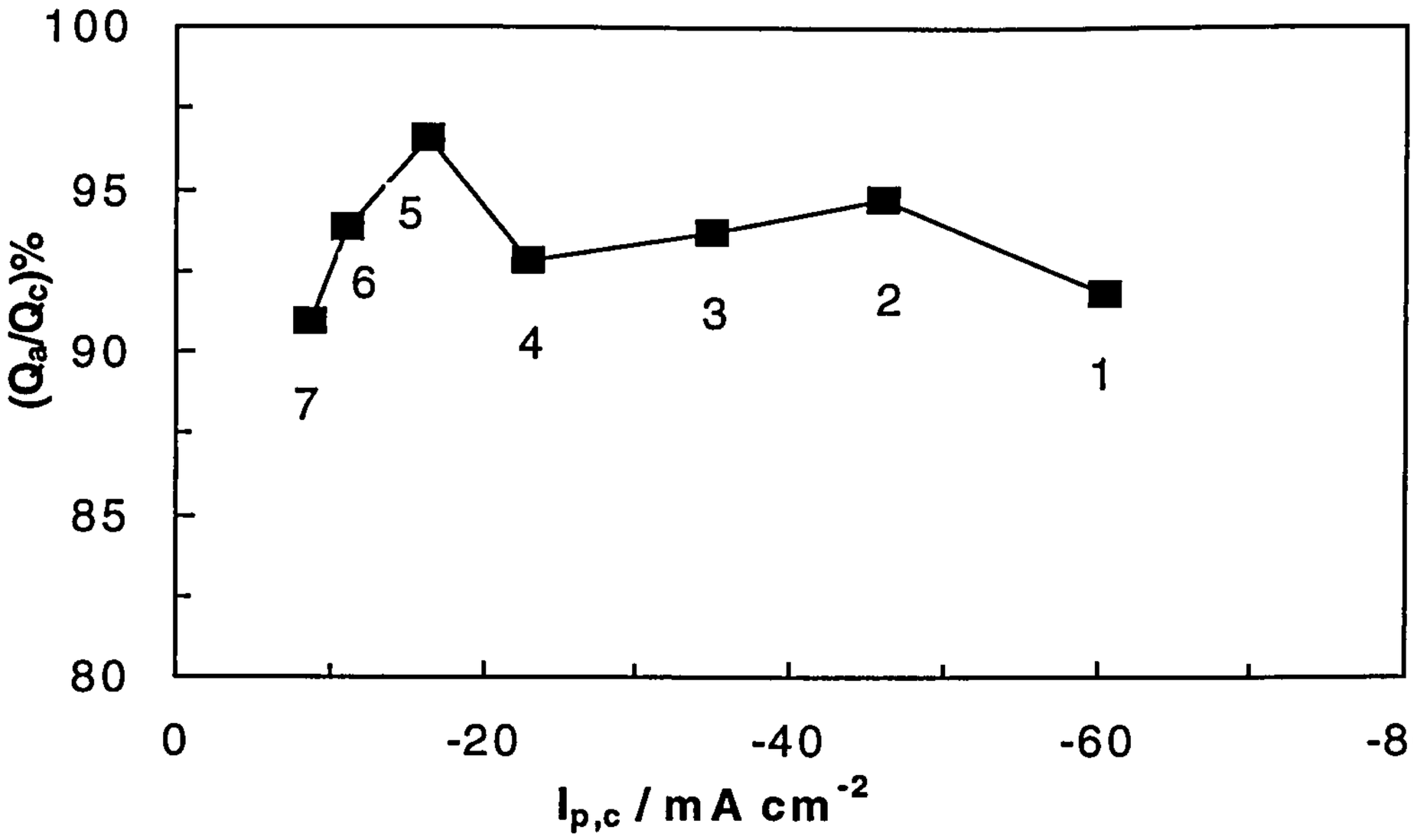

Fig. 3.1.4 . The coulombic efficiency of aluminium plating and stripping on tungsten as a function of the cathodic peak current density at 25°C. Sweep rate (V s^{-1}): (1) 0.01; (2) 0.02; (3) 0.10; (4) 0.25; (5) 0.05; (6) 0.5; (7) 1.0.

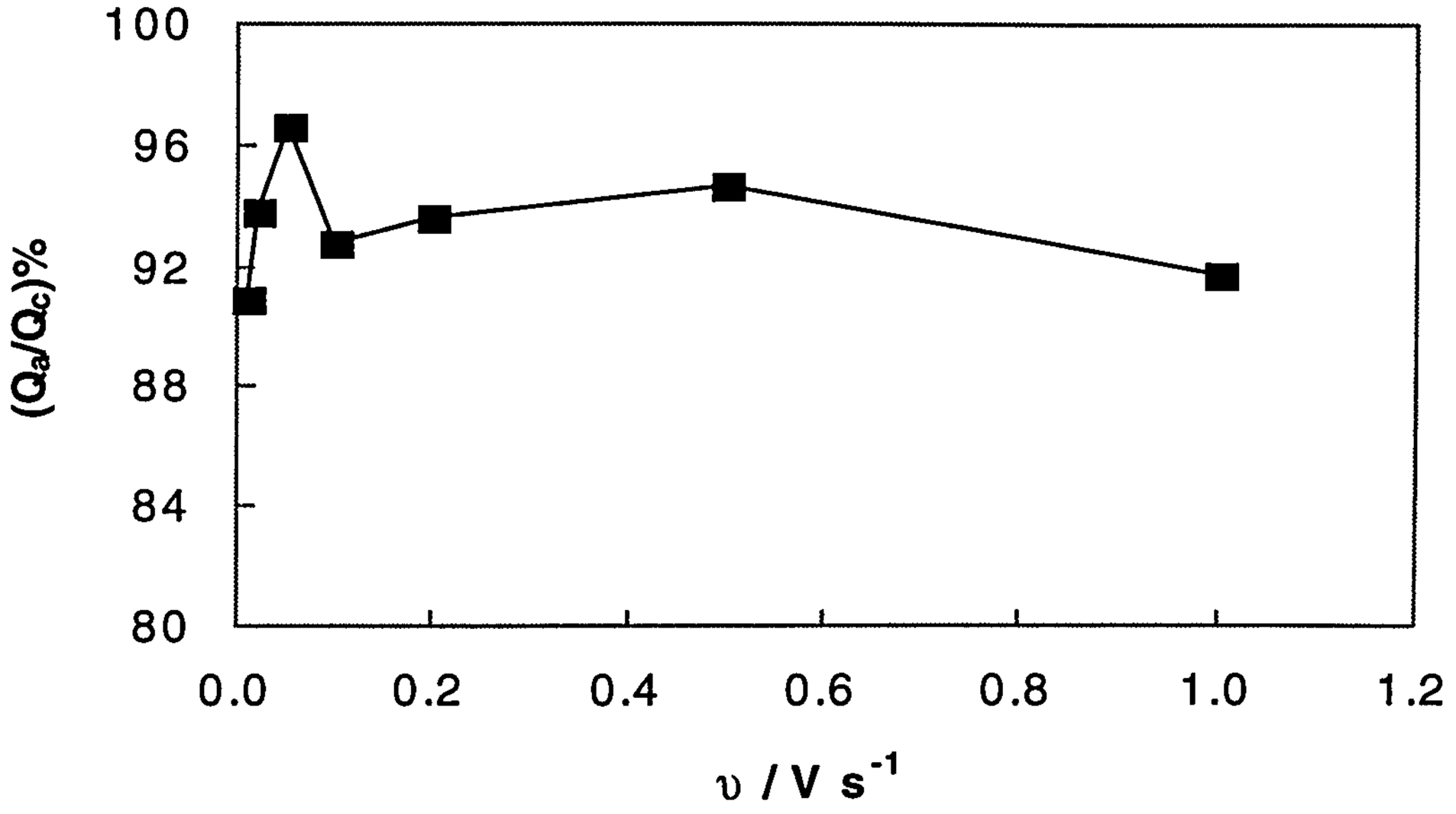

Fig. 3.1.5 . The coulombic efficiency of aluminium plating and stripping on tungsten as a function of sweep rate at 25°C.

One possibility is that a chemical corrosion reaction occurred between the deposited aluminium and the melt or its impurities as already reported for other molten salt systems $AlCl_3$ + BPC [180], $AlCl_3$ + NaCl [181], and $AlCl_3$ + LiCl + $DMSO_2$ [65]. The consequence of the reported corrosion reaction was a loss of coulombic efficiency. So, the greater the corrosion, the lower the coulombic efficiency. Since slow scan rates correspond to longer exposure times, and corrosion would be proportional to the time, greater corrosion would occur at lower scan rates (**Fig. 3.1.5**).

Another possibility may be the reduction of some electroactive impurities (one of these was probably H_2O), which occurs before the deposition of aluminium [65], until their depletion in diffusion layer. The charge Q_{imp} necessary for reducing these impurities in the diffusion layer would increase with a fall in the current density (slower sweep rates).

The third possibility results from the features of room-temperature organic melts. In the high temperature inorganic $AlCl_3$-MCl systems, *e.g.*, $AlCl_3$-NaCl melt, aluminium deposition occurred from the reduction of both $AlCl_4^-$ and $Al_2Cl_7^-$

ions [181], and therefore if the $Al_2Cl_7^-$ ion concentration dropped below that required for the applied potentials or current densities then the deposition from $AlCl_4^-$ ions would also occur. 100% coulombic efficiencies were therefore observed for all melt compositions. In the acidic organic melts $AlCl_3$-R^+Cl^- (where R^+ are BP^+, MEI^+ or $TMPA^+$ ions) the next most readily reduced species after the $Al_2Cl_7^-$ ions were the R^+ cations. In aluminium deposition from $AlCl_3$-BPC melts, if the $Al_2Cl_7^-$ ion concentration dropped below that required for the applied current densities, reduction of the BP^+ cations occurred and the plating efficiency dropped below 100% hence resulting in the apparently low stripping percentages [121].

A fourth possibility was an alloying effect which has been reported in some high temperature inorganic melts [182, 183]. In those melts it was confirmed that alloying was taking place and that a solid solution was formed. It has been found that tungsten alloyed with aluminium to form both intermetallic compounds and solid solutions [184]. The amount of metal stripped from the solid solution during the anodic process was less than that in forming the solid solution during the cathodic process, because of the low diffusion rates in the alloy.

In the present work, the poor adhesion of aluminium deposits to tungsten substrate was observed. This could be an important reason for the low coulombic efficiency. It was observed that during deposition and stripping on glassy carbon substrate in $AlCl_3$-NaCl melt [185], some aluminium deposits fell off into the melt, showing poor adherence to the electrode.

Since the decrease in coulombic efficiency with decreasing current density also happened on the non-metallic glassy carbon electrode (see **Chapter 4**) and with stirring, the contributions from alloying and the reduction of $AlCl_4^-$ ions were excluded. The influence of impurities should also be small because the melts were very pure as shown by the very small residual currents. Thus, the corrosion reaction between fresh aluminium deposits and the melts, and the poor adhesion of the deposits to the tungsten substrate were probably the main reasons for the decrease in the coulombic efficiency at lower current densities.

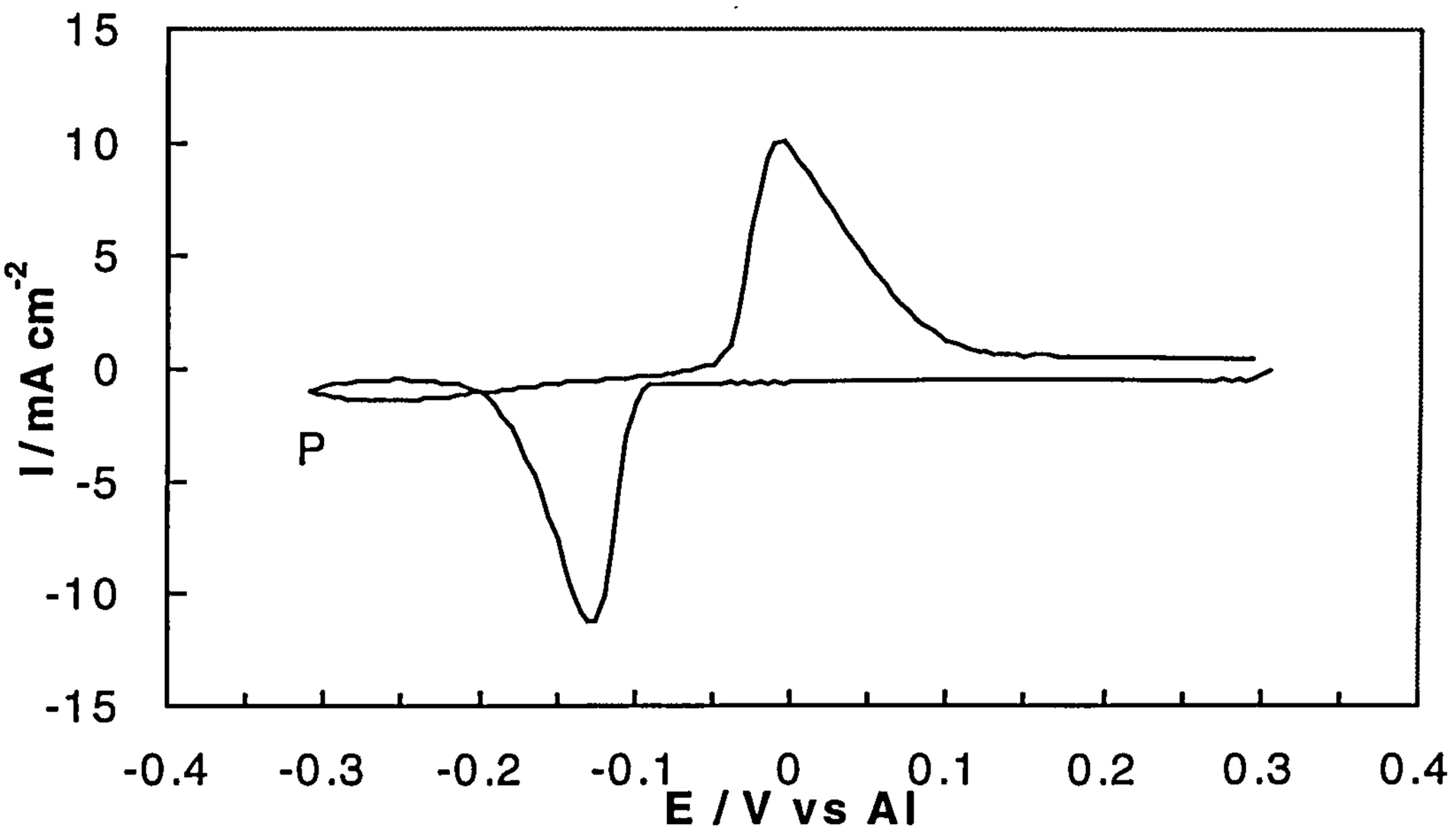

Fig. 3.1.6. Cyclic voltammogram of 2:1 $AlCl_3$-TMPAC melt on tungsten at 25°C. Sweep rate: 0.01 V s^{-1}.

3.1.4 Passivation of the Electrodes

After long storage time or at low sweep rates (< 50 mV s^{-1}), a current loop (**P**) starting around -0.3 V at low sweep rates was observed (**Fig. 3.1.6**), following the bulk deposition of aluminium, whereas the first current loop was seen at -0.1 V (**Fig. 3.1.1**). The current loop **P** became bigger when potentials increased more negatively, and a corresponding anodic prepeak (**P′**) occurred at -0.1 V (**Fig. 3.1.7**). Both peak currents increased as deposition potentials shifted negatively.

It was unclear what caused the prepeaks, but they probably resulted from the decomposition of the melt, *i.e.* the reduction of $TMPA^+$ or $AlCl_4^-$ ions. Basically, the $AlCl_4^-$ ion concentration was very low in the acidic melt as mentioned before. However, in quiescent melts the concentration of $Al_2Cl_7^-$ ions near the electrode surface would decrease with the more negative deposition potentials and the acidity of the melt would be changed locally, resulting in larger the concentration of the $AlCl_4^-$ ions. Thus, variation of $AlCl_4^-$ activity might affect

the shape of the voltammograms, especially at more negative deposition potentials. Besides the reduction of the $Al_2Cl_7^-$ ions, the W-Al alloying effect might cause the prepeaks, especially at very low sweep rates or very negative deposition potentials. To better understand the prepeaks, further spectroscopic experiments, such as NMR, IR, X-ray diffraction would be required for characterising the structure of the melt.

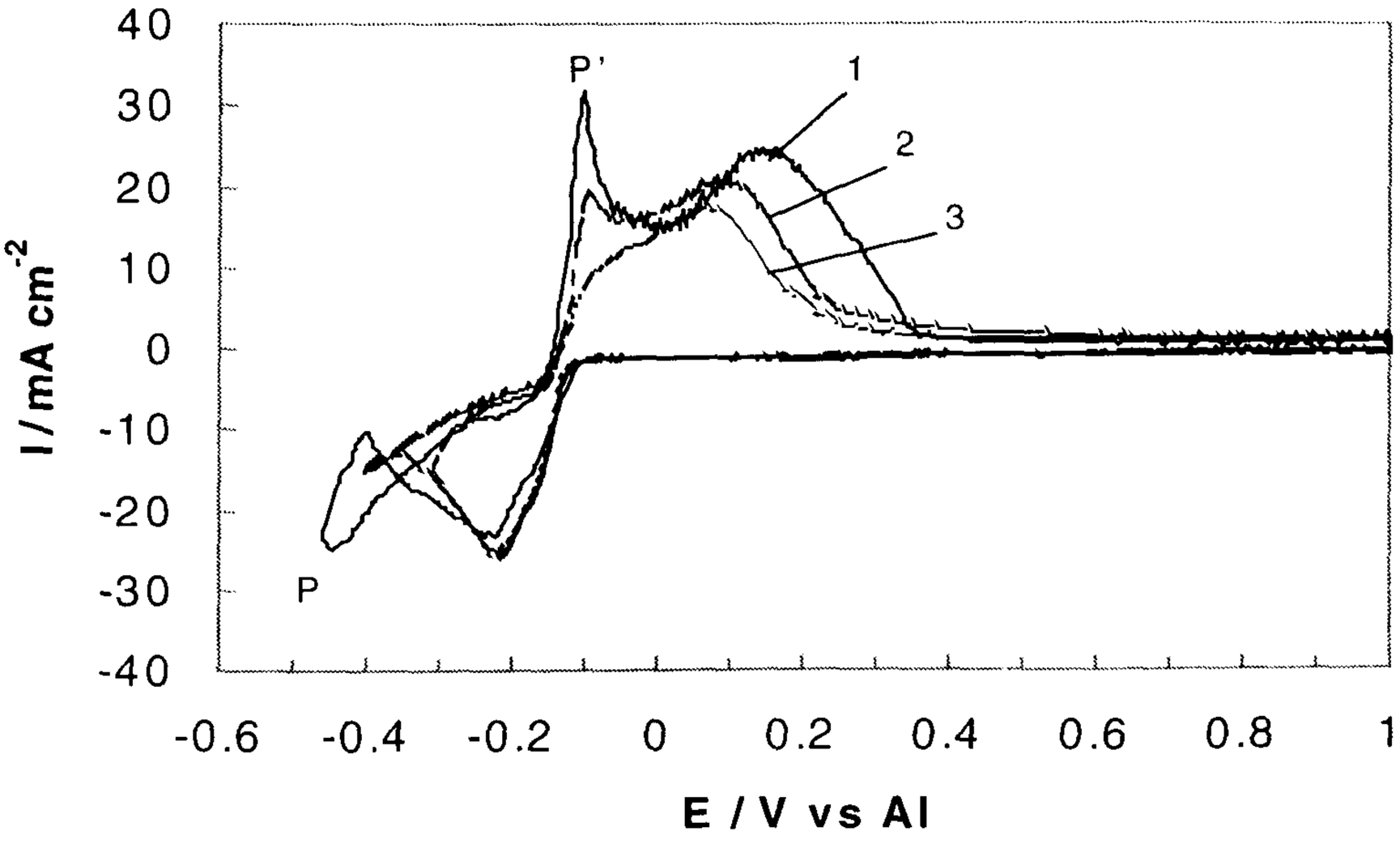

Fig. 3.1.7. Cyclic voltammograms of 2:1 $AlCl_3$-TMPAC melt on tungsten at 25°C. Sweep rate: 0.10 V s^{-1}. Switching potentials: (1). -0.5 V; (2). -0.4 V; (3). -0.3 V.

Coinciding with the occurrence of the peaks **P** and **P'**, black dense adherent layer was found either on both cathode and anode. Also, a passivation phenomenon was observed with a resultant sudden decrease in the anodic current after long storage times (**Fig. 3.1.8**). This passivation was attributed to the formation of an insoluble, poorly conducting layer of $AlCl_3$ on the electrode surface, which could result from the reaction between aluminium and Cl^- ions in the melt. The result was agreed with that from the $AlCl_3$-MEIC melt [**186**], in which the thickness and/or of

the compactness of this passivating layer were found to consequently grow as the storage time increased.

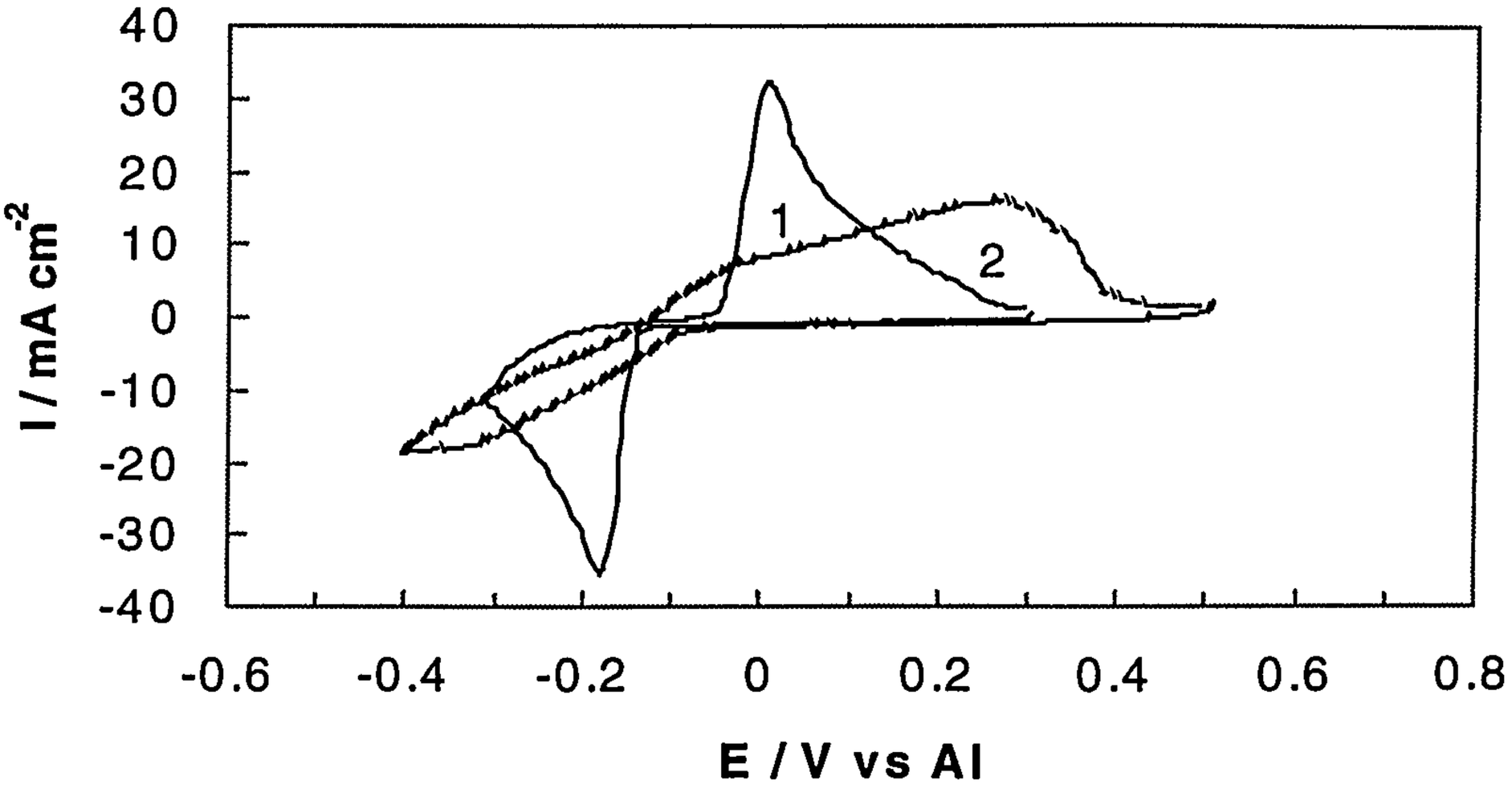

Fig. 3.1.8. Cyclic voltammograms of 2:1 $AlCl_3$-TMPAC melt on tungsten at 25°C. Sweep rate: 0.10 V s^{-1}. Storage time: (1) 5 h and (2) 5 days.

3.1.5 Underpotential Deposition (UPD)

In order to characterise the prepeaks **B** and **B′** in **Fig. 3.1.1**, higher sweep rates were used. A close examination of the 1 V s^{-1} voltammogram in **Fig. 3.1.9** revealed two distinct cathodic peaks: one, at 0.1 V (**A**) and the otherat 1.8 V (**B**). Like that observed in the $AlCl_3$-BPC system [121], peak **A** was attributed to the underpotential deposition (UPD) of aluminium, that is, the deposition at potentials (at 0.1 V) positive of the bulk deposition. The term UPD is usually invoked to describe the deposition of submonolayer quantities of metal onto a foreign metallic substrate where the deposited species has an activity less than unity. The anodic peak **A′** therefore corresponded to the stripping of the UPD layer. The peaks **B** and

B′ which were only visible at very high sweep rates, implying a low concentration, may have been due to impurities in the melts.

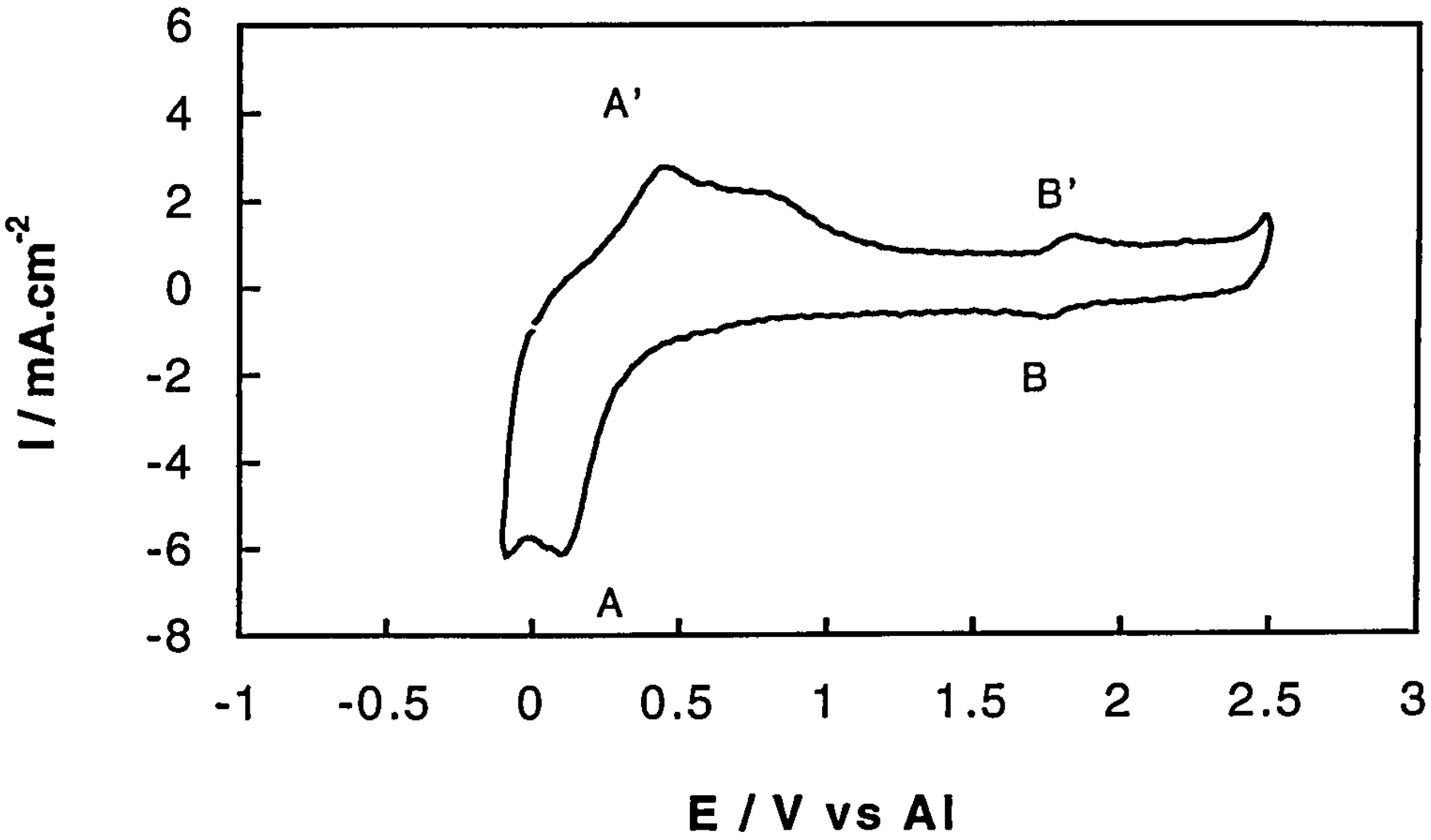

Fig. 3.1.9. Cyclic voltammogram on tungsten in 2:1 $AlCl_3$-TMPAC melt at 25°C. Sweep rate: 1.0 V s^{-1}.

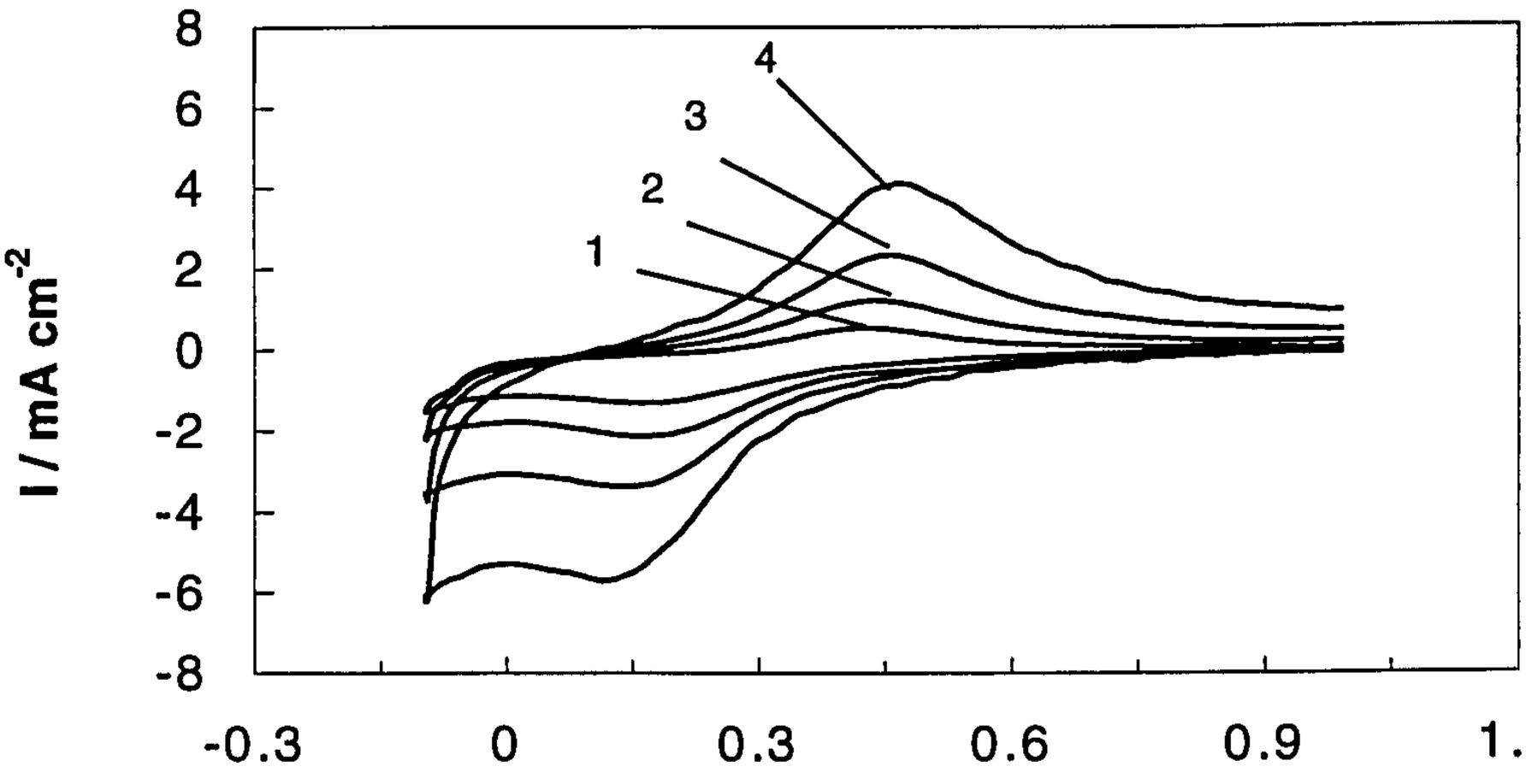

Fig. 3.1.10. Voltammograms revealing underpotential deposition and stripping of aluminium on tungsten in 2:1 $AlCl_3$-TMPAC melt at 25°C. Sweep rates (V s^{-1}) were: (1) 0.1; (2) 0.25; (3) 0.5; (4) 1.0.

The sequence of aluminium UPD preceding bulk deposition is clearly shown in **Fig. 3.1.10**. It should be pointed out that in all voltammograms in this thesis related to UPD the constant background currents were subtracted off. Since the background current was very small (about 1 mA cm^2), the correction affected only UPD currents but not bulk deposition currents. Thus, the sweeps in **Fig. 3.1.10** are net currents. The corresponding stripping peaks were apparent on the reverse scan. The charges under both the UPD peaks and the corresponding stripping peaks are collected in **Table 3.1.3**. Since a monolayer of aluminium (r = 1.43 nm) with the density of bulk aluminium corresponds to a charge of 0.68 mC cm^{-2} **[121]**, the UPD process on tungsten corresponds to about 3.4 ~ 6.4 monolayer equivalents. These values were calculated assuming the electrode to be perfectly smooth and flat. Any roughness would reduce the calculated thickness. It therefore appears that a surface phase was formed which consisted either of a few monolayers of aluminium or alternatively a thicker deposit of a compound containing partially reduced aluminium species. This latter possibility seems highly unlikely.

Table 3.1.3 Cumulative charges for the UPD and the corresponding stripping of aluminium on tungsten

v (V s^{-1})	Q_a (mC cm^{-2})	Q_c (mC cm^{-2})	Q_a/Q_c%
0.10	4.36	3.52	80.0
0.20	3.24	2.53	78.0
0.50	3.08	2.40	78.0
1.00	2.34	1.81	77.0

It should be noted that the number of the monolayers was higher than those in reported previous investigations **[177,136,187]**. It may result from the possibility that the electrochemically active area was greater than the geometric area as a result of roughening of the electrode by the electrochemical cleaning process **[128]**, where the tungsten surface was cleaned by evolution of substantial quantities of chlorine gas with consequent removal of oxide impurities adsorbed from the melts. The

peak current densities of the UPD peaks were proportional to υ (**Fig. 3.1.11**) in agreement with the results observed in $AlCl_3$-BPC melts [121] and $AlCl_3$-NaCl system [188]. The $I_{p,c}$ *vs.* υ plot was linear, as expected for a reversible surface constrained process. Also, the plot did not pass through the origin, proving that the UPD process was not diffusion controlled. It should be pointed out that the linear $I_{p,c}$ *vs.* υ dependence was obtained from the curves corrected for the background currents. Without the correction for the background currents only linear $I_{p,c}$ *vs.* $\upsilon^{1/2}$ plots were obtained. Such a result was found by Chryssoulakis et al. [187] who had no explanation as to how such UPD processes could be diffusion controlled. In practice, the diffusion controlled condition should not occur until the surface concentration of $Al_2Cl_7^-$ ions near the electrode was exhausted.

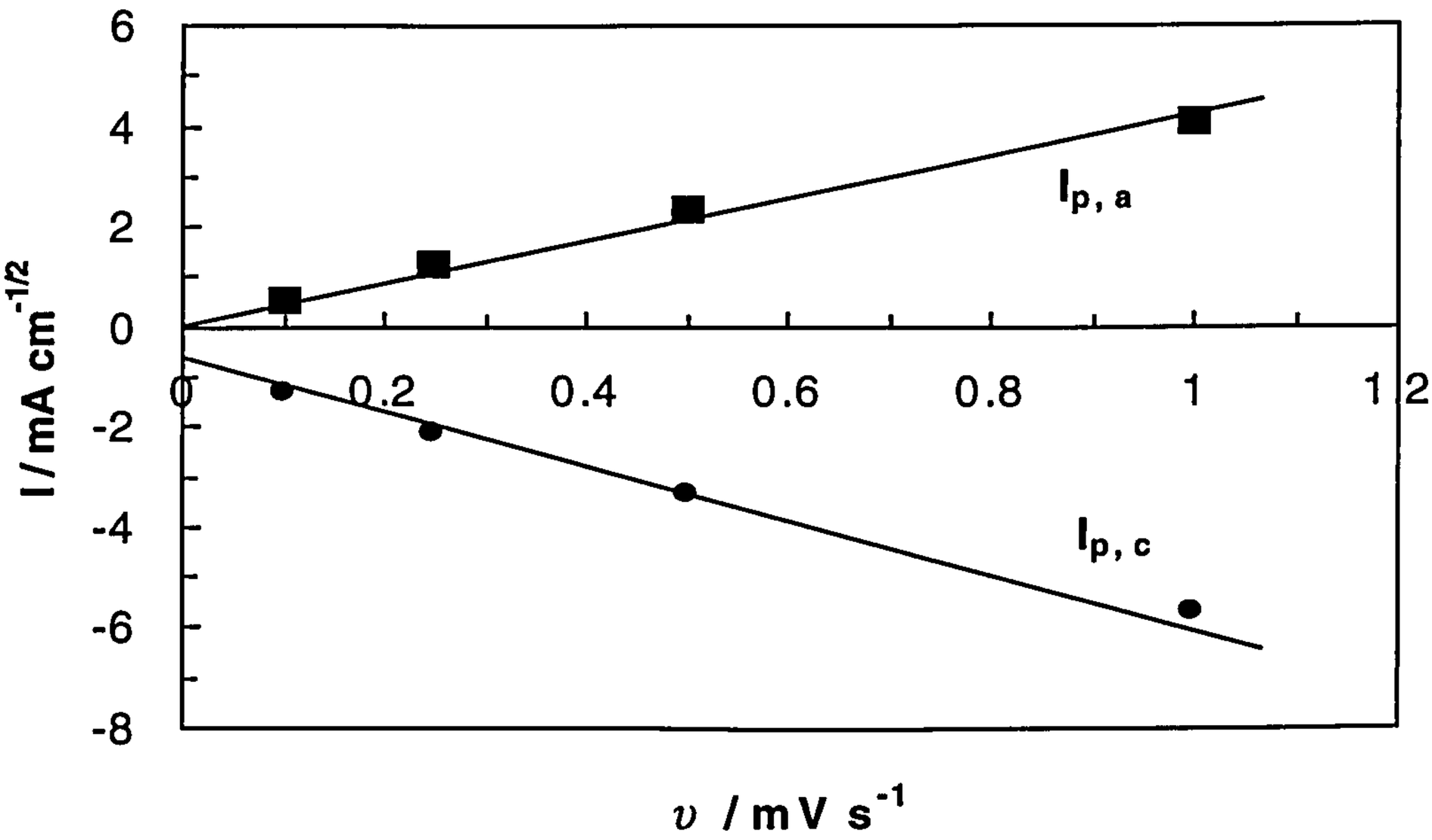

Fig. 3.1.11. Plot of cathodic and anodic peak currents vs. sweep rate for aluminium UPD on tungsten in 2:1 $AlCl_3$-TMPAC melt at 25°C.

According to **Table 3.1.3**, the coulombic efficiencies were about 78%, suggesting the apparent retention of a small portion of the underpotential deposition aluminium. The charges of the UPD increased with decreasing scan

rates, implying an effect of time in the process. There is no clear explanation for this behaviour at present.

3.1.6 Nucleation Analysis

In contrast to the voltammetric method, a well-developed quantitative formalism exists for analysing phase formation under conditions of constant overpotential, or supersaturation. Thus, chronoamperometry was chosen to examine the deposition kinetics of aluminium in more detail.

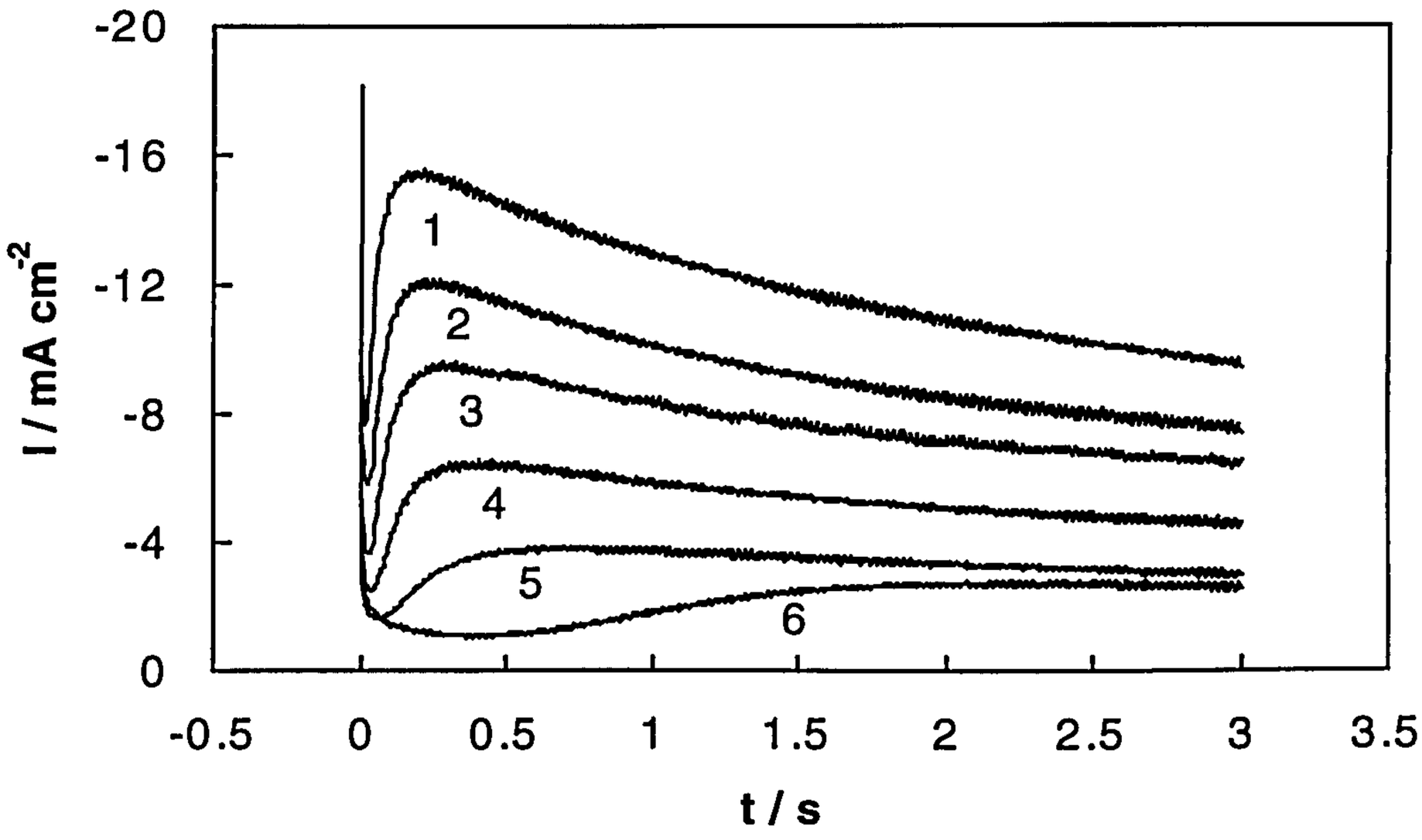

Fig. 3.1.12. A series of potentiostatic current transients for aluminium deposition on tungsten in 2:1 $AlCl_3$-TMPAC melt at 25°C. Applied potentials (V) were: (1) -0.19; (2) -0.18; (3) -0.17; (4) -0.16; (5) -0.15; (6) -0.14.

Representative current transients are shown in **Fig. 3.1.12.** These experiments were performed in quiescent solutions by the double potential step technique, where the potential was stepped from an initial value of 0.0 V, the rest potential, to potentials sufficiently negative to initiate the nucleation process, and finally back 0.0 V. For the time scale examined, the nucleation/growth behaviour of aluminium was first observed at -0.15 V, in agreement with the observation in

the voltammograms. The shape of the current transients was typical of diffusion-limited nucleation and growth of a metal deposit on a foreign metal substrate [189]. The features of these transients can be characterised as follows.

Firstly, the current-time transients exhibited a sharp spike in the current due to charging of the electrode double-layer after the potential step was applied.

Then, a rising current followed almost immediately due to the formation and subsequent growth of aluminium nuclei on the electrode surface. This corresponded to an increase in the electroactive area as independent nuclei grew and/or the number of nuclei increased. During this stage of growth the nuclei developed hemispherical diffusion zones around themselves and as these zones overlapped, hemispherical mass-transfer gave way to linear mass-transfer to what was effectively a planar electrode surface.

Consequently, the current exhibited a broad maximum, I_m, whose position on the time axis, t_m, depended upon the magnitude of the potential step. The maxima in these transients were caused by coalescence of the individual diffusion zones surrounding the growing crystallites [189].

After passing through the maximum, the current decreased with a linear I *vs.* $t^{-1/2}$ relationship (**Fig. 3.1.13**) showing that diffusion control was established after the initial nucleation (**Eqn. 2.2.1**).

From a series of such current transients it was possible to construct sampled voltammograms at some constant time within the diffusion controlled region. A typical one is shown in **Fig. 3.1.14.** The shape of this curve was consistent with the deposition of an insoluble product and a plot of $log[(I_d - I)/I]$ *vs.* E (where I is the current at the potential E and I_d is the diffusion-limited current) was linear (**Fig. 3.1.15**). A value of -0.186 V for the formal electrode potential, E°′ was obtained from the potential axis intercept. In the $AlCl_3$-NaCl melt at 175°C [190], the deposition reaction was found to be perfectly reversible on the basis of the pulse voltammtric data. The quasi-reversibility found in the present system, which is similar to in the $AlCl_3$-BPC melt [121], is probably, in part, due to the lower

temperature of the solvent. At the potentials corresponding to the plateau current, the current showed a linear dependence on $t^{-1/2}$, for pulse times greater than 1 s and less than 20 s, indicating that the process was diffusion controlled.

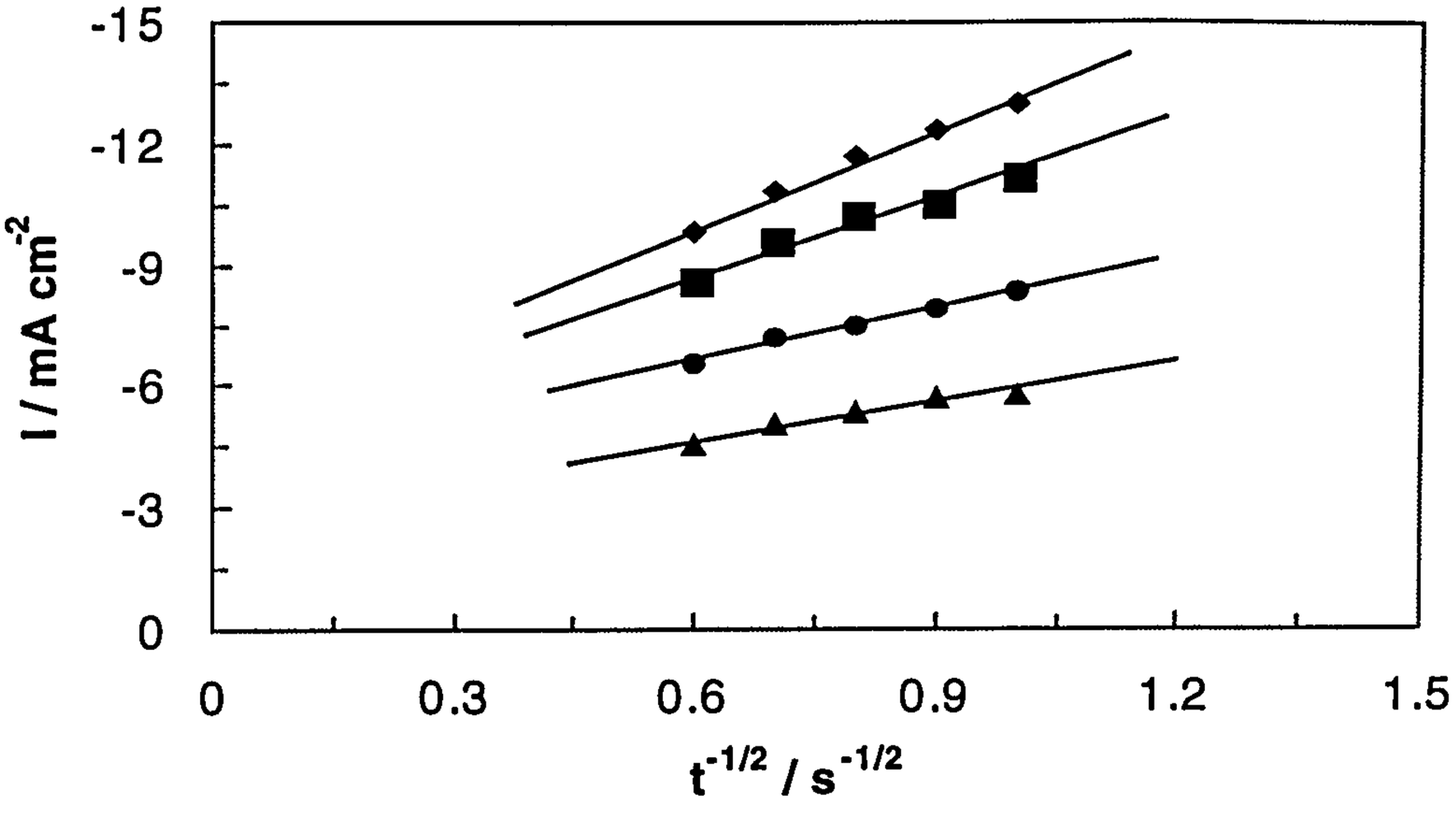

Fig. 3.1.13. Plots of *I vs.* $t^{1/2}$ from current-time transients obtained at (1) -0.18 V; (2) -0.20 V; (3) -0.22 V and (4) -0.24 V.

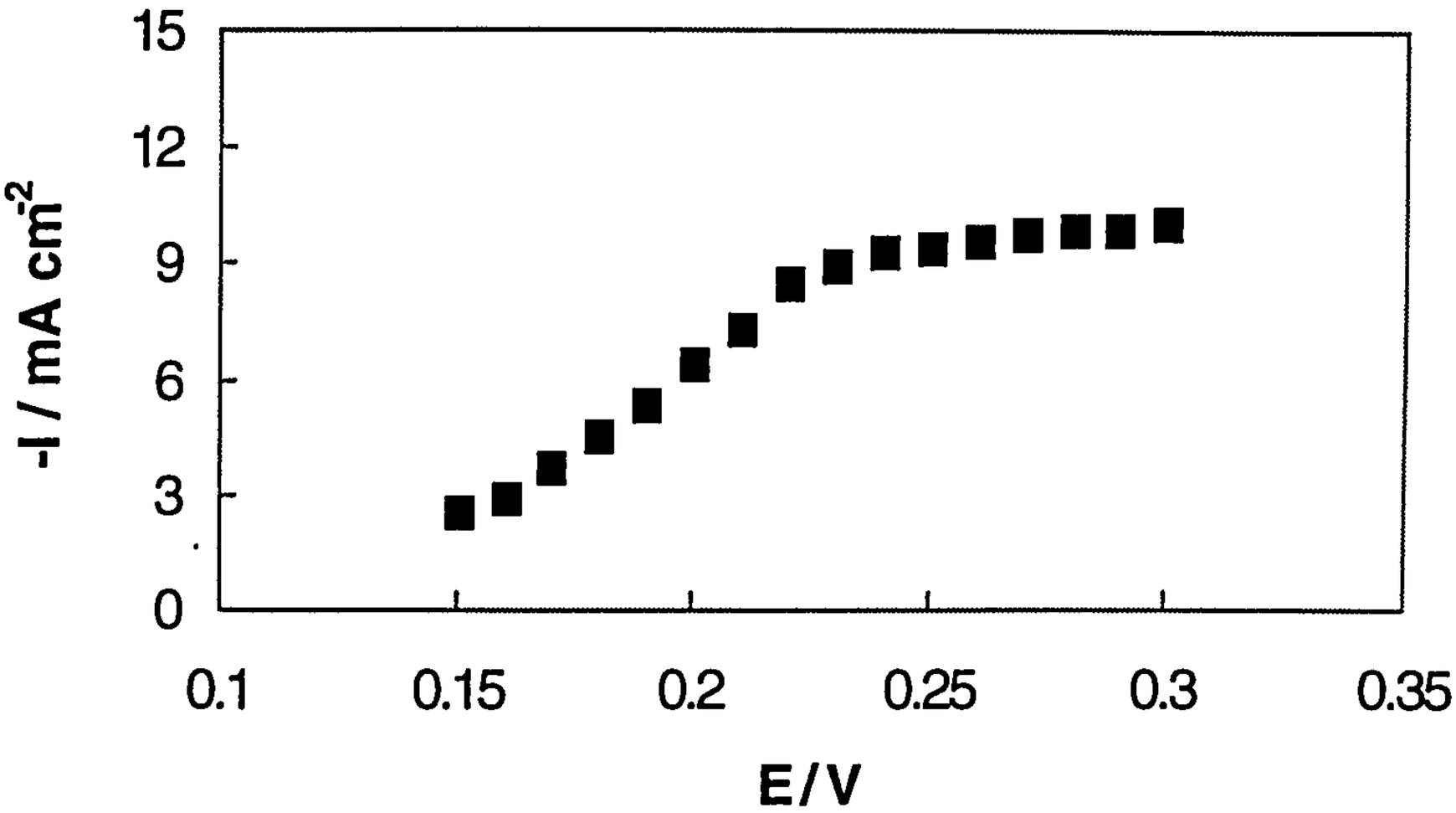

Fig. 3.1.14. Sampled voltammogram constructed from current-time transients shown in **Fig. 3.1.12** sampled at 0.8 s.

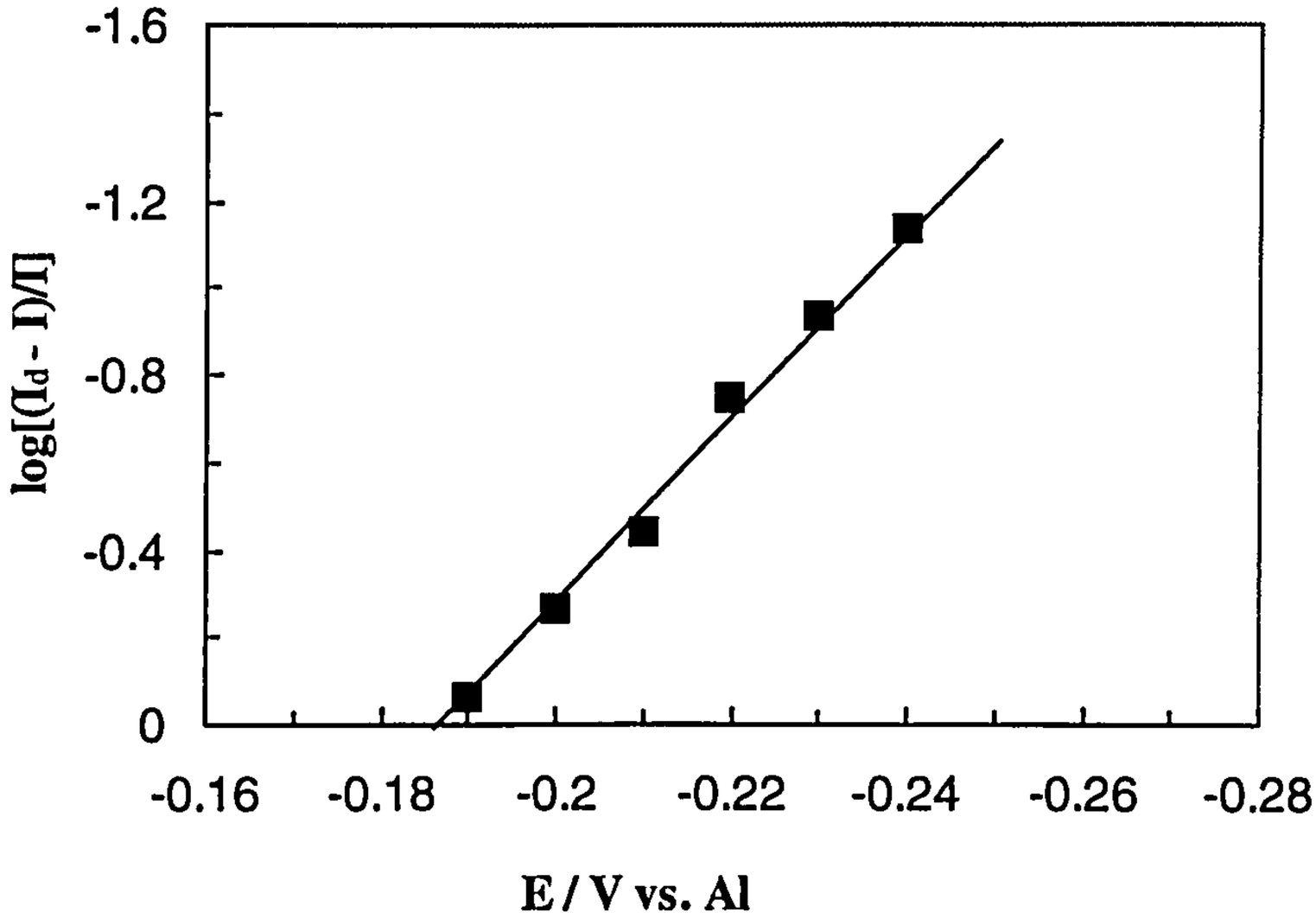

Fig.3.1.15. A Plot of $log\left[(I_d - I)/I\right]$ *vs. E* corresponding to the voltammogram in **Fig. 3.1.14.**

The various models that have been developed to describe the diffusion controlled nucleation and growth processes taking place during bulk metal

deposition were recently summarised [191]. The models involving instantaneous nucleation, (which corresponds to fast nucleation on a small number of active sites such that all sites are immediately converted to nuclei), and progressive nucleation, (which corresponds to slow nucleation on a large number of active sites), with hemispherical diffusion-controlled growth of nuclei [148] have been found to be appropriate for representing metal deposition in most systems. These models may have been relevant in the present case as well. Therefore, the rising portions of typical current-time transients recorded on tungsten electrodes were analysed and compared to these two models.

In the case of instantaneous nucleation, the total current at higher overpotentials is:

$$I(t) = nFN\pi\ M^{1/2}(2Dc)^{3/2}\rho^{-1/2}t^{1/2} \qquad (3.1.4)$$

where N is the number density of active sites, c the bulk concentration of electroactive species, nF the molar charge of the electrodepositing species, M the molecular weight of the deposited metal, and ρ its density. In the case of progressive nucleation:

$$I(t) = \frac{2}{3}nFAN\pi\ M^{1/2}(2Dc)^{3/2}\rho^{-1/2}t^{3/2} \qquad (3.1.5)$$

where A is the nucleation rate constant.

The first model is applicable if the rising current is proportional to $t^{1/2}$, whereas the second model is indicated if the current increases linearly with $t^{3/2}$. However, it was more convenient to first normalise the current by I_m and to then examine the linearity with t of a plot of the resulting quotient, I/I_m, raised to the appropriate power. Plots of $(I/I_m)^{2/3}$ and $(I/I_m)^2$ vs. t were constructed from current-time data taken from the ascending portions of three current-time transients similar to those shown in **Fig. 3.1.12**. These are depicted in **Fig. 3.1.16** and **Fig. 3.1.17**. It

can be seen that only the plot for instantaneous nucleation shows appreciable linearity during the initial stages.

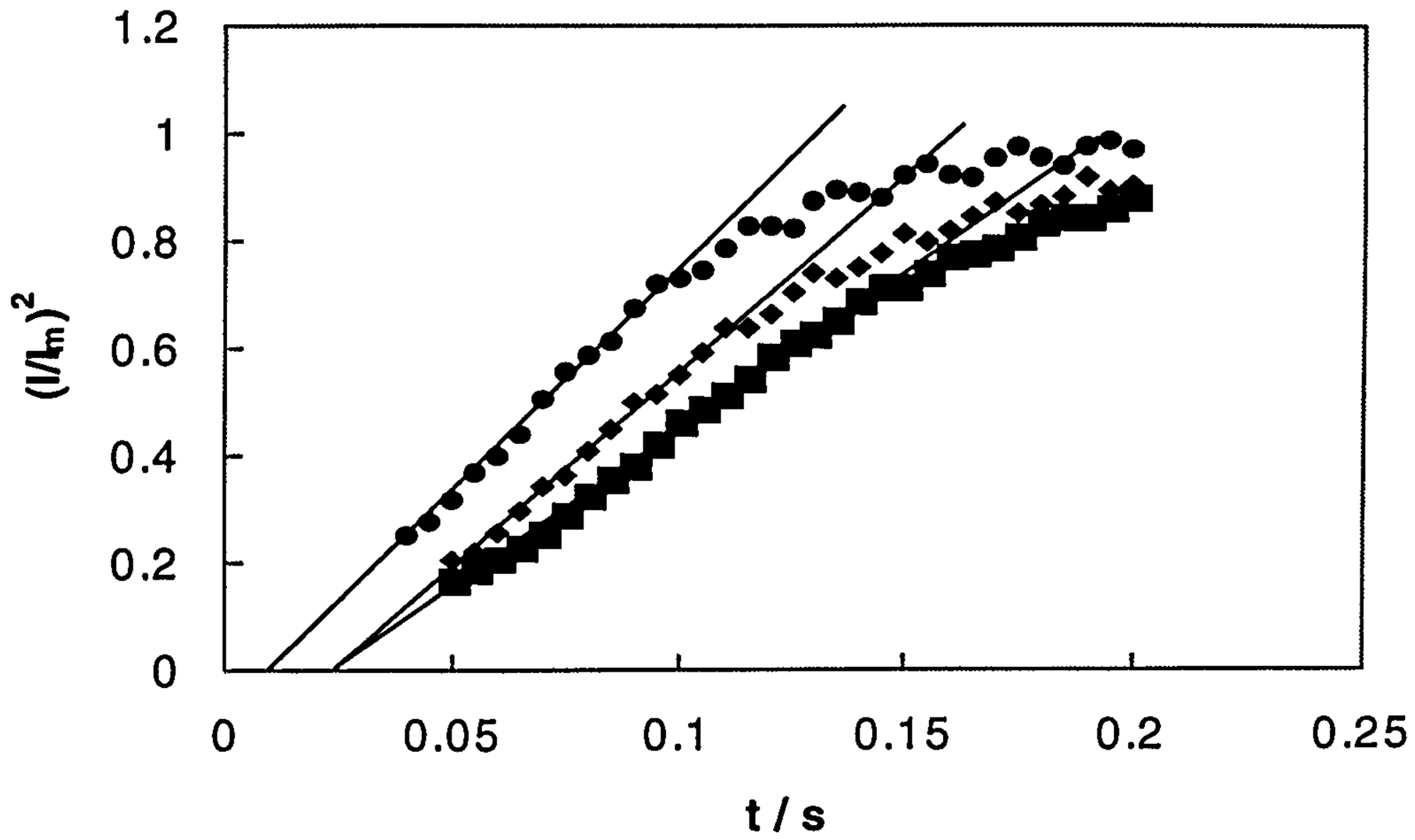

Fig. 3.1.16. Plot of $(I/I_m)^2$ *vs. t* constructed from the current-time transients shown in **Fig. 3.1.12:** (1) -0.20 V; (2) -0.21 V, (3) -0.22 V. Linearity indicates instantaneous nucleation.

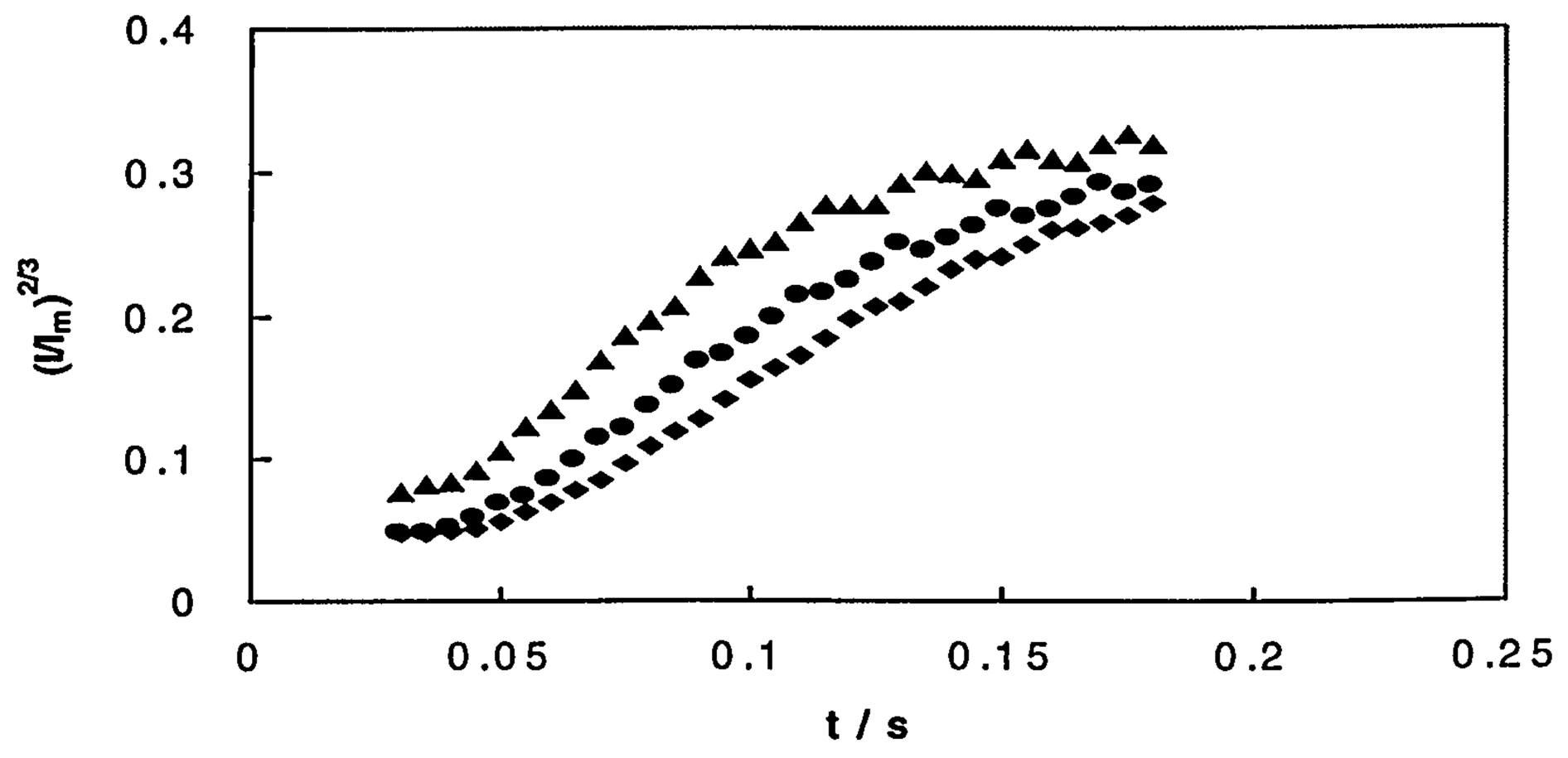

Fig. 3.1.17. Plot of $(I/I_m)^{2/3}$ *vs. t* constructed from the current-time transients shown in **Fig. 3.1.12:** (1) -0.20 V; (2) -0.21 V and (3) -0.22 V. Curvature indicates that progressive nucleation is not followed.

A more definitive confirmation for adherence to the nucleation models can be made by comparing data from the entire experimental current-time transient to the following appropriate dimensionless theoretical equation [148]:

$$(I/I_m)^2 = (t/t_m)^{-1}\left(\frac{1-\exp[-xt/t_m+\alpha\ (1-\exp(-xt/\alpha\ t_m))]}{1-\exp[-x+\alpha\ (1-\exp(-x/\alpha\ ))]}\right)^2 \qquad (3.1.6)$$

where

$$x = bt_m \qquad (3.1.7)$$

and

$$\alpha = b/A \qquad (3.1.8)$$

$$b = N\pi\ D(\pi cM/\rho)^{1/2} \qquad (3.1.9)$$

The two limiting cases of **Eqn. 3.1.6** correspond to instantaneous nucleation ($\alpha \rightarrow 0$, x=1.2564) and progressive nucleation ($\alpha \rightarrow \infty$), respectively [148]:

$$(I/I_m)^2 = 1.2254(t/t_m)^{-1}(1\text{-}\exp[-2.3367(t/t_m)^2])^2 \qquad (3.1.10)$$

$$(I/I_m)^2 = 1.9542(t/t_m)^{-1}(1\text{-}\exp[-1.2564(t/t_m)])^2 \qquad (3.1.11)$$

In order to make an effective comparison between theory and experiment, it was necessary to apply a correction to the experimental data in order to account for an induction time, t_0, preceding the onset of nucleation.

In electrocrysallisation [192], induction times may arise in three ways. The first and most generally considered cause of time-lag in electrochemical nucleation is related to the non-steady state of nucleation [193,194,195,196,197,198,199]. Induction times can also be attributed to the stochastic nature of nucleation. This

type of induction time obeys Poissonian probability. Therefore, with a macro-electrode having a large number of possible nucleation sites, this time-lag would be vanishingly small. Finally, a time-lag should also appear if some kind of electrochemical transformation of the electrode surface was required before nucleation and growth could occur.

Apparently, for the deposition of aluminium on tungsten, induction times from the above mentioned sources were not significant compared to the time scale of nucleation and growth. t_0 could be obtained from the intercept of the straight lines of I *vs.* $t^{1/2}$ [189]. In all the data sets examinated, the magnitude of t_0 was generally less than 5 ms, and so no time correction was necessary.

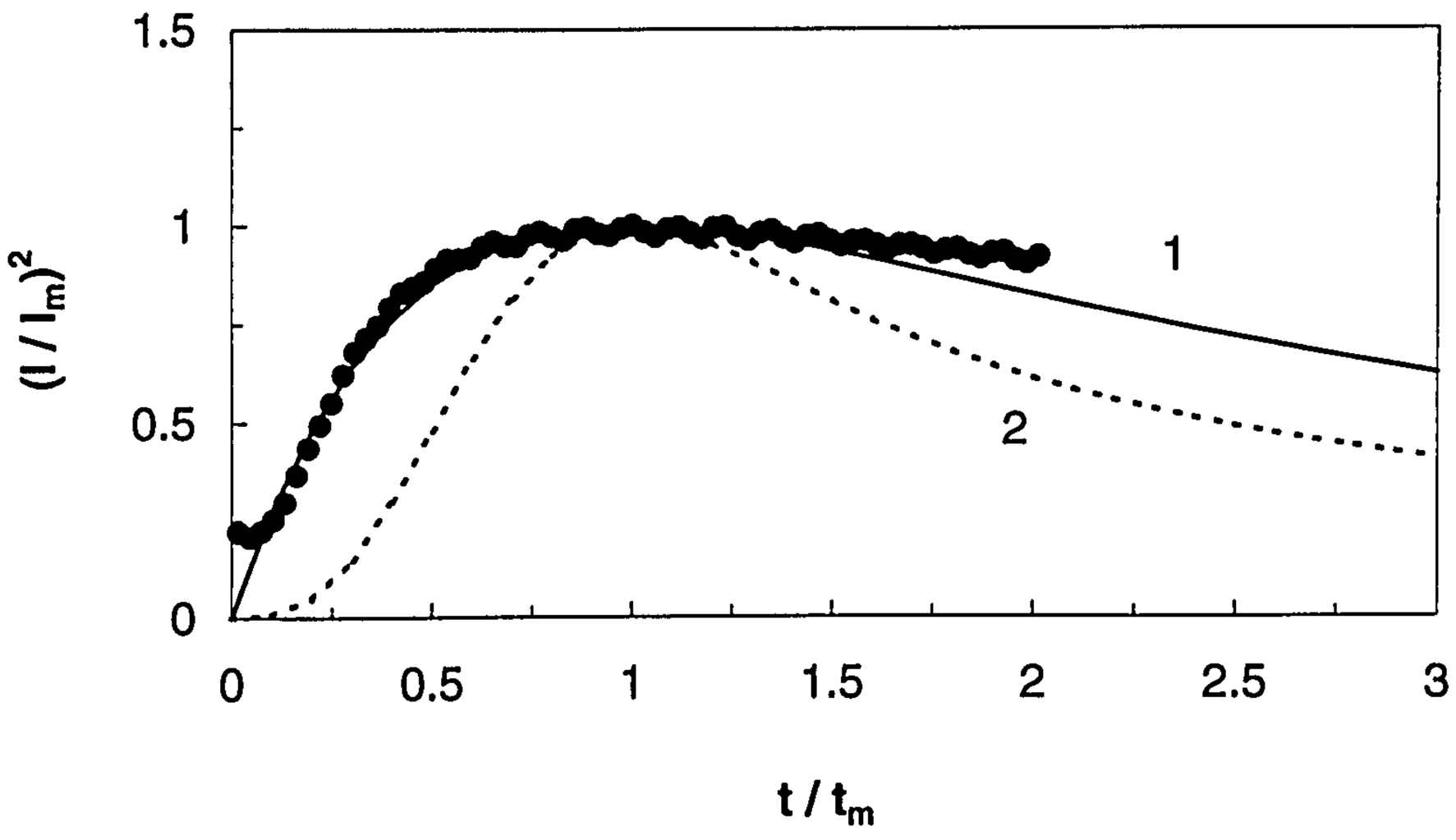

Fig. 3.1.18. Comparison of the dimensionless experimental data derived from the current transients with the theoretical models for diffusion controlled three dimensional instantaneous (1) and progressive (2) nucleation and growth.

The dimensionless analysis of the experimental data revealed that alumnium electrodeposition occurred by three dimensional diffusion-controlled instantaneous nucleation and growth, as shown in **Fig. 3.1.18**. It is possible to obtain information about the diffusion coefficient, D of $Al_2Cl_7^-$ and the number

density of active sites, N, from I_m and t_m of the respective transients. Specifically, for instantaneous nucleation:

$$(I_m)^2 t_m = 0.1629(nFc)^2 D \quad (3.1.12)$$

$$I_m = 0.6382nFcD(kN)^{1/2} \quad (3.1.13)$$

where:

$$k = (8\pi cM/\rho)^{1/2} \quad (3.1.14)$$

The calculated diffusion coefficients and chronoamperometric data are collected in **Table 3.1.4**. The average D value, 2.45×10^{-7} cm^2 s^{-1} agreed with the mean value of 2.17×10^{-7} cm^2 s^{-1} from cyclic voltammetry. However, the values of N, for potentials from -0.2 to -0.3 V, proved to be much smaller than the atomic density of the substrate ($\approx 10^{15}$ cm^{-2}), and this result suggested that the number of active sites could indeed be a serious limitation for nucleus formation in the early stages of phase formation.

Table 3.1.4 Chronoamperometric data for Aluminium nucleation

E vs. Al (V)	$10^3 I_m$ (A cm^{-2})	t_m (s)	$10^6 (I_m)^2 (t_m)$ (A cm^{-2} s)	$10^7 D$ (cm^2 s^{-1})	$10^{-6} N$ (sites cm^{-2})
-0.23	-11.07	0.28	3.25	2.68	2.03
-0.24	-12.10	0.28	3.95	2.25	2.37
-0.25	-13.71	0.22	3.85	2.50	2.81
-0.26	-14.38	0.24	4.71	2.55	2.48
-0.27	-16.25	0.17	4.23	2.18	4.12
-0.28	-17.32	0.18	5.04	2.40	3.57
-0.29	-18.35	0.17	5.39	2.35	3.83
-0.30	-18.85	0.18	5.90	2.73	3.17

It is noteworthy that similar values of N were observed in other systems, 10^6 cm^{-2} for potentials from 1.5 to 1.7 V in $AlCl_3$-LiCl-$DMSO_2$ system [66] and $10^6 \sim 10^8$ cm^{-2} for potentials from -0.075 to -0.30 V in $AlCl_3$-MEIC melts [128] for the

cases of aluminium nucleation on tungsten substrates. To properly understand the significance of these values and the data in **Table 3.1.4**, it is necessary to examine the physical phenomena occurring during the deposition process [148].

As the first nuclei were formed, they grew and drew electroactive species from solution producing a diffusion zone which was depleted in the electroactive species. As this depleted diffusion zone grew out into solution (three dimensional growth), its growth projected onto the electrode surface was seen as a two dimensional zone which was depleted of the electroactive species. Within this two dimensional diffusion zone, further nucleation was inhibited (*i.e.* continued nucleation occurred only on the electrode surface uncovered by the diffusion zones) and this diffusion zone was therefore referred to as the nucleation exclusion zone. Because of the development of this exclusion zone around each growing nucleus, the actual density of nuclei formed was much less than the number density of active nucleation sites (N) on the electrode surface. The development of this exclusion zone meant that the nucleation process was almost complete at t_m. In fact, 95% of nuclei have formed by t_m.

Besides the above-mentioned influence of the diffusion zones, the active nucleation sites, are typically defects in the surface layer of the substrate [200]. As previously pointed out, corrosion, alloying and passivation phenomena occurred during deposition of aluminium on tungsten in the melt. These factors would affect the number of active sites. Additionally, the differences of morphology and structure between the fresh aluminium deposits and tungsten substrate might also explain why the N values were always smaller than the atomic density of the substrate.

Since the aluminium deposits were poorly adherent to tungsten, SEM photomicrographs were not obtained.

3.1.7 Convolution Analysis

The convolution technique offers a number of advantages in the treatment of potential sweep data. For a reversible reduction reaction in a voltammetric experiment:

$$E = E_{1/2} + \frac{RT}{nF} \ln \frac{m_l - m_t}{m_t} \qquad (2.2.11)$$

the curve of m_t *vs.* E for the forward and backward scans superimpose, with m_t returning to zero at sufficiently positive potentials. This behaviour has been verified experimentally [157,159]. For a quasi-reversible reaction, however, the forward and backward m_t curves do not coincide.

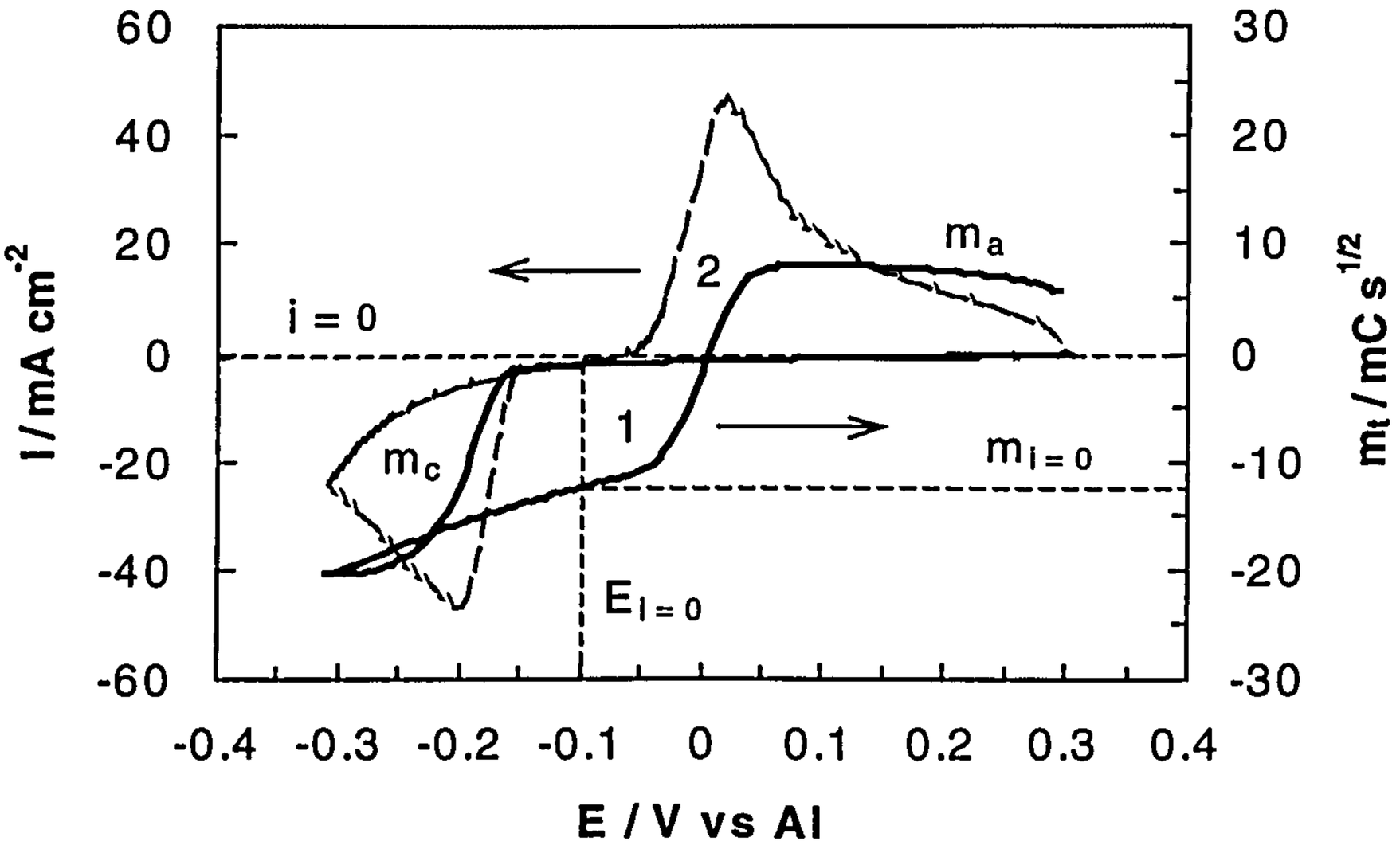

Fig. 3.1.19. Convoluted (1) and cyclic (2) voltammograms for Al deposition and stripping from tungsten at 0.1 V s^{-1}, and analysis of $E_{1/2}$ in accordance of **Eqn. 2.2.15.**

Curve (1) in **Fig. 3.1.19** is a typical convolution current-potential transient for aluminium deposition and stripping processes. Obviously, the deposition $m_{t,c}$ and stripping $m_{t,a}$ currents did not superimpose, showing clear quasi-reversible character. This lock of superimposition resulted from the shift of the $E_{p,c}$ and $E_{p,a}$

values from reversible values. As convolution theory predicts, when the deposition process was purely diffusion controlled at -0.3 V, the surface concentration of $Al_2Cl_7^-$ ions, $c(0,t)$, was zero, and the transformed current m_c reached a limiting value m_l. On the reverse scan, m_a crossed m_c to form a very clear nucleation current loop, in good agreement with the observation in voltammetric results (**Fig. 3.1.6**). According to **Eqn. 2.2.15**:

$$E_{1/2} = E_{i=0} - \frac{RT}{F} \ln \frac{m_l - m_{i=0}}{m_{i=0}} \qquad (2.2.15)$$

the reversible $E_{1/2}$ for this quasi-reversible deposition process was estimated to be -0.07 V. This value was more positive than the -0.142 V estimated from voltammetry.

Fig. 3.1.20 shows convolution deposition currents at various sweep rates transformed from **Fig. 3.1.2**. As can be seen, the m_c *vs.* E plots shift to negative potentials with increasing sweep rate rather than superimpose as expected. The potential scale should be independent of υ (**Eqn. 2.2.14**):

$$E = \frac{RT}{\alpha nF} \ln \frac{k^\circ}{D^{1/2}} + \frac{RT}{\alpha nF} \ln \frac{m_l - m_c(1 + e^{(nF/RT)(E-E_{1/2})})}{i} \qquad (2.2.14)$$

When the process is under diffusion control, $c(0,t) \rightarrow 0$, $m_c \rightarrow m_l$, forming a plateau in the m_c *vs* E plot.

Interestingly, the m_c *vs* E plots (**Fig. 3.1.20**) exhibited peaks rather than the plateau as the sweep rate decreased. This m_c only depends upon $D^{1/2}$ and bulk concentration c_o (**Eqn. 2.2.8**):

$$m_l = nFAD_o^{1/2} c_o \qquad (2.2.8)$$

and c_o was a constant. Thus, the decrease in m_t might be indicative of a decrease D. It was possibly caused by a solid layer from a corrosion reaction, which changed apparent D values. Similar results were observed for the stripping curves. In the stripping case it might be caused by the formation of a passivating layer on the working electrode.

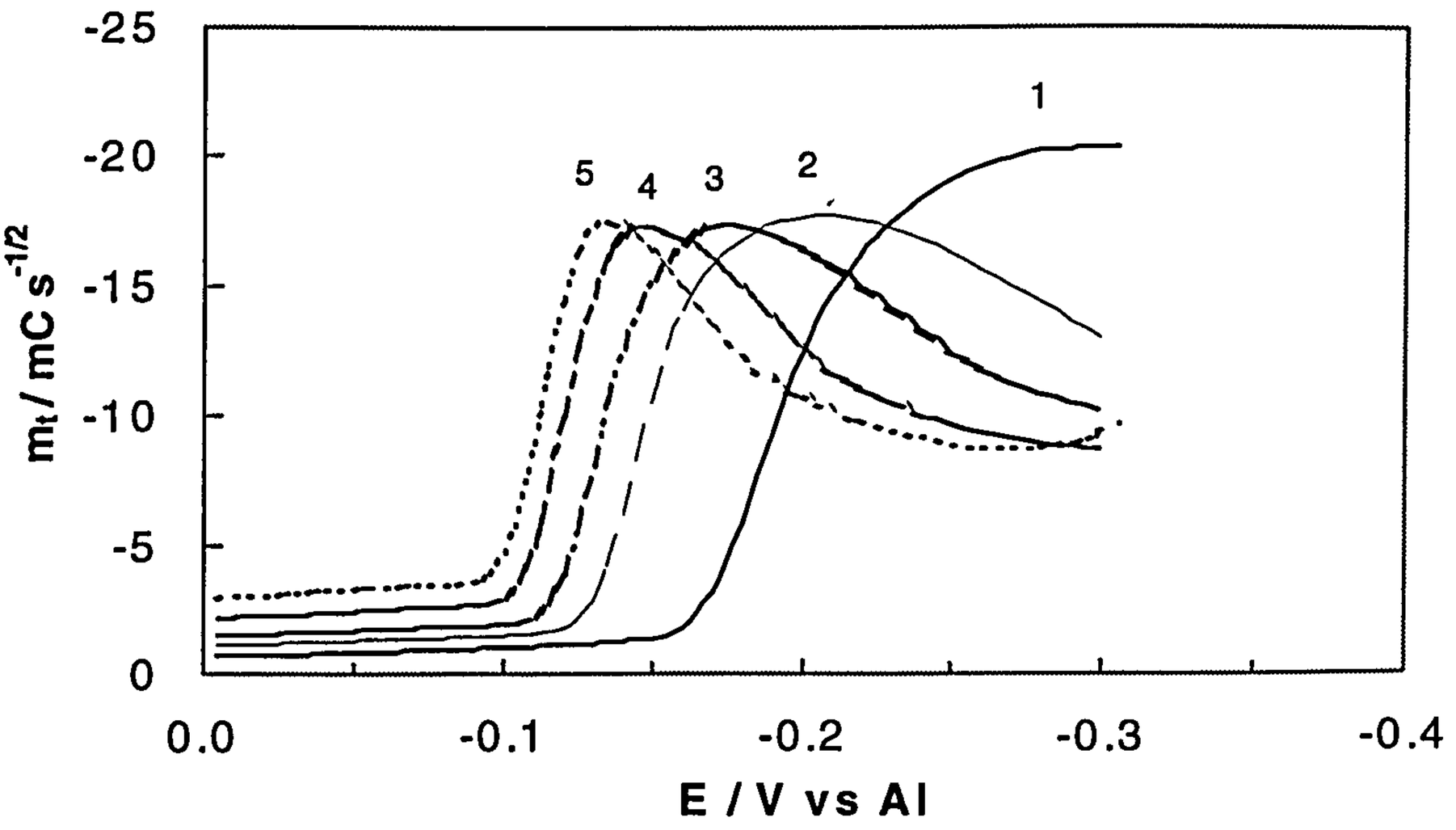

Fig. 3.1.20. Convoluted deposition currents transformed from **Fig. 3.1.2** at sweep rates: (V s^{-1}): (1) 1.0; (2) 0.5; (3) 0.25; (4) 0.10; (5) 0.05; (6) 0.02.

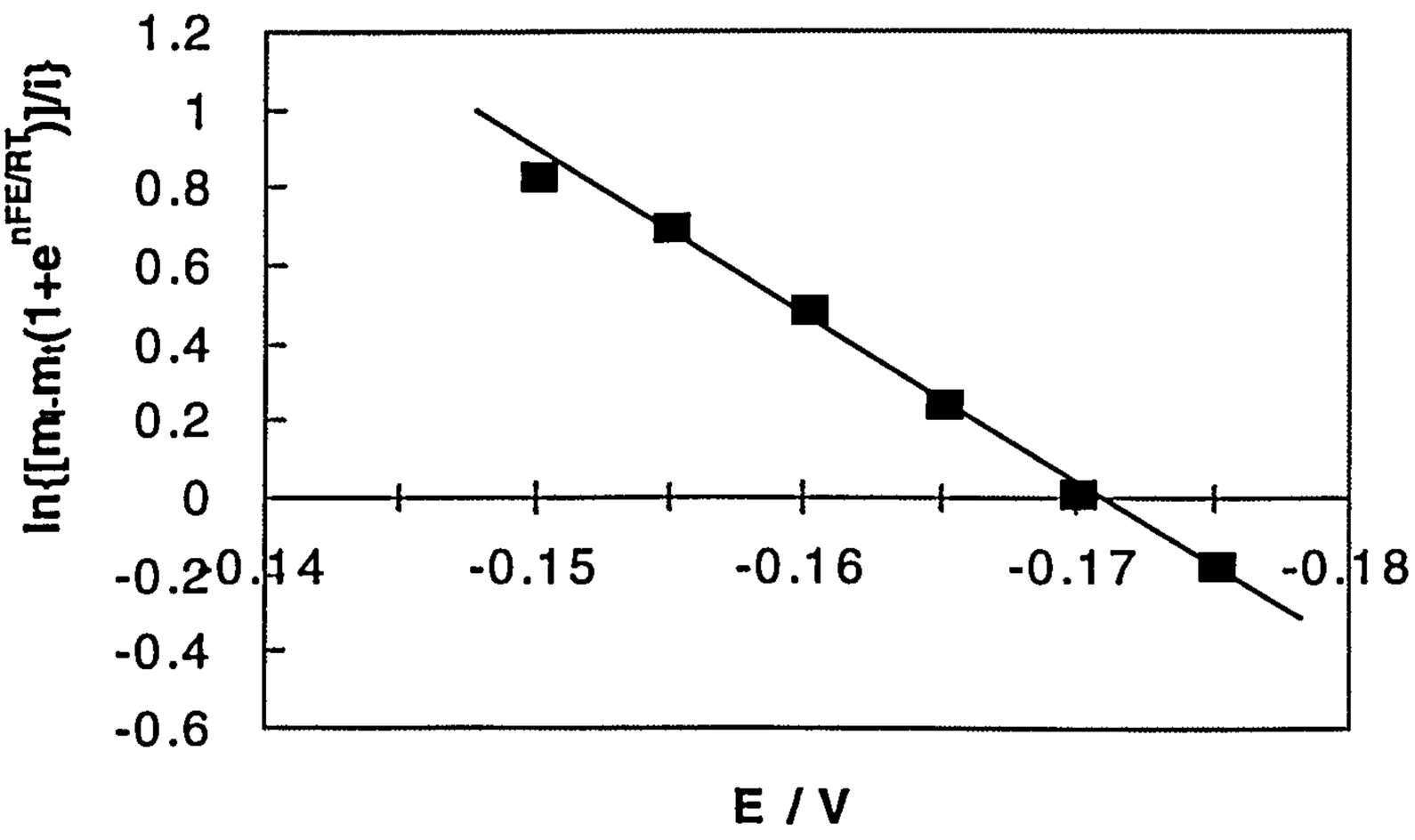

Fig. 3.1.21. Logarithmic analysis for the covoluted voltammogram (curve 1 in Fig. 3.1.19).

According to **Eqn. 2.2.14** from the slope and intercept of **Fig. 3.1.21**, α and k° were calculated to be 0.44 and 4.75×10^{-4} cm s^{-1}, respectively.

3.2 ALUMINIUM ELECTRODEPOSITION FROM THE DILUTED MELT

Generally, room temperature molten salts have slightly higher viscosities and lower conductivities in comparison with those of aqueous electrolytic solutions and high temperature molten salts. Some aromatic compounds have been used as cosolvents to decrease the viscosity and increase the conductivity of organic haloaluminate molten salts [121,133], or as solvents to dissolve the inorganic analogues [201]. These solutions were suitable for the electrodeposition of aluminium. Basically, in order to maintain the reversibility of the Al electrode, solvents should be weak Lewis bases so as to not react with $AlCl_3$ and thus influence equilibrium **Eqn. 1.3.7** unfavourably:

$$AlCl_4^- + AlCl_3 \rightleftharpoons Al_2Cl_7^- \qquad (3.2.1)$$

The Lewis basicity of a number of solvents wasempirically determined by Gutmann [202,203] who described them in terms of a donor number (DN) and classified the halogenated aromatics as weak Lewis bases. Zawodzinski et al. [204] categorised potential cosolvents on the basis of their relative donor ability to the donor ability of an ambient temperature chloroaluminate melt, which in turn is dependent upon its mole fraction. The basic melts had a DN above 27 and the acidic DN values below -14.5. In acidic melts, only the lowest possible positive DN cosolvents could preserve the characteristics of the reversible aluminium electrode and the $Al_2Cl_7^-$ ions. Cosolvents with negative donor numbers would not react with acidic melts, but these seem to be no solvents in this category.

Recent work in this area [133], where acidic $AlCl_3$-MEIC and $AlCl_3$-TMPAC melts were used as model electrolytes to test several candidates from the lowest DN solvents, found most of them to be either immiscible or not to have

acceptable electrochemical properties. Only the halogenated aromatics, especially 1,2-dichlorobenzene (1,2-DCB) were miscible and showed low reactivity toward the melts [205]. The electrochemical behaviour of $AlCl_3$-TMPAC melts diluted by 1,2-DCB on alumnium electrodes was investigated [134], revealing that aluminium stripping was not affected by 1,2-DCB. However, dilution with 1,2-DCB beyond 80% by volume appeared to have an adverse effect on conductivity. Since little information about the diluted melts is available, in this section 1:2 $AlCl_3$-TMPAC melt diluted with 50% volume of 1,2-DCB were electrochemically investigated on tungsten working electrodes.

3.2.1. The Bulk Deposition and UPD of Aluminium

Since the 0.60 M (80% volume cosolvent) melt displayed similar electrolytic resistance to the neat (3.09 M) melt, whereas the 1.55 M melt (50% volume cosolvent) gave a resistance 40% less than the neat meat melt [134], the 1.55 M melt was chosen as diluted system.

After mixing euqal volume of 1,2-DCB and neat melt, increasing deposition and stripping currents were immediately observed (**Fig. 3.2.1**). These were attributed to the decrease of viscosity and the corresponding increase in ionic mobility and conductivity. Also, dilution might cause a decrease in the degree of association of ion pairs or ion aggregates, which apparently dominate the neat state [206,207,208]. Although the dilution had a beneficial effect on the viscosity and the conductivity, the positive limit for chlorine evolution was decreased, occurring at 1.8 V instead of 2.6 V in the case of the neat melt. It was observed that the background current was larger than that in the neat melt and the coloration of the solution became slight brown. These could be caused by impurities in the 1,2-DCB.

Voltammetric analysis of Al deposition and stripping processes from the diluted solutions showed the following features: $E_{p,c}$, $|E_{p,c} - E_{p,a}|$ and $|E_{p,c} - E_{p/2,c}|$ shifted negatively as scan rates increased; $I_p \upsilon^{-1/2}$ was independent of υ ;and $I_{p,a}/I_{p,c}$ was close to unity. All these were consistent with quasi-reversible and diffusion controlled deposition and stripping processes.

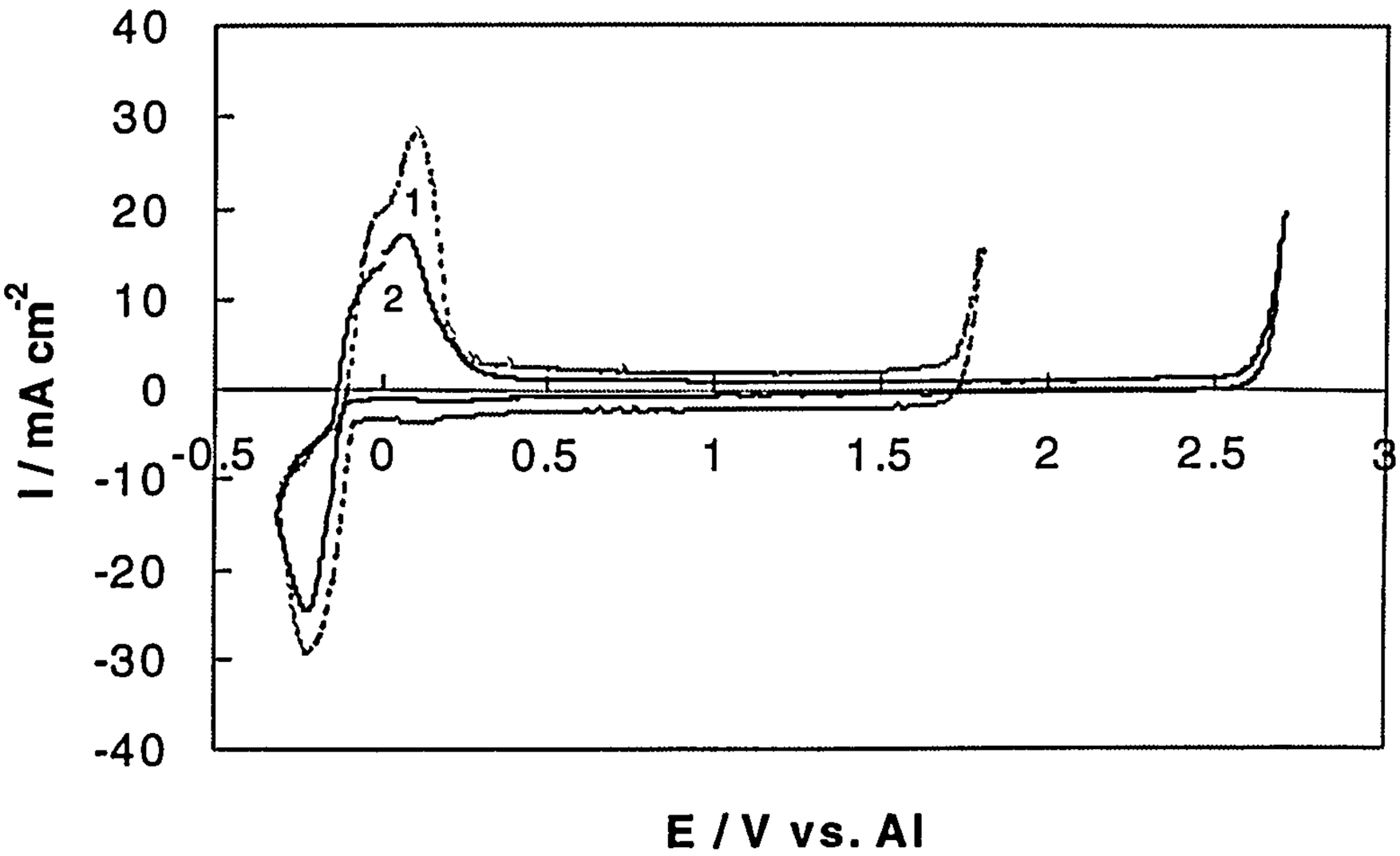

Fig. 3.2.1. Voltammograms for 2:1 $AlCl_3$-TMPAC melts with 50% (1) and without (2) 1,2-DCB at 0.1 V s^{-1}

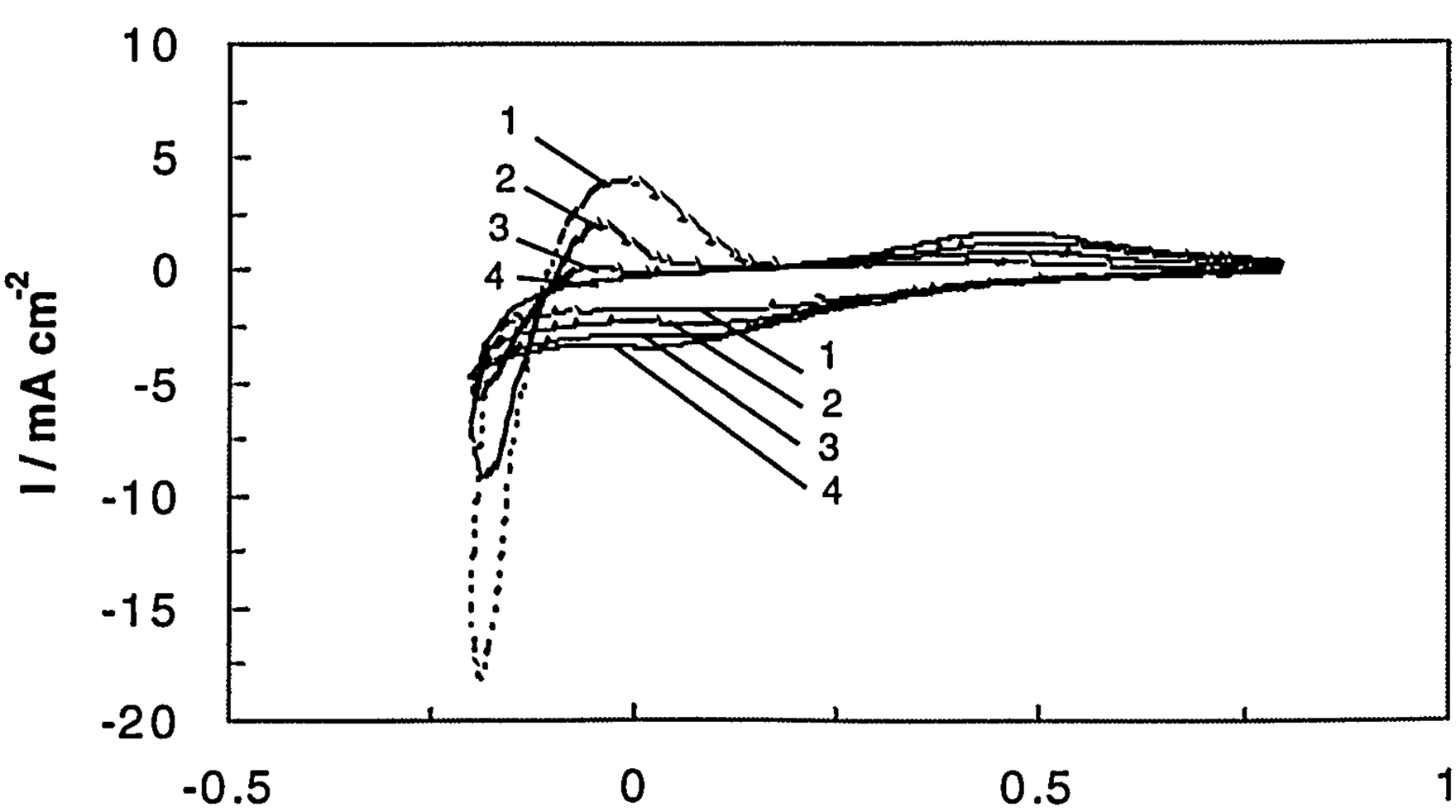

Fig. 3.2.2. Voltammograms of Al UPD on a tungsten electrode in the 2:1 $AlCl_3$- TMPAC melts diluted by 50% volume of 1,2-DCB with the correction of the background current (25°C). Sweep rates (V s^{-1}) were: (1) 0.1; (2) 0.25; (3) 0.5; (4) 1.0.

Fig. 3.2.2 shows aluminium UPD in the diluted system at various sweep rates with the correction of the background current. These charge corresponded to 3 ~ 10 monolayers. The range was large in the neat melt, implying that UPD was easier in the diluted melts than in the neat melts. UPD in the diluted systems was still surface controlled, shown by the linearity of I_p *vs* υ . Bulk deposition processes at -0.14 V involved nucleation. It is noteworthy that the deposition currents increased as υ decreased. This was probably because the switching potential (-0.2 V) in **Fig. 3.2.2** did not reach the peak potential (-0.22 V) for bulk deposition and consequently the process was not diffusion controlled. In this conditions the surface processes such as nucleation were dominant. Since the formation and growth of nuclei increased with time, the increase in currents, resulting from the formation and growth of nuclei, followed the decreasing sweep rates.

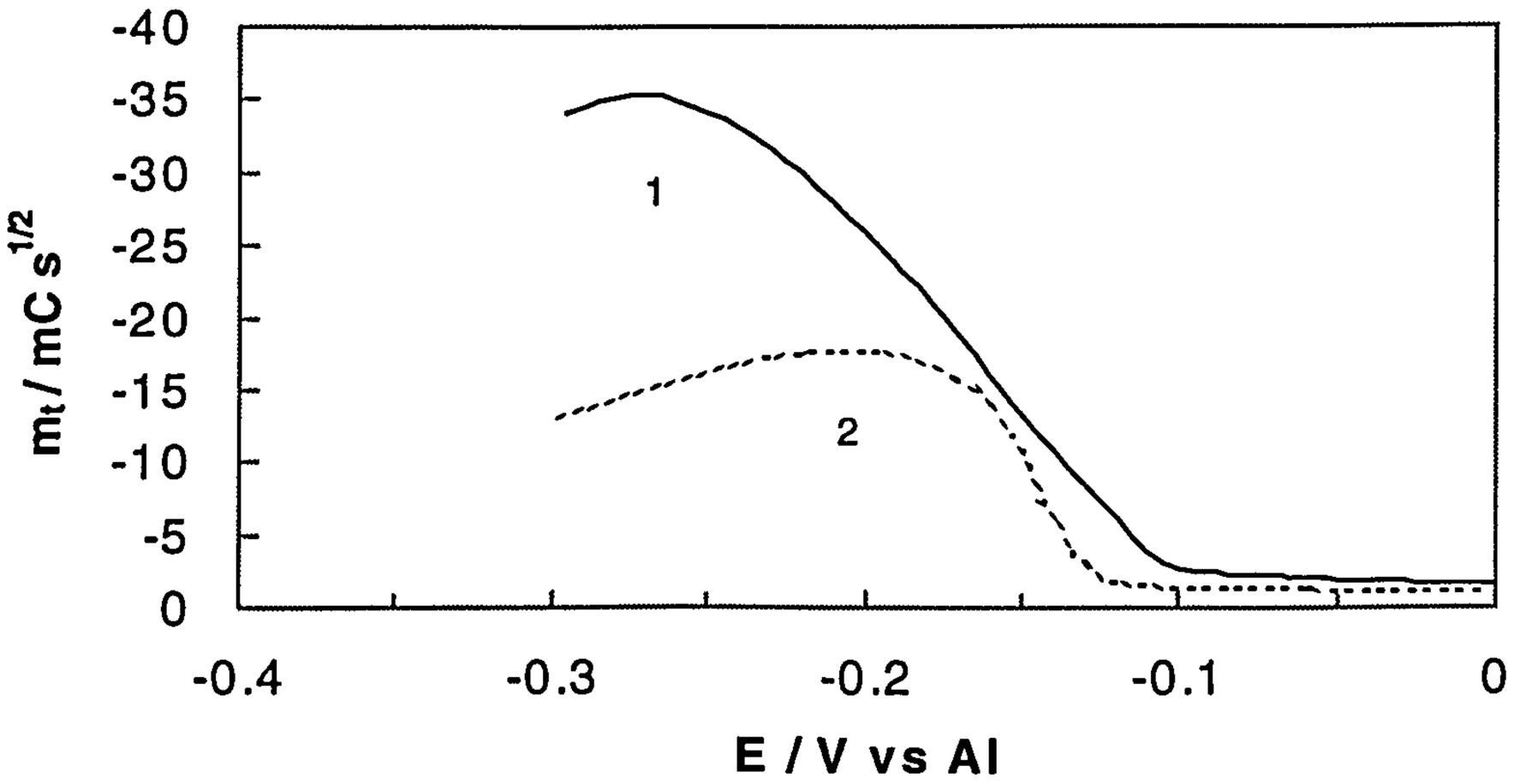

Fig. 3.2.3. Convolution analysis of Al deposition currents in 2:1 $AlCl_3$-TMPAC melts with 50% volume (1) and without (2) 1,2-DCB at 0.1 V s^{-1}

Convolution analysis (**Fig. 3.2.3**) revealed that the peak potential of Al deposition in the diluted melt shifted negatively relative to the neat melt, and, correspondingly, $E_{1/2}$ shifted from -0.07 V (the neat melt) to -0.11 V. These shifts, which were not obvious in the voltammogram (**Fig. 3.2.1**), indicated that reduction

of $Al_2Cl_7^-$ ions became more difficult in the diluted melts, although dilution increased the conductivity of electrolytic solutions.

From the convoluted voltammograms, D, α and k° for aluminium deposition were evaluated. The value of 6.5×10^{-5} for D was two orders greater than that for the neat melt, confirming the dilution effect. α was 0.40 , closed to 0.44 in the neat melt. The value of 8.32×10^{-3} for k° was one order 4.75×10^{-4} bigger than in the neat melt, suggesting the deposition reaction was faster in the diluted melt.

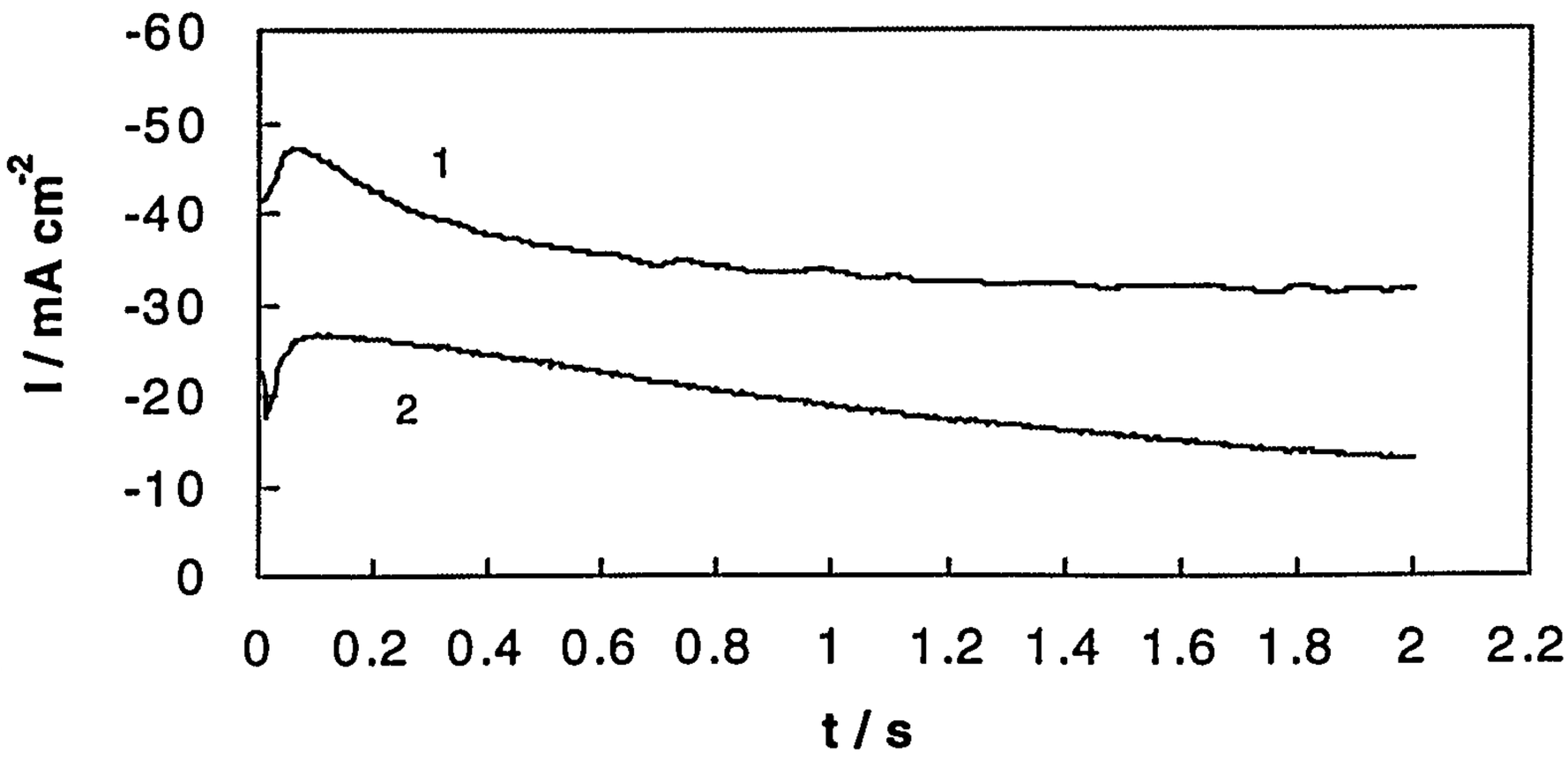

Fig. 3.2.4. Comparison of current-time transients of Al deposition in 2:1 $AlCl_3$-TMPAC melts with 50% volume (1) and without (2) 1,2-DCB at -0.2 V.

3.2.2 Nucleation Analysis

Chronoamperometric plots of alumnium deposition from the diluted (**curve 1**) and the neat (**curve 2**) melts are shown in **Fig. 3.2.4.** Obviously, in the diluted melt, the nucleation current was higher, and the maximum followed by Cottrel behaviour came earlier, implying diffusion controlled conditions were easier to reach. However, there was noise on the plateau, which could be attributed to cathodic passivation or corrosion. In fact, a black grainy layer was observed on the

working electrode. Similar to that in the neat melt, the deposition process in the diluted melt also involved instantaneous nucleation and diffusion limited growth, confirmed by the dimensionless analysis (**Fig. 3.2.5**).

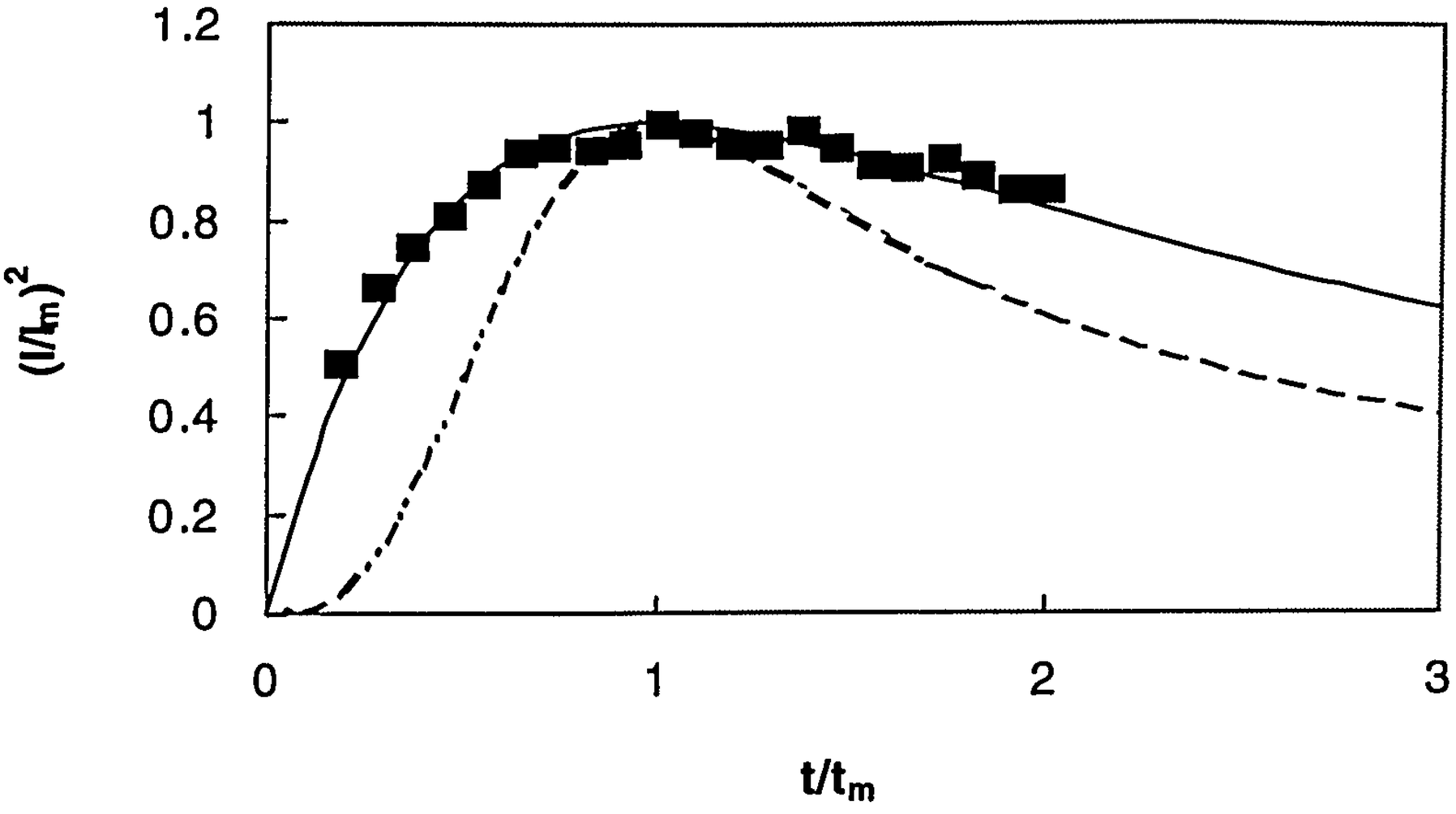

Fig. 3.2.5. Comparison of the dimensionless experimental data (■) derived from the current transients shown in **Fig. 3.2.5** (**curve 1**) with the theoretical models for diffusion controlled three dimensional instantaneous and progressive nucleation and growth.

Chapter 4

ALUMINIUM ELECTRODEPOSITION ON ALUMINIUM AND GLASSY CARBON

Since the anodic passivation, the corrosion reaction and alloying effect were involved in the deposition and stripping processes of aluminium on tungsten from 2:1 $AlCl_3$-TMPAC melts, and electrodepositions of metals are strongly related to the electrode materials, naturally, it is concerned if these phenomena would be happening on aluminium itself, and non-metal substrate, glassy carbon. As aluminium was used as the anode and reference electrode, it would be interesting to know how it worked as the working electrode. As was expected, no allying effect would be observed on glassy carbon because it is an inert, non-metal electrode. Therefore, to better understanding electrochemical behaviours of aluminium, glassy carbon in 2:1 $AlCl_3$-TMPAC melts, Al deposition and stripping processes on aluminium and glassy carbon were investigated in this chapter.

4.1 ALUMINIUM ELECTRODE

4.1.1 Voltammetric Studies

Fig. 4.1.1 shows a set of typical voltammograms for 2:1 $AlCl_3$-TMPAC melt on high pure (5N) aluminium electrode at various sweep rates. The residual current density in the window was about 0.2 mA cm^{-2}, less than 1.0 mA cm^{-2} on tungsten, proving that in the latter case, the contribution to the residual current density was partially from impurities in tungsten. Furthermore, these voltammograms exhibited current loops typical of deposition processes

requiring nucleation overpotentials at all sweep rates. However, there was no evidence of an UPD prewave seen on the tungsten electrode, suggesting that the occurrence of UPD was highly dependent upon the electrode substrate.

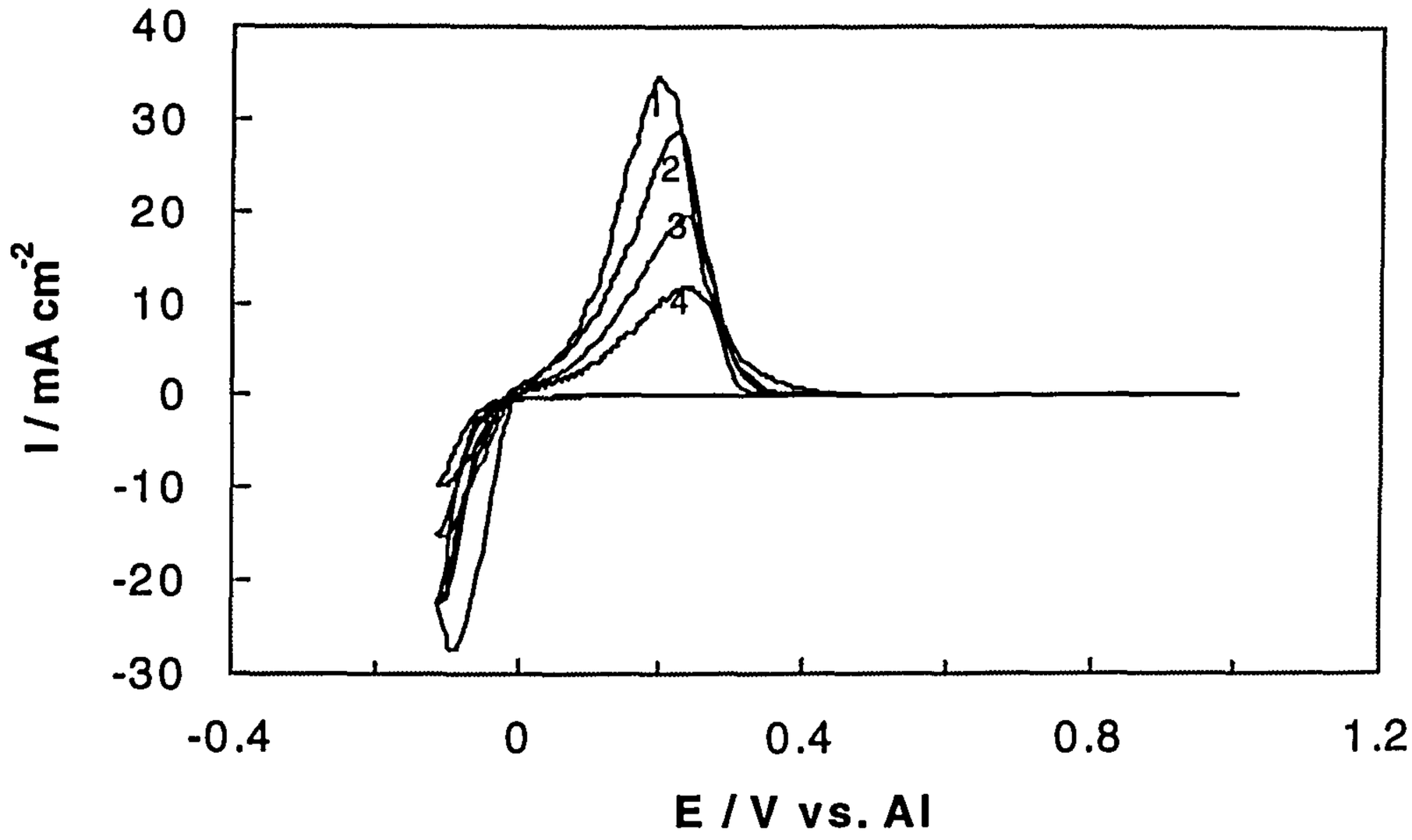

Fig. 4.1.1. Voltammograms for deposition and stripping of aluminium on aluminium electrode from 2:1 $AlCl_3$-TMPAC melt at 25°C. Sweep rates (V s^{-1}): (1) 0.20; (2) 0.10; (3) 0.05; (4) 0.02.

At higher sweep rates, aluminium deposition occurred at -0.02 V, compared with -0.18 V on tungsten. It is evident that aluminium was more easily deposited on itself than on tungsten and other foreign substrates [185]. Upon sweep reversal, a stripping peak was observed immediately. However, the ratios of $I_{p,a}/I_{p,c}$ were greater than unity, and the coulombic efficiencies were over 200%, indicating that dissolution of electrode itself was involved in the stripping process. Generally, in order to strip the deposits on the working electrode, between two experiments the potential was held 5 min at 1.0 V. On aluminium electrodes, however, the pre-treatment caused increases in the deposition and stripping currents (**Fig. 4.1.2**). The increases were due to either extra $Al_2Cl_7^-$ ions from the dissolution of aluminium electrode or roughening of the surface.

4.1.2 Passivation-Dissolution of Electrodes

In contrast to tungsten electrodes, $E_{p,a}$ shifted slightly positively, and the irreversibility of the deposition-stripping process increased with decreasing sweep rates. This was assigned to increasing passivation of the anode. With more negative switching potentials (-0.4 V) and longer times (lower sweep rates), the separation of deposition and stripping peaks (**A** and **D**) became bigger and a small anodic peak (**C**) occurred at -0.1 V (**Fig. 4.1.3**). Similar results were observed in some inorganic melts [185] in which the peak **C** was assigned to a porous, but insoluble oxide film on the electrode surface.

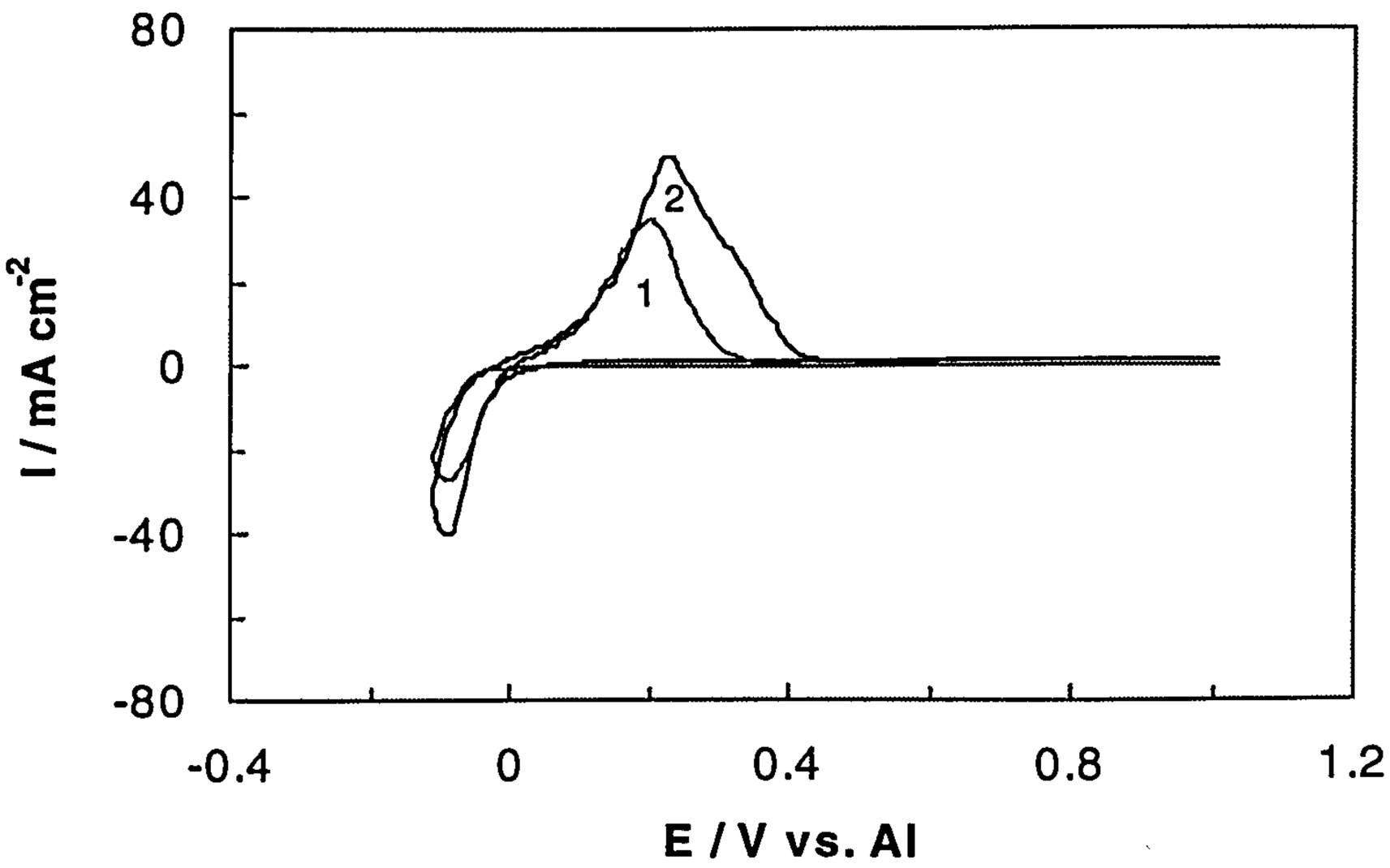

Fig. 4.1.2. Cyclic voltammograms for deposition and stripping of aluminum on aluminium electrode from 2:1 $AlCl_3$-TMPAC melt at 25°C and 0.10 V s^{-1}. Curve (1) results after holding the working electrode at 1.0 V for 1 min and curve (2) results from 5 min at 1.0 V.

Analysis of a coulombic efficiencies (**Fig. 4.1.4**) derived from **curve 1** in **Fig. 4.1.3** shows that, the ratio of Q_C/Q_{A+B} was only 0.18 and a well-defined low-intensity stationary current plateau (**E**) between two stripping peaks followed peak **C**. These were characteristic of the passivation state. $Q_a/Q_c = 1$ occurred at 0.34 V, whereas the total $Q_a/Q_c = 1.17$, greater than unity, attributing to dissolution of aluminium electrode. Therefore, the whole stripping of aluminium involved an active passivation-dissolution process [211,212]

which consisted of the formation of a passivation layer and the dissolution of the electrode.

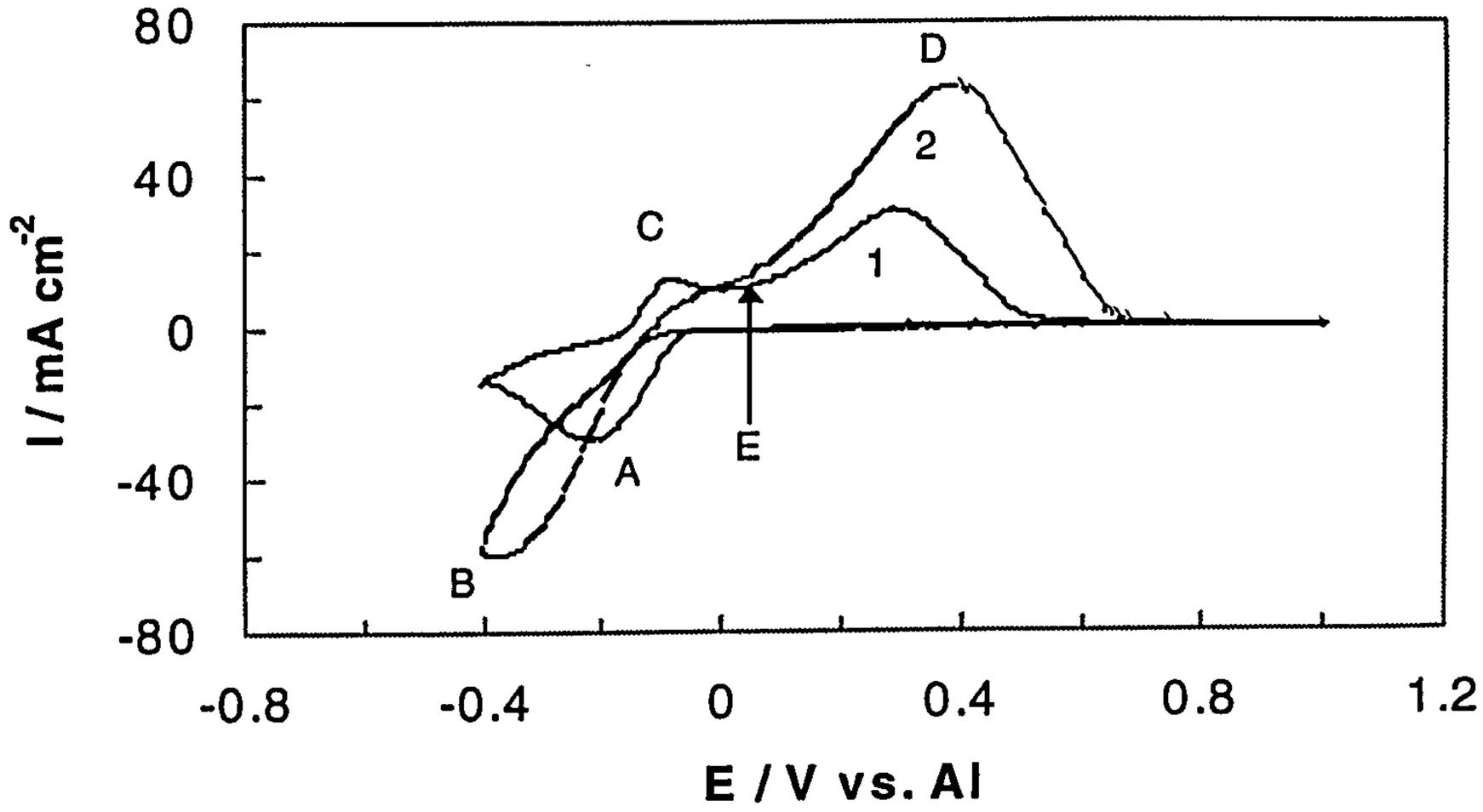

Fig. 4.1.3. Cyclic voltammograms of 2:1 $AlCl_3$-TMPAC melt on aluminium electrode after (1) 1 day and (2) 5 days at 25°C. Sweep rate: 0.10 V s^{-1}.

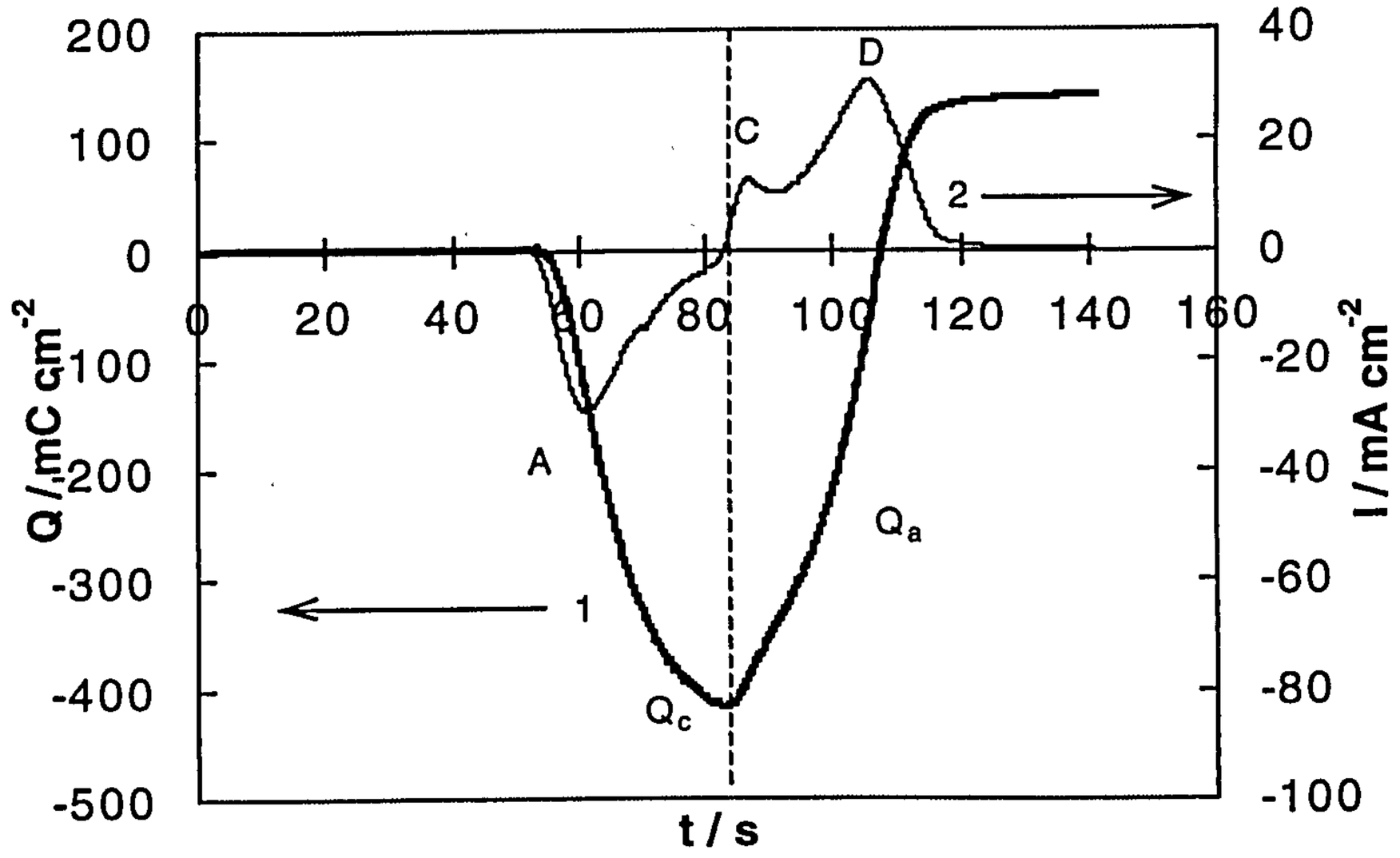

Fig. 4.1.4. Charge analysis of aluminium deposition and stripping (1) and its corresponding current-time transient (2) derived from **curve 1** in **Fig. 4.1.3.**

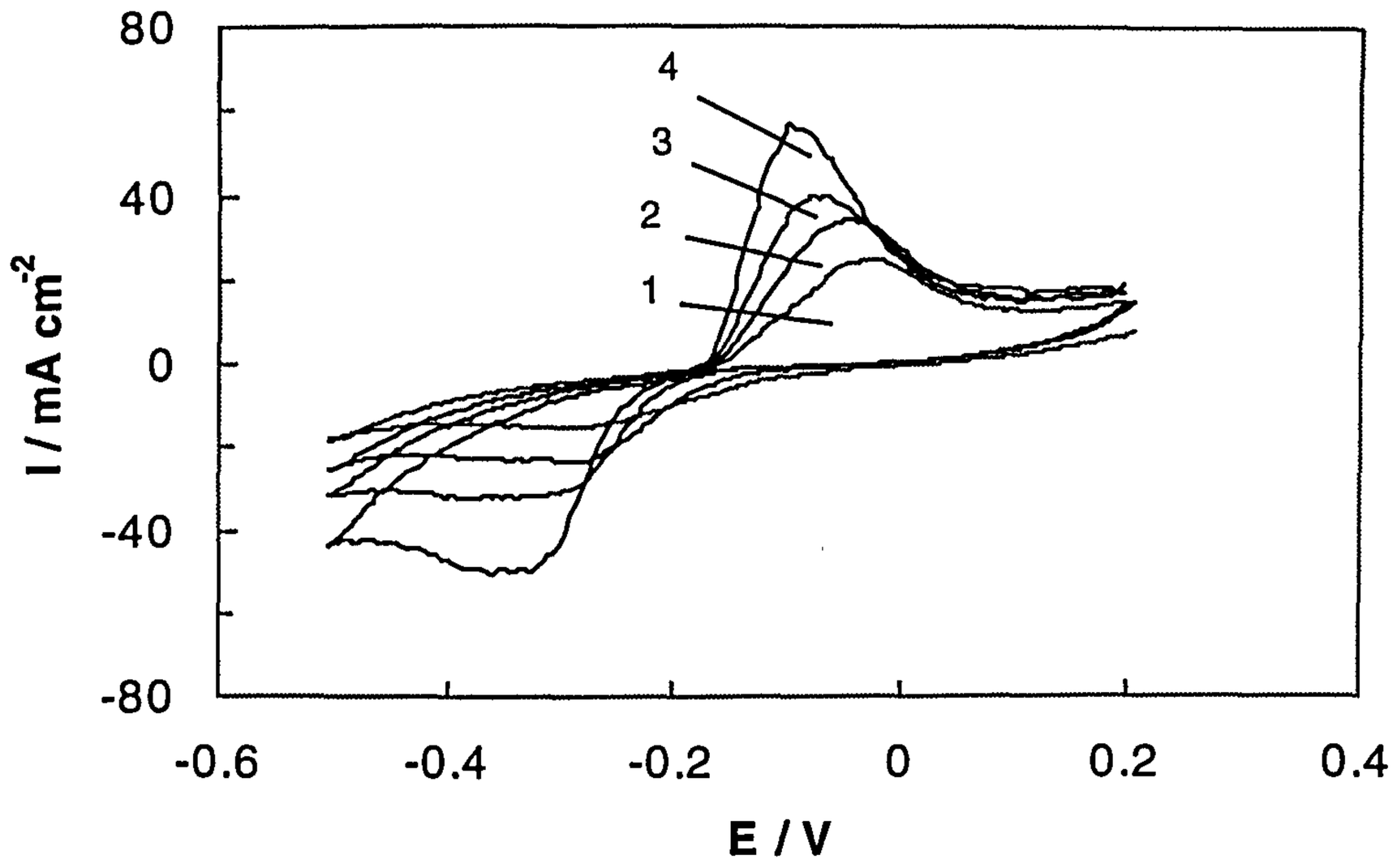

Fig. 4.1.5. Voltammograms for deposition and stripping of aluminium on aluminium from 2:1 $AlCl_3$-TMPAC melt within a narrow potential range which excluded the dissolution of aluminium. Sweep rates (V s^{-1}): (1) 0.20; (2) 0.10;(3) 0.05;(4) 0.02. t = 25°C

In order to better understand the surface passivation, voltammograms at various sweep rates were carried out within a narrow potential range which excluded aluminium dissolution (**Fig. 4.1.5**). Notably, $E_{p,c}$ shifted negatively, compared to **Fig. 4.1.5**. This might be due to the change of the electrode surface after the passivation-dissolution process.

Passivation was confirmed by the fact that $E_{p,a}$ shifted slightly positively with decreasing sweep rates. $I_p \sim \upsilon^{1/2}$ plots were linear (**Fig. 4.1.6**), indicating that the stripping process was diffusion controlled. However, the $I_{p,a} \sim \upsilon^{1/2}$ plot did not pass through the origin, suggesting kinetic limitations caused by passivation of the electrode. Also, the $I_p \sim \upsilon^{1/2}$ relationships can be explained on the basis of Müller's passivation model [211] if the film formation process was under ohmic resistance control [210,211]. The change in ohmic resistance was caused by the spread of the insulating passivation layer across the electrode surface.

The expressions for the peak current and potential in the Muller's passivation model are [210,212]:

$$I_p = (nF\rho\kappa / M)^{1/2} A_0(1-\theta_p)\upsilon^{1/2} \quad (4.1.1)$$

$$E_p = E_0 + (nF\rho\kappa / M)^{1/2}[(\delta / \kappa) + R_0 A_0(1-\theta_p)]\upsilon^{1/2} \quad (4.1.2)$$

where κ is the specific conductivity of the solution inside the film, ρ is the film density, θ_p is the fraction of the initial electrode surface covered, A_0 is the bare surface area, δ is the film thickness, M is its average molar mass, and R_0 is the resistance of the external circuitry.

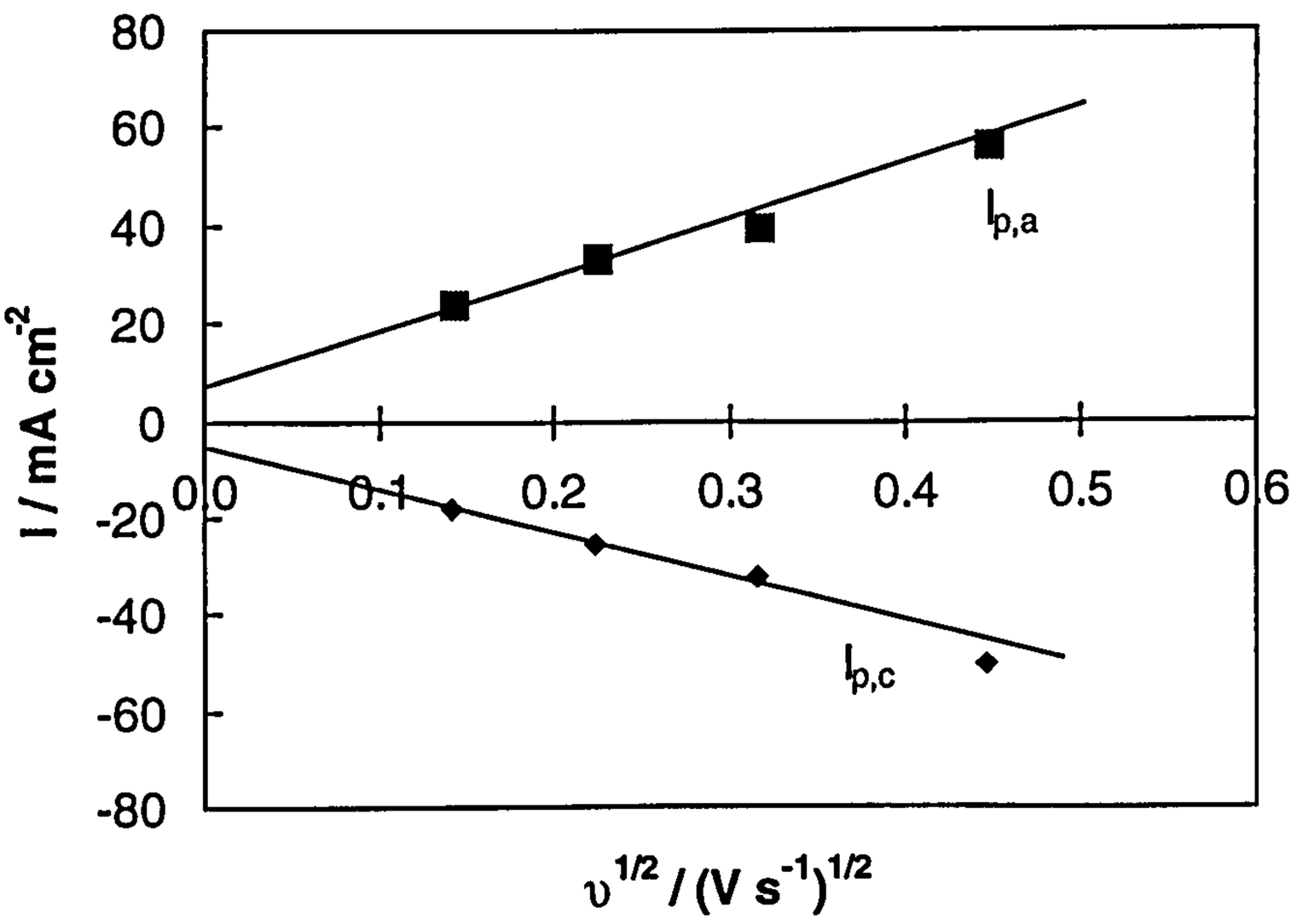

Fig. 4.1.6. Plot of cathodic and anodic peak currents vs. square root of sweep rate for aluminium deposition and stripping on aluminium electrode in 2:1 $AlCl_3$-TMPAC melt at 25°C.

Since the passivation film was not characterised, θ_p, δ and R_0 cannot be determined. However, **Eqn. 4.1.2** predicts a linear relationship between E_p upon $\upsilon^{1/2}$, which has been verified by the results shown in **Fig. 4.1.7.** It is evident that the dependence of $E_{p,a}$ and $\upsilon^{1/2}$ was linear. Extrapolation of $E_{p,a}$ and $\upsilon^{1/2}$ to the potential axis gave the value of -0.27 V, the spontaneous film formation potential, E_f.

Analysis of convolution voltammograms showed that the reversible $E_{1/2}$ of Al deposition on aluminium in **Fig. 4.1.1**, was 0.0 V, more positive than -0.07 V on tungsten, in agreement with the conclusion that aluminium was easier to deposit on itself than on tungsten and foreign substrates. The diffusion coefficient was 8.0×10^{-7} cm^2 s^{-1}, which can be compared to the values of 1.03×10^{-6} cm^2 s^{-1} and 1.02×10^{-6} cm^2 s^{-1} for 0.19 M and 0.38 M melts diluted by 1,2-DCB [134]. The k° value of 1.37×10^{-4} cm s^{-1} was slightly smaller than 4.75×10^{-4} cm s^{-1} on tungsten.

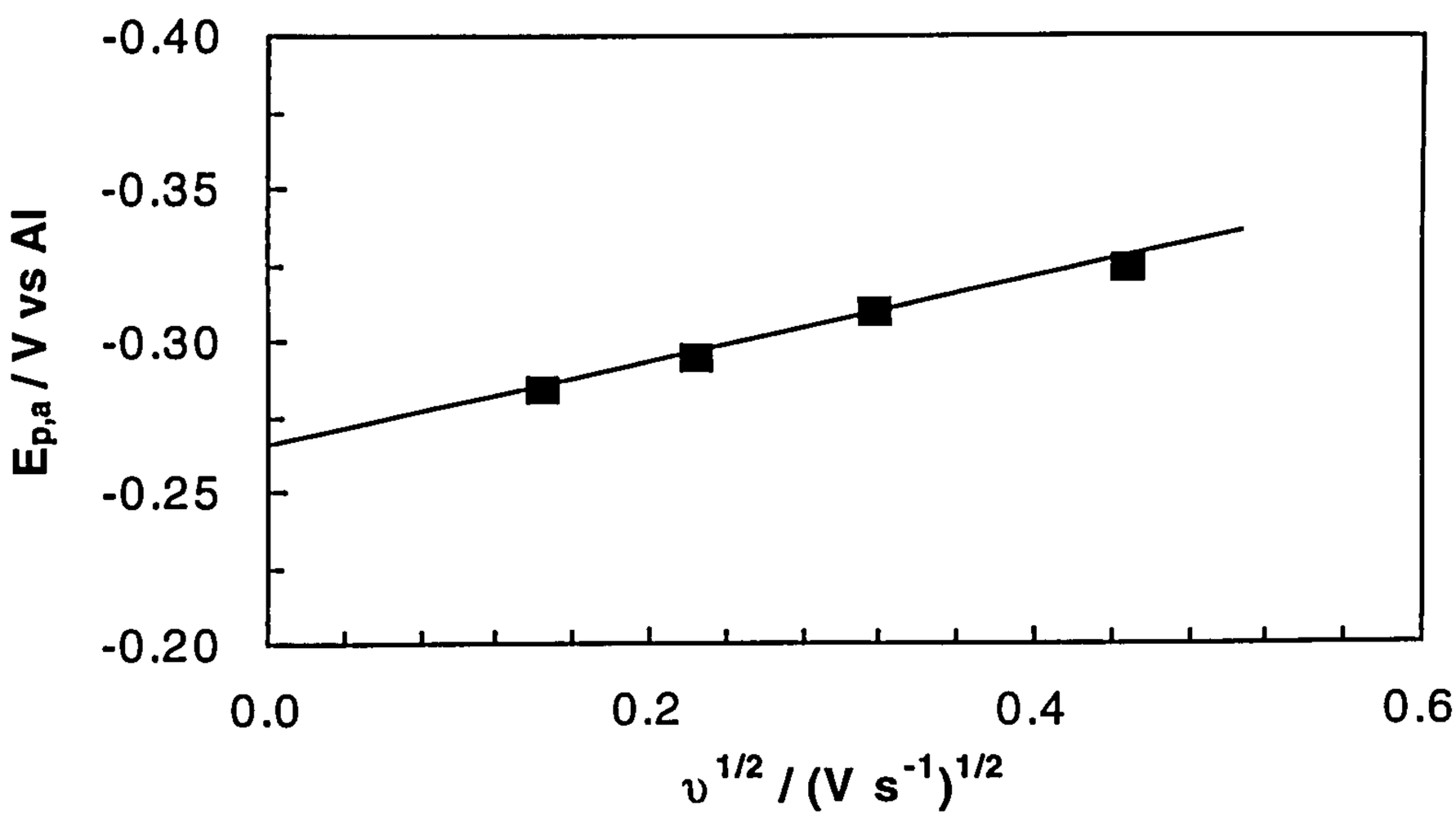

Fig. 4.1.7. $E_{p,a} \sim \upsilon^{1/2}$ plot for aluminium stripping derived from **Fig. 4.1.5.**

4.1.2 Nucleation Analysis

In order to gain greater insight into the nucleation processes occurring on aluminium electrodes, potential-step experiments were performed by stepping potential from 0.0 V, where no aluminium was deposited or stripped, to potentials sufficiently negative to initiate the nucleation process. The nucleation began at -0.10 V. Representative examples of transients obtained on aluminium are shown **Fig. 4.1.8**. Similar to the observations on tungsten, the currents on the rising portions of the transients linearly varied with $t^{1/2}$ which indicated that instantaneous nucleation was occurring followed by hemispherical diffusion controlled three-dimensional growth of the nuclei.

After passing the maxima, the transients exhibited the usual $t^{-1/2}$ current decay, *i.e.* mass-transport-controlled behaviour. Furthermore, analysis of dimensionless transients (**Fig. 4.1.9**) confirmed that a three-dimensional diffusion controlled instantaneous nucleation and growth process was involved in bulk aluminium deposition.

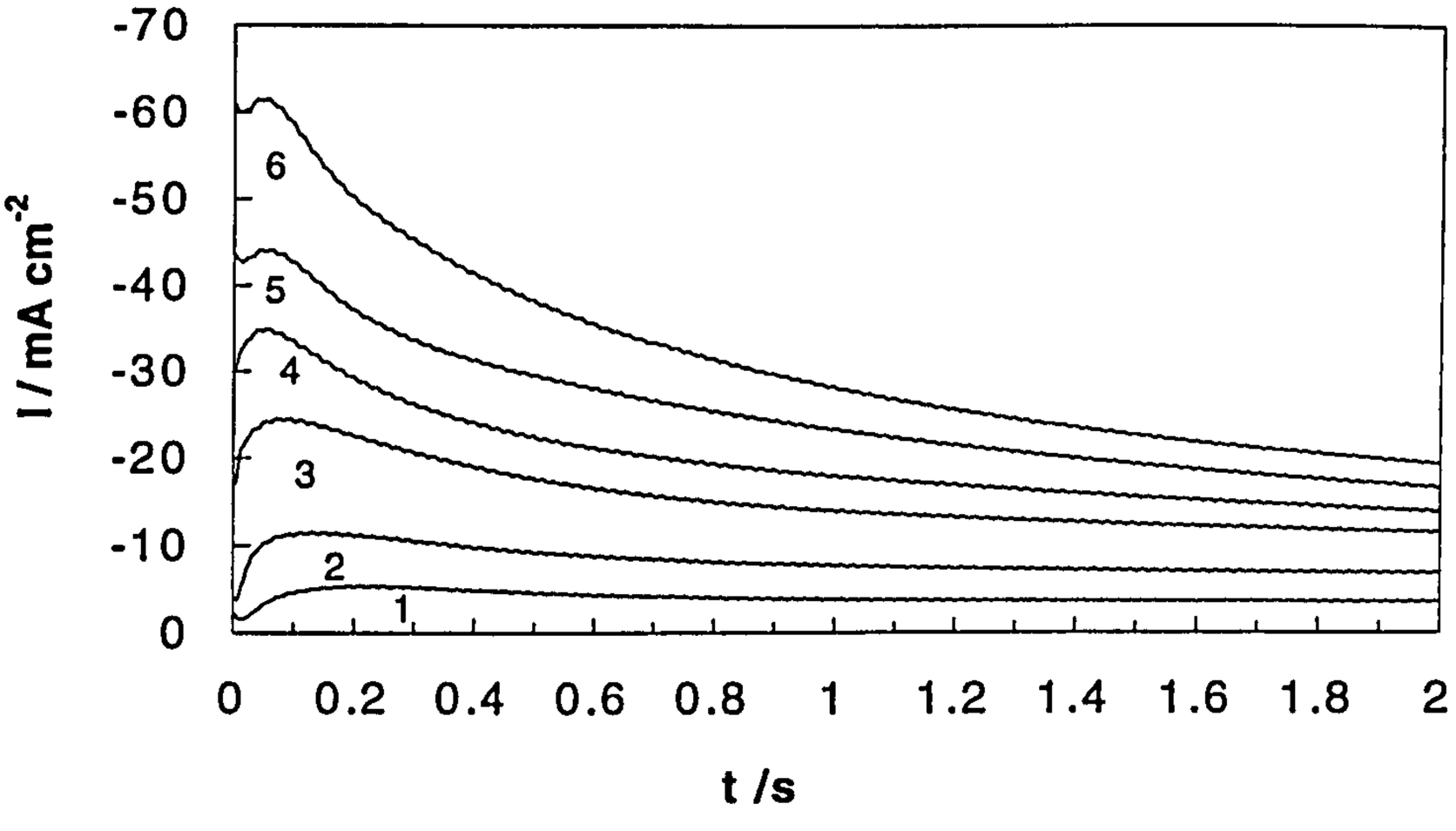

Fig. 4.1.8. A series of potentiostatic current transients for aluminium deposition on aluminium in a 2:1 $AlCl_3$- TMPAC melt at 25°C at various applied potentials (V): (1) -0.08; (2) -0.10; (3) -0.12; (4) -0.14; (5) -0.16; (6) -0.18.

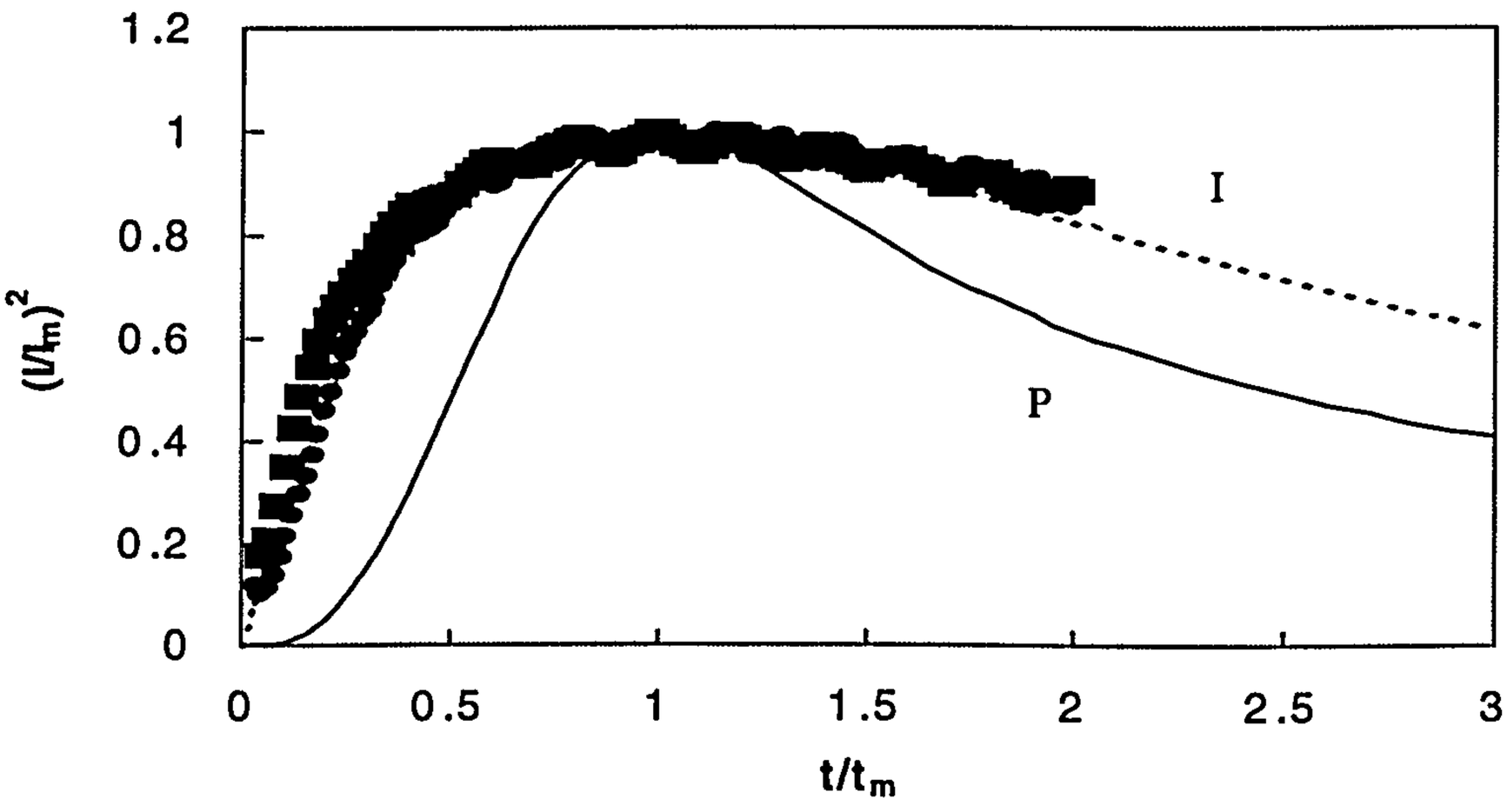

Fig. 4.1.9. Comparison of the dimensionless experimental data derived from **Fig. 4.1.8** with the theoretical models for diffusion controlled three dimensional instantaneous (I) and progressive (P) nucleation and growth.

4.2 GLASSY CARBON ELECTRODE

4.2.1 Voltammetric Studies

A cyclic voltammogram of aluminium deposition and stripping on glassy carbon in 2:1 $AlCl_3$-TMPAC melt at 0.1 V s^{-1} is shown in **Fig. 4.2.1.** As can be seen, some voltammetric features were identical to those on tungsten. Upon sweeping toward negative potentials, aluminium was initially deposited at -0.18 V and on the reverse scan stripping occurred at 0.0 V (**A'**). The deposition process involved nucleation, and the peak potential of apparent UPD (**B**) was approximately 0.1 V. Integration of deposition and stripping peaks indicated 92% of the deposited aluminium was recovered during stripping. A UPD charge of 6.48 mC cm^{-2} suggested that about 20 monolayers of aluminium surface phase was formed prior to bulk deposition. However, about 2 mA cm^{-2} of residual current density in the window indicated that glassy carbon was less pure than tungsten and aluminium. Besides this, a small irreversible anodic wave (**C**) was found at 2.22 V. It was unclear whether it resulted from impurities in the glassy carbon substrate or the oxidation of the electrode itself.

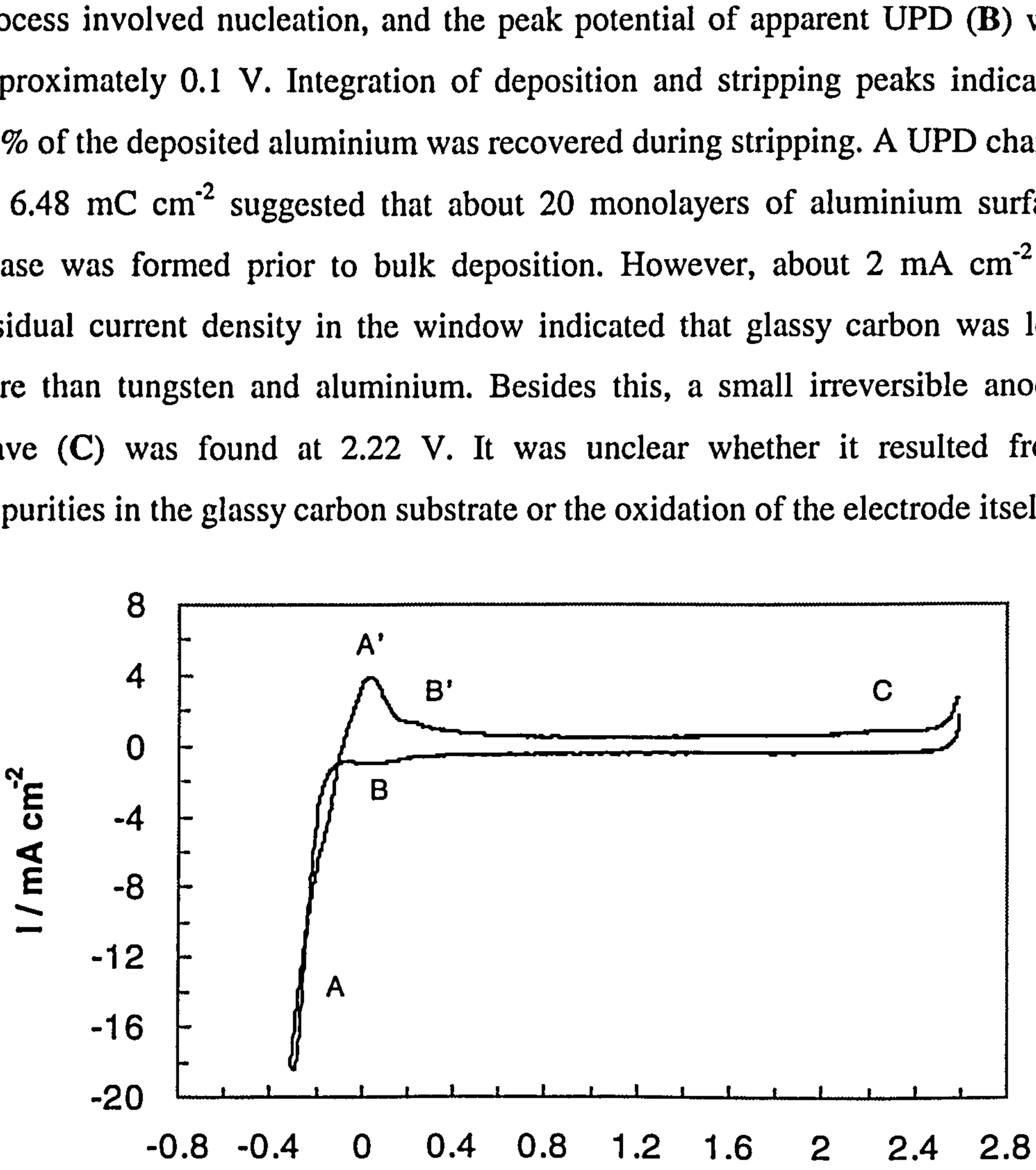

Fig. 4.2.1. Cyclic voltammograms for 2:1 $AlCl_3$-TMPAC melt on glassy carbon at 25°C. Sweep rate was 0.1 V s^{-1}.

Further voltammograms (**Fig. 4.2.2**) were recorded at various sweep rates. The peak current density of wave **C** increased linearly with sweep rate. Two small prewaves **A** and **B** at *ca.* 1.0 V and 1.6 V, respectively, were observed at high sweep rates (1.0 V). They could be due to impurities in the glassy carbon. Moreover, the UPD waves were very ambiguous and totally disappeared at higher sweep rates. It is noteworthy that all prewaves and the apparent UPD waves above were vanished after several potential cycles, proving that these wave were strongly dependent upon the surface state of the glassy carbon electrode. So, pre-treatment of the glassy carbon was very important prior to collecting data.

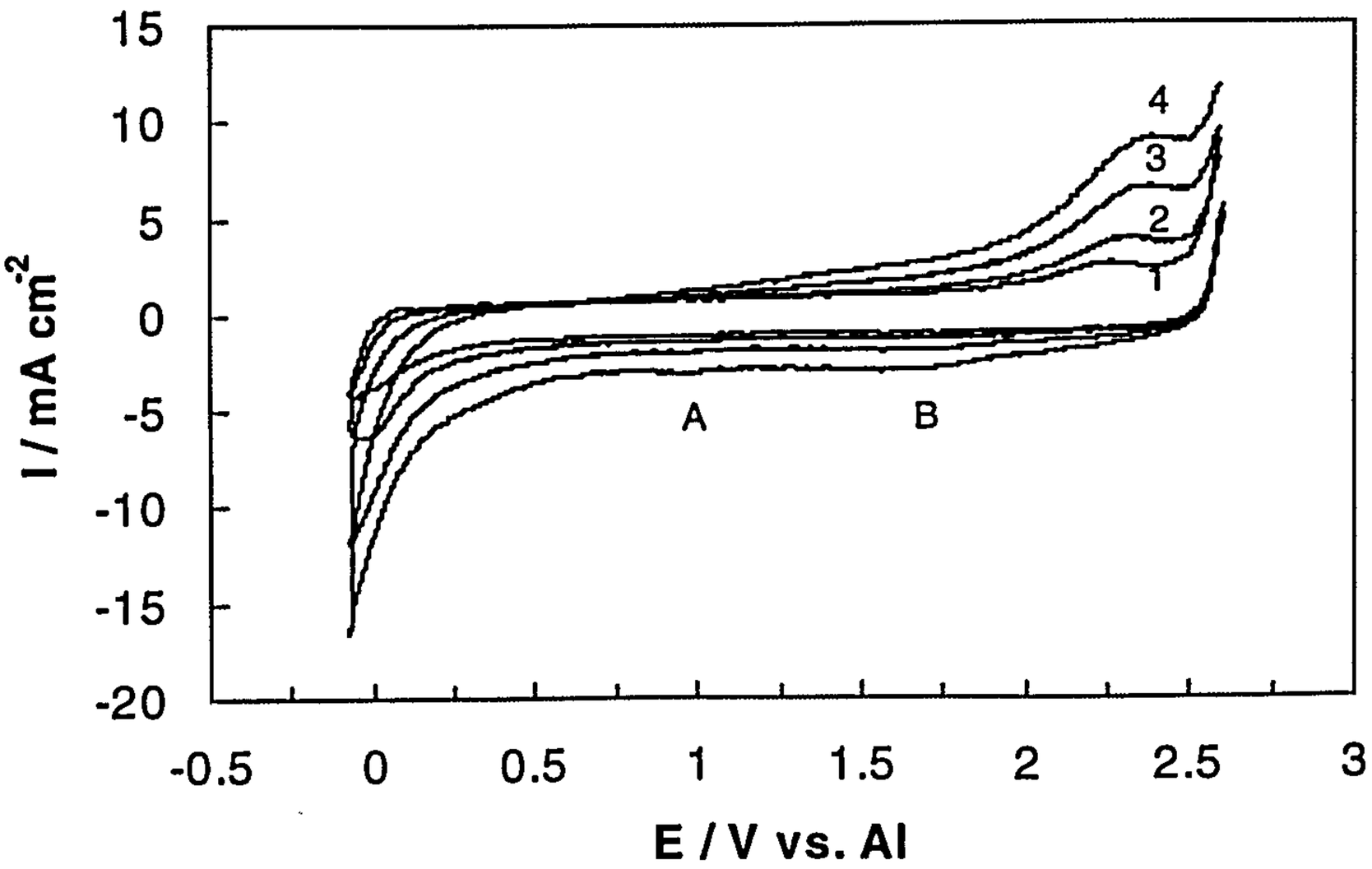

Fig. 4.2.2. Voltammograms for 2:1 $AlCl_3$- TMPAC melt on glassy carbon at 25°C. Sweep rates were: (1) 0.1; (2) 0.25; (3) 0.5; (4) 1.0 V s^{-1}.

4.2.2 Bulk Deposition of Aluminium

Fig. 4.2.3 shows voltammograms of aluminium bulk deposition and stripping on glassy carbon at various sweep rates with the pre-treatment of electrode described in **Sec.2.1.3**. No UPD waves were seen as expected. In agreement with those on aluminium and tungsten, $E_{p,c}$ shifted negatively, and $|E_{p,c} - E_{p,a}|$ increased with increasing sweep rates (**Table 4.2.1**). Furthermore, $I_{p,a}/I_{p,c}$ was less than unity. $|E_{p,c} - E_{p,a}|$ was greater than the 0.02 V theoretical

value expected for reversible process, and $I_{p,c} \sim \upsilon^{-1/2}$ plots were linear (**Fig. 4.2.4**). Taken together, these results suggested the deposition of aluminium on glassy carbon was quasi-reversible and diffusion controlled.

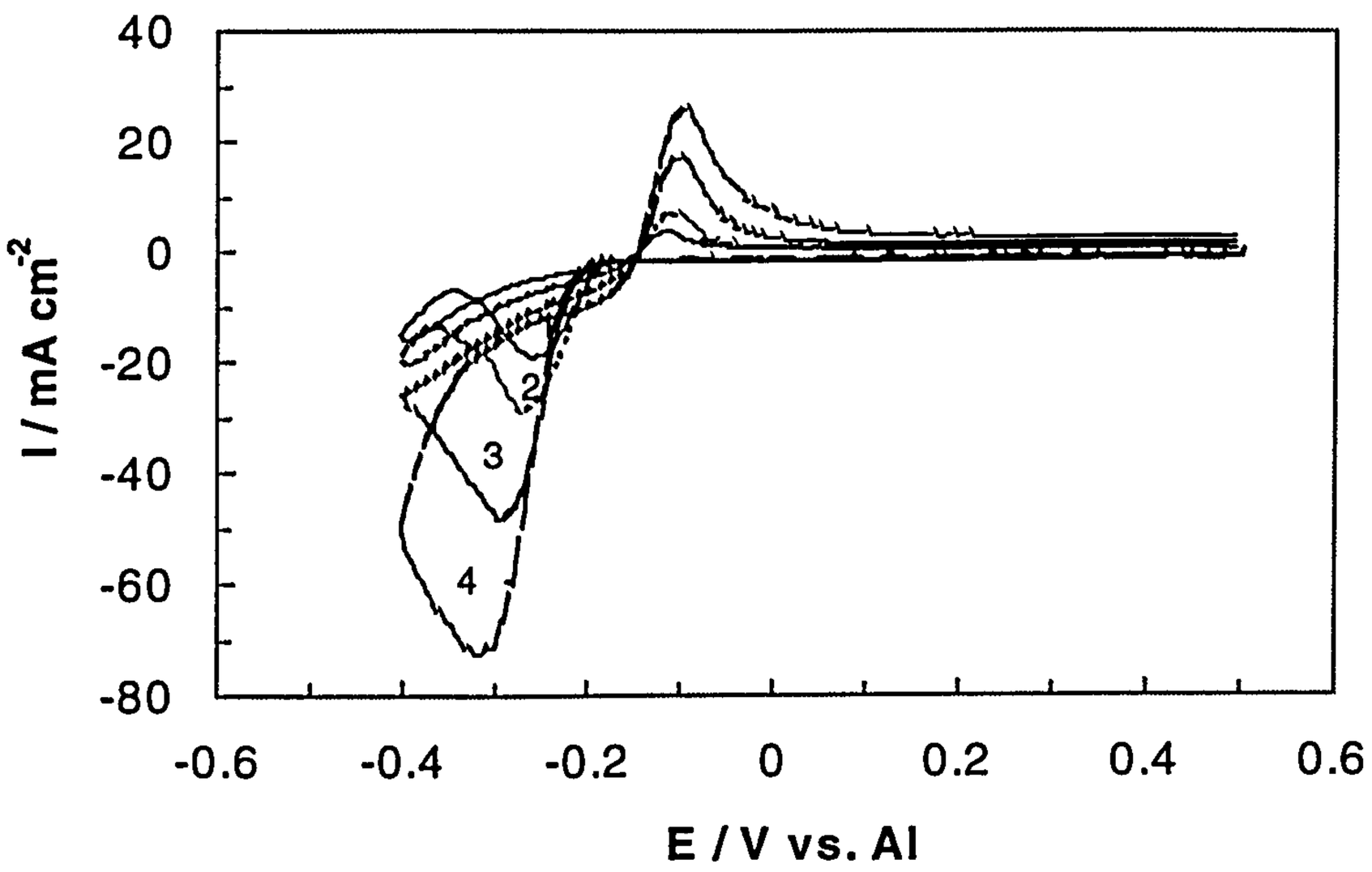

Fig. 4.2.3. Voltammograms for deposition and stripping of aluminium on glassy carbon from 2:1 $AlCl_3$-TMPAC melt within a narrow potential range at 25°C. Sweep rates were (1) 0.20; (2) 0.10; (3) 0.05; (4) 0.02 V s^{-1}.

Table 4.2.1. Voltammtric data for aluminium deposition on glassy carbon from 2:1 $AlCl_3$-TMPAC melts

υ (V s^{-1})	$I_{p,c}$ (mA cm^{-2})	$I_{p,c}\,\upsilon^{-1/2}$ (mA cm^{-2} $V^{-1/2}$ $s^{1/2}$)	$I_{p,a}/I_{p,c}$	$E_{p,c}$ (V)	$\lvert E_{p,c} - E_{p,a} \rvert$ (V)
0.01	-18.73	-1.87	0.22	-0.26	0.14
0.02	-28.51	-4.03	0.27	-0.27	0.16
0.05	-48.06	-10.75	0.36	-0.30	0.19
0.1	-72.37	-22.88	0.36	-0.32	0.22

Similar to tungsten (**Fig. 3.1.2**), second current loops were found at low sweep rates. Obviously, an alloying effect, one of the possible explanations for the current loop on tungsten, was excluded because glassy carbon is not metal. Thus, it could be assigned to other possibilities, such as the reduction of $TMPA^+$ or $AlCl_4^-$ ions, especially the latter. The loop increased with decreasing sweep rate and at lower sweep rate, more charge and more deposition occurred. The increased charge would result in a local concentration of $AlCl_4^-$ ions much

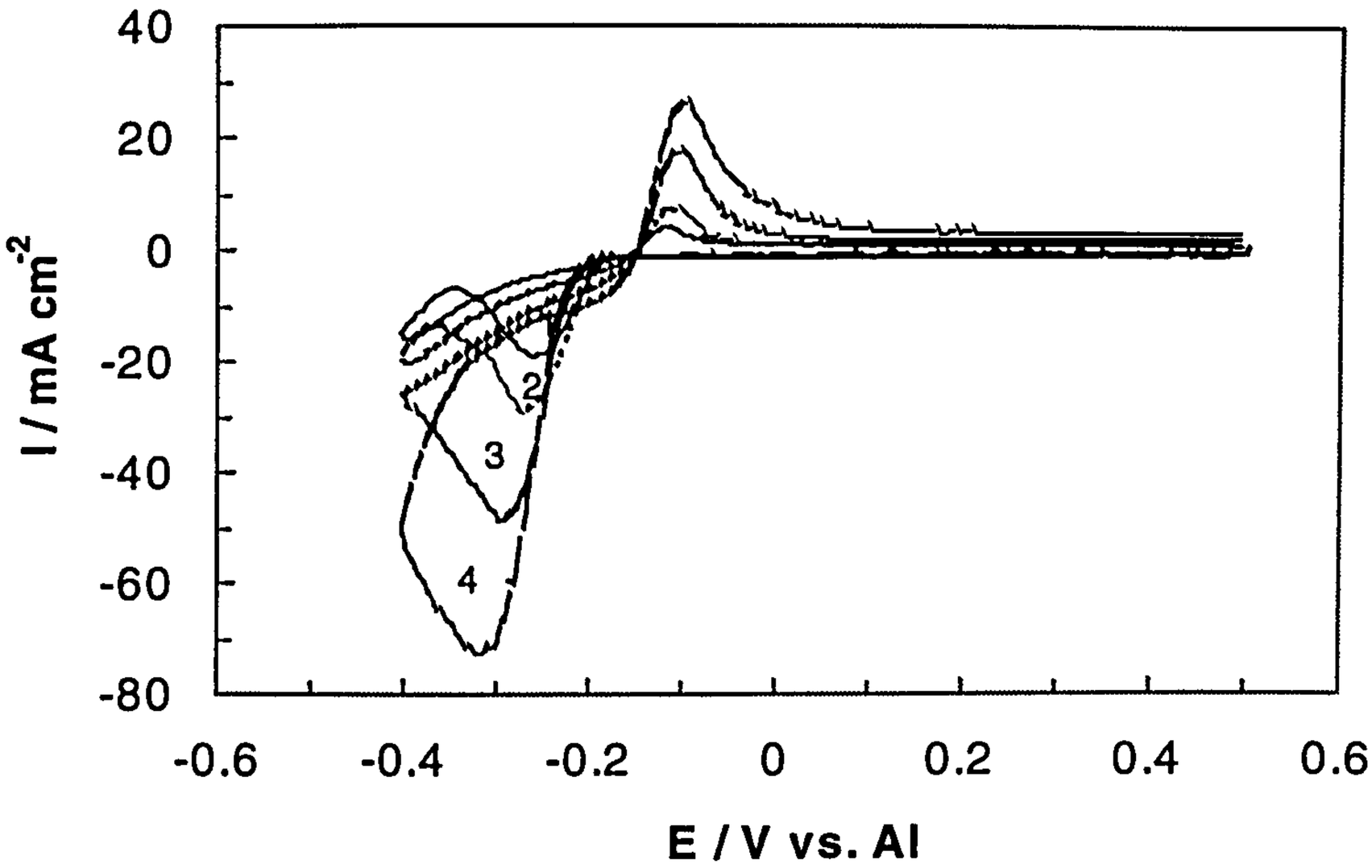

Fig. 4.2.3. Voltammograms for deposition and stripping of aluminium on glassy carbon from 2:1 $AlCl_3$-TMPAC melt within a narrow potential range at 25°C. Sweep rates were (1) 0.20; (2) 0.10; (3) 0.05; (4) 0.02 V s^{-1}.

Table 4.2.1. Voltammtric data for aluminium deposition on glassy carbon from 2:1 $AlCl_3$-TMPAC melts

υ (V s^{-1})	$I_{p,c}$ (mA cm^{-2})	$I_{p,c}\,\upsilon^{-1/2}$ (mA cm^{-2} $V^{-1/2}$ $s^{1/2}$)	$I_{p,a}/I_{p,c}$	$E_{p,c}$ (V)	$\lvert E_{p,c} - E_{p,a}\rvert$ (V)
0.01	-18.73	-1.87	0.22	-0.26	0.14
0.02	-28.51	-4.03	0.27	-0.27	0.16
0.05	-48.06	-10.75	0.36	-0.30	0.19
0.1	-72.37	-22.88	0.36	-0.32	0.22

Similar to tungsten (**Fig. 3.1.2**), second current loops were found at low sweep rates. Obviously, an alloying effect, one of the possible explanations for the current loop on tungsten, was excluded because glassy carbon is not metal. Thus, it could be assigned to other possibilities, such as the reduction of $TMPA^+$ or $AlCl_4^-$ ions, especially the latter. The loop increased with decreasing sweep rate and at lower sweep rate, more charge and more deposition occurred. The increased charge would result in a local concentration of $AlCl_4^-$ ions much higher than in the bulk. In some sense, the electrode acted as an aluminium-modified electrode and the second current loop typical of nucleation could arise from the reduction of $AlCl_4^-$ ions.

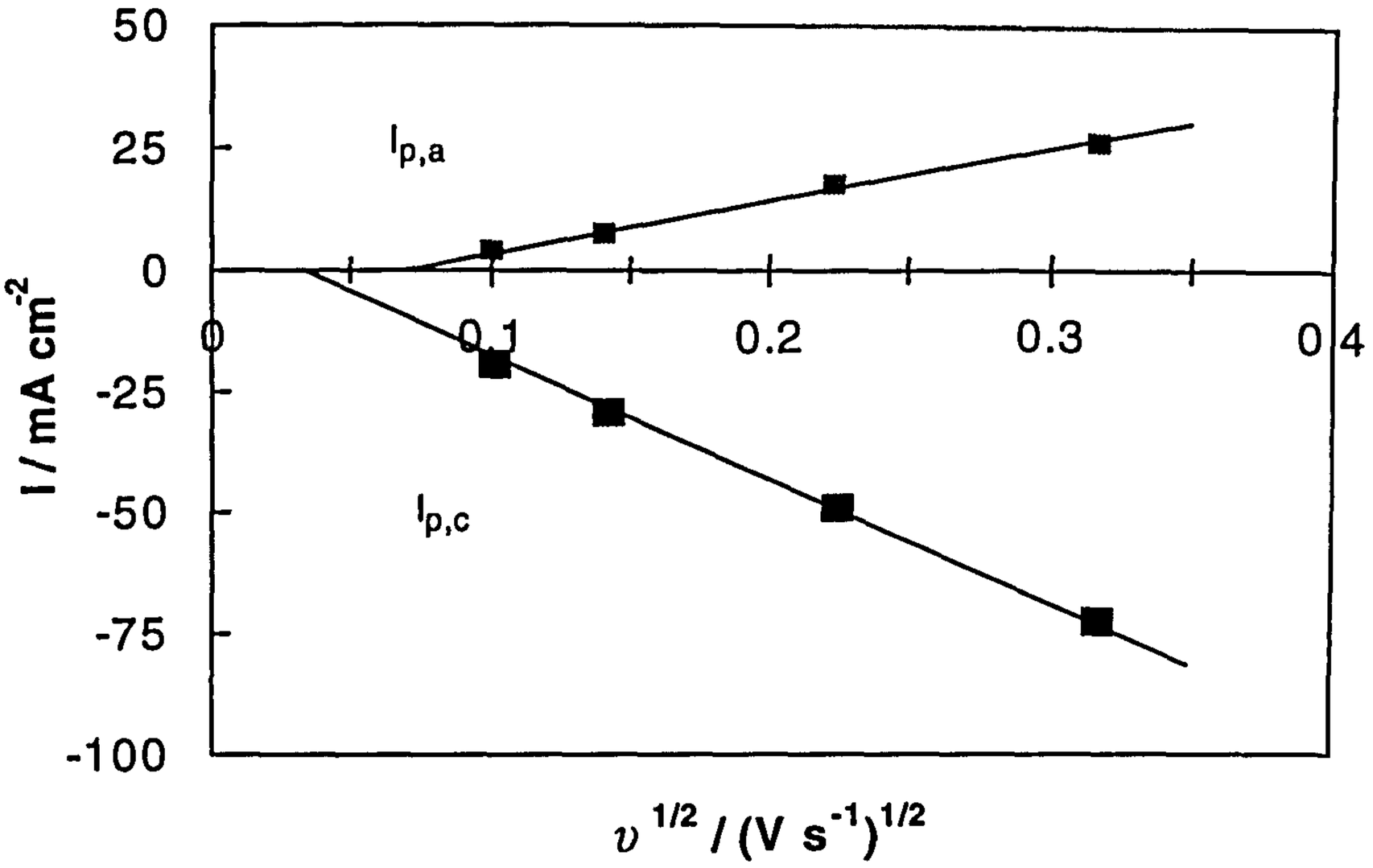

Fig. 4.2.4 Plot of cathodic and anodic peak currents vs. square root of sweep rate for deposition and stripping of aluminium on glassy carbon in 2:1 $AlCl_3$-TMPAC melt at 25°C.

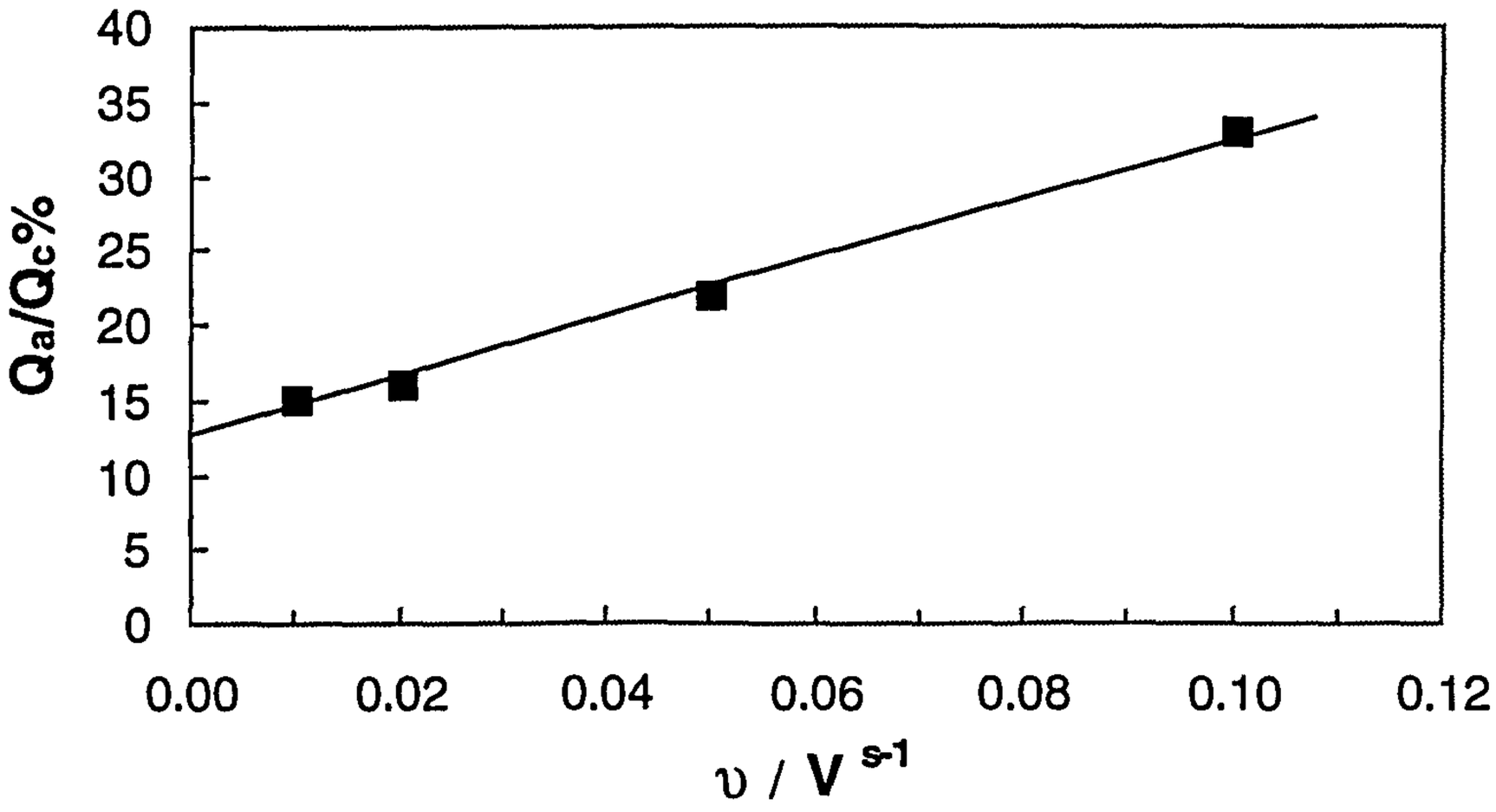

Fig. 4.2.5 . The coulombic efficiency of aluminium plating and stripping on glassy carbon as a function of sweep rate at 25°C.

In contrast to a coulombic efficiency over 90% on tungsten, the coulombic efficiency on glassy carbon was remarkably low, below 35%, and decreased linearly with increasing sweep rate (**Fig. 4.2.5**). The very low

coulombic efficiency for the latter could be attributed to the poor adhesion of aluminium deposits to the glassy carbon substrate. It was observed in $AlCl_3$-NaCl melts [185] that small aluminium pieces fell off into the melt during deposition and stripping and that small aluminium particles remained on the electrode surface during chlorine gas evolution, apparently adhering poorly to the electrode.

4.2.3 Nucleation Analysis

Analysis of the nucleation processes on glassy carbon was similar to that on aluminium electrode. Potential-step experiments were performed by stepping potential from 0.0 V, where no aluminium electrode was deposited, to potentials sufficiently negative to initiate the nucleation process. Nucleation was initiated at -0.20 V. Representative examples of transients obtained on aluminium are shown **Fig. 4.2.6.** Similar to the observation on tungsten, the currents on the rising porting of transients linearly varied with $t^{1/2}$ which indicated that instantaneous three-dimensional nucleation was occurring followed by hemispherical diffusion controlled growth of the nuclei. After passing the maxima, the transients exhibited the usual $t^{-1/2}$ current decay, *i.e.* mass-transport controlled behaviour. Furthermore, analysis of dimensionless transients (**Fig. 4.2.7**) confirmed that a three-dimensional diffusion controlled instantaneous nucleation and growth process was involved in bulk aluminium deposition. The calculated chronoamperometric data are collected in **Table 4.2.2.**

Table 4.2.2. Chronoamperometric data for aluminium nucleation on glassy carbon

E *vs* Al (V)	$10^3 I_m$ (A cm^{-2})	t_m (s)	$10^6 (I_m)^2 (t_m)$ (A cm^{-2} s)	$10^5 D$ (cm^2 s^{-1})	$10^{-6} N$ (sites cm^{-2})
-0.22	-27.39	0.15	11.25	0.78	1.34
-0.24	-36.03	0.10	12.98	0.88	1.82
-0.26	-41.59	0.11	19.03	1.01	1.45
-0.28	-45.73	0.12	25.09	1.17	1.12
-0.30	-56.68	0.09	28.91	1.35	1.40

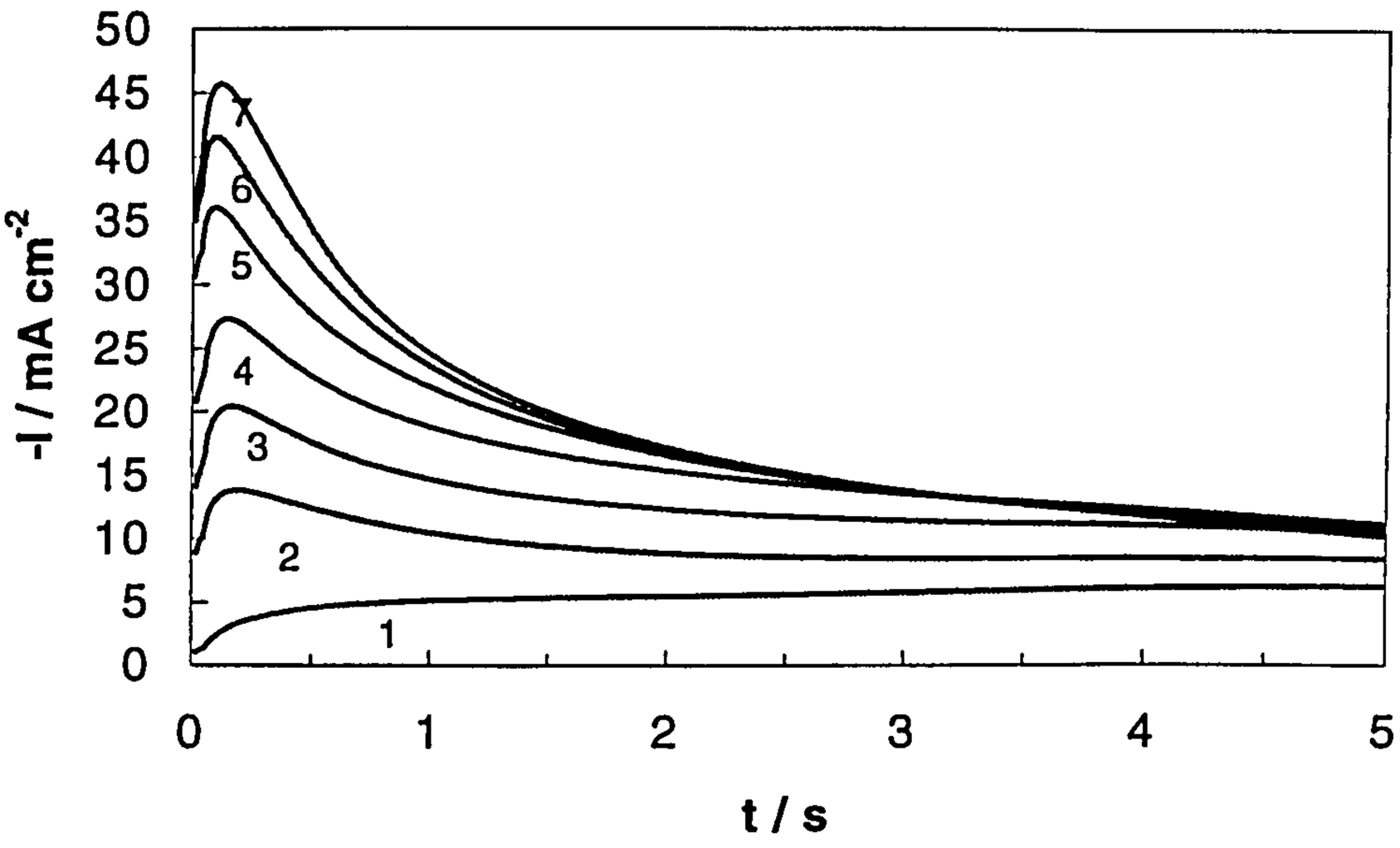

Fig. 4.2.6. A series of potentiostatic current transients for aluminium deposition on glassy carbon in 2:1 $AlCl_3$- TMPAC melt at 25°C at various applied potentials (V): (1) -0.15; (2) -0.20; (3) -0.22; (4) -0.24; (5) -0.26; (6) -0.28.

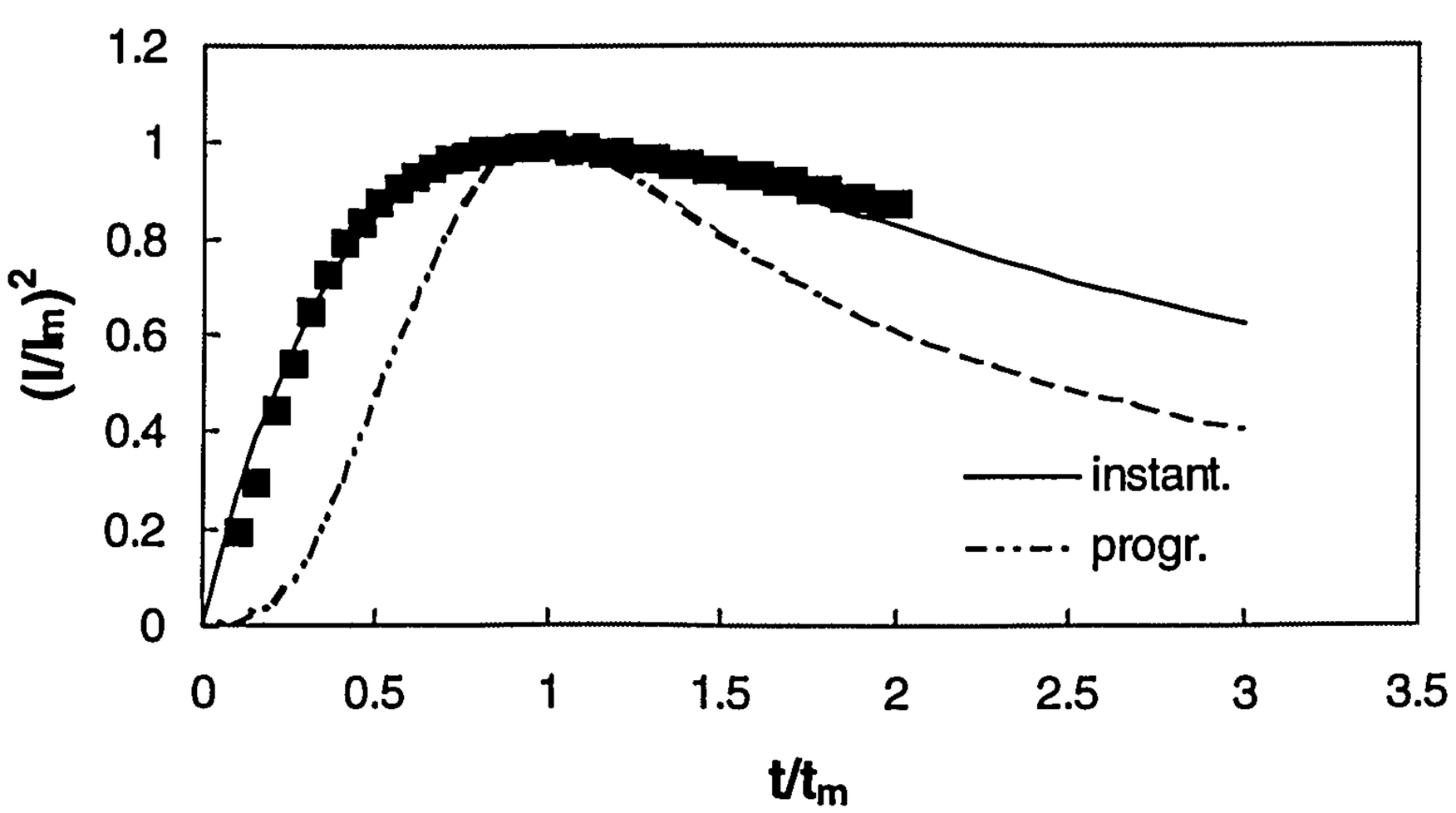

Fig. 4.2.7. Comparison of the dimensionless experimental data derived from **Fig. 4.2.6** with the theoretical models for diffusion controlled three dimensional instantaneous and progressive nucleation and growth.

CHAPTER 5

ELECTRODEPOSITIONS OF ALUMINIUM AND ITS ALLOYS ON NICKEL AND PLATINUM

5.1 INTRODUCTION

Since the role of UPD in the formation of certain alloys, especially aluminium alloys, is well known [213], it is necessary to understand the UPD behaviour of aluminium on various metal substrates from room temperature molten salts. Therefore, nickel and platinum were also studied as working electrodes for aluminium deposition from 2:1 $AlCl_3$-TMPAC melts.

A growing interest in the electrodeposition of new alloys and in fundamental processes controlling alloy formation has led to renewed interest in UPD phenomena [188,214,215,216]. Because of the electrochemical inertness of platinum, little information about Al-Pt alloys has been reported. In contrast, the electrodeposition of a number of Al-Ni alloys has been demonstrated from inorganic chloroaluminate molten salts, mainly acidic $AlCl_3$-NaCl melts [188]. Recently, Moffat has proposed an UPD mechanism for the electrodeposition of Al-Ni alloys from an $AlCl_3$-rich $AlCl_3$-NaCl molten salt electrolytes [188]. In this system, the Al-Ni alloys formed at potentials positive of bulk Al (*i.e.* in the aluminium UPD region) and negative of bulk Ni electrodeposition. Additionally, the composition of the Al-Ni alloys was found to be a function of the deposition potential and was correlated with the free energy of alloy formation.

Electrodeposition of similar Al-Ni alloys has been reported in room temperature chloroaluminate molten salt electrolytes [217,218,219]. More recently,

the formation of Al-Ni alloys in a $AlCl_3$-BPC melt was confirmed using scanning electron microscopy/energy dispersive spectroscopy (SEM/EDS) analysis of electrodeposits [220]. They found that ca. 10 atom percent Al was incorporated into the alloy for potentials positive of bulk Al electrodeposition. Although the formation of these Al-Ni alloys in room temperature molten salts was previously disputed [221], the electrodeposition of Al-Ni alloys from the $AlCl_3$- MEIC melt has recently been confirmed [220].

Generally, a necessary condition required for binary alloy, AB, formation is given by the equalities [188]:

$$E_A + \eta_A = E_B + \eta_B \tag{5.1.1}$$

$$E_A^\circ + \frac{RT}{nF}\ln(\frac{a_{A^+}}{a_A}) + \eta_A = E_B^\circ + \frac{RT}{nF}\ln(\frac{a_{B^+}}{a_B}) + \eta_B \tag{5.1.2}$$

where E°_i (i = A and B) is the thermodynamic reversible potential given by the Nernst equation and η_i represents the kinetic overpotential or degree of supersaturation for metal i. This general statement has several limiting cases which have been outlined in the classic treatises by Brenner [222] and Gorbunova and Polukarov [223]. The reversible potentials, and the metallurgy of several intermetallic compounds were measured [224]. The effect of intermetallic compound formation is represented in **Eqn. 5.1.2** by the activity, a_i, of the alloy constituents, yielding a positive shift of the reversible potential for each constituent away from that characteristic for the pure state. This is equivalent to the formal description of the phenomenon of UPD [215]. Consequently, it is to be expected that UPD phenomena play a central role in alloy formation in these systems. In fact, in many UPD systems, alloy formation by interdiffusion of the substrate and UPD layer is also well known [213,225].

In contrast, the role of UPD in the deposition of thick alloy electrodeposits has received less attention. In this instance UPD of more active species may occur

simultaneously with the deposition of the more noble species, such as the deposition of compound semiconductors, like CdTe [226]. Investigations of Ni and Pt working electrodes in 2:1 $AlCl_3$-TMPAC melts could present opportunities to explore the synthetic pathways of Al-Ni or Al-Pt alloy formation in more detail. Consequently, a variety of electrochemical techniques were implemented which allowed a clear separation and identification of the processes involved in phase formation.

Chapter 5. ELECTRODEPOSITIONS OF ALUMINIUM AND ITS ALLOYS ON Ni AND Pt

5.2 NICKEL

5.2.1 Voltammetric Behaviour on Nickel electrode

The voltammetric behaviour of the 2:1 $AlCl_3$-TMPAC melt with nickel electrodes was investigated. A representative cyclic voltammogram at 0.1 V s^{-1} on the smaller nickel electrode is shown in **Fig. 5.2.1**. The potential sweep began at 2.7 V *vs.* the Al reference electrode. The first cathodic wave **A** started at 0.5 V and rose to a peak at 0.2 V, similar to UPD of aluminium on tungsten. However, the peak current density on nickel was much higher than that on tungsten. Passing the peak potential, a current plateau extended to approxmately -0.22 V, where the second cathodic peak (**B**) started and peaked at -0.36 V, associated with aluminium deposition. On the reverse scan, four anodic waves were observed. Waves **B′** at -0.16 V and **A′** at 0.5 V seemed to correspond to stripping peaks of **B** and **A**. Two other larger waves were found at 1.0 V (**C**) and 1.34 V (**D**), respectively.

5.2.2 Charge Analysis

The charge analysis of **Fig. 5.2.1** is shown in **Fig. 5.2.2**. The total coulombic efficiency Q_a/Q_c was 1.35, greater than unity. However, $Q_{A'}/Q_A$ was approximately unity whereas $Q_{B'}/Q_B$ was only 0.35, indicating that most of the charge passed in deposition in wave **A** was released while only a small part of the deposited aluminium (**B**) was dissolved in peaks **B′**. In addition, $Q_{A'+B'}/Q_c$ was 0.71, also suggesting some residual deposits were retained on the surface of the electrode. It can be seen in **Fig. 5.2.2** that waves **C** and **D** have occurred before $Q_a/Q_c = 1$. Therefore, the stripping charge for the residual deposits has partially contributed to that for waves **C** and **D**. Since the residual deposits contained the rest of the aluminium after peaks **A′** and **B′**, the stripping of the remaining aluminium was involved in peaks **C** and **D.**

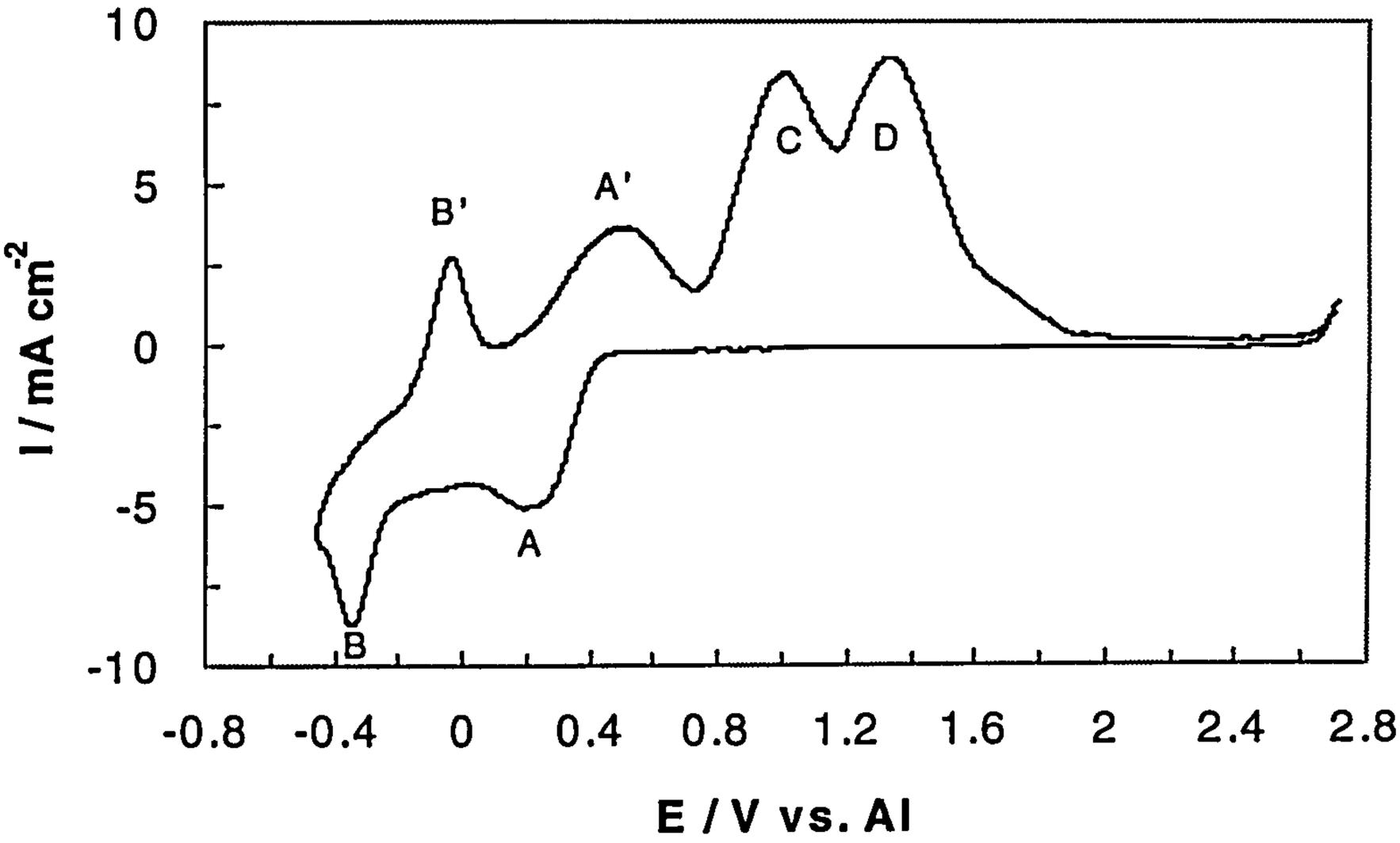

Fig. 5.2.1. Cyclic voltammograms of 2:1 $AlCl_3$-TMPAC melt on nickel wire (ϕ=2 mm) at 25°C. Sweep rate: 0.1 V s^{-1}.

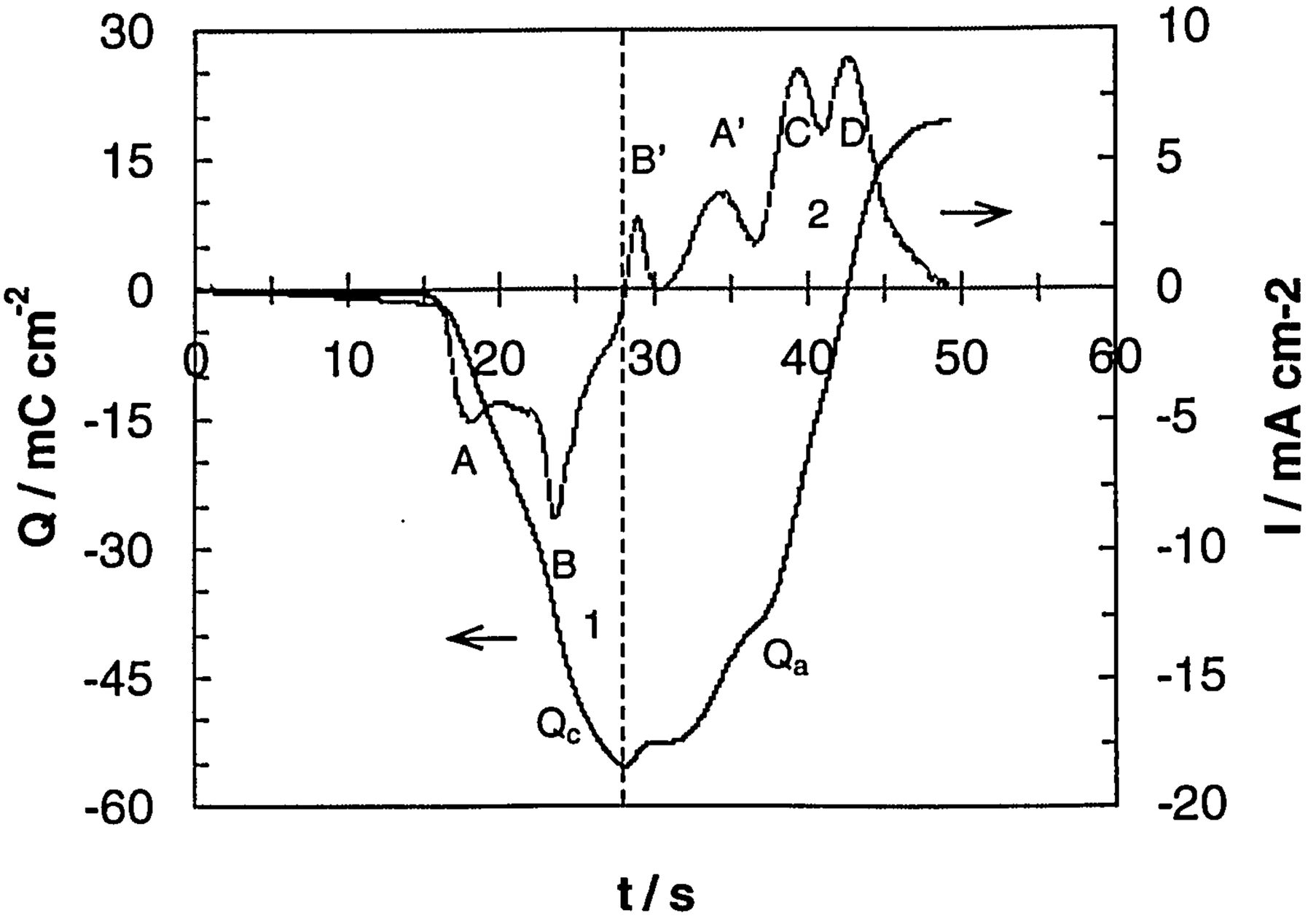

Fig. 5.2.2. Charge analysis of aluminium deposition and stripping (1) and its corresponding current-time transient (2) derived from **Fig. 5.2.1.**

Considering that the total coulombic efficiency was greater than unity, similar to that found on an aluminium electrode, it is reasonable to assume that the extra charge resulted from the dissolution of the nickel electrode. Since Q_{C+D} was nearly 80% of Q_a and much greater than Q_c, seemingly, such a large charge could not come from only the stripping of the remaining aluminium, so dissolution of the nickel electrode was indicated.

5.2.3 Deposition and Stripping of Ni(II) Species

To better understand waves **C** and **D**, a series of cyclic voltammetric experiments at different negative switching potentials were carried out. The initial potential was held at 2.0 V, where no nickel deposition took place, for 5 s prior to every scan. Voltammograms recorded as a function of the switching potential, E_λ , are shown in **Figs. 5.2.3** and **5.2.4**. In **Fig. 5.2.3** the voltammogram with E_λ =0.35 V (**curve 1**) shows that the wave **A** in **Fig. 5.2.1** started at 0.55 V with a very small cathodic current density I_A. The reverse scan exhibited two anodic waves (**C** and **D**) with peak potentials E_p 0.94 V and 1.3 V, respectively. Extending E_λ to 0.3 V (**curve 2**), I_A, $I_{p,C}$, and $I_{p,D}$ increased greatly.

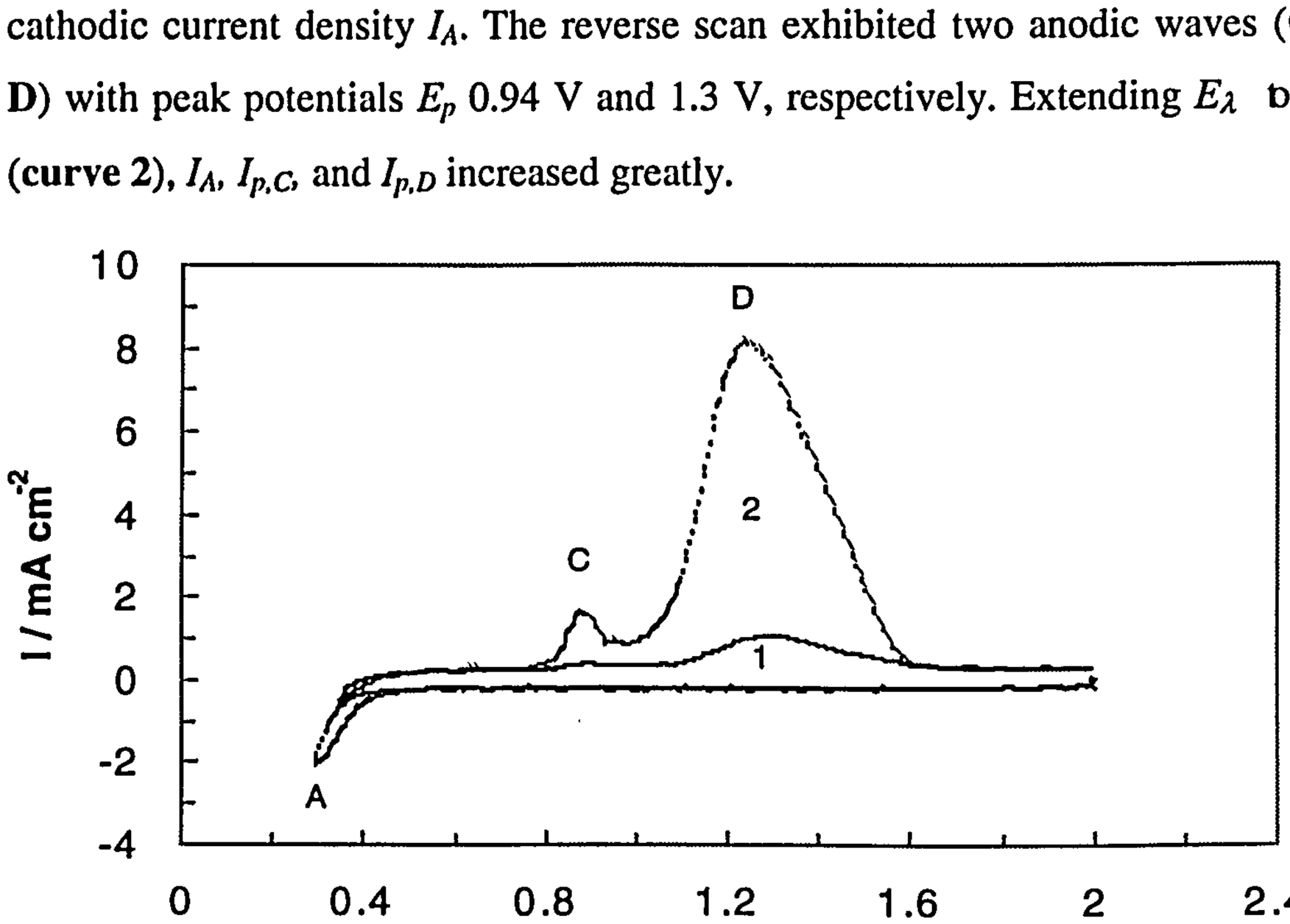

Fig. 5.2.3. Cyclic voltammograms of 2:1 $AlCl_3$-TMPAC melt on nickel at 25°C. Switching potentials: (1). 0.35 V; (2). 0.3 V. Sweep rate: 0.10 V s^{-1}.

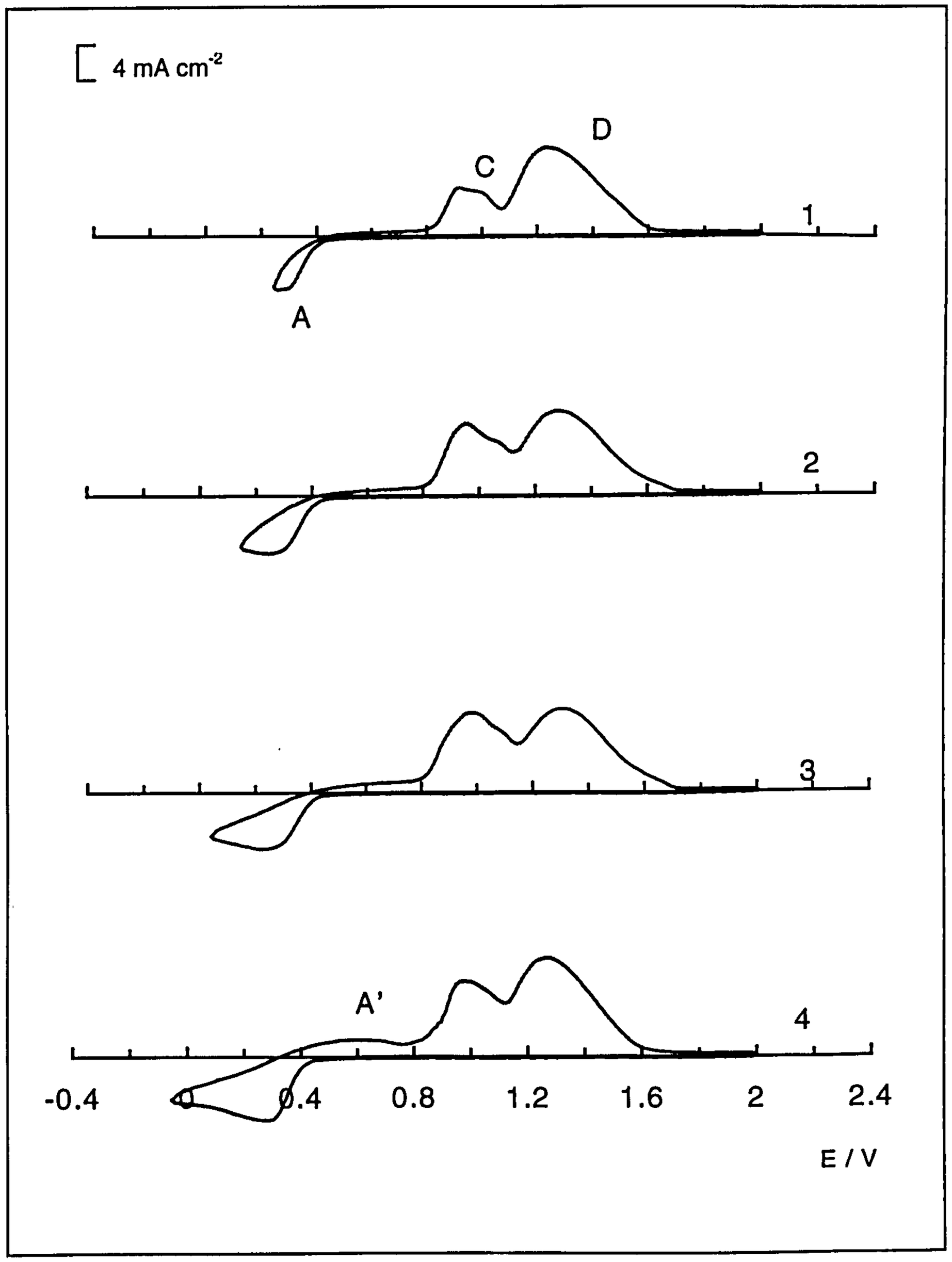

Fig. 5.2.4. Cyclic voltammograms of 2:1 $AlCl_3$-TMPAC melt with nickel electrodes at 25°C. Switching potentials: (1) 0.25 V; (2) 0.15 V; (3) 0.05 V; (4) -0.10 V. Sweep rate: 0.10 V s^{-1}.

As E_λ was made progressively more negative, from 0.25 to -0.05 V (**Fig. 5.2.4**), the peak **A** occurred at 0.22 V (**curve 2**) initially, and then E_p shifted slightly to 0.28 V (**curve 4**). Meanwhile, the anodic current densities of the plateau region between 0.5 and 0.7 V increased slowly and finally formed a much broader wave **A′** with E_λ = -0.05 V (**curve 4**). Moreover, when E_λ >0.0 V (**curve 1 ~ 3**), I_p of waves **C** and **D** increased, $E_{p,C}$ moved positively and $E_{p,D}$ shifted negatively. Besides these peaks, two shoulders were found following peaks **C** and **D**, respectively. As E_λ decreased below 0.0 V (**curve 4**), accompanied by the occurrence of wave **A′**, $I_{p,C}$ decreased while $I_{p,D}$ continued to rise.

According to the previous results on tungsten and glassy carbon, the peak **A** might be related to a UPD process involving an Al-Ni alloying effect because of the proximity of peak **A** to the onset of aluminium UPD. However, compared with the very small charge, 3.52 mC cm^{-2}, for UPD on tungsten at 0.1 V s^{-1}, the large values for peak **A**, from 18 ~ 31 mC cm^{-2} (**curves 1 ~ 4** in **Fig. 5.2.4**), suggested that the UPD of aluminium or an alloy was more obvious on nickel than on tungsten. Integration of **Fig. 5.2.3** gives a coulombic efficiency of about 90% for Q_A/Q_C, which was typical for all curves with E_λ positive of 0.0 V, indicating that most of the deposition charge was stripped before peak **D** occurred. Thus, peak **C** corresponded to the de-alloying process of the alloy deposition. Notably, although the fresh melt was initially nickel free, the nickel electrode could be dissolved at the holding potential of 2.0 V, resulting in the existence of a small amount of nickel ions in the melt.

Similar results were reported in a 5.0×10^{-2} M solution of Ni(II) on a glassy carbon electrode in 2:1 $AlCl_3$-MEIC melts [218], where the nickel deposition wave with E_p = 0.38 V was considered to result from the reduction of Ni(II) solvated by the melt:

$$Ni^{2+} + 2e^- = Ni \qquad (5.2.1)$$

It should be noted that the solutions of Ni(II) in those melt were prepared by the controlled potential coulometric anodisation of the nickel electrode at an applied potential of 1.40 V. Accordingly, in the present work, Ni(II) species contributing to the peak **A** should at least in part come from the dissolution of nickel electrode at the holding potential of 2.0 V. However, the role of Ni(II) species was by the small area nickel electrodes and the shorter holding times (only 5 s) at the beginning of the sweeps.

The characteristics of peak **D** were still less clear. Like the results on aluminium, it might be assigned to the dissolution of the nickel electrode at very positive potentials. However, it seemed to be impossible that such a large amount of nickel was dissolved from the electrode. On the other hand, unlike the case of aluminium electrode, where stripping of the aluminium deposits and the dissolution of the aluminium electrode formed a continuous wave, in the present case waves **C** and **D** were well separated. Considering the $Al_2Cl_7^-$ and Cl^- concentrations in the melt, wave **D** was likely to result from the following reaction:

$$Ni + nAl_2Cl_7^- \rightleftharpoons [Ni(Al_2Cl_7)_n]^{(2-n)} + 2e^- \qquad (5.2.2)$$

or

$$Ni + nCl^- \rightleftharpoons [NiCl_n]^{(2-n)} + 2e^- \qquad (5.2.3)$$

It is well known that divalent nickel ions exist in the $NiCl_4^{2-}$ state in concentrated chloride molten salts [227,228,229], although no complexed nickel ions were found in the acidic $AlCl_3$-BPC melt [217].

If the nickel electrode was dissolved by forming nickel complexes, after the first scan the concentration of Ni(II) species in the melt should increase, resulting in more deposition of nickel during the following scan, which could be the main source of Ni(II) species for the deposition of a Ni-rich alloy. Thus, the nickel deposits in the alloy likely resulted from the reduction of Ni(II) complexes rather than Ni^{2+} ions. This inference has been substantiated by the addition of Ni(II) species to the melt (see **Chapter 7**). Also, the energy dispersive x-ray spectroscopy

(EDS) analysis of Ni-Al alloy electrodeposited from 2:1 $AlCl_3$-MEIC melts [218] found the presence of 20 (atom%) of chlorine in the deposits.

Fig. 5.2.5 shows that at E_λ =0.3 V, $I_{p,A}$, $I_{p,C}$ and $I_{p,D}$ increased with sweep rates in the range of 0.01 ~ 0.05 V s^{-1} (**curves 3 ~ 5**). Peak **C** disappeared at sweep rates below 0.05 V s^{-1}. These results indicated that since no aluminium deposition was involved in the reduction process at E_λ =0.3 V, peaks **C** and **D** were strongly associated with the dissolution of the nickel electrode.

Considering the existence of various valence states of nickel ions reacted with $Al_2Cl_7^-$ or Cl^- ions in the melt, according to **reaction 5.2.2** or **reaction 5.2.3,** the shoulders following wave **C** and **D** could result from reactions with different n values. Since stable $NiCl_4^-$ ions exist extensively in concentrated Cl^- ion molten salts, wave **D** might be related to **reaction 5.2.3**. If so, the shoulders before and after wave **D** likely involve reactions containing $[NiL_n]^{(2-n)}$ ions (where L is $Al_2Cl_7^-$ or Cl^-) for n < 4 and n > 4, respectively. On the other hand, no complexed Ni(II) ions were found in $AlCl_3$-BPC [217] and $AlCl_3$-MEIC melts [218], suggesting that organic cations $TMPA^+$ could play a favourable role in **reaction 5.2.2** or **reaction 5.2.3.**

5.2.4 Deposition and stripping of bulk aluminium and Al-Ni alloy

As E_λ became more negative from -0.15 to -0.45 V (**Fig. 5.2.6**), the peak currents of **A, C** and **D** changed slightly, while $I_{p,A'}$ increased clearly. This increase became more obvious when E_λ reached the potential region of bulk aluminium deposition. In contrast to the constant peak current densities, $I_{p,B}$, of aluminium bulk deposition, $I_{p,B'}$ increased with negatively shifting E_λ as expected, and was much lower than $I_{p,B}$ or $I_{p,A'}$. Associated with the small $Q_{B'}/Q_B$ value, 0.35, clearly, more than half the aluminium deposits were stripped at more positive potentials, especially that of peak **A′**.

Interestingly, in the cases where E_λ <-0.3 V, following the stripping of the bulk aluminium deposition, the anodic current densities decreased to slightly negative values in the range between 0.05 ~ 0.15 V. Similar phenomena were

found in $AlCl_3$-NaCl molten salts [188]. Those was considered to be a consequence of the continued deposition of nickel which overcompensated and/or obscured any partial anodic process that might be occurring under these mixed potential conditions.

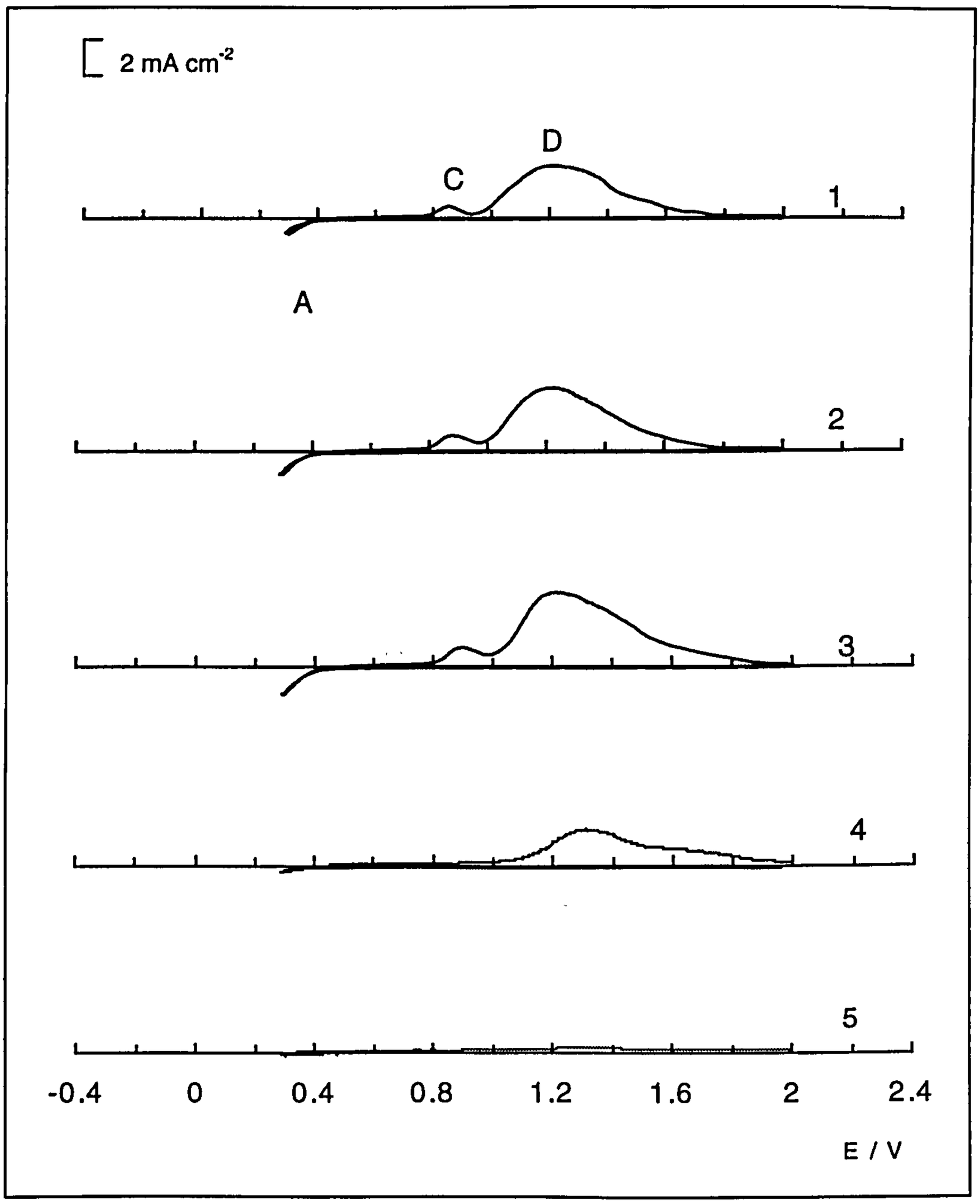

Fig. 5.2.5. Voltammograms for 2:1 $AlCl_3$-TMPAC melts with nickel electrodes at 25°C. Sweep rate ($V\ s^{-1}$): (1) 0.20; (2) 0.10; (3) 0.05; (4) 0.02; (5) 0.01.

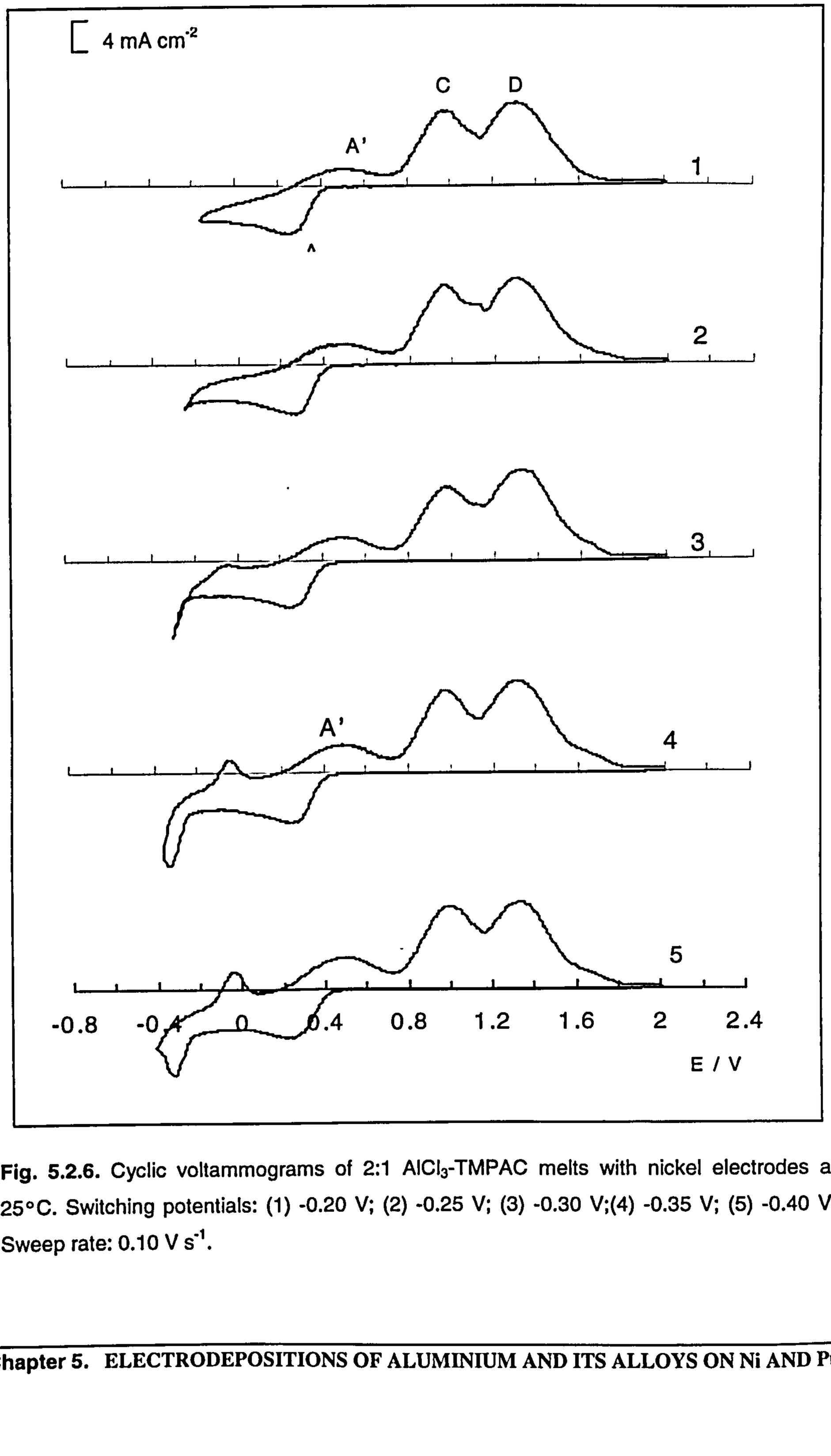

Fig. 5.2.6. Cyclic voltammograms of 2:1 $AlCl_3$-TMPAC melts with nickel electrodes at 25°C. Switching potentials: (1) -0.20 V; (2) -0.25 V; (3) -0.30 V;(4) -0.35 V; (5) -0.40 V. Sweep rate: 0.10 V s^{-1}.

It should be noted that UPD of aluminium played an important role in the depositions of Ni-Al alloys and bulk aluminium. After passing the peak potential of wave **A**, the deposition current density did not decrease with the expected $t^{-1/2}$ kinetics associated with a diffusion limited reaction. Instead, the current density exhibited a current plateau 4 mA cm^{-2} as E_λ passed below 0.0 V, indicating that the UPD of aluminium was involved in the deposition of the Ni-Al alloy. On the other hand, from the development of wave **A′**, it can be seen that wave **A′** was basically a current plateau which was slightly higher than the back ground current density when E_λ was approaching negatively to 0.0 V (**Fig. 5.2.4**). Thus, wave **A** was attributed to the deposition of a nickel-rich alloy.

As E_λ became more negative, approaching the deposition potential of bulk aluminium, current density of wave **A′** increased. Wave **A′** was developing broad (**Fig. 5.2.6**), suggesting a strong interaction between the deposit and the electrode substrate.

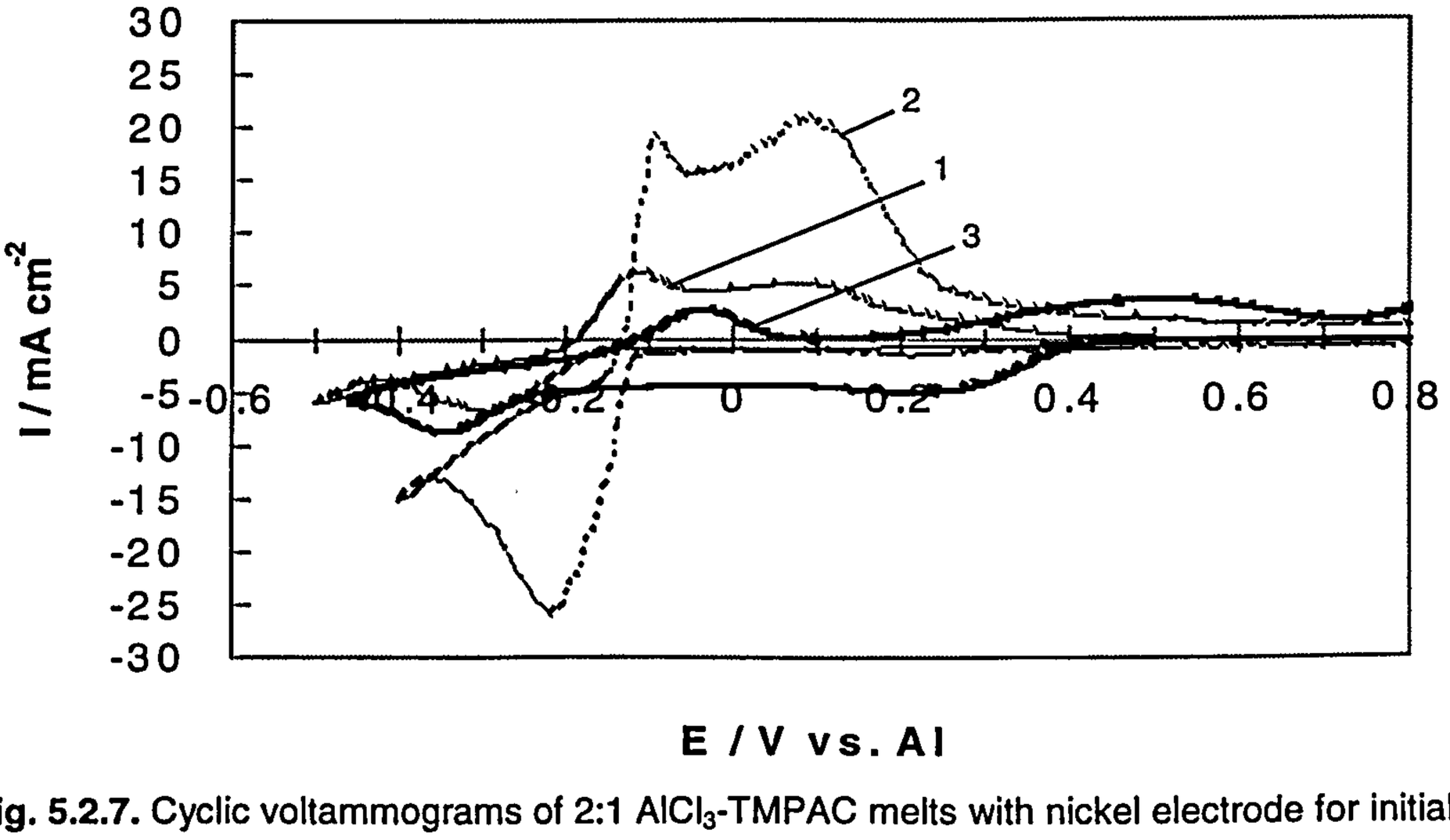

Fig. 5.2.7. Cyclic voltammograms of 2:1 $AlCl_3$-TMPAC melts with nickel electrode for initial potentials: (1) 0.50 V; (2) 2.7 V; and on tungsten (3). Sweep rate: 0.10 V s^{-1}.

It is noteworthy that the peak potential of bulk aluminium was -0.34 V, which was more negative than -0.15 V on tungsten and -0.06 V on aluminium, and

much further from the reversible potential of aluminium. Since the alloying occurred positive to 0.0 V, it is probable that bulk aluminium was deposited on a surface modified by Ni-Al alloy deposits.

In order to further understand the deposition of bulk aluminium on the nickel substrate, scans were initiated from *ca.* 0.5 V, which was far from the stripping potential of nickel so that the influence of nickel dissolution should be minimised. A typical voltammogram with E_λ = -0.5 V is shown in **Fig. 5.2.7** (**curve 1**), which was very similar to the voltammogram on tungsten (**curve 3**). The main difference between them was that the current densities for aluminium deposition and stripping on nickel were much smaller than those on tungsten. The smaller current densities on Ni could be caused by the formation of the alloy on the surface of the nickel electrode. As can been seen in **curve 1**, a UPD plateau started at 0.48 V and the subsequent deposition of bulk aluminium occurred at -0.295 V, about -0.05 V more positive than that in the case of scans beginning at a potential of 2.7 V (**curve 2**). A nucleation loop occurred at potentials more negative than -0.4 V, indicating the probable reduction of $AlCl_4^-$ ions. The reverse scan exhibited two stripping peaks at -0.21 V and 0.08 V, respectively. Both of them formed actually a very broad wave, suggesting a strong interaction between the deposits and the electrode substrate, or the possible passivation of the electrode, similar to aluminium electrodes.

Fig. 5.2.8 shows voltammograms of aluminium deposition and stripping on nickel starting from an initial potential of 0.5 V. As the sweep rates decreased, the starting potentials of the nucleation loops shifted positively. At the lower sweep rate of 0.02 V s^{-1}, following aluminium stripping waves B and C, the anodic scan exhibited the third wave (**D**) at 0.22 V. This potential coincided with the onset of the UPD stripping (wave **A'** in **Fig. 5.2.1**). The peak current densities of bulk deposition and stripping of aluminium were linear with $\upsilon^{1/2}$ (**Fig. 5.2.9**). However, $I_{p,c} \sim \upsilon^{1/2}$ did not pass through the origin indicating kinetic limitations caused by the nucleation step.

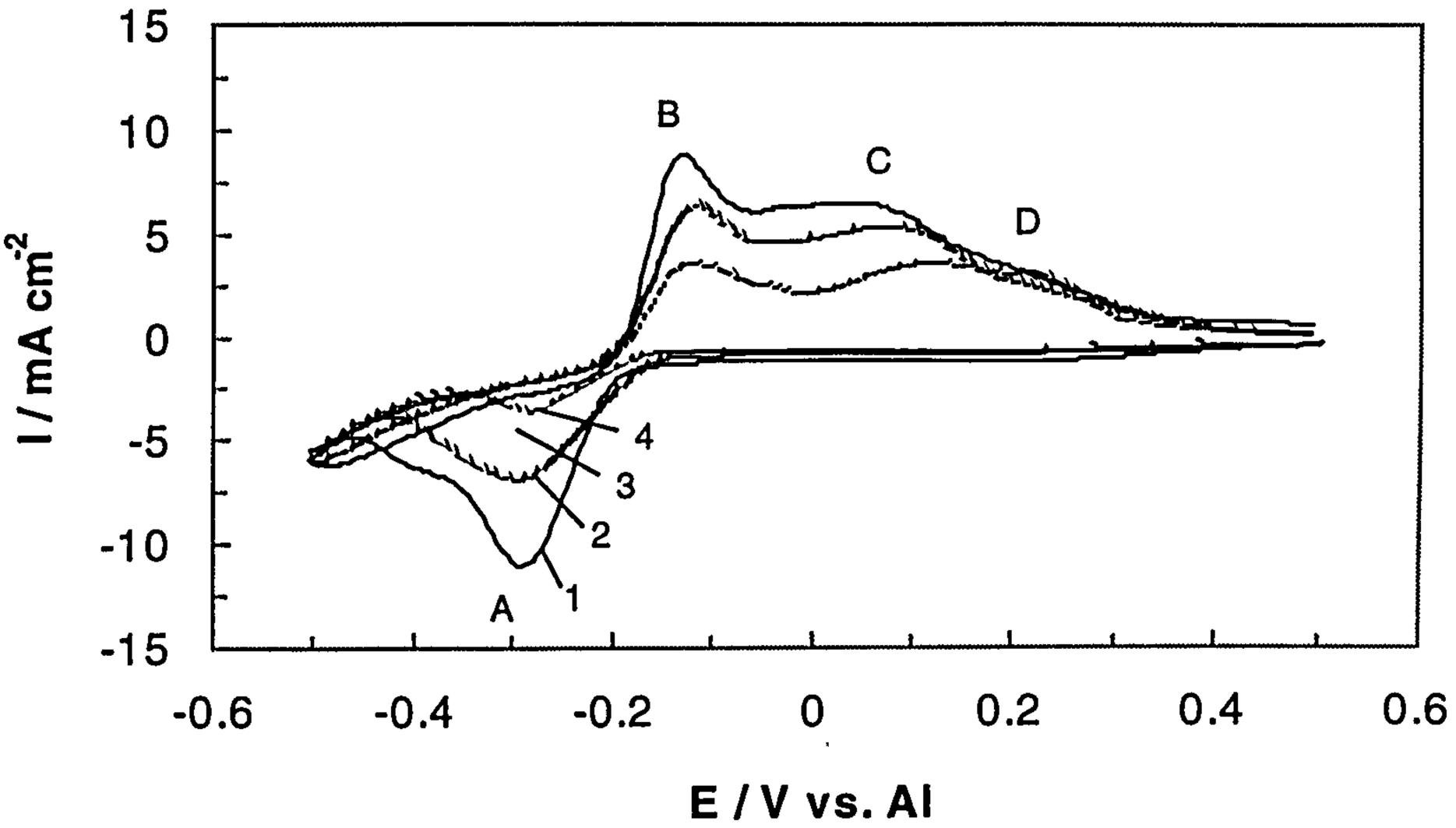

Fig. 5.2.8. Voltammograms for deposition and stripping of aluminium on nickel electrodes from 2:1 $AlCl_3$-TMPAC melts at 25°C. Sweep rates: (V s^{-1}): (1) 0.20; (2) 0.10; (3) 0.05; (4) 0.02.

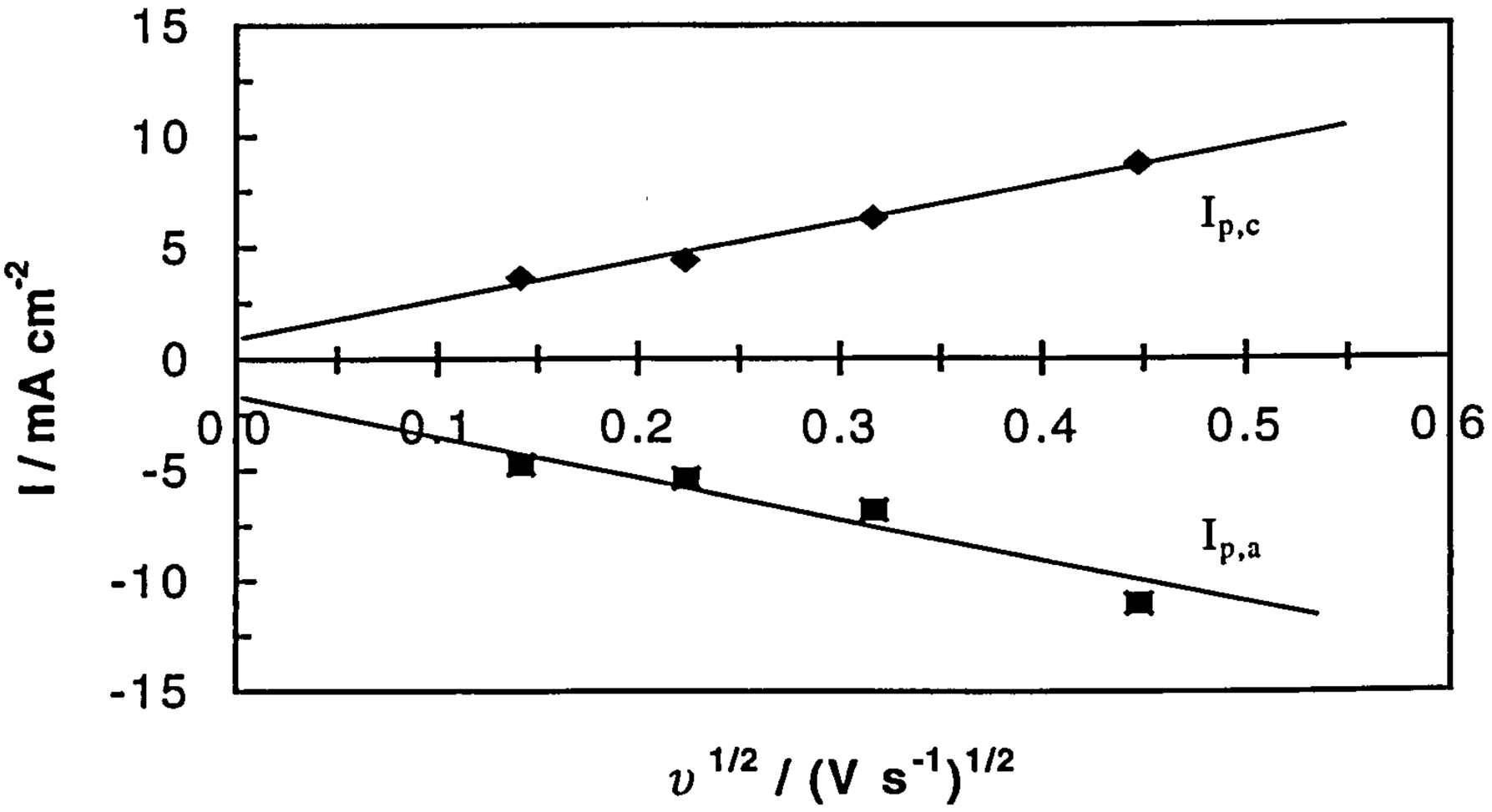

Fig. 5.2.9. Plot of cathodic and anodic peak currents vs. square root of sweep rate for aluminium deposition and stripping on nickel in 2:1 $AlCl_3$-TMPAC melts at 25°C.

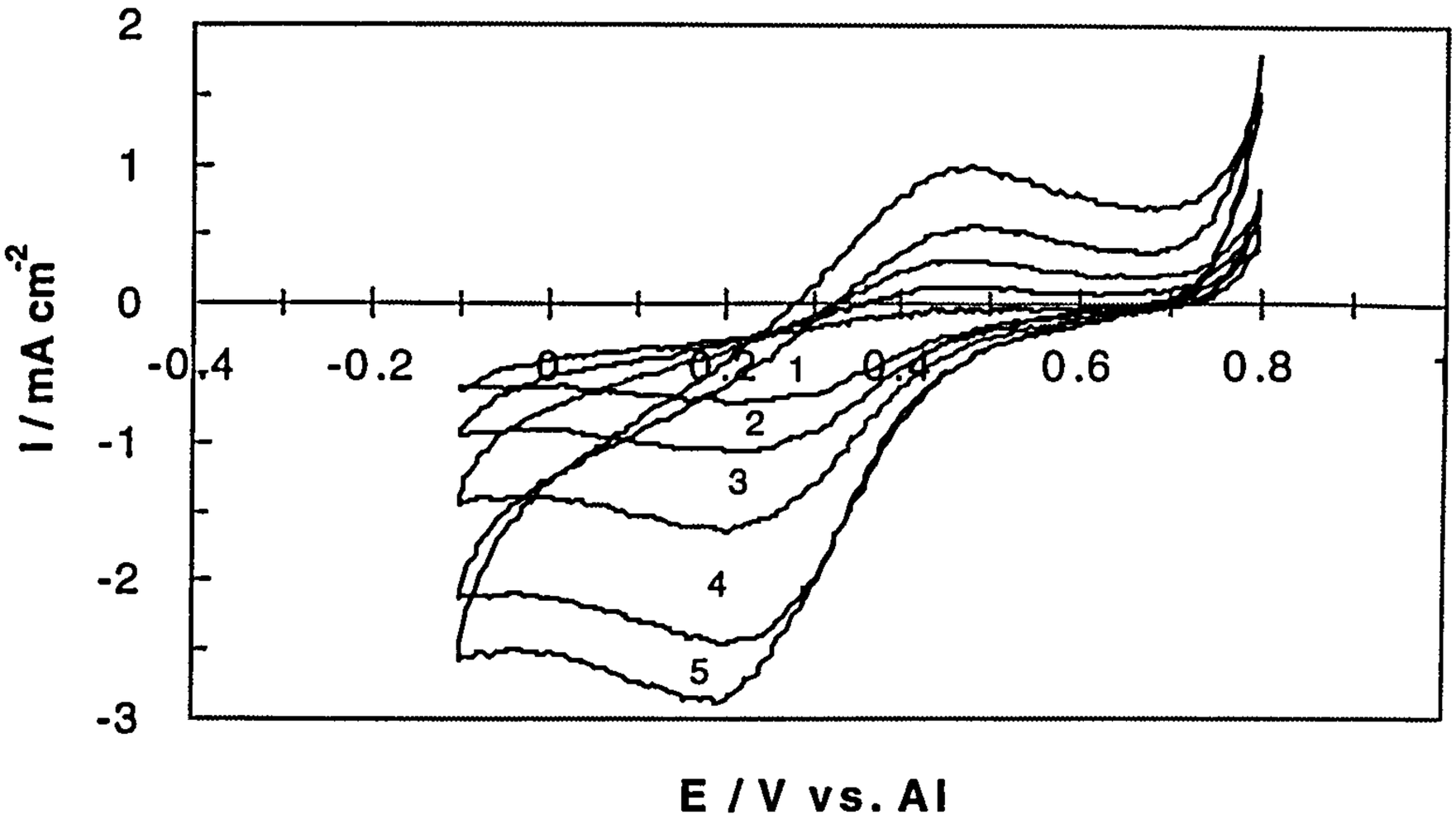

Fig. 5.2.10. Voltammograms, with correction of the background current, revealing Al-Ni alloy deposition and stripping on nickel in 2:1 $AlCl_3$- TMPAC melts at 25°C. Sweep rates ($V\ s^{-1}$): (1) 0.1; (2) 0.25; (3) 0.5; (4) 0.75; (5) 1.0.

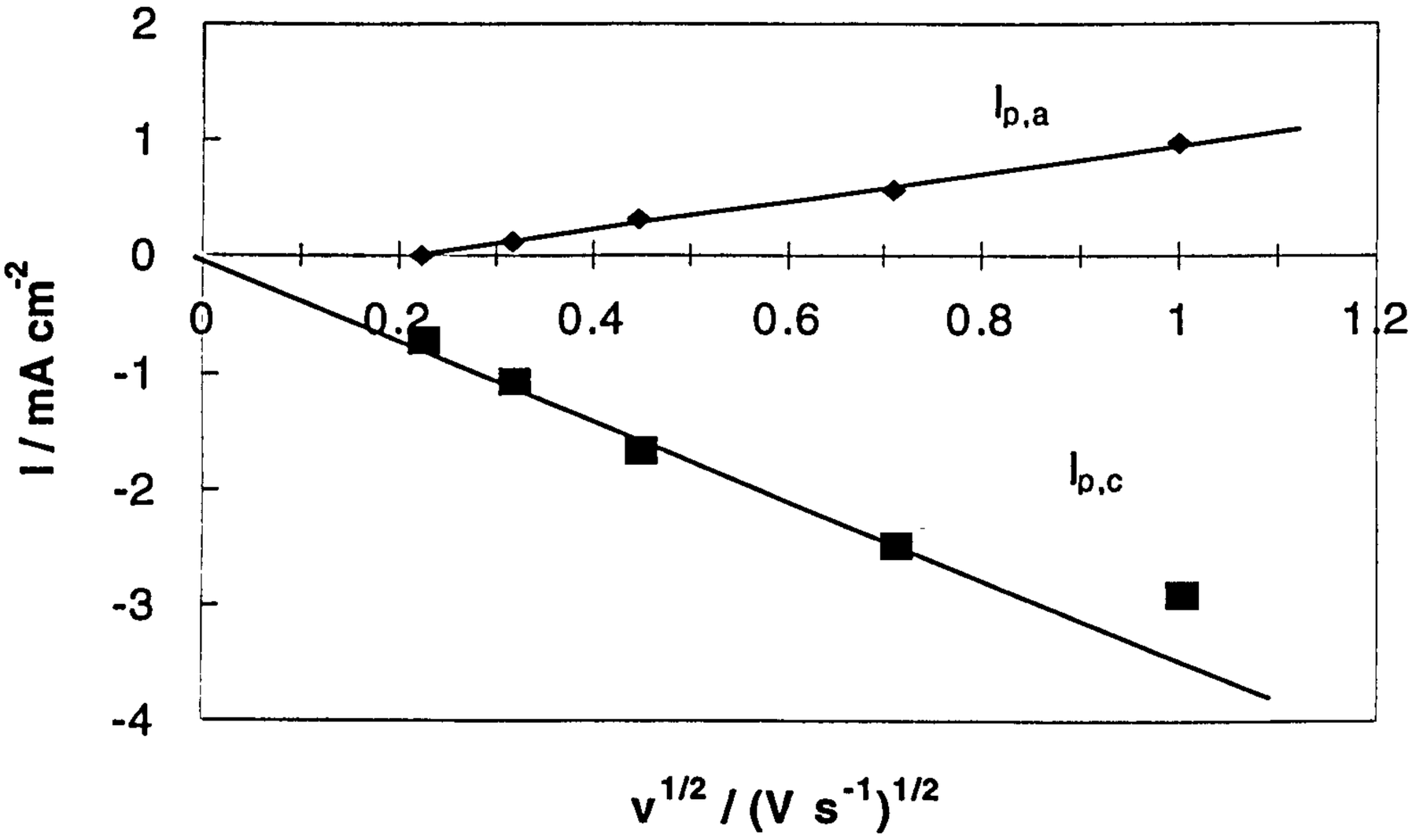

Fig. 5.2.11. Plot of cathodic and anodic peak currents vs. square root of sweep rate for underpotential deposition and stripping of aluminium on nickel in 2:1 $AlCl_3$-TMPAC melts at 25°C.

To examine deposition and stripping of the Ni-Al alloy, a potential scan was performed between -0.1 and 0.8 V, which covered the aluminium UPD and deposition of the Ni-Al alloy. A collection of voltammograms at various sweep rates, corrected for the background current, is shown in **Fig. 5.2.10**. Clearly, the current densities for stripping were much smaller than those for deposition. This could be caused by the reactions discussed before, in which some nickel was stripped with the formation of Ni(II) complexes with either $Al_2Cl_7^-$ or Cl^- ions in the melt. Like the aluminium UPD on tungsten, consideration of the charge of the deposited Ni-Al alloy indicated deposits of 2 ~ 7 monolayers on the surface. However, the $I_{p,c} \sim \upsilon^{1/2}$ plot was linear and passed through the origin (**Fig. 5.2.11**), suggesting that the alloy deposition on nickel was diffusion controlled, unlike the surface controlled process found on tungsten.

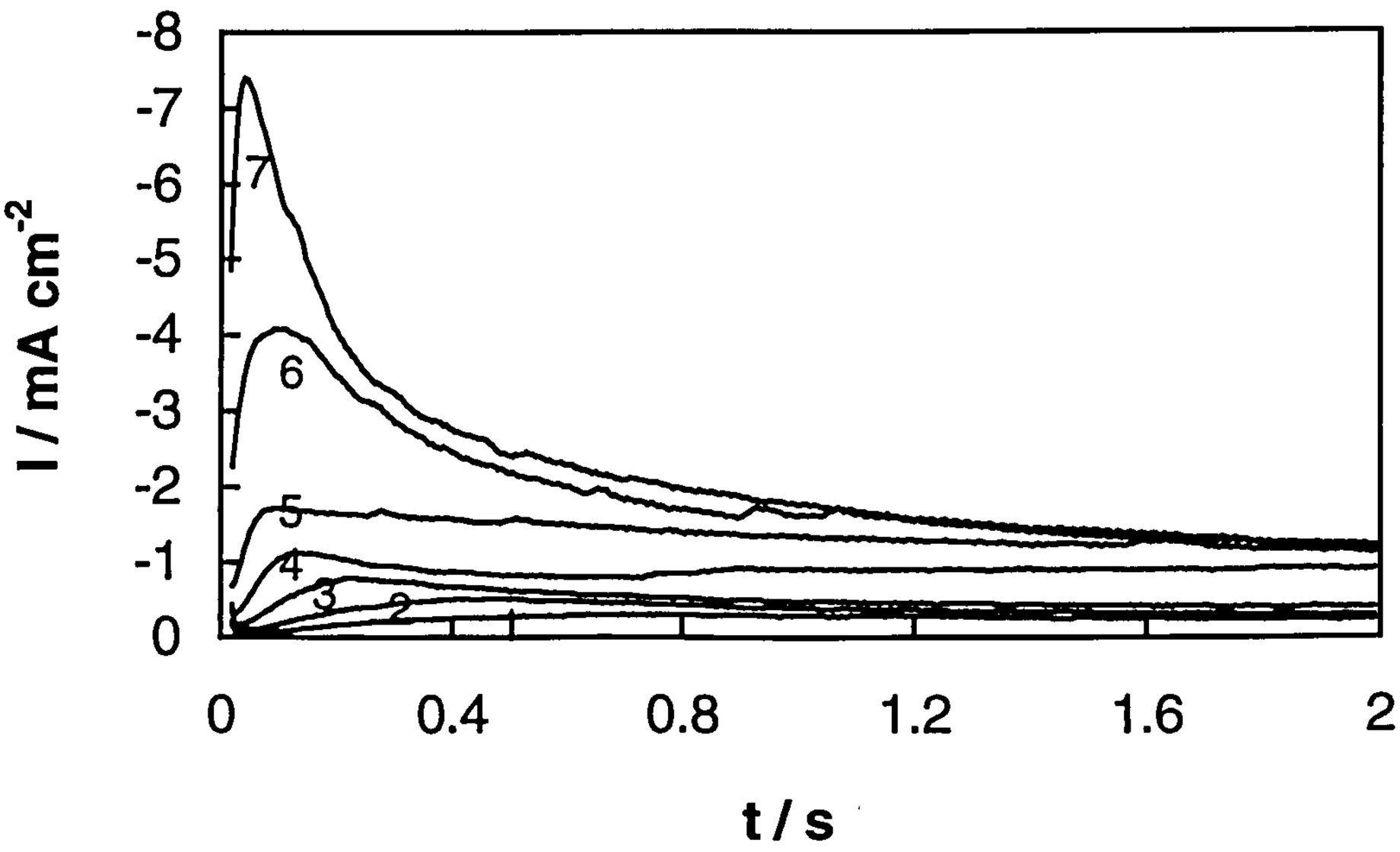

Fig. 5.2.12. Potential-step current transients for Al-Ni alloy deposition on nickel in 2:1 $AlCl_3$- TMPAC melts at 25°C at applied potentials (V): (1) -0.20; (2) -0.19; (3) -0.18; (4) -0.17; (5) -0.16; (6) -0.15; (7) -0.14.

5.2.5 Nucleation Analysis

In order to probe the mechanism of Ni-Al alloy deposition on nickel, chronoamperometric experiments were carried out by stepping the potential from 2.0 V, where no nickel deposition took place, to a value sufficiently negative to initiate the formation of nickel nuclei. In all cases, the final potential returned to 2.0 V, where all deposits on the electrode would be stripped completely, giving a clean surface of electrode for the next transient. Examples of some typical current-time transients resulting from these potential-step experiments are shown in **Fig. 5.2.12.** As can been, these transients demonstrated that the deposition of the Ni-Al alloy displayed classic nucleation-growth behaviour. That is, the current density rose due to the formation of the nuclei, and reached a maximum when the diffusion zones of the growing nuclei began to overlap, and finally decreased, following the Cotrell equation characteristic of diffusion control. The time t_m corresponding to I_m was dependent upon the applied potential, becoming shorter as the potential was made more negative.

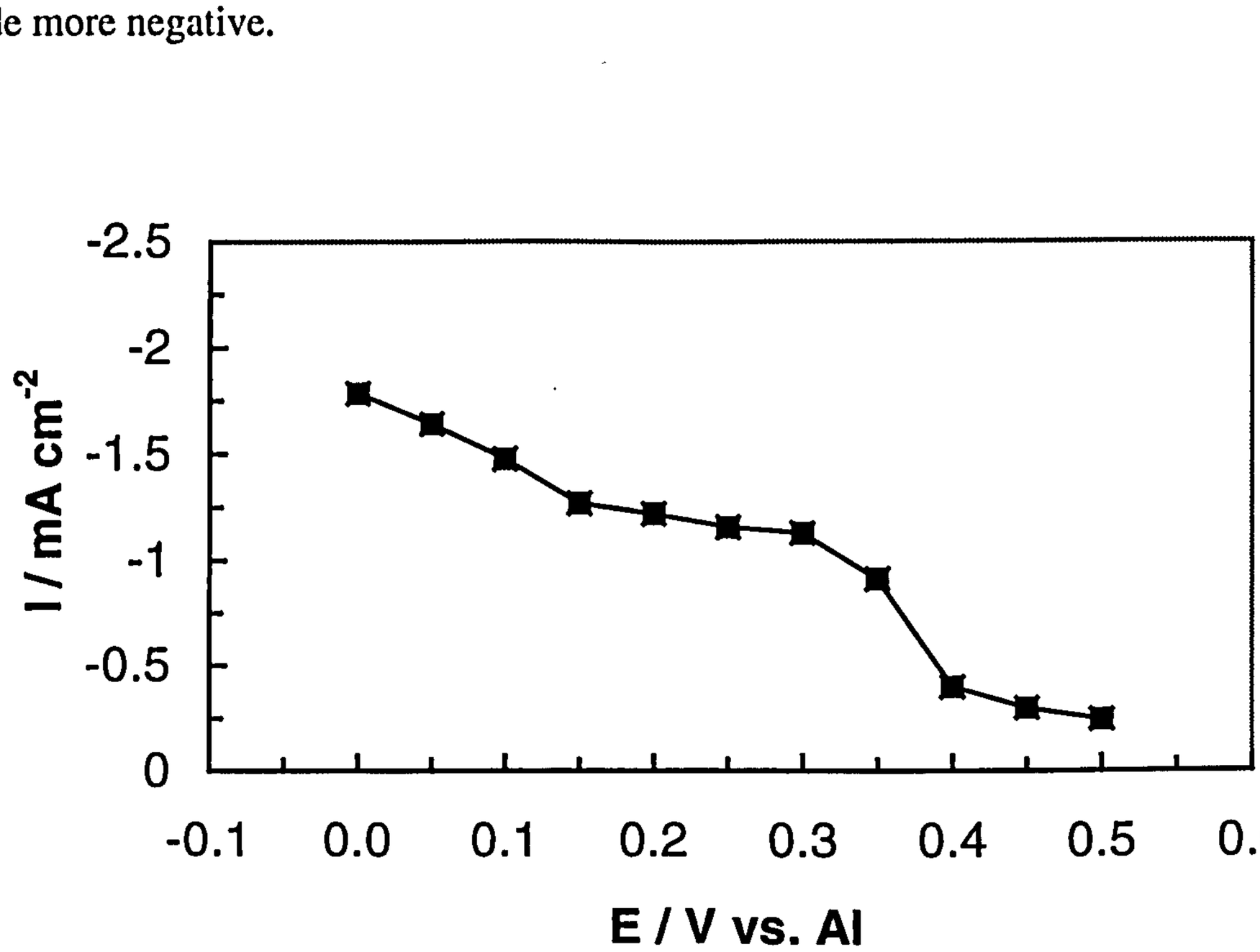

Fig. 5.2.13. A sampled current voltammogram constructed from current-time transients shown in **Fig. 5.2.12** at 0.8 s.

A sampled voltammogram constructed from a series of transients acquired at different potentials on nickel at 0.8 s is shown in **Fig. 5.2.13**. This voltammogram did not exhibit a clear limiting current density plateau which would be expected if the deposition of nickel was the sole reduction process. Instead, the current density increased almost continuously as the potential decreased. This result was in good agreement with that observed in $AlCl_3$-MEIC melts [218]. Accordingly, **Fig. 5.2.13** suggested that the reduction of Ni(II) species became diffusion limited below 0.35 V and then the co-deposition of aluminium occurred simultaneously with the diffusion-controlled deposition of nickel.

It has been demonstrated during previously (**Chaters 3** and **4**) that aluminium deposition on tungsten, aluminium and glassy carbon involved a three-dimensional instantaneous nucleation process followed by hemispherical diffusion-controlled growth of the developing nuclei. Instantaneous nucleation on a fixed number of active sites and progressive nucleation are two limiting cases of metal deposition. Intermediate cases lying between these two limiting models are considered to involve progressive nucleation, but on a finite number of active sites. The theoretical transients for this case is represented by **Eqn. 3.1.6** [148]:

$$(I/I_m)^2 = (t/t_m)^{-1}\left(\frac{1-\exp[-xt/t_m+\alpha\ (1-\exp(-xt/\alpha\ t_m))]}{1-\exp[-x+\alpha\ (1-\exp(-x/\alpha\ ))]}\right)^2 \qquad (3.1.6)$$

and the potential dependent nucleation rate constant per active site, A, can be obtained from **Eqn. 5.2.4** [148]:

$$A = x/\alpha\ t_m \qquad (5.2.4)$$

Dimensionless experimental plots $(I/I_m)^2$ *vs.* t/t_m taken from the transients for the Al-Ni alloy deposition in **Fig. 5.2.12** were compared with the theoretical dimensionless curves. A typical example is shown in **Fig. 5.2.14**. The experimental

curve fell between the two limiting models, indicating the Al-Ni alloy deposition followed progressive nucleation on a limited number of active sites. The resulting values of x and α were 1.82 and 0.35, respectively. These values yields nucleation rate constants of 130 s^{-1}. Since the compositions of Al(III) and Ni(II) species in the alloy were unknown, the values of D and N could not be calculated.

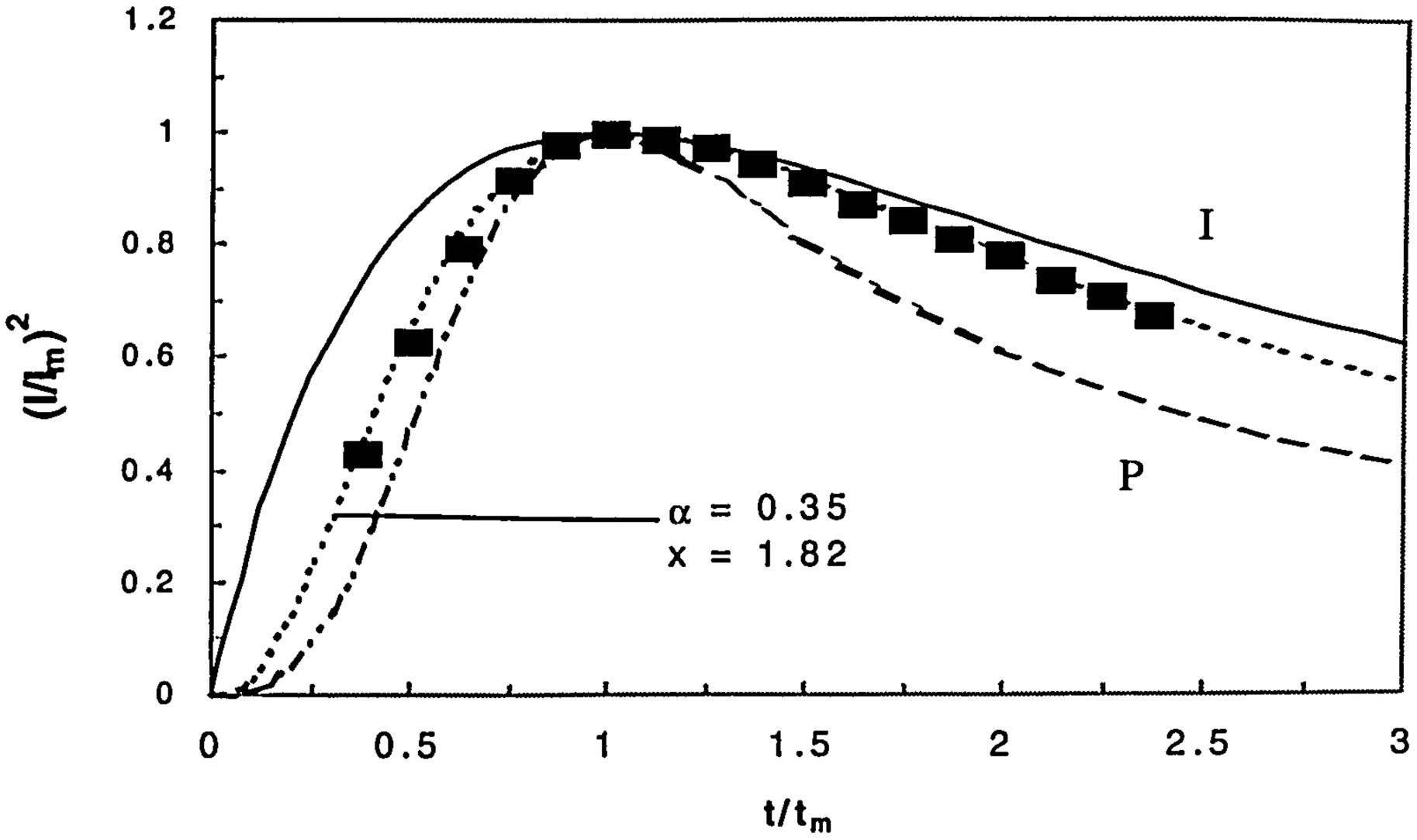

Fig. 5.2.14. Comparison of the dimensionless experimental data derived from **Fig. 5.2.12** with the theoretical models for diffusion controlled three dimensional instantaneous (I) and progressive (P) nucleation and growth.

As similar treatment for the nucleation of bulk aluminium was also carried out. The stepping potential initiated at 0.0 V, where the Ni deposition effect would be minimised. Representative transients are collected in **Fig. 5.2.15**. The dimensionless analysis (**Fig. 5.2.16**) indicated that the bulk aluminium deposition on nickel substrate from 2:1 $AlCl_3$-TMPAC melts involved three-dimensional instantaneous nucleation followed by hemispherical diffusion-controlled growth of the developing nuclei. The values of D and N were calculated to be 2.3×10^{-8} cm^2 s^{-1} and 5.2×10^5 sites cm^{-2}, respectively.

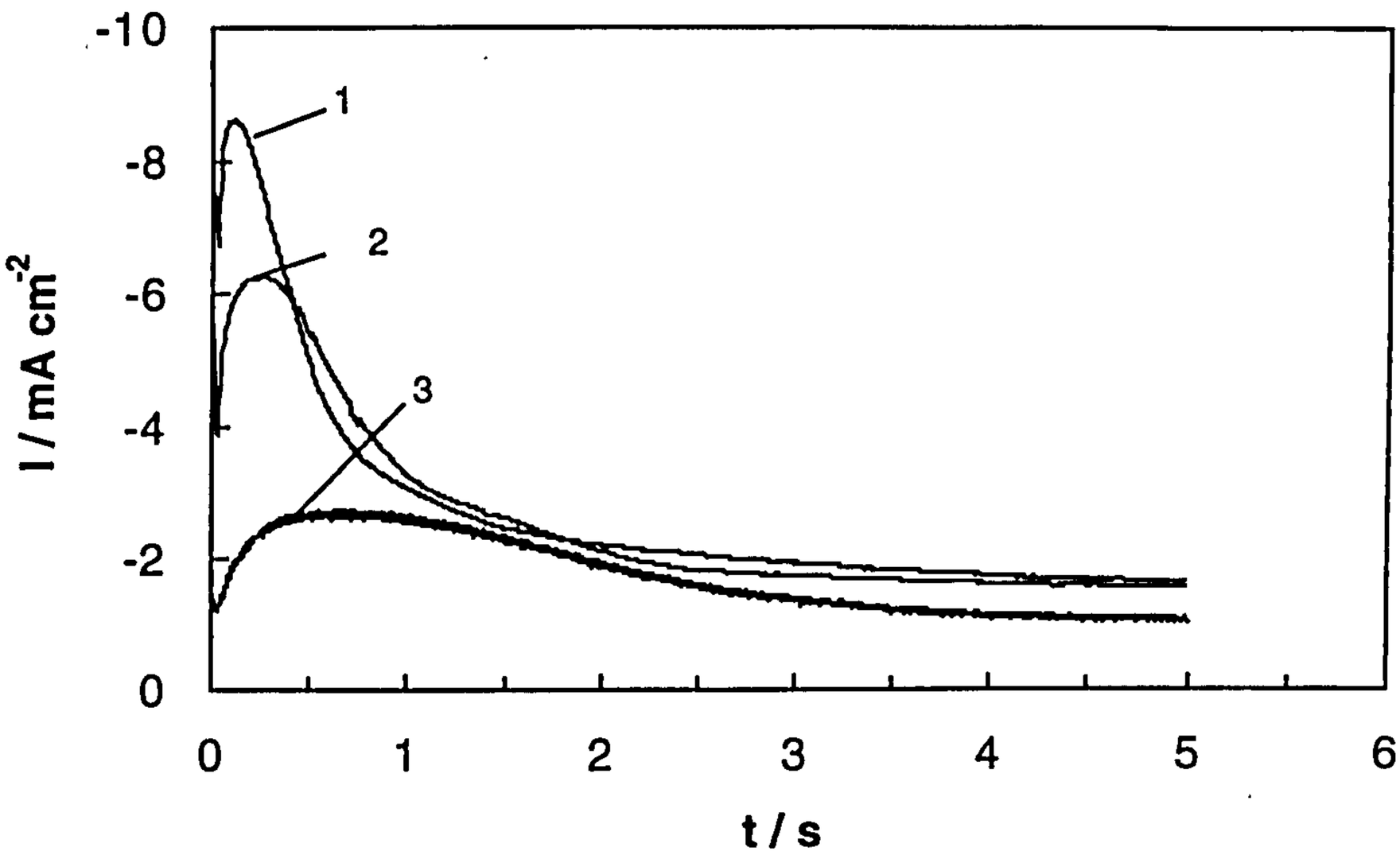

Fig. 5.2.15. Potential-step current transients for bulk aluminium deposition on nickel in 2:1 $AlCl_3$- TMPAC melts at 25°C at applied potentials (V): (1) -0.19; (2) -0.18; (3) -0.17.

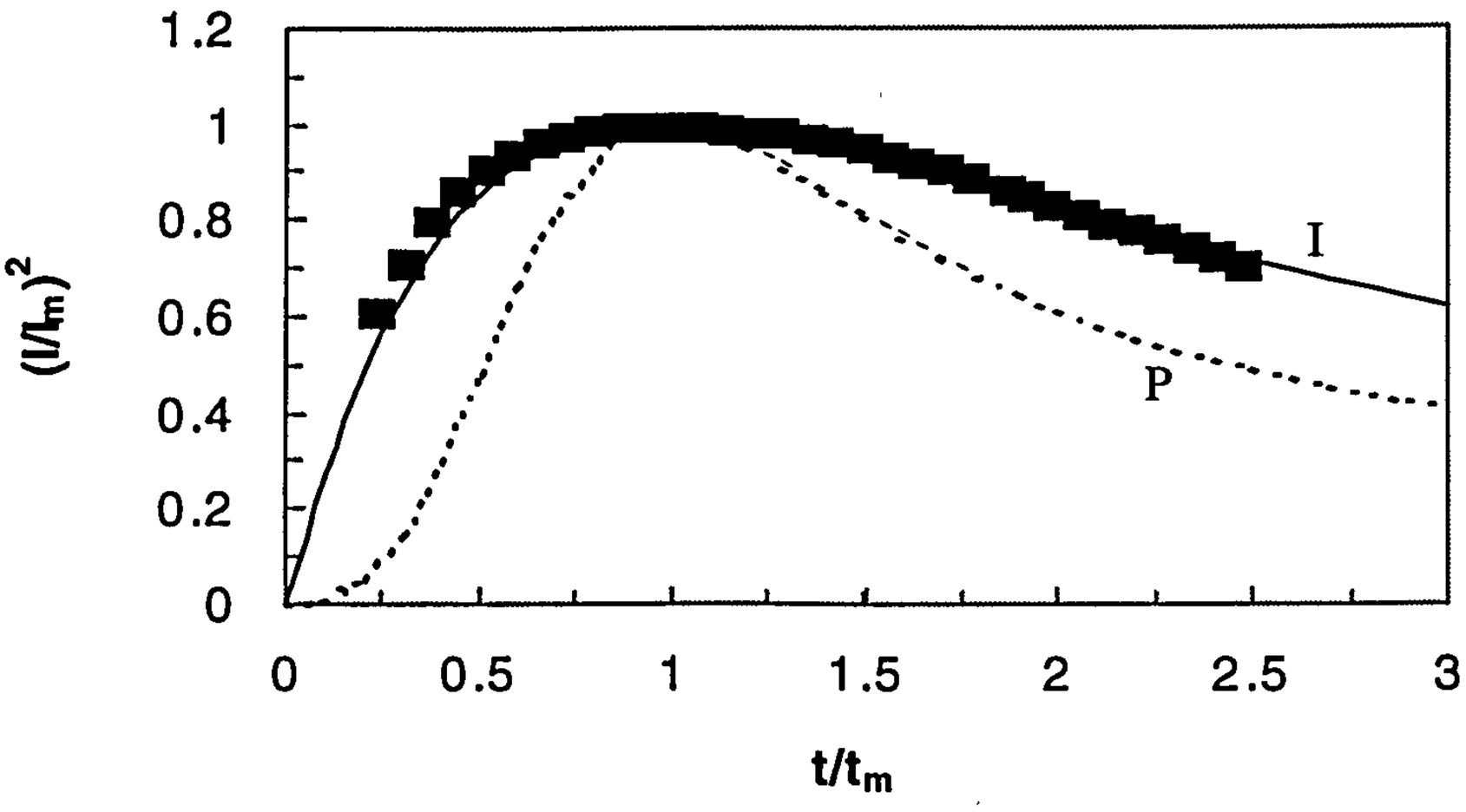

Fig. 5.2.16. Comparison of the dimensionless experimental data derived from **Fig. 5.2.15** with the theoretical models for diffusion controlled three dimensional instantaneous and progressive nucleation and growth.

5.3 PLATINUM ELECTRODE

5.3.1 Voltammetric Behaviour

A typical cyclic voltammogram for 2:1 $AlCl_3$-TMPAC melts with platinum at 0.1 V s^{-1} is shown in **Fig. 5.3.1**. Interestingly, the voltammetric behaviour of the melt with platinum was very similar to that on nickel. The potential scan began from *ca.* 2.6 V. As for the case of nickel, $E_{p,B}$ was more negative than observed on tungsten and glassy carbon electrodes and this might be due to the surface of electrode being modified by the alloy. On the reverse scan, waves **B′** and **A′** at -0.1 V and 0.4 V, respectively, corresponded to the stripping of aluminium and the Al-Pt alloy deposits. In addition, two irreversible waves **D** and **E** occurred at 1.0 V and 1.3 V respectively. Like the case on the nickle electrode, they were assigned to the oxidation of platinum and the $Al_2Cl_7^-$ and Cl^- ions in the melt:

$$Pt + nL^- \rightleftharpoons [PtL_n]^{(2-n)} + 2e^- \qquad (5.3.1)$$

where L is either $Al_2Cl_7^-$ and Cl^-.

A detailed investigation was performed using different negative switching potentials E_λ from 0.4 V to - 0.5 V (**Fig. 5.3.2**). Wave **E** occurred with E_λ equal to 0.375 V (**curve 1**), which was the onset of wave **A**. With the extension of E_λ to 0.325 V (**curve 2**), wave **D** was observed. Since the current densities of waves **D** and **E** increased with decreasing E_λ, which traversed the deposition potential range of **A** and **B**, this confirmed that the stripping of aluminium and the alloy deposits were also involved in the development of waves **D** and **E**.

Integration (**Fig. 5.3.3**) of **Fig. 5.3.1** showed that the coulombic efficiencies $Q_{A'}/Q_A$, $Q_{B'}/Q_B$ and $Q_{A'+B'}/Q_A$ were 0.42, 0.64 and 0.35, respectively. This suggested that after waves **A′** and **B′** some residual deposits of aluminium or its alloy with platinum were retained on the electrode surface, or part of deposits took part in **Reaction 5.3.1**. On the other hand, the overall

coulombic efficiency $Q_A/Q_C$was 1.17, indicating some extra charge was involved in waves **D** and **E**.

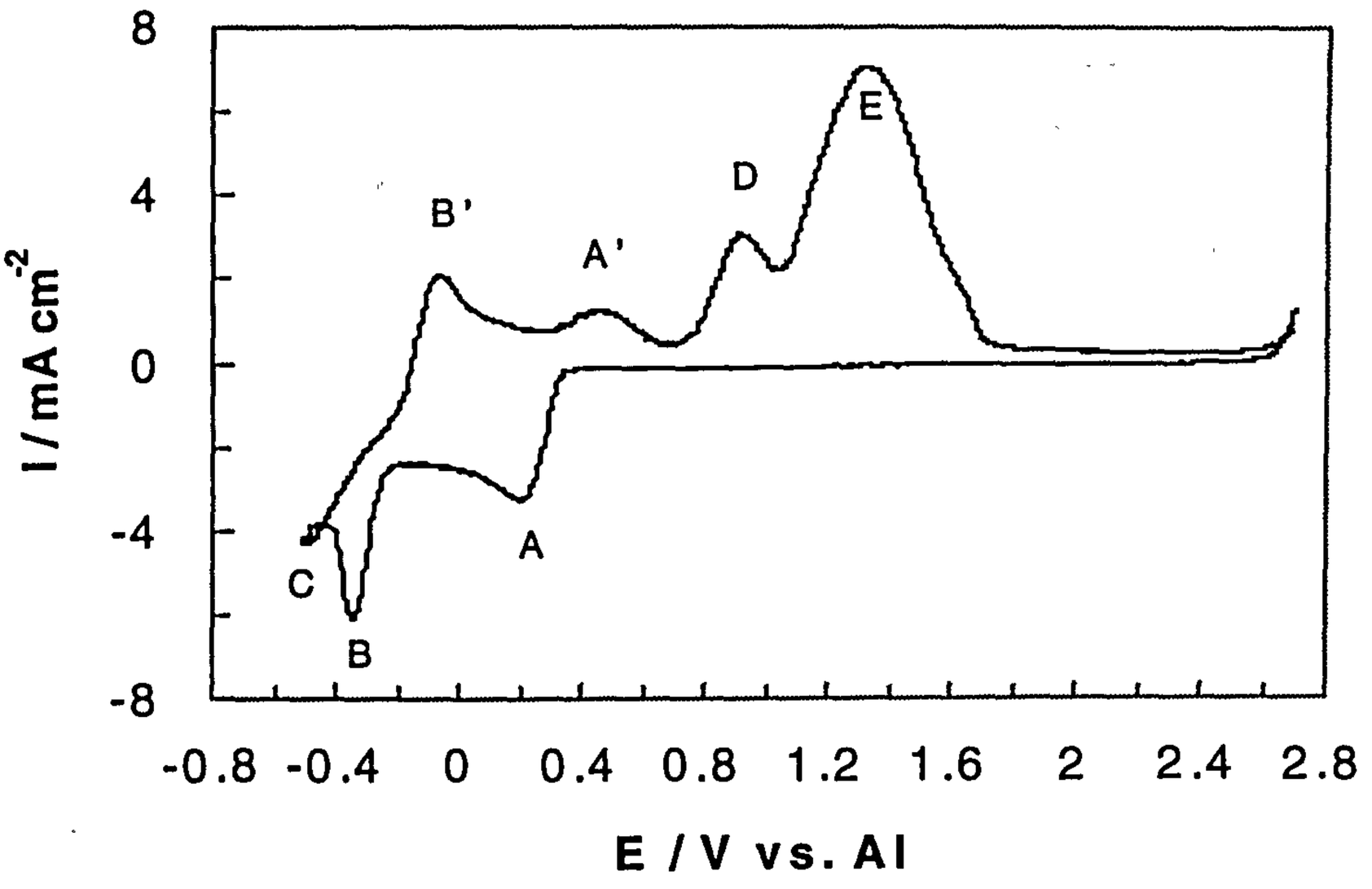

Fig. 5.3.1. Cyclic voltammogram of a 2:1 $AlCl_3$-TMPAC melt with platinum at 25°C. Sweep rate: 0.1 V s^{-1}.

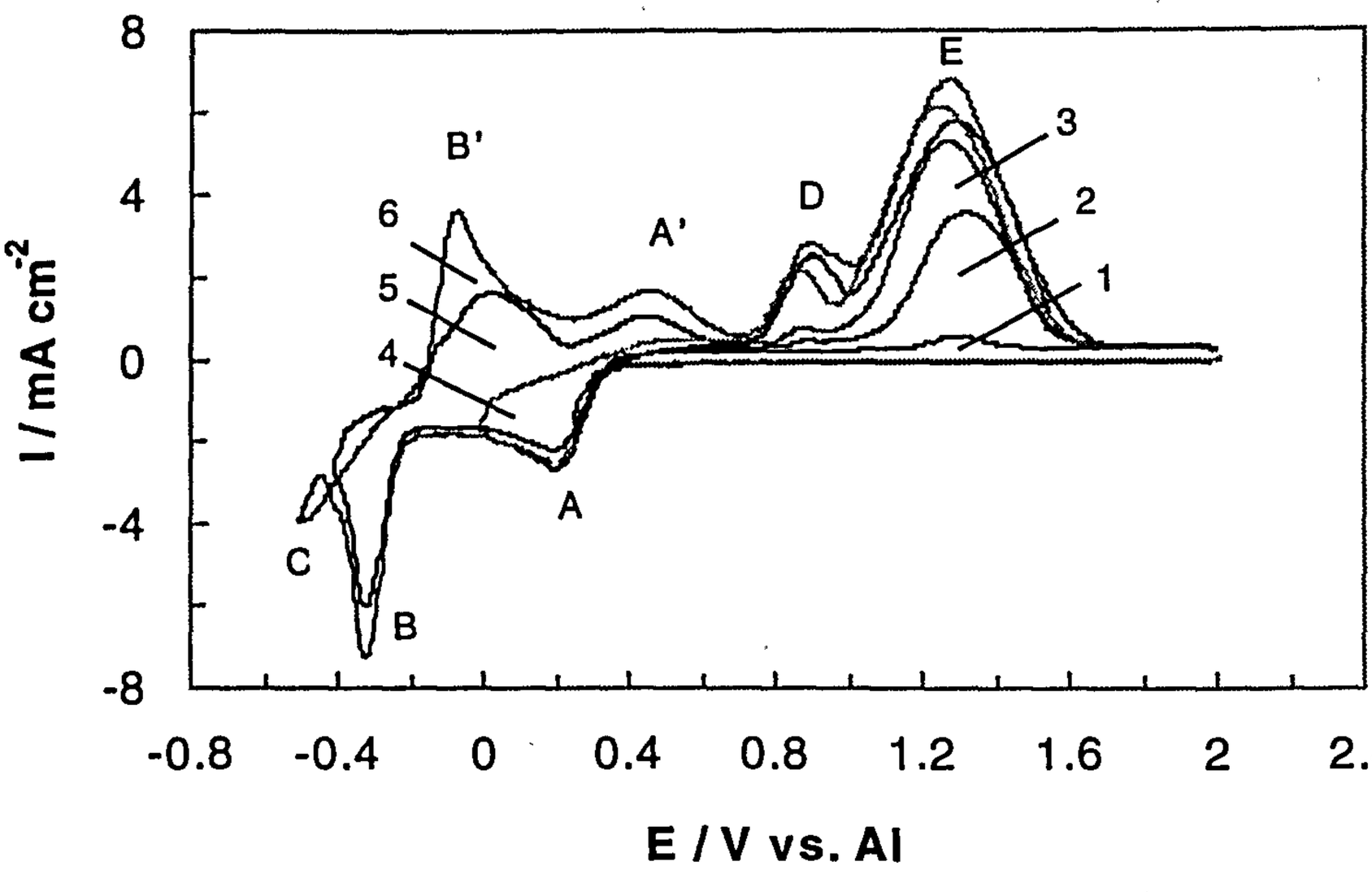

Fig. 5.3.2. Cyclic voltammograms of 2:1 $AlCl_3$-TMPAC melts with Pt at 25°C. Switching potentials: (1) 0.35 V; (2) 0.30 V. (3) 0.20 V; (4). -0.25 V; (4) 0.00 V; (5) -0.40 V; (6) -0.50 V. Sweep rate: 0.10 V s^{-1}.

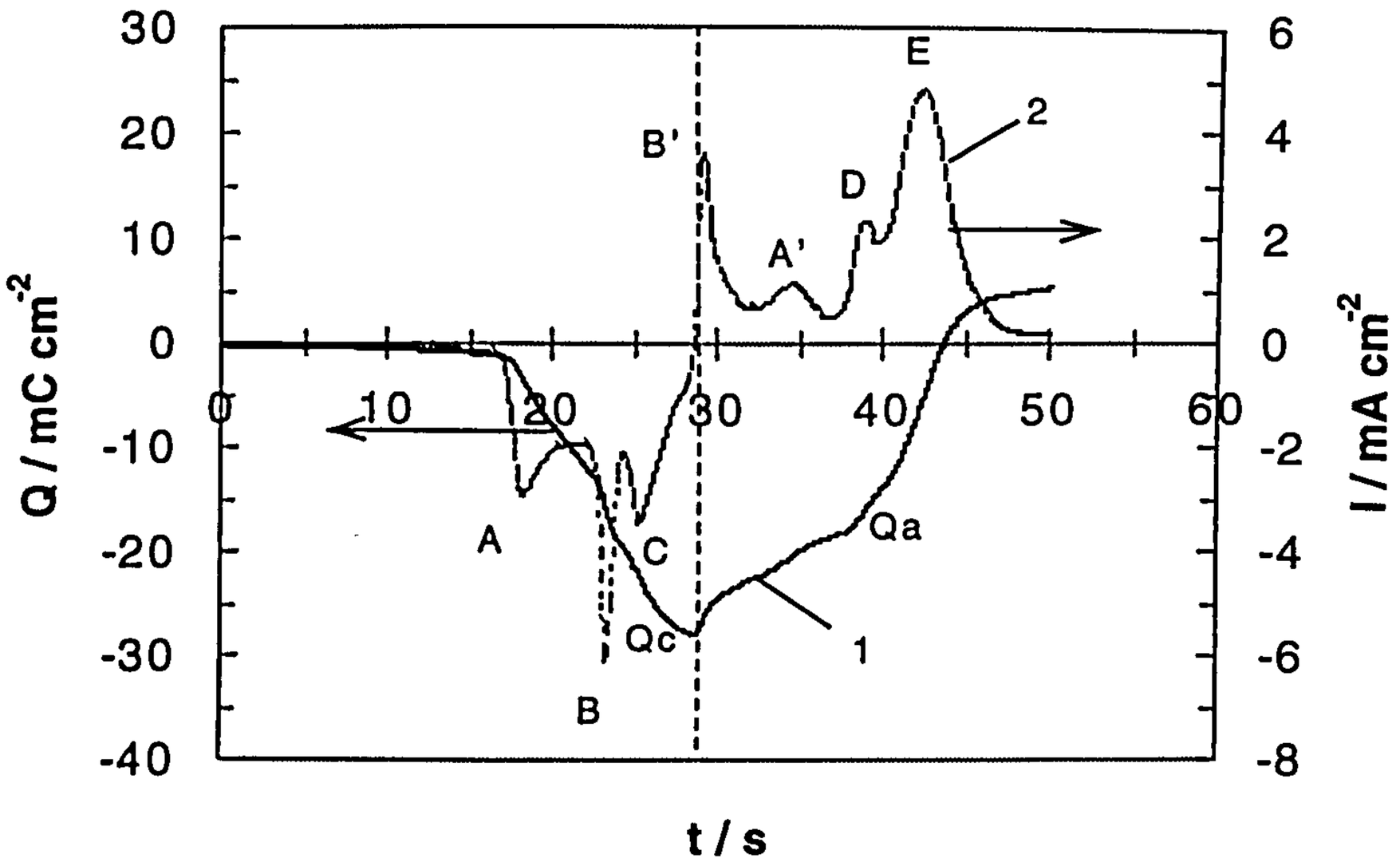

Fig. 5.3.3. Charge analysis of aluminium deposition and stripping (1) derived from **Fig. 5.3.1** and its corresponding current-time transient (2).

Voltammograms of the bulk deposition of aluminium at various sweep rates were also examined. As seen in **Fig. 5.3.4**, $E_{p,c}$ moved positively with increasing sweep rates. These values were over 0.1 V more positive than -0.375 V when the initial potential was 2.0 V, reflecting the different states of the electrode surface. In the former case the modification of the electrode by the alloy was minimised. Therefore the electrode surface was much "cleaner", which was confirmed by the ratio $I_{p.a}/I_{p,c}$ which was nearly unity and a coulombic efficiency of 98% for aluminium deposition and stripping. In additional, $I_{p.a}$ and $I_{p,c}$ were linear with the square root of the sweep rate (**Fig. 5.3.5**), indicating that the processes were diffusion controlled.

Similarly, the voltammetric investigation of deposition and stripping of the alloy (**Figs. 5.3.6** and **5.3.7**) gave the same conclusion. It proved that the formation of the Al-Pt alloy was also diffusion controlled. However, the $I_{p,c} \sim \upsilon^{1/2}$ plot did not pass through the origin and the ratio of $I_{p.a}/I_{p,c}$ was much less than one suggesting kinetics limitation.

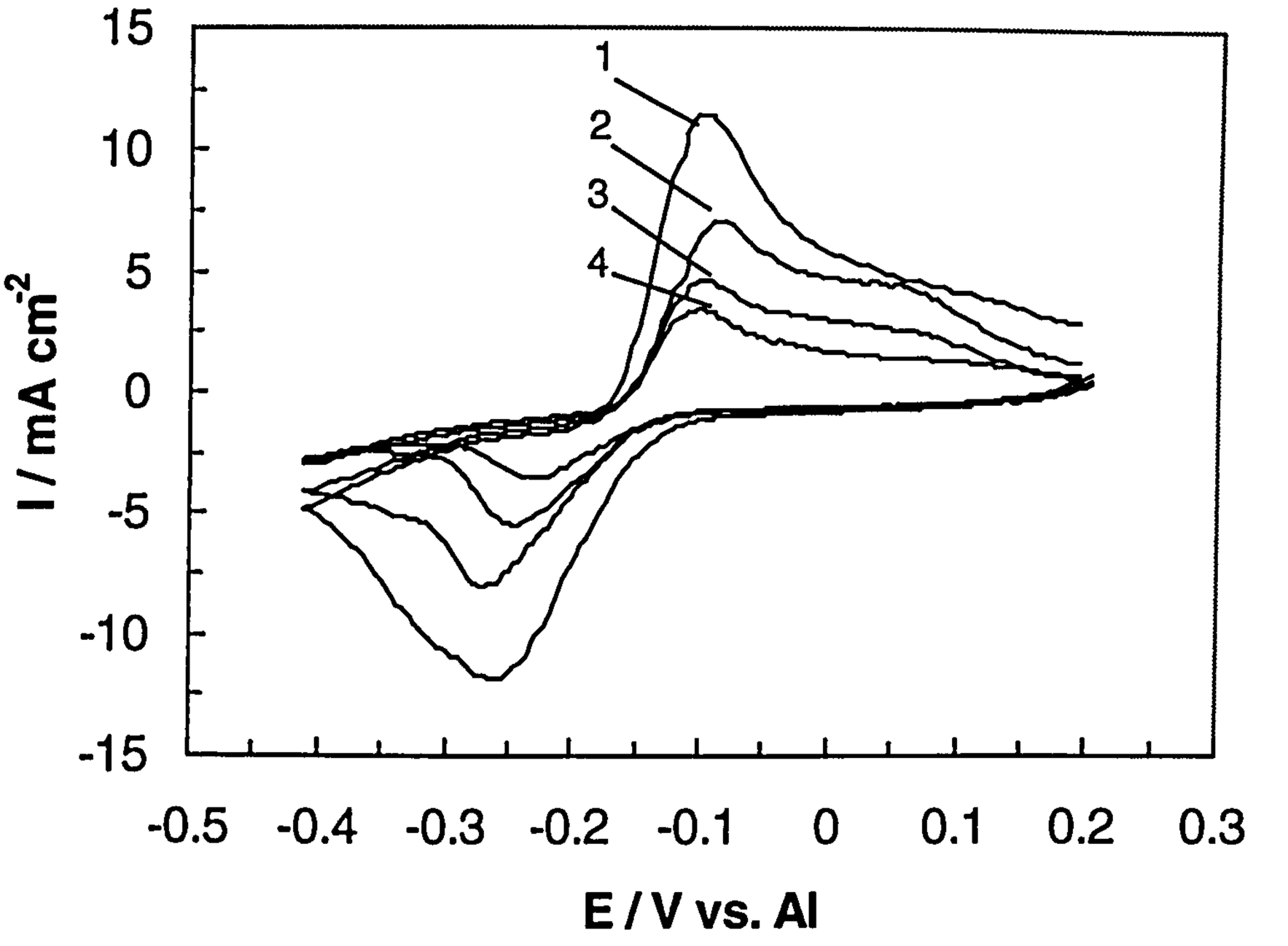

Fig. 5.3.4. Voltammograms for deposition and stripping of aluminium on platinum from 2:1 $AlCl_3$-TMPAC melts at 25°C. Sweep rates: (V s^{-1}): (1) 0.20;(2) 0.10;(3) 0.05;(4) 0.02.

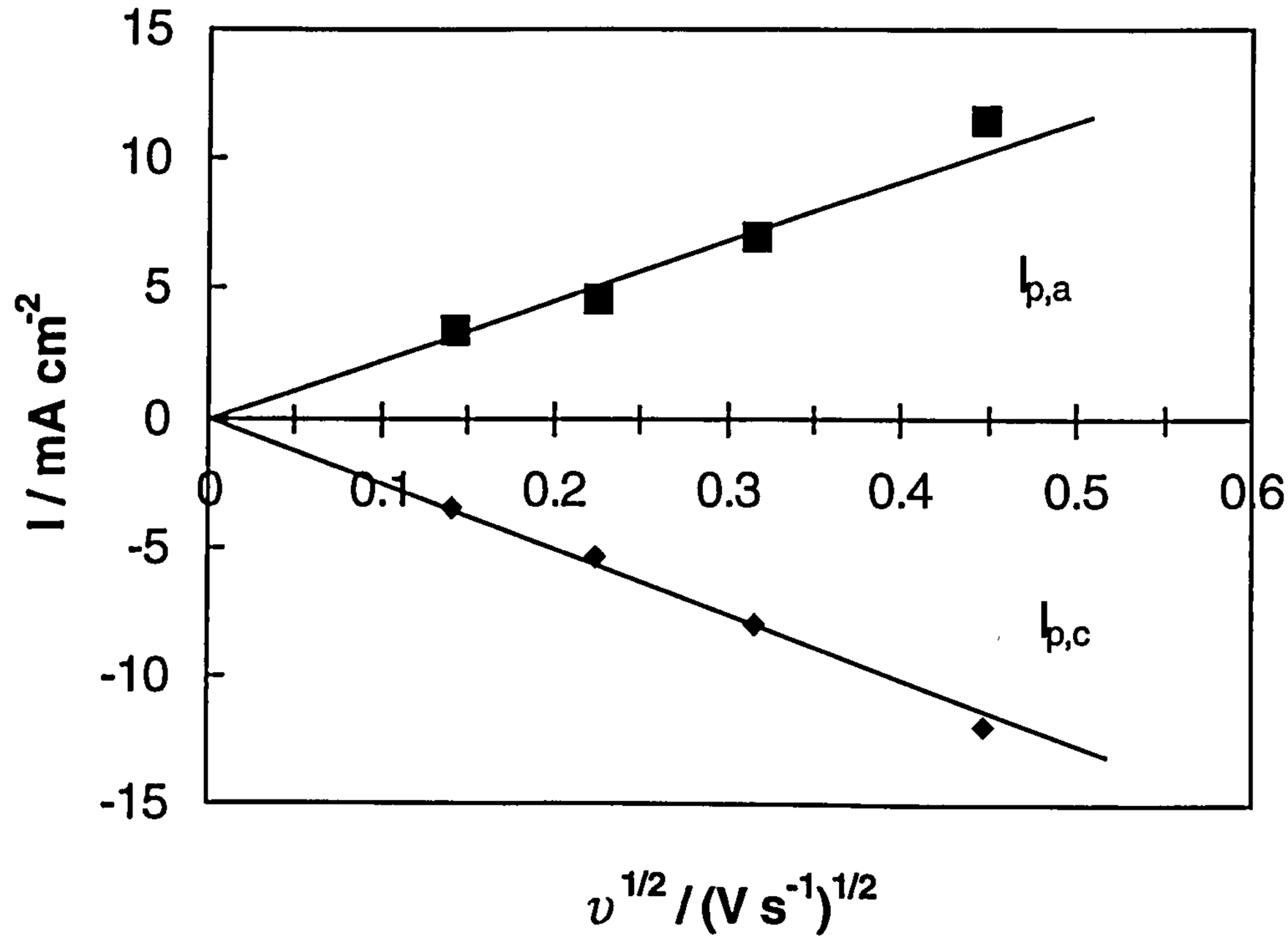

Fig. 5.3.5. Plot of cathodic and anodic peak currents vs. square root of sweep rate for aluminium deposition and stripping on platinum from 2:1 $AlCl_3$-TMPAC melts at 25°C.

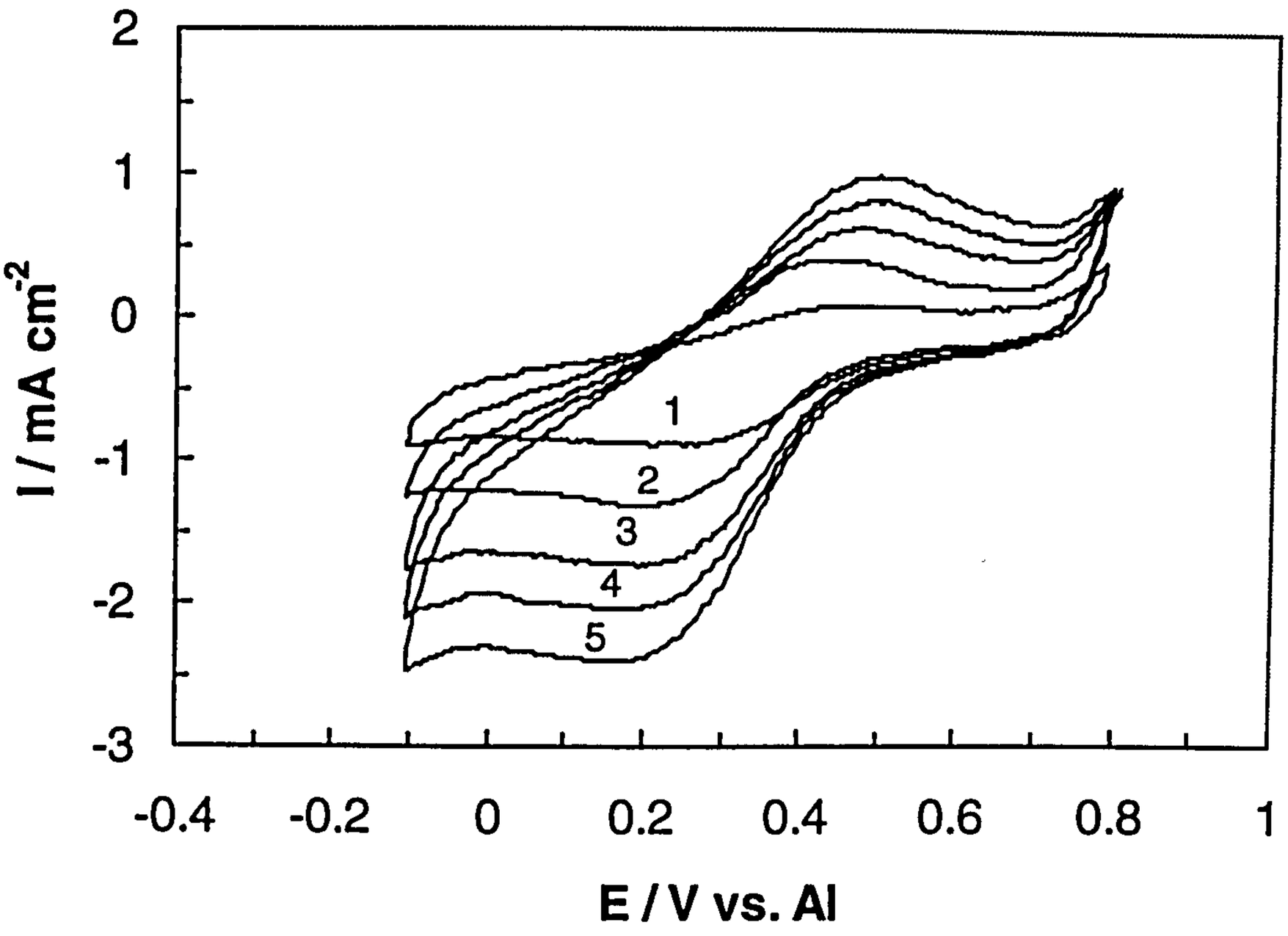

Fig. 5.3.6. Voltammograms, with correction of the background current, revealing Al-Pt alloy deposition and stripping on platinum from 2:1 $AlCl_3$-TMPAC melts at 25°C. Sweep rates (V s^{-1}): (1) 0.1; (2) 0.25; (3) 0.5; (4) 0.75; (5) 1.0.

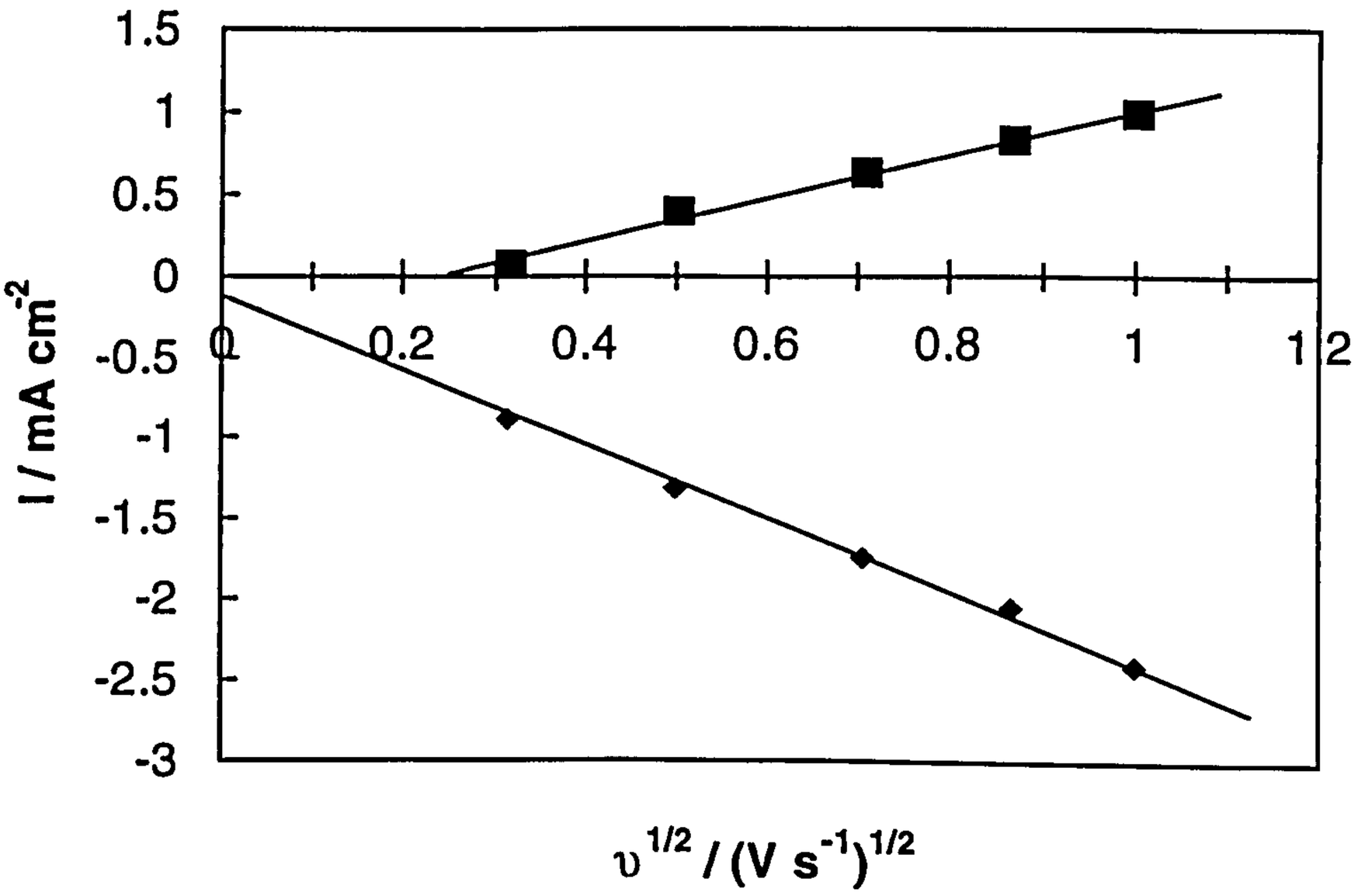

Fig. 5.3.7. Plot of cathodic and anodic peak currents vs. square root of sweep rate for underpotential deposition and stripping of aluminium on platinum from 2:1 $AlCl_3$-TMPAC melts at 25°C.

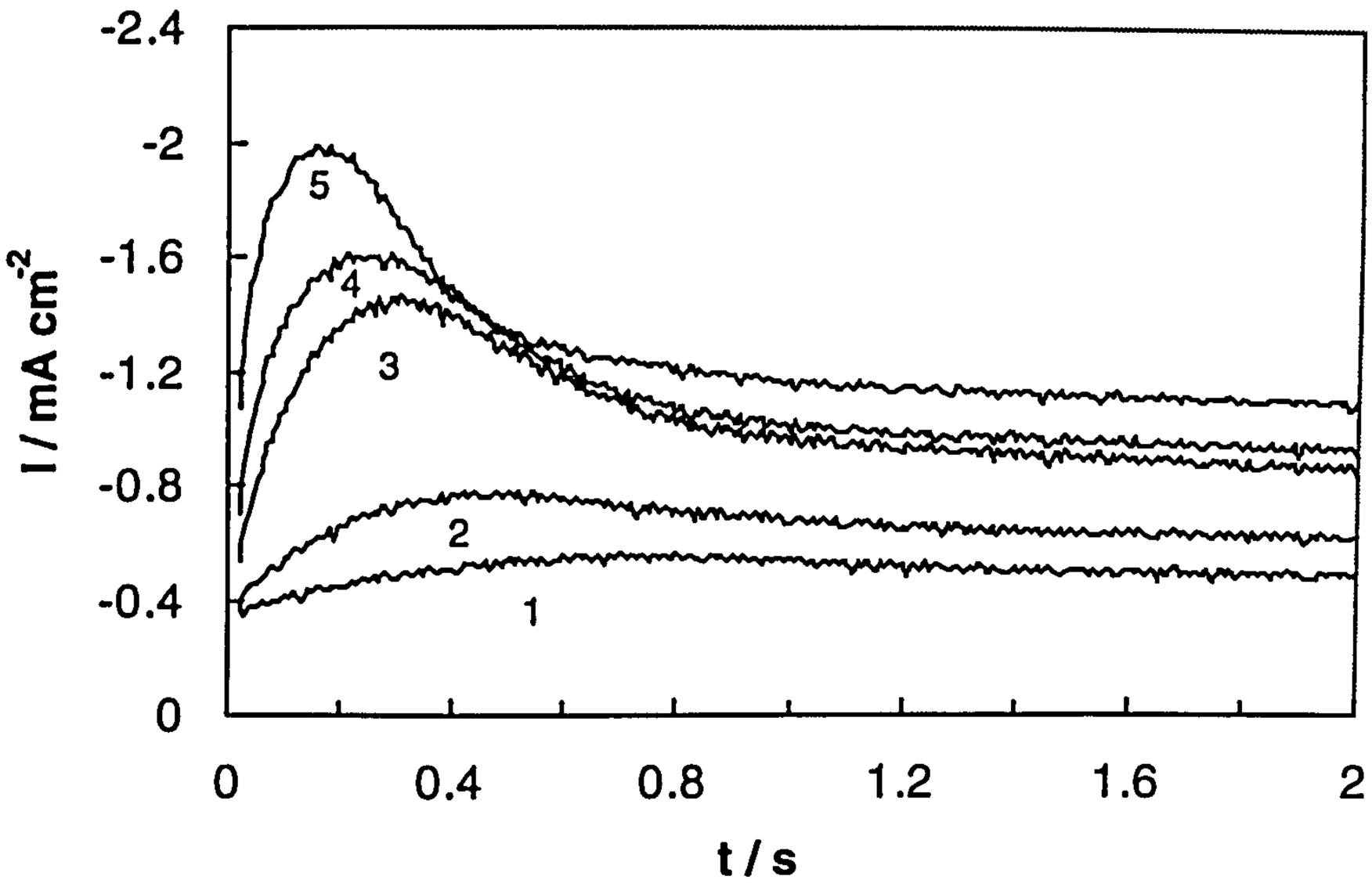

Fig. 5.3.8. Potential-step current transients for aluminium deposition on platinum from 2:1 $AlCl_3$-TMPAC melts at 25°C at applied potentials (V): (1) -0.16; (2) -0.18; (3) -0.20; (4) –0.22; (5) –0.24.

5.3.2 Nucleation Analysis

Although the voltammetric behaviour of the melt on platinum and nickel looked very similar, that did not mean that they would have similar chronoamperometric behaviour. As shown in **Fig. 5.3.8**, despite the fact that the current-time transients of the bulk deposition of aluminium exhibited increasing currents typical of the formation and growth of nuclei, the dimensionless analysis (**Fig. 5.3.9**) revealed the nucleation process was instantaneous at short times and became progressive after t_m. This development reflected the aluminium deposition on platinum was different from that on the nickel.

It is noteworthy that at the same potentials, the nucleation currents of bulk aluminium deposition on platinum were far less than those on either the the nickel, or the alloy deposition (**Fig. 5.3.10**). In the latter case, the nucleation process was progressive (**Fig. 5.3.11**), similar to that on nickel. Values of 1.85

and 0.30 for x and α respectively allowed the calculation of the average value of nucleation rate constants as 182 s^{-1}.

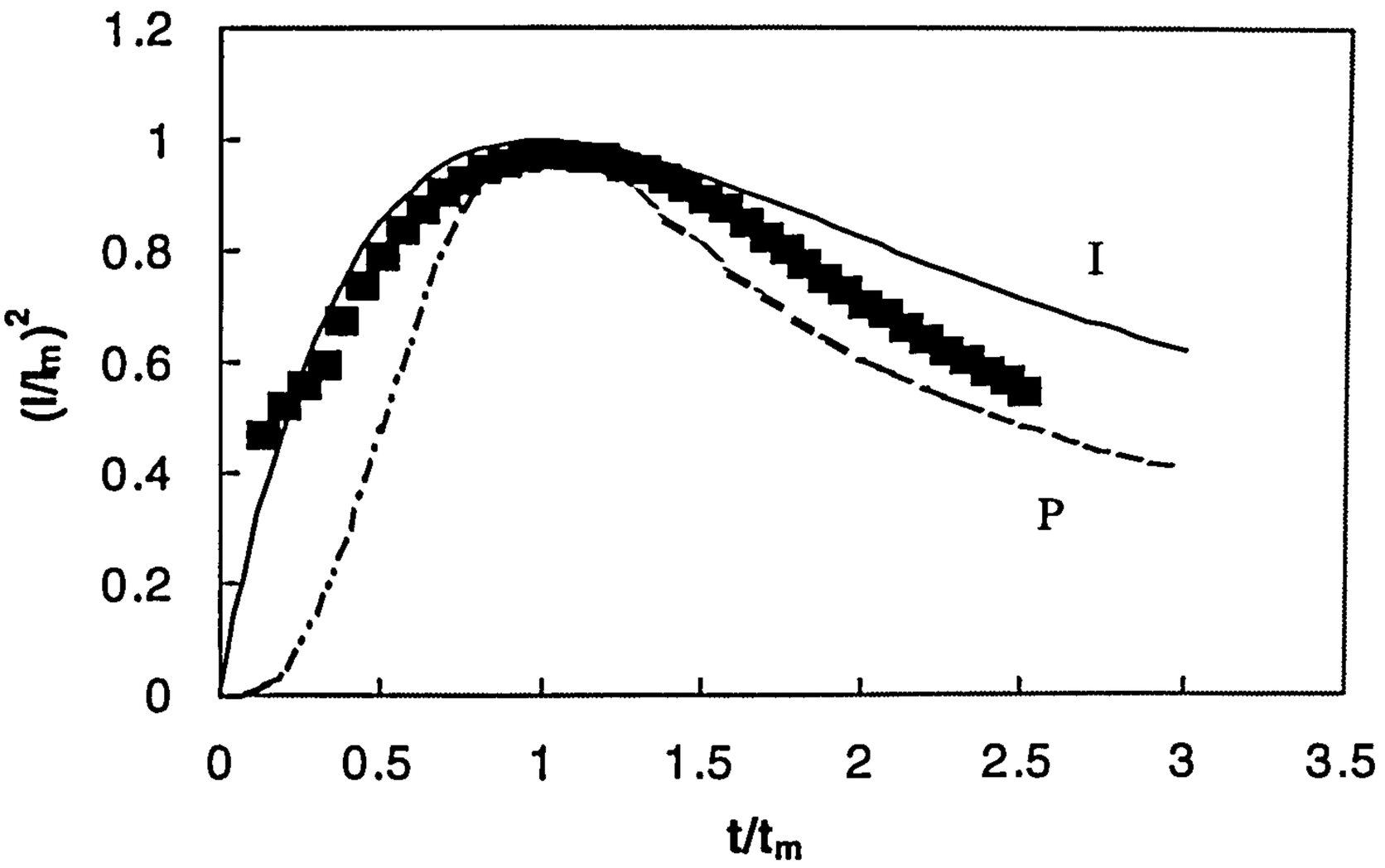

Fig. 5.3.9. Comparison of the dimensionless experimental data derived from **Fig. 5.3.8** with the theoretical models for diffusion controlled three dimensional instantaneous (I) and progressive (P) nucleation and growth.

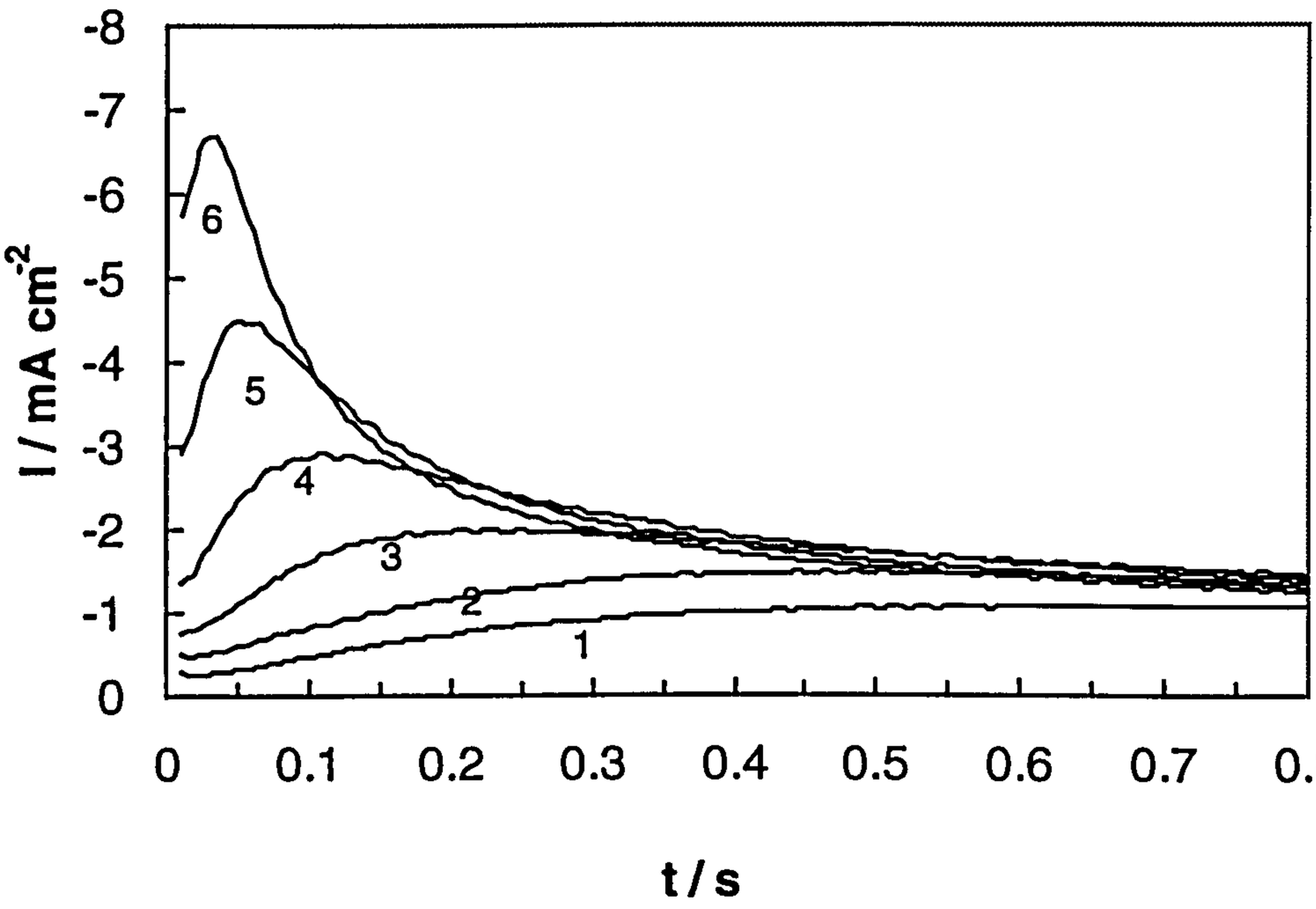

Fig. 5.3.10. Potential-step current transients for Al-Pt alloy deposition on platinum in 2:1 $AlCl_3$- TMPAC melts at 25°C. Applied potentials (V) were: (1) 0.40; (2) 0.35; (3) 0.30; (4) 0.25; (5) 0.20; (6) 0.15.

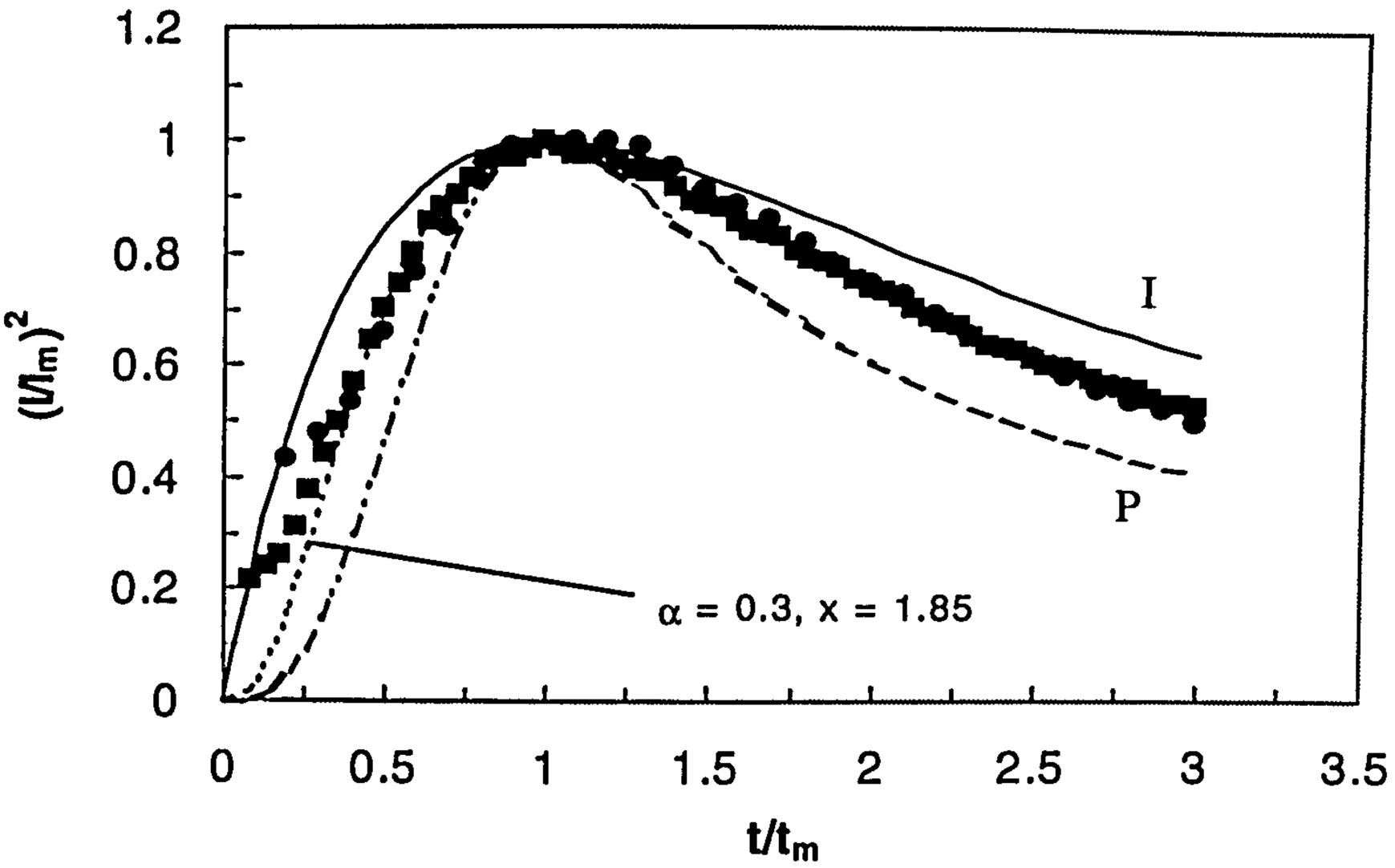

Fig. 5.3.11. Comparison of the dimensionless experimental data derived from **Fig. 5.2.15** with the theoretical models for diffusion controlled three dimensional instantaneous and progressive nucleation and growth.

CHAPTER 6

ALUMINIUM ELECTRODEPOSITION FROM MELTS WITH NICKEL IONS

6.1 CHARACTERISTICS OF MELTS WITH Ni(II) IONS

In order to better understand the voltammetric behaviour of Ni(II) species, the characteristics of the melt with 0.1 mM $NiCl_2$ added were investigated on glassy carbon and tungsten substrates. It should be pointed out that at room temperature the solubility of $NiCl_2$ in 2:1 $AlCl_3$-TMPAC melts was very low and, in fact, 0.1 mM was nearly a saturated concentration.

Such low solubility might result from the change of the acidity of the melt. In accordance with **Eqn. 1.3.4**:

$$2AlCl_4^- \rightleftharpoons Al_2Cl_7^- + Cl^- \qquad (1.3.4)$$

the addition of $NiCl_2$ would the increase the concentration of Cl^- ions which would shift the above equilibrium to the left, resulting in a lower concentration of $Al_2Cl_7^-$ ions, *i.e.*, the acidity of the melt would decrease.

Typical voltammograms on glassy carbon with (**curve 1**) and without (**curve 2**) Ni(II) ions are shown in **Fig. 6.1.1**. Compared with **curve 2**, a new pair of peaks (**A** and **A'**) were found in **curve 1**. Peak **A** at *ca.* 0.65 V might be assigned to the reduction of Ni(II) ions and the corresponding stripping peak **A'** occurred around 1.2 V. The difference of the peak potentials was 0.55 V indicative of the

irreversibility of the process. Similar to the observation on nickel electrodes, after passing $E_{f,A}$, the cathodic current density decreased slowly, suggesting the involvement of Ni-Al alloying effect. And then it was followed by a plateau and a board wave **C** due to the formation of Ni-Al alloy and aluminium UPD. However, the current density on wave **C** was higher than that in the nickel-free melt (**curve 2**), proving the contribution of Ni deposition to the alloy. Like the nickel-free melt, the current density loop **B** crossed at -0.07 V, suggesting that the similar aluminium nucleation was involved in the deposition of bulk aluminium.

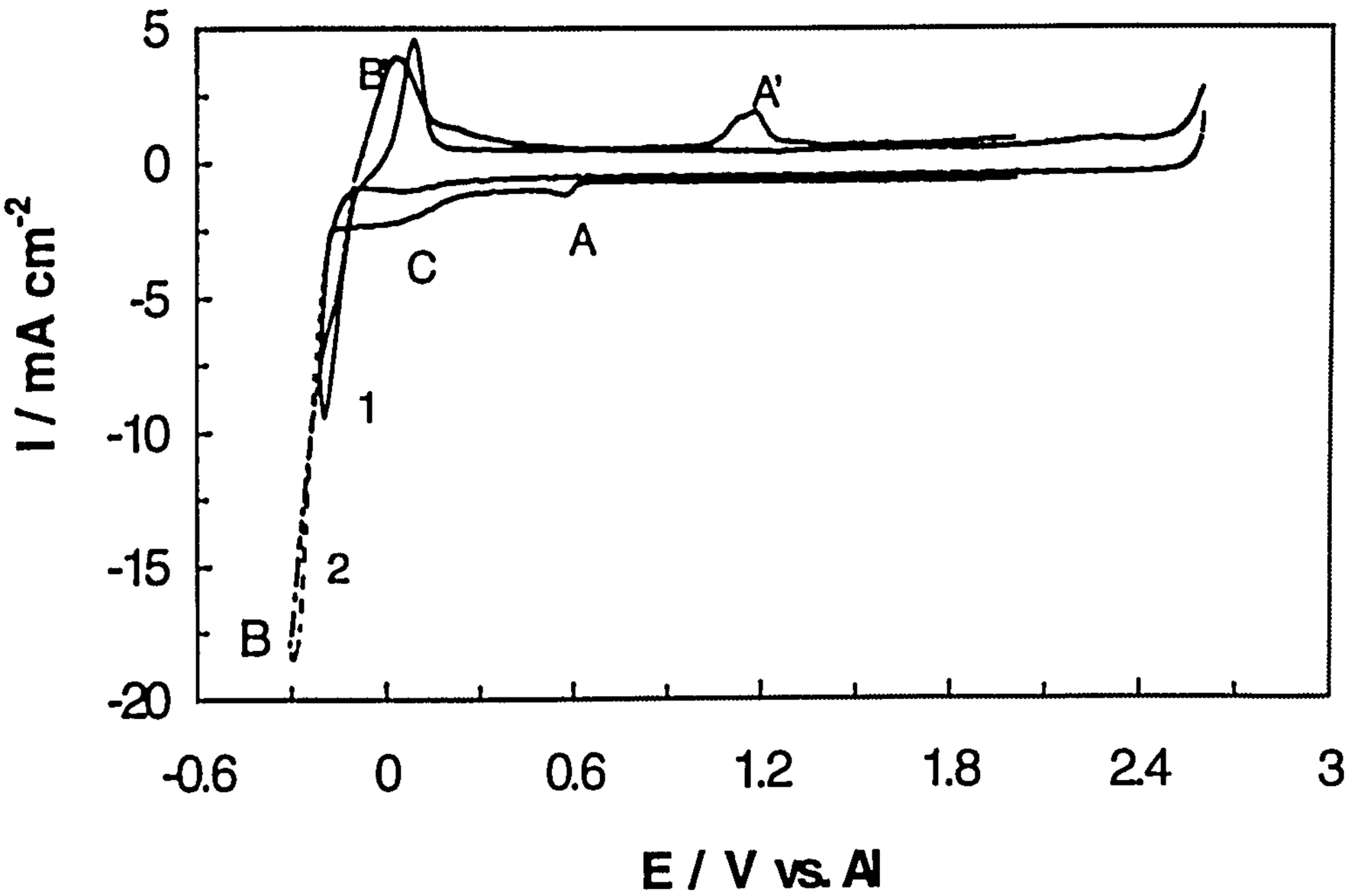

Fig. 6.1.1. Cyclic voltammograms of 2:1 $AlCl_3$-TMPAC melts on glassy carbon with (1) and without (2) 0.1 mM Ni^{2+} at 25°C. Sweep rate: 0.1 V s^{-1}.

In comparison to those in **curve 2**, the addition of Ni(II) species obviously affected the bulk aluminium deposition and stripping. Not only did the bulk aluminium deposition and stripping peaks in **curve 1** become more well-defined, but also the coulombic efficiency increased from 35% of **curve 2** to 48% of **curve 1**. The latter was obtained from **Fig. 6.1.2**. This effect might be caused by the adding $NiCl_2$ which served as the strong electrolytes to increase conductivity of the

melt. However, the fact of the coulombic efficiency lower than 50% still demonstrated the very poor adhesion of the aluminium deposits to glassy carbon and the reason could be same as the discussion for the nickel-free melt in **Sec. 4.2.2.** In **Fig. 6.1.2** the charge for the UPD wave **C** was calculated to be 7.78 mC cm^{-2}, corresponding to 10 monolayer equivalents of aluminium. Interestingly, the coulombic efficiency of nickel deposition and stripping was 110%, implying that other processes seemed to be involved in the nickel stripping.

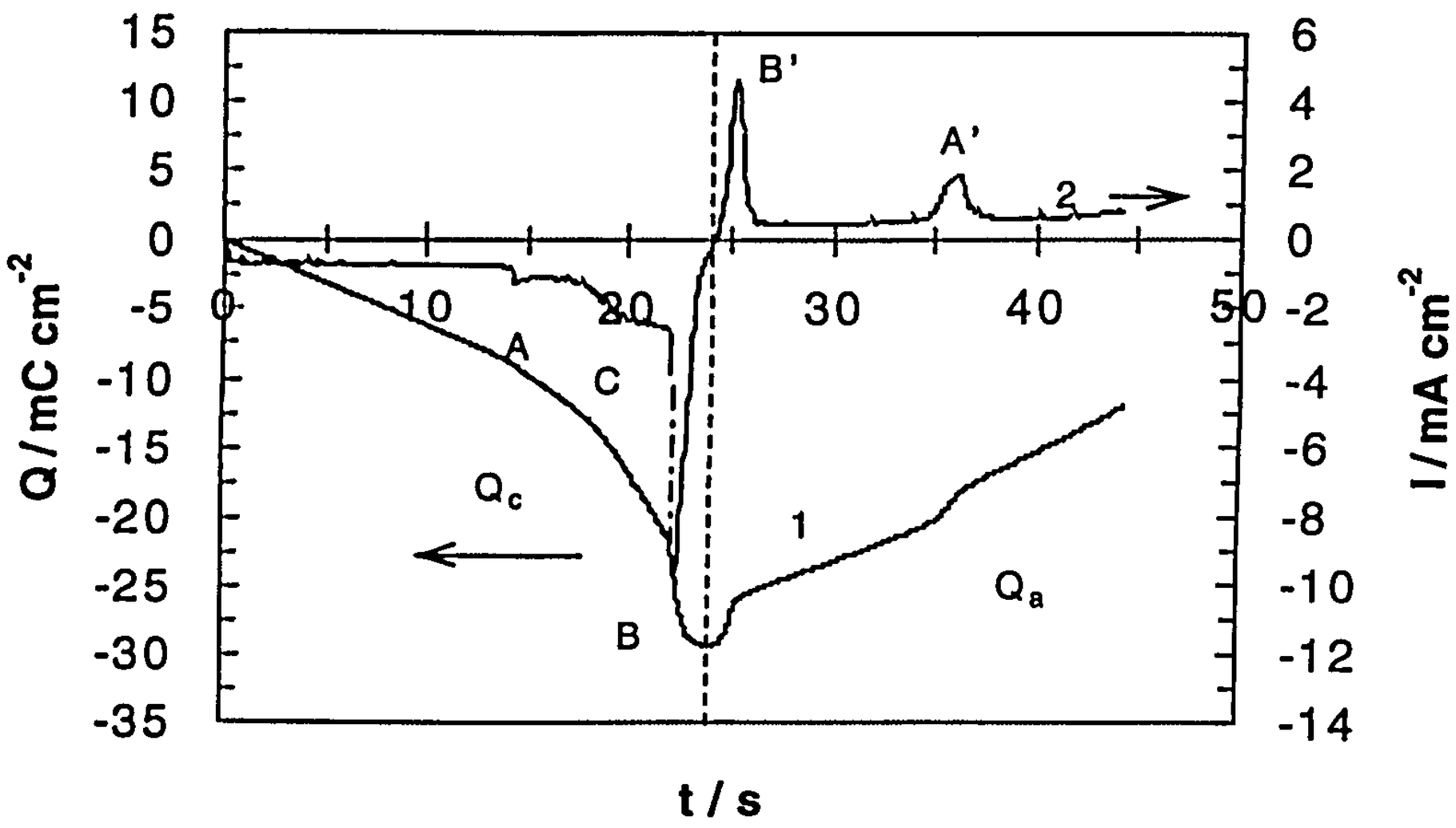

Fig. 6.1.2. Charge analysis (1) obtained from the corresponding current-time transient (2) din **Fig. 6.1.1.**

Fig. 6.1.3 shows a comparison of voltammograms for the pure melt on nickel electrode (**curve 1**) and for the nickel-containing melt on glassy carbon (**curve 2**). The peak potential of the nickel deposition wave **C** was about 0.3 V more positive than that of Ni-Al alloy deposition peak **A**. Clearly, the nickel deposition involved in wave **A** did not result from the uncomplexed Ni^{2+} ions. This could be evident that the reaction occurring between the nickel electrode and most Ni(II) species involved in waves **A, A', D** and **E** came from the reaction. This was further confirmed by the fact that only a small wave **C'** appeared rather than three large peaks **A', D** and **E,** corresponding to nickel deposition wave **C**. It should be

noted that peak **C'** appeared to be composed of two peaks at 1.12 V and 1.20 V, respectively. The potential of the former peak was close to that of the shoulder following wave **D** in **curve 1**, whereas the latter one located at the onset of wave **E**. According to the analysis in **Chapter 5**, it was probable that the fresh nickel deposits were complexed by Cl^- or $TMPA^+$ ions in the melt according to the reactions **5.2.2** and **5.2.3**. Since the extra charge was required for the reactions, it caused the value of Q_c'/Q_c to be greater than unity.

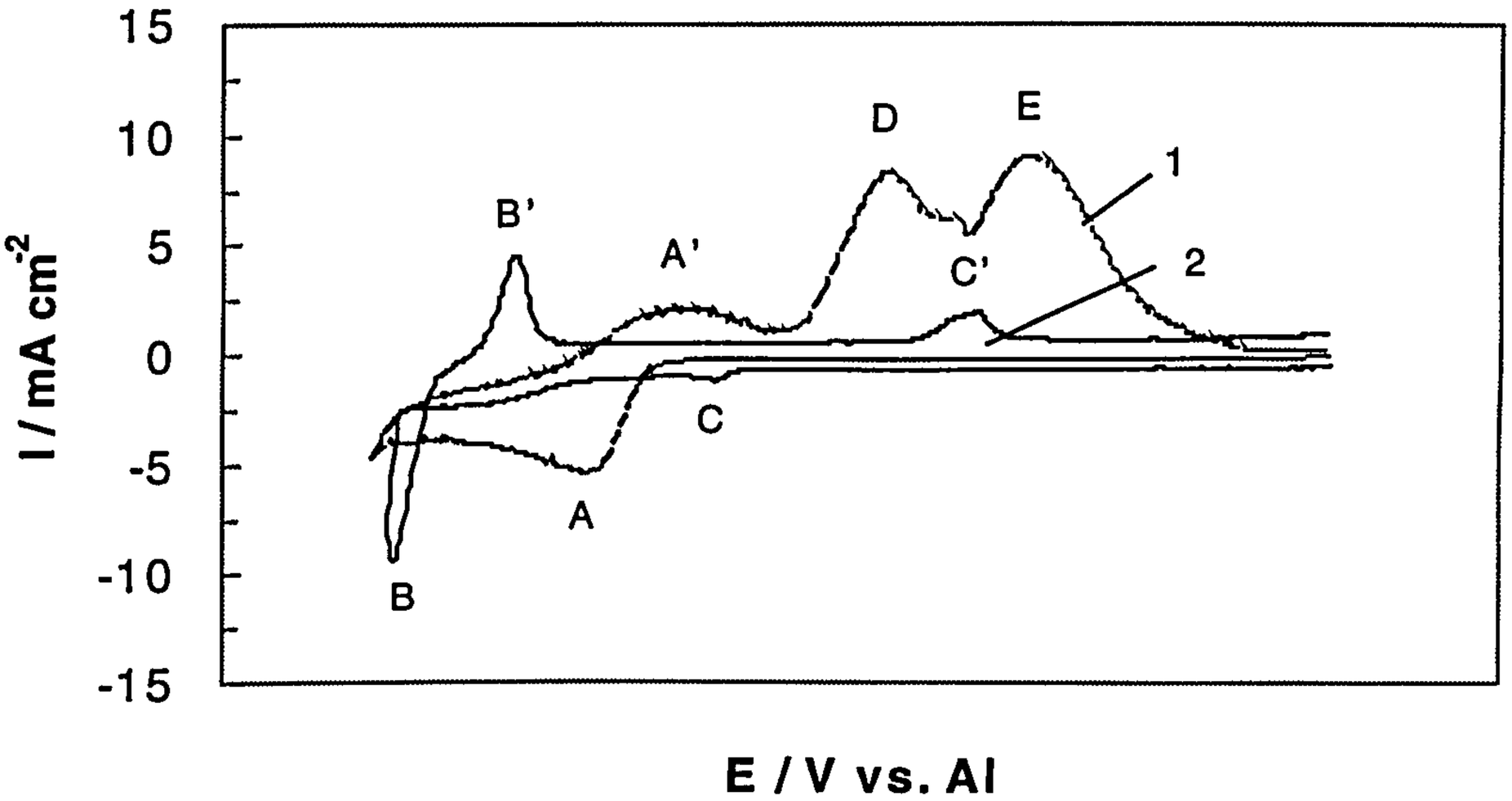

Fig. 6.1.3. Cyclic voltammograms of 2:1 $AlCl_3$-TMPAC melts without added Ni^{2+} ions on nickel (1) and glassy carbon with 0.1 mM Ni^{2+} ions on glassy carbon (2) at 25 °C. Sweep rate: 0.1 V s^{-1}.

To reveal how the alloying effect influenced waves **C** and **C'**, the voltammetric experiments were performed at different switching potentials. As the switching potentials increased negatively from 0.5 V to -0.2 V (**Figs. 6.1.4**), $I_{p,C}$ decreased slightly after $E_\lambda < E_{p,C}$ (**Fig. 6.1.5**), whereas $I_{p,C'} \sim E_\lambda$ plots exhibited a peak as shown in **Fig. 6.1.6**. $I_{p,C'}$ rose in the E_λ range of 0.2 ~ 0.5 V, which covered the plateau region of the involved alloy, and reached a maximum when E_λ approached the onset of wave **C**. As E_λ passed through the aluminium UPD

region, $I_{p,C}$, decreased and the minimum value was observed prior to the occurrence of bulk aluminium deposition.

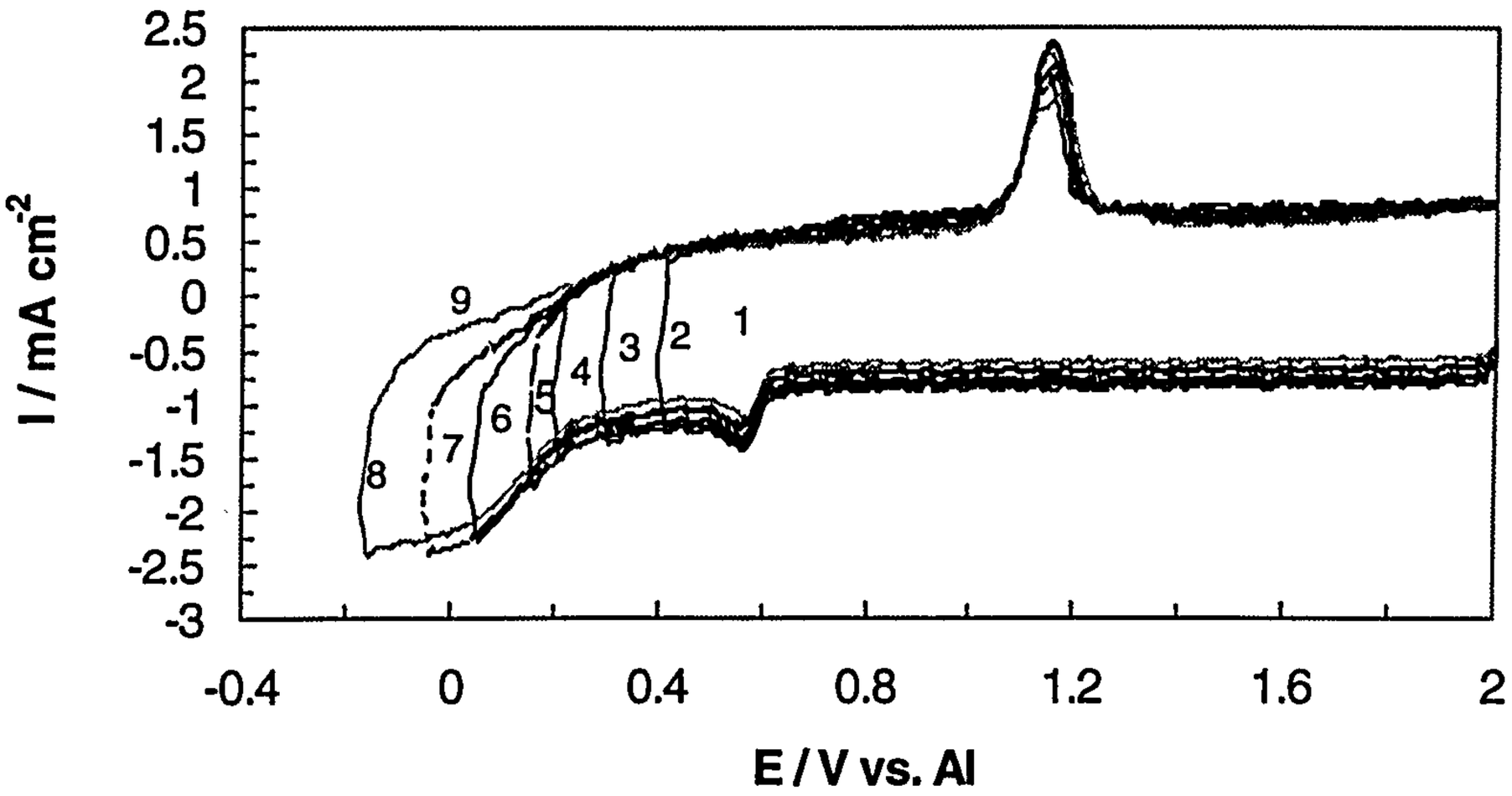

Fig. 6.1.4. Cyclic voltammograms of 2:1 $AlCl_3$-TMPAC melts with 0.1 mM Ni^{2+} ions on glassy carbon at 25°C. Switching potentials: (1) 0.5 V; (2) 0.4 V; (3) 0.3 V; (4) 0.2 V; (5) 0.15 V; (6) 0.05 V; (7) -0.05 V; (8) -0.15 V; (9) -0.2 V. Sweep rate: 0.10 V s^{-1}.

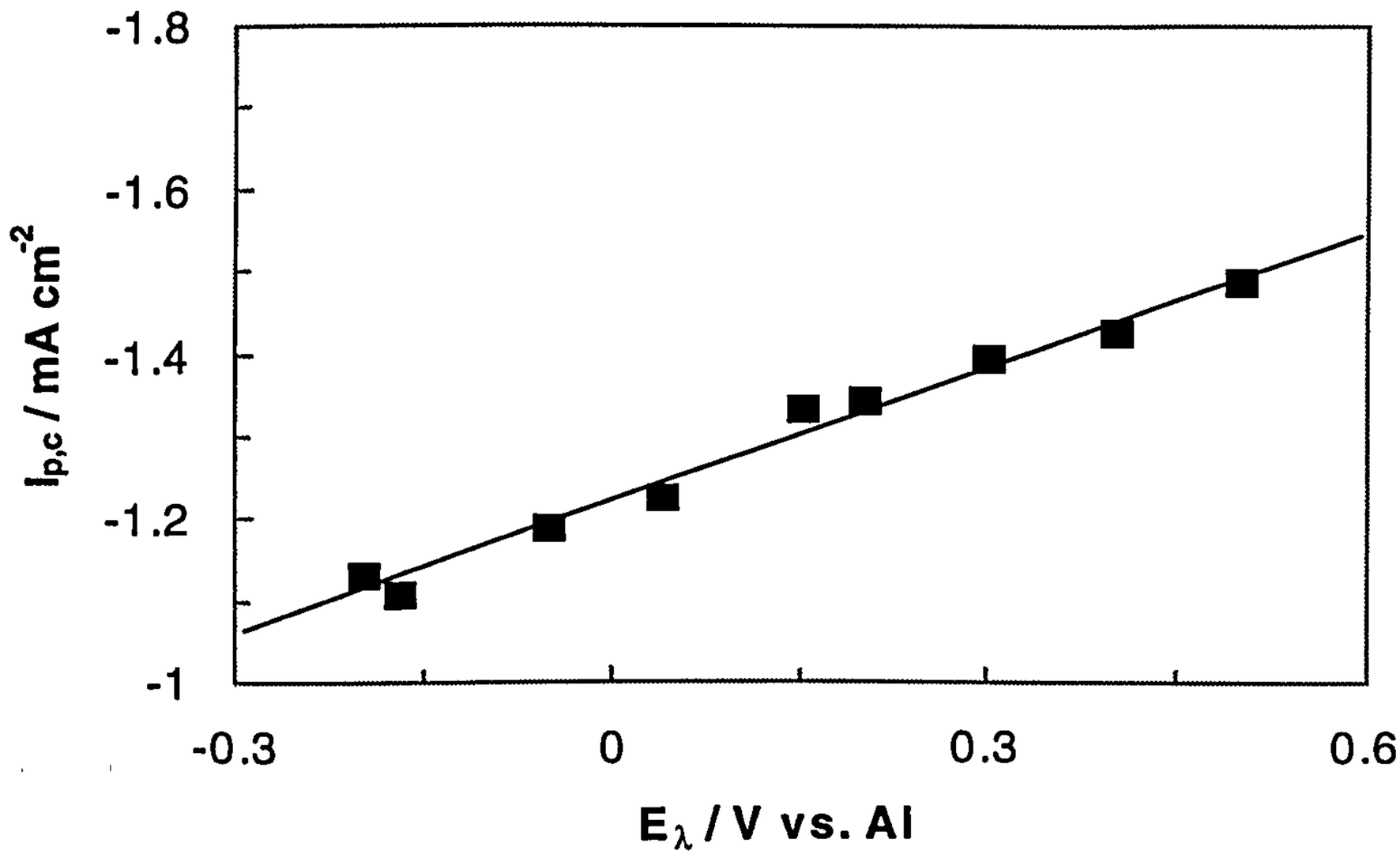

Fig. 6.1.5. Plot of $I_{p,c}$ *vs.* E_λ for aluminium deposition on glassy carbon in 2:1 $AlCl_3$-TMPAC melt with 0.1 mM Ni^{2+} ions at 25°C. Sweep rate: 0.10 V s^{-1}.

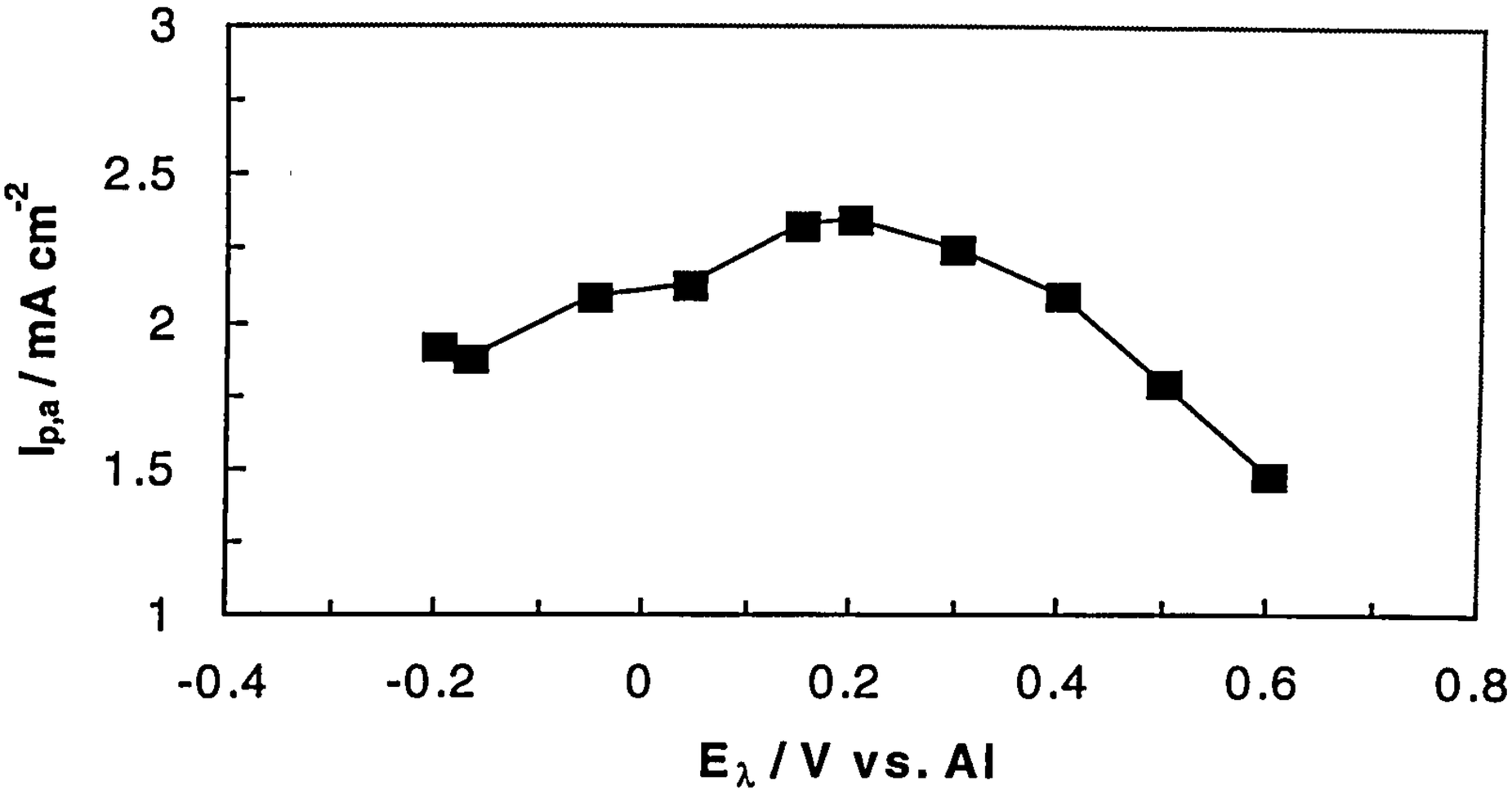

Fig. 6.1.6. Plot of $I_{p,a}$ *vs.* E_λ for aluminium stripping on glassy carbon in 2:1 $AlCl_3$-TMPAC melt with 0.1 mM Ni^{2+} ions at 25°C. Sweep rate: 0.10 V s^{-1}.

The above results revealed that the development of the peak current, $I_{p,C'}$,mainly resulted from the nickel component in the Ni-Al alloy. The linear decrease for $I_{p,C} \sim E_\lambda$ plots might be caused the irreversibility of nickel or Ni-Al alloy deposition and stripping. This irreversibility possibly arose from the alloying effect or the oxidation between the fresh deposits and the melt. If the deposits at $E_{p,C}$ are from the original Ni^{2+} ions, as E_λ shifted negatively, the concentration of original Ni^{2+} ions would decrease with increasing alloying or oxidation, resulting in the linear decrease for $I_{p,C} \sim E_\lambda$ plots. On the other hand, when E_λ was within the plateau range, wave **C'** was due mainly to the stripping of nickel and the Ni-rich alloy deposits. The contribution from both of them caused the increase for $I_{p,C}$ and the maximum before $E_\lambda \geq 0.15$ V. After that point, the contribution of nickel deposits was constant, whereas that from the alloy decreased with the decreasing nickel composition in the alloy deposits, resulting in of the decreasing $I_{p,C'} \sim E_\lambda$ plots.

Based on the voltammetric results, convolution analysis for wave **C** in **Fig. 6.1.3** was carried out and compared with that on nickel electrode. Typical samples

are illustrated in **Fig. 6.1.7.** In the case of nickel deposition on glassy carbon (**curve 1**), convolution current density, m_t, rose more quickly prior to the occurrence of the reduction wave than that on nickel electrodes (**curve 2**). Apparently, the reduction of Ni^{2+} ions seemed to start at the beginning of the scan, much earlier than expected at 0.6 V, where wave **C** occurred. Further, no limiting convolution current was found as expected for a diffusion-controlled process, consistent with the observation in CV studies of Ni^{2+} ions. This further proved that the alloy deposition following the reduction of Ni^{2+} ions was involved in wave **C**. Similar results were obtained from **curve 2**, although the reduction of Ni^{2+} ions before the alloy deposition was not very clear.

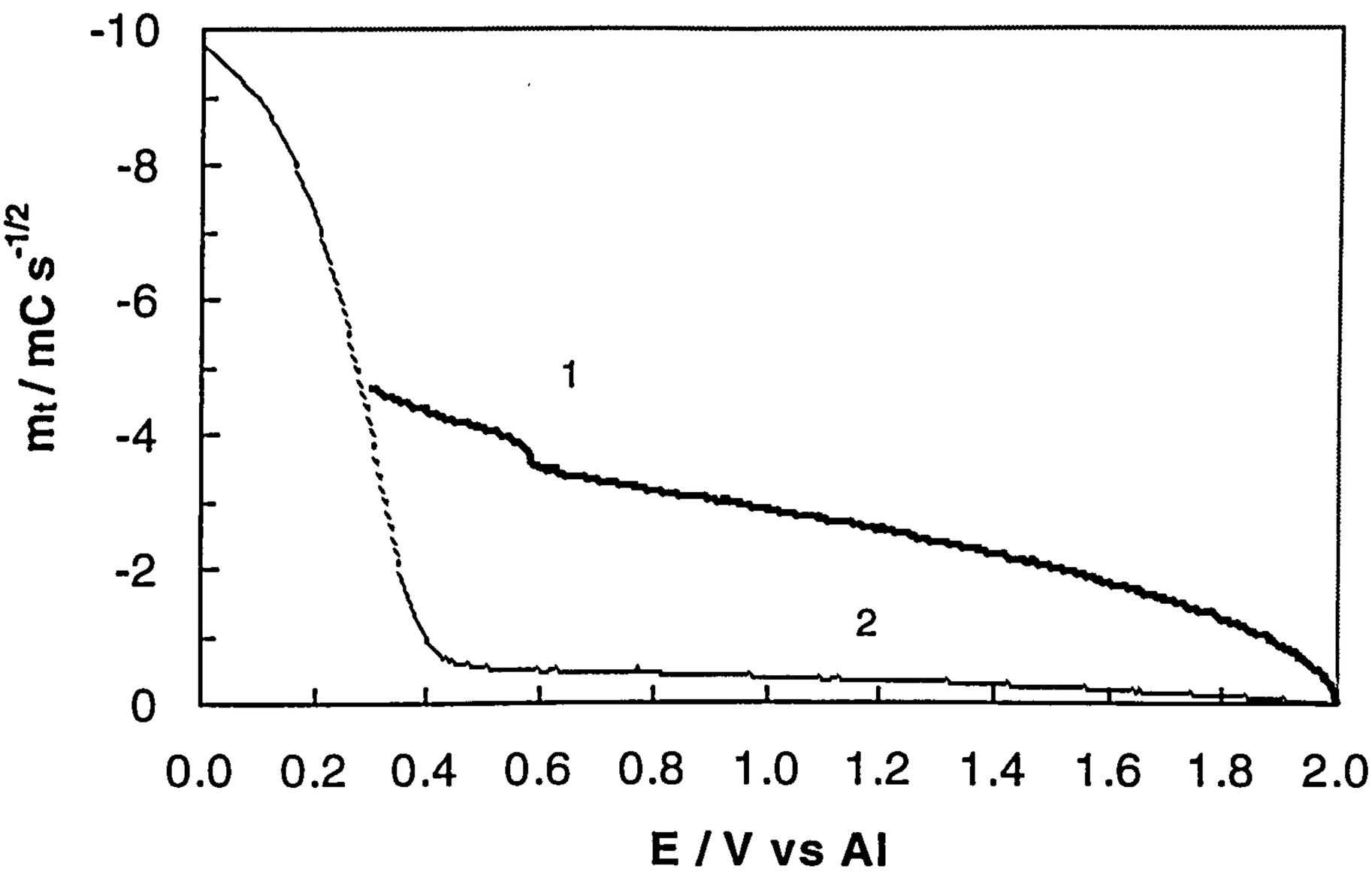

Fig. 6.1.7. Convoluted aluminium deposition currents in 2:1 $AlCl_3$-TMPAC melts on glassy carbon with 0.1 mM Ni^{2+} ions added (1) and without Ni^{2+} ions on nickel (2) at 25 °C. Sweep rate: 0.10 Vs^{-1}.

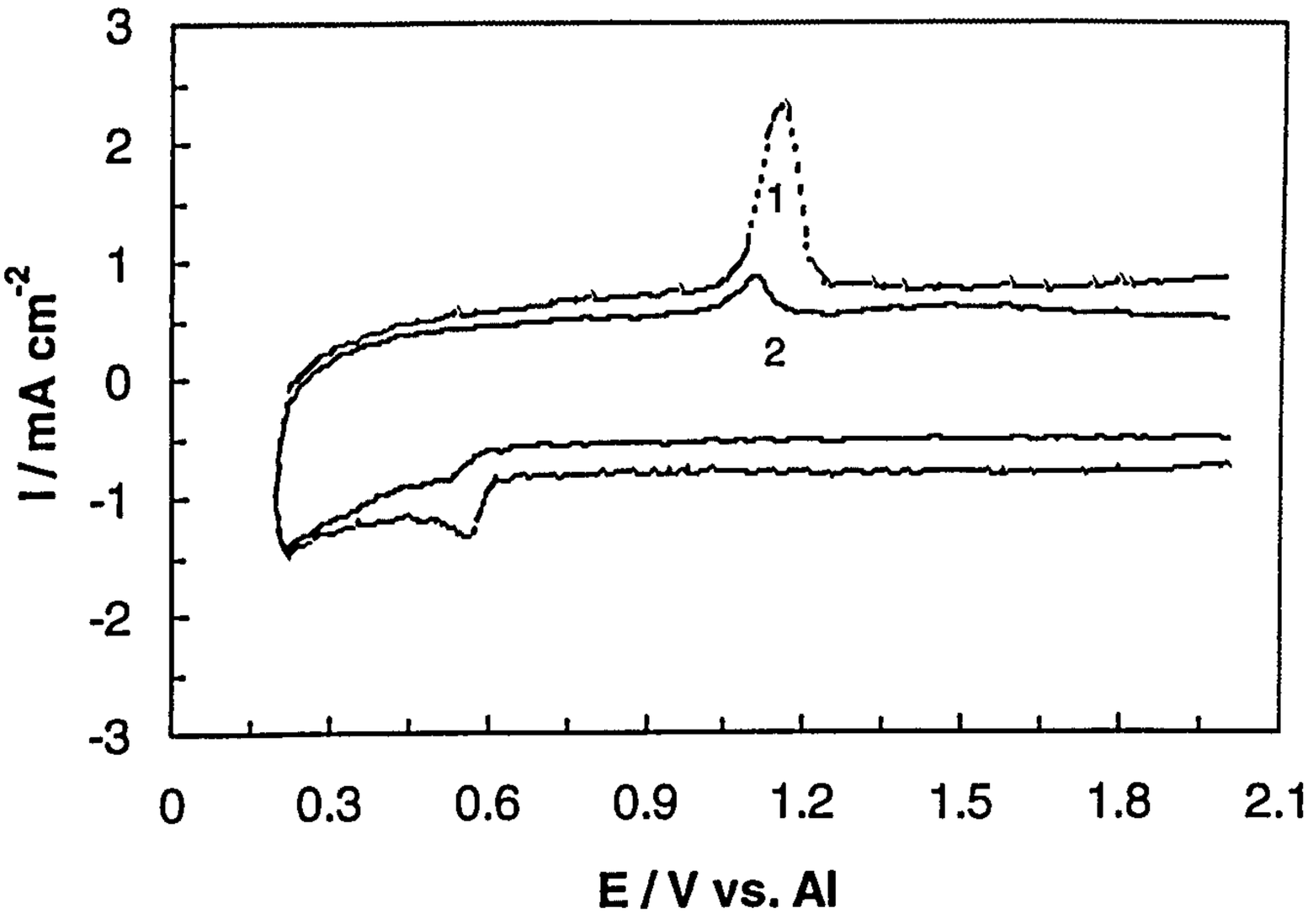

Fig. 6.1.8. Cyclic voltammograms of 2:1 $AlCl_3$-TMPAC melts with 0.1 mM Ni^{2+} ions on glassy carbon (1) and tungsten (2) at 25°C. Sweep rate: 0.1 V s^{-1}.

6.2 NUCLEATION ANALYSIS

6.2.1 The Formation of Ni-Al Alloy

A quantitative analysis of the deposition processes of bulk aluminium and Ni-Al alloy were performed by chronoamperometry. For the alloy deposition the potentials were stepped from an initial 2.0 V to the values indicated. A representative set of current-time transients obtained is shown in **Fig. 6.2.1.** Unlike the observations for nickel electrodes, no rising current typical of a nucleation process was found in these transients. Instead, the current decayed according to $t^{-1/2}$ kinetics while the magnitude at a given time was a function of potential. The $t^{-1/2}$ dependence indicated that linear diffusion was dominant such that the increased current could not be attributed to an increase in area that would occur with a nucleation and growth mechanism.

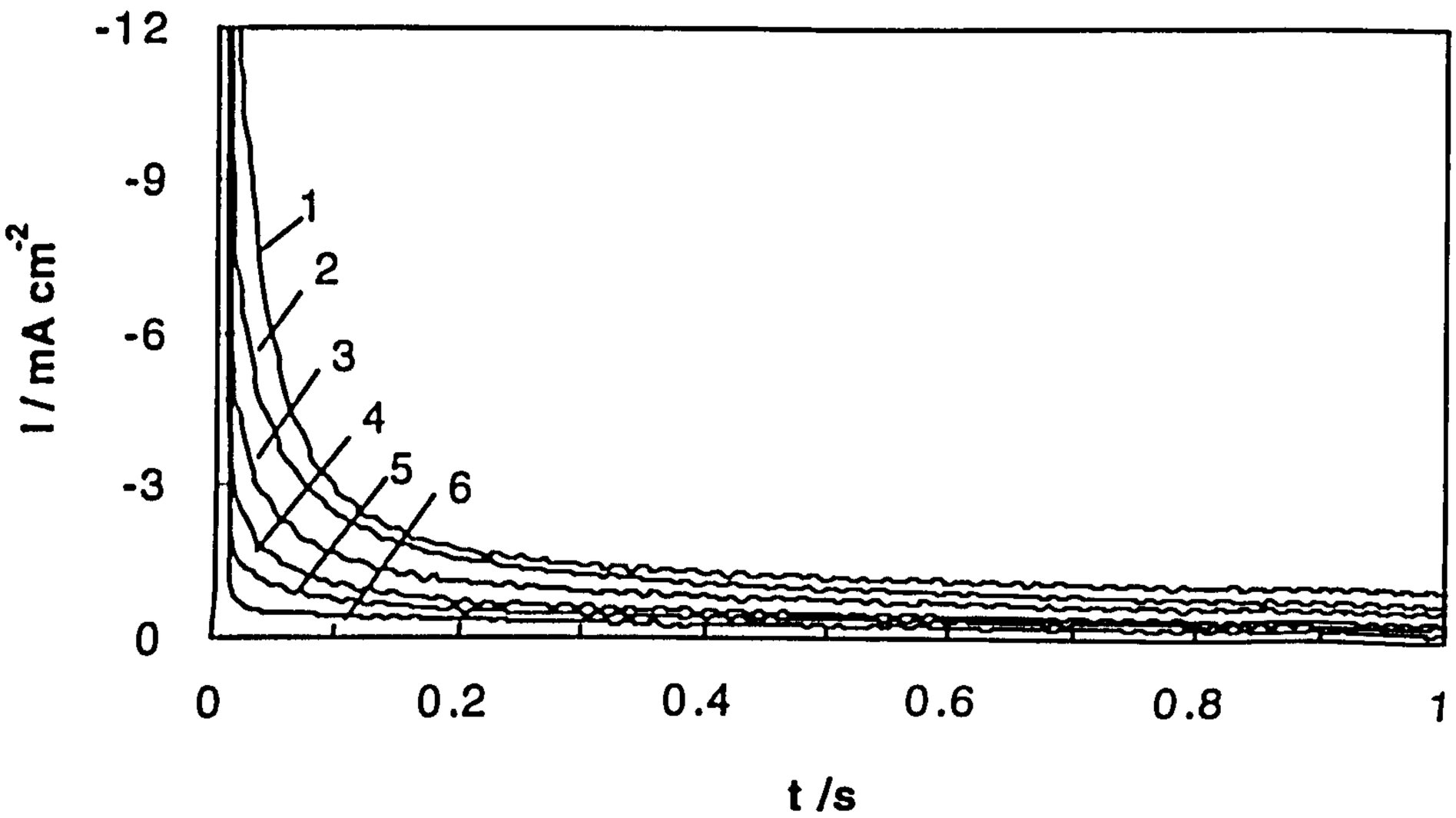

Fig. 6.2.1. Potential-step current transients for Al-Ni alloy deposition on glassy carbon in 2:1 $AlCl_3$-TMPAC melts with 0.1 mM Ni^{2+} ions at 25°C. Applied potentials are: (1) -0.19; (2) -0.18; (3) -0.17; (4) -0.16; (5) -0.15; and (6) -0.14V.

The effect of potential on the magnitude of the current was illustrated in the sampled current voltammogram shown in **Fig. 6.2.2.** The current at 0.5 V

represented the current for nickel reduction on glassy carbon. Thus, the increasing current observed with more negative potential should be due to codeposition of aluminium. As can be seen, when the potential was below 0.4 V a linear increase in current occurred, associated with the deposition of an alloy in which aluminium composition was a function of the potential. In this instance, the formation of the deposits was dominated by the thermodynamics of the alloy formation.

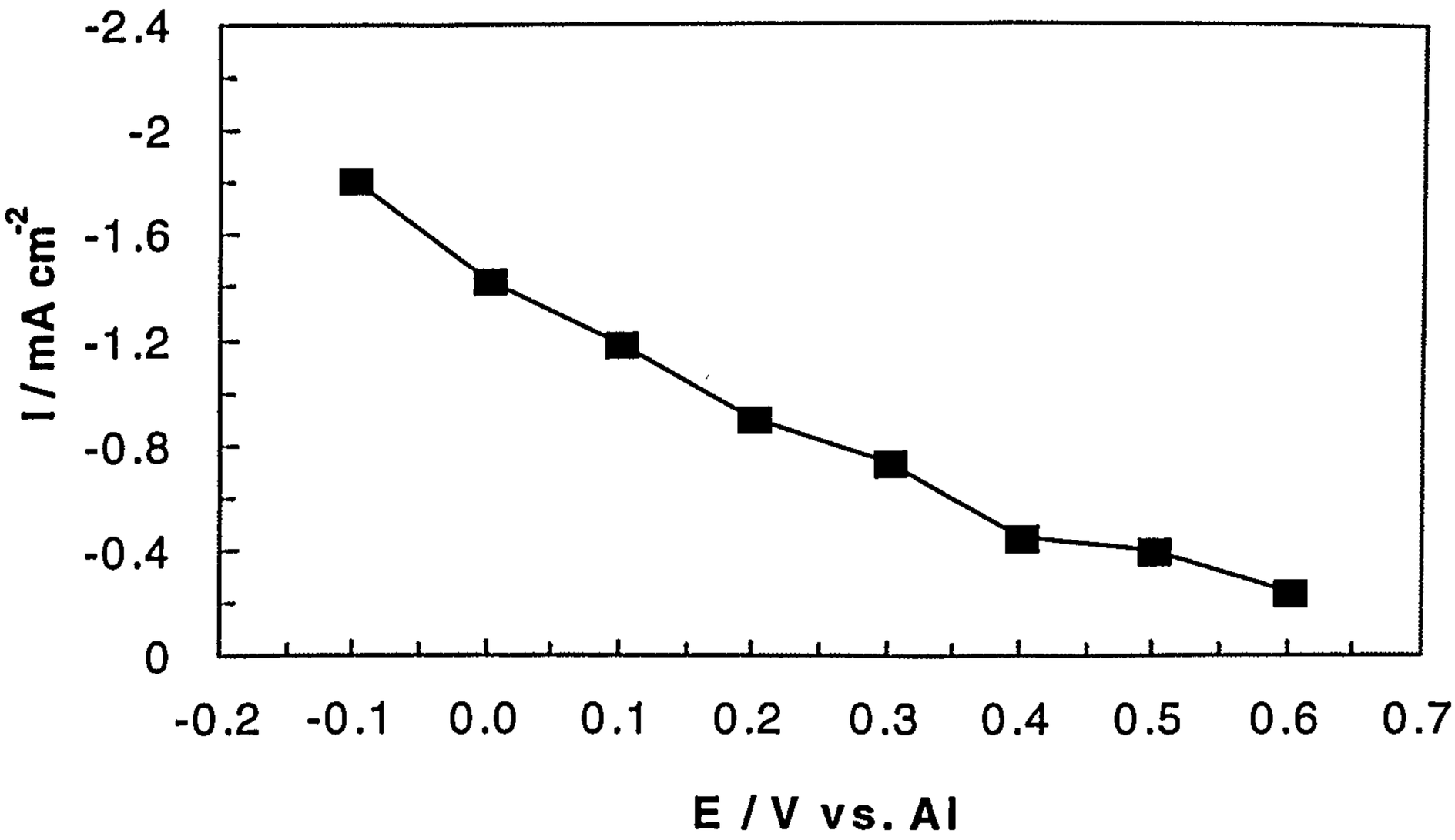

Fig. 6.2.2. Sampled current voltammogram constructed from current-time trnsients shown in **Fig. 6.2.1.**

6.2.2 The Bulk Aluminium Deposition

The bulk aluminium deposition process on glassy carbon in 2:1 $AlCl_3$-TMPAC melts with 0.1 mM Ni^{2+} ions at 25°C was also examined by chronoamperometry. Current-time transients of the initial potential starting at 0.0 V were identical with those from the nickel-free melt on glassy carbon in **Chapter 4.** For the current case of the melt containing $NiCl_2$, the potentials were stepped from an initial potential of 2.0 V to values where aluminium nucleation occurred. **Fig. 6.2.3** shows a set of typical current-time transients. The increasing current typical of the formation of growing nuclei on the surface of the electrode was found to occur at potentials more negative than -0.18 V, agreeing with the observation from

the nickel-free melt. However, after the maximum, the decreasing current decayed more slowly than $t^{-1/2}$. Only at –potentials less than 0.4 V did the current decay follow the Cottrell equation. The corresponding chronoamperometric data is summarised in **Table 6.2.1.** The average values for D and N were 2.74×10^{-8} cm^2 s^{-1} and 1.68×10^{-5} sites cm^{-2}, respectively.

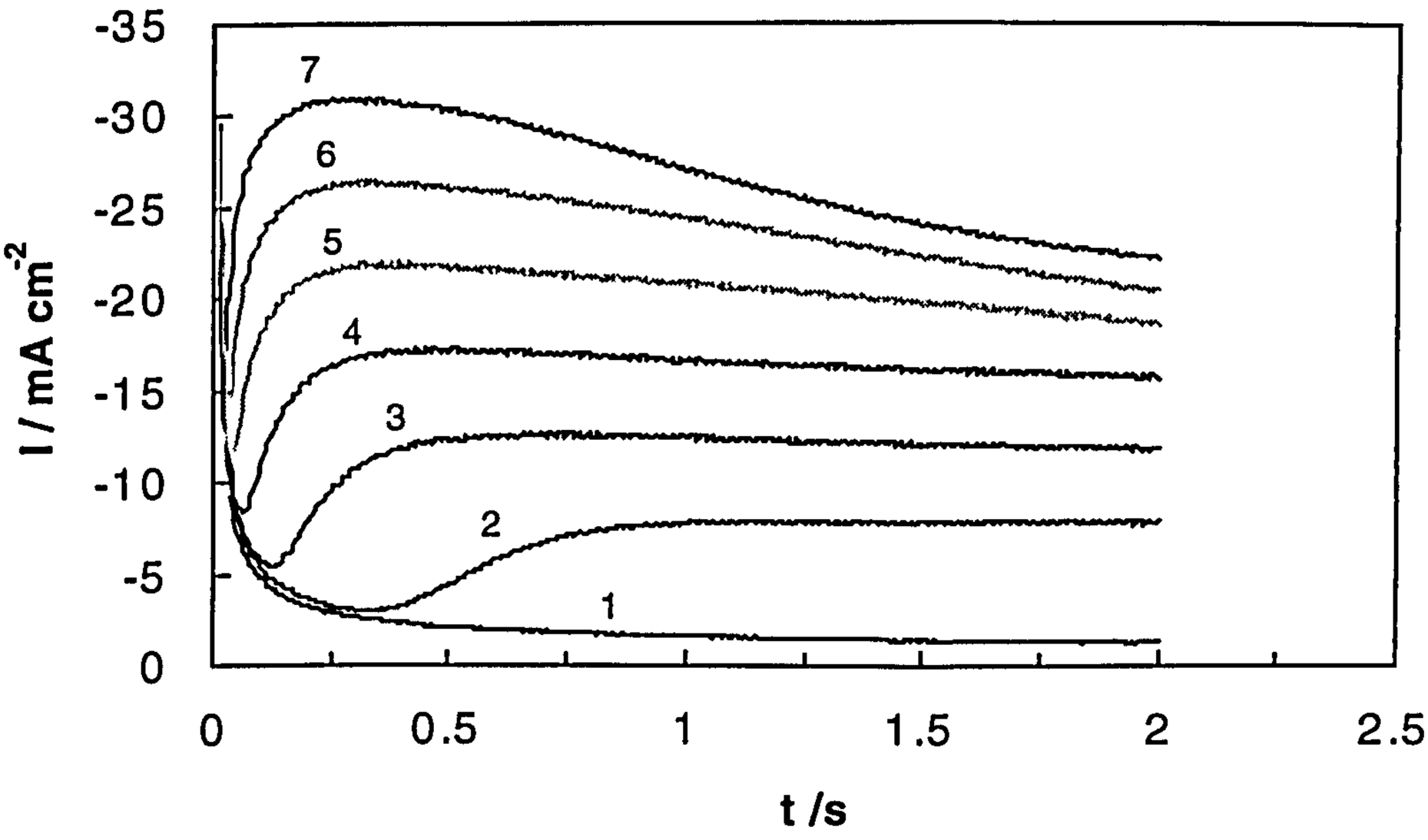

Fig. 6.2.3. Potential-step current transients for aluminium deposition on glassy carbon in 2:1 $AlCl_3$-TMPAC melt with 0.1 mM Ni^{2+} ions at 25°C. Applied potentials are: (1) -0.16; (2) -0.20; (3) -0.24; (4) -0.28; (5) -0.32; and (6) -0.36; and (7) –0.40V.

Table 6.2.1. Chronoamperometric data for Aluminium nucleation from the melt containing $NiCl_2$ on the glassy carbon electrode

E vs. Al (V)	$10^3 I_m$ (A cm^{-2})	t_m (s)	$10^6 (I_m)^2 (t_m)$ (A cm^{-2} s)	$10^8 D$ (cm^2 s^{-1})	$10^{-5} N$ (sites cm^{-2})
-0.32	-22.00	0.36	17.18	2.11	1.92
-0.34	-24.22	0.34	19.36	2.38	1.83
-0.36	-26.42	0.33	23.38	2.87	1.50
-0.38	-28.80	0.31	25.71	3.16	1.47
-0.40	-30.95	0.27	25.86	3.18	1.68

Notably, in the case of 2:1 $AlCl_3$- TMPAC melts with 0.1 mM Ni^{2+} ions on glassy carbon, when the initial potential was 2.0 V, times to reach the maximum

currents, t_m, were larger and the maximum currents, I_m were smaller, compared with the results for the nickel-free melt on tungsten from initial potentials of 0.0 V (**Table 4.2.2**),. These differences of t_m, and I_m from the melts with and without nickel ions indicated the completely different states of the electrode surfaces in the two cases. The comparison of the sampled voltammograms of the two cases (**Fig. 6.2.4**) demonstrated that in the nickel-free melt a slight rising current plateau characteristic of a diffusion limited process started at -0.26 V (**curve 2**). In contrast, no such plateau was found in the latter case, instead, the current increased linearly with more negative shifting potentials.

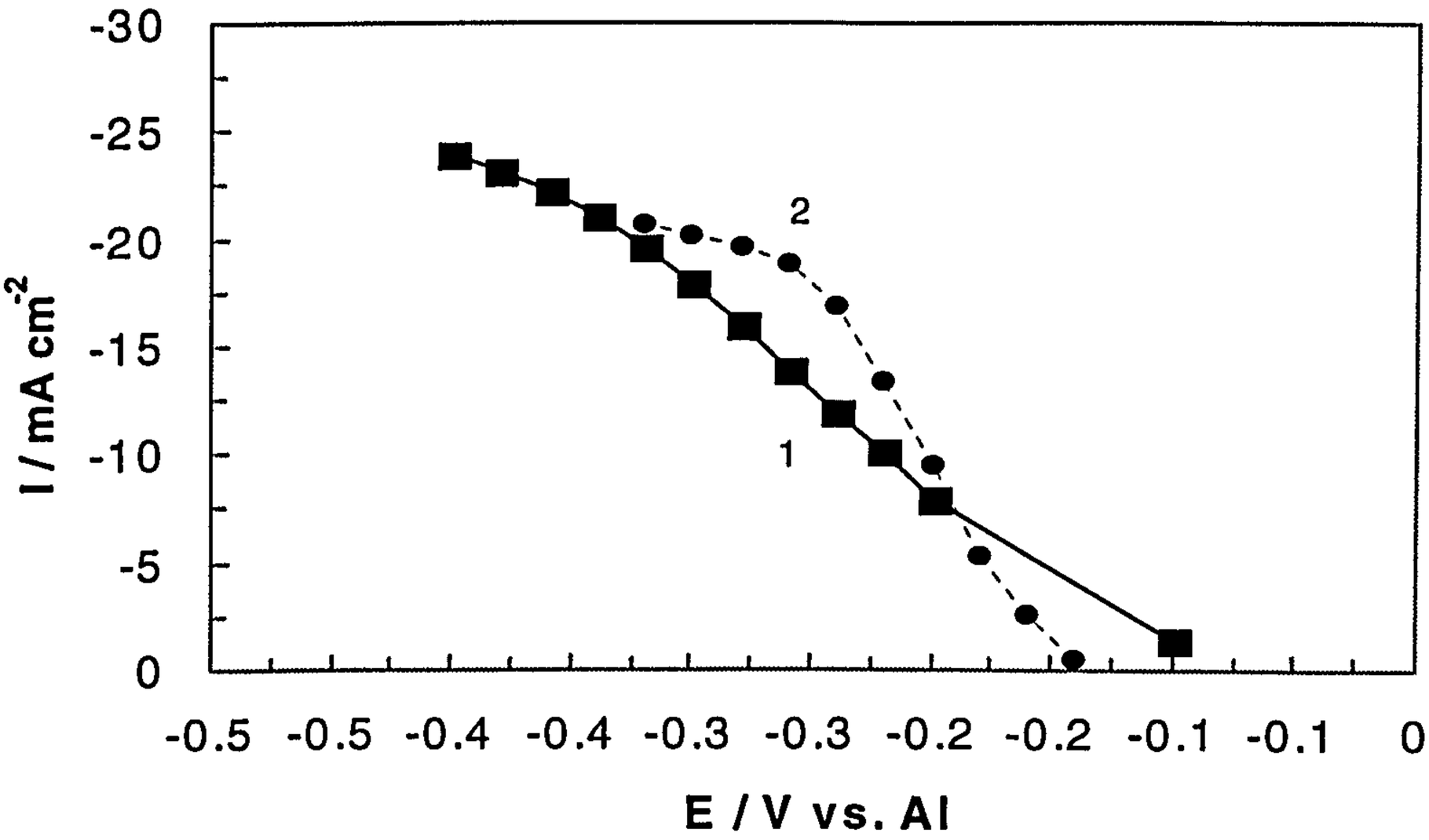

Fig. 6.2.4. Comparison of sampled current voltammograms constructed from current-time transients for aluminium deposition on glassy carbon in 2:1 $AlCl_3$-TMPAC melts with (1) and without (2) 0.1 mM Ni^{2+} ions at 25°C.

Dimensionless analysis (**Fig. 6.2.5**) revealed that the bulk aluminium deposition on the electrode modified by the alloy deposits involved three dimensional instantaneous nucleation and growth. There is no clear explanation for the deviation of the experimental data after t_m from the theoretical curve.

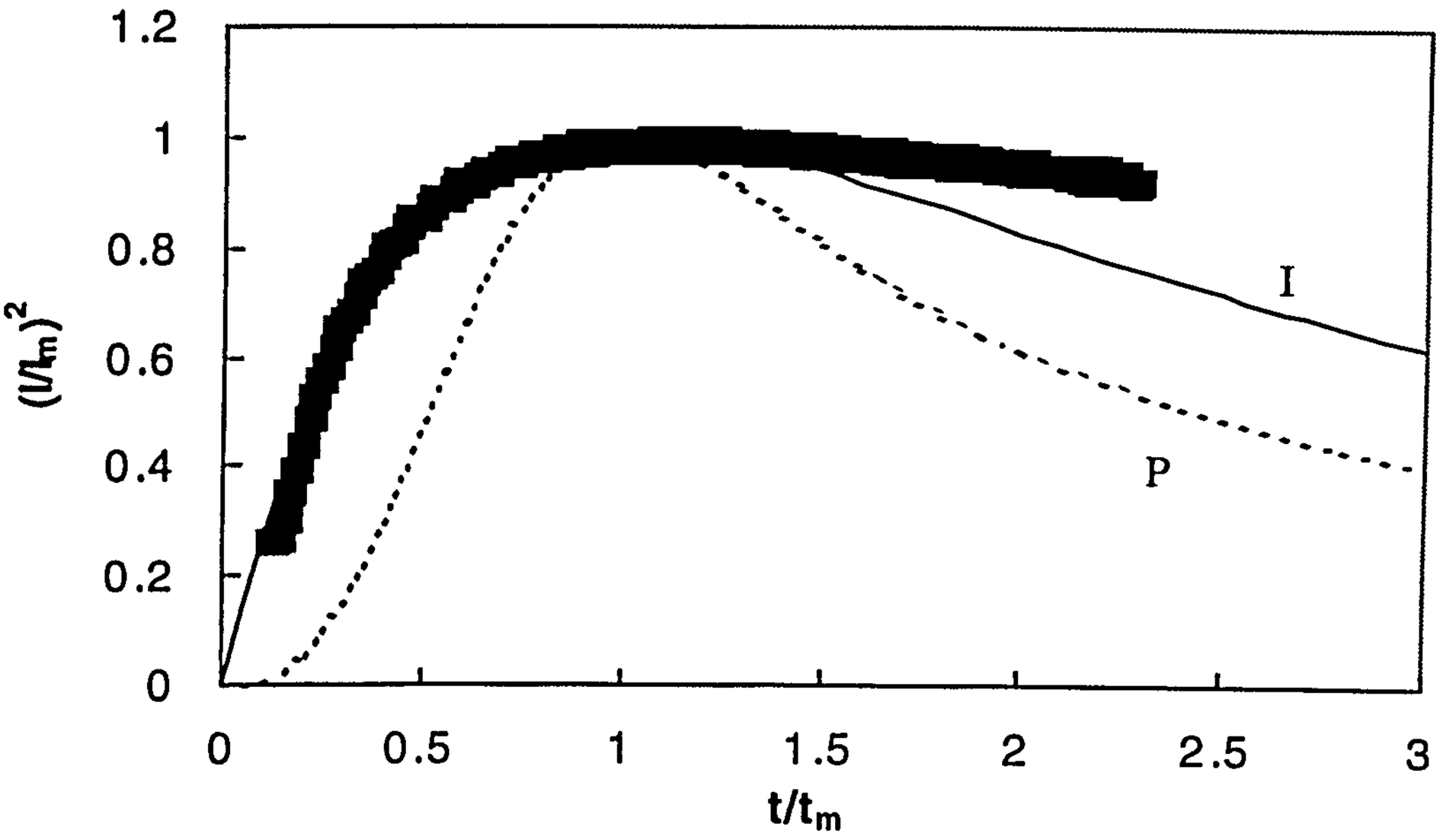

Fig. 6.2.5. Comparison of the dimensionless experimental data derived from **Fig. 6.2.3** with the theoretical models for diffusion controlled three dimensional instantaneous and progressive nucleation and growth.

Chapter 7

CONCLUSIONS AND A PROPOSED GENERAL REACTION SCHEME

7.1 CONCLUSIONS

Through the investigations of the electrodeposition of aluminium from room temperature 2:1 $AlCl_3$-TMPAC molten salts on various substrates with staircase cyclic voltammetry, chronoamperometry, convolution voltammetry electrochemical techniques, the following conclusions can be drawn:

1. The electrodeposition of aluminium can be achieved on tungsten, aluminium, platinum, nickel and glassy carbon substrates from 2:1 $AlCl_3$-TMPAC molten salts at room temperature. However, deposits were granular and poorly adherent.
2. The reduction of $Al_2Cl_7^-$ ions was quasi-reversible and diffusion controlled. the influence of the equilibrium reaction:

$$2AlCl_4^- \rightleftharpoons Al_2Cl_7^- + Cl^- \qquad (1.3.4)$$

Besides, the aluminium deposition could be associated with the reduction of the resulting product $AlCl_4^-$ ions following locally changes in acidity of the melts, and a corrosion reaction between fresh aluminium deposits and the melt. Accordingly, the mechanism for aluminium electrodeposition from 2:1 $AlCl_3$-TMPAC melts was likely similar to that for the acidic $AlCl_3$-BPC melts [136]:

$$Al_2Cl_7^- + 3e^- \rightleftharpoons Al + 7AlCl_4^- \quad (1.3.7)$$

$$AlCl_4^- + 3e^- \rightleftharpoons Al + 4Cl^- \quad (1.3.6)$$

$$Al + X \longrightarrow \text{Products (corrosion)} \quad (1.3.10)$$

where X represents organic cations or impurities.

3. The bulk depositions of aluminium on all electrodes except platinum involved three-dimensional instantaneous nucleation process followed by hemispherical diffusion-controlled growth of the developing nuclei. On platinum the nucleation process was characteristic of instantaneous nucleation at short time which tended to progressive nucleation at longer time.
4. The phenomena of aluminium UPD were found on all electrodes but not on aluminium itself, indicating that process that the occurrence of UPD was highly dependent upon electrode materials. The UPD layers on the surface of the electrodes corresponded to about 2 ~ 10 aluminium monolayer equivalents.
5. Aluminium alloying was observed to be involved in the UPD processes on the foreign metal substrates. The UPD was a surface controlled process on tungsten, whereas it was diffusion controlled on nickel and platinum. The UPD processes on tungsten and platinum were under the limitation of kinetics.
6. On nickel and platinum, the electrodes and the nickel and platinum components in fresh deposits were likely to react with $Al_2Cl_7^-$ and Cl^- ions in the melt as the following reaction:

$$M + nA^- \rightleftharpoons [MA_n]^{(2-n)-} + 2e^- \quad (7.1.1)$$

where M: Ni, Pt; A^-: $Al_2Cl_7^-$, Cl^-.

7. Passivation phenomena were observed to occur on all electrodes. These could result from a black layer formed by $AlCl_3$ precipitates. Particularly, on aluminium the stripping of aluminium involved an active dissolution-passivation process.
8. The 1,2-DCB dilution of $AlCl_3$-TMPAC melts had a beneficial effect on increasing aluminium deposition and stripping currents by decreasing viscosity and the degree of association of ion pairs or ion aggregates of the melt, thereby increasing the conductivity of the melt.

7.2 A PROPOSED GENERAL REACTION SCHEME

7.2.1 Problems and Solutions

As discussed above, although aluminium can be electrodeposited on various substrates from 2:1 $AlCl_3$-TMPAC molten salts at room temperature, to form the basis for an Al-plating system, it is still necessary to resolve some problems encountered in this thesis work. These problems included the poor adhesion of the deposits to the substrates, the passivation of the electrodes, the corrosion of fresh deposits, the higher viscosity and the lower conductivity of the melts, and the deterioration of the plating bath.

In a sense, the solutions of the above problems seem to depend upon seeking suitable additives. According to their intrinsic properties, room temperature molten salts can dissolve not only inorganic salts such as metal chlorides but also many organic compounds (**Sec. 1.3.1**). Therefore, there is an extensive choice of additives for improving the present Al-plating system.

The lack of aluminium deposits on the substrates might come from the poor adhesion of the deposits to the polished mirror-like surface of the electrodes. This type of the electrode surface was suitable for studies of deposition involving nucleation and growth but not for adherence of deposits.

Furthermore, the use of a Schlenk line made the controlled removal of the electrode difficult.

In a private communication, Dr. A. Abbott suggested that a bright shiny adherent Al deposit could be obtained by abrading the surface with a very rough glass paper, and then pickling quickly in aqua regia, and finally degreasing usually in a chlorinated solvent. Since this treatment would create a very rough surface with a large number of defects, this method is unsuitable for studies of nucleation.

In addition to the problems of the system, some experimental results were also not completely clear. As seen with the electrochemical techniques used in this thesis, the compositions of alloys were not quantitatively determined; the current loops following the bulk deposition of aluminium were not characterised; the passivation of the electrodes and the oxidation reactions between fresh deposits or electrodes and Cl^- or $Al_2Cl_7^-$ ions in the melts were not structurally analysed. Therefore, in order to more satisfactorily characterise the processes involved, further experiments will be required. These would involve NMR for analysis of the melts, EDS for the structure characterisation of the electrode surface, SEM for morphology of the deposits, chronopotentiometry for the corrosion study of the electrodes or fresh deposits, and recording multi-sweep voltammograms for the mechanism investigation of the electrode processes.

Moreover, since the physico-chemical properties of the Al-plating systems are strongly dependent upon the composition of the melts and temperature, the thermodynamics of the melts will be very interesting.

7.2.2 A Proposed General Reaction Scheme

Although many excellent properties of ambient temperature molten salts are known, only a few systems have been extensively studied up to now. Wider recognition and commercial use still develop slowly, mainly because of preparation and/or stability difficulties, or lower conductivities. Therefore,

investigation of new compounds capable of forming low-temperature molten salts with inorganic salts such as $AlCl_3$ should be undertaken to find melts which are easier to prepare than the MEIC type and which display a wider window of electrochemical stability than BPC type. Such new materials may represent useful electrolytes for electrodeposition work.

Basically, preparation of MEIC and BPC and their derivatives is based on the general neutralisation reaction [90]:

$$RN + R'X \longrightarrow RR'N^+X^- \qquad (7.2.1)$$

where RN is the aromatic amine and R′X the alkyl halide of interest.

The syntheses of *N*-ethylpyridinium bromide, *N*-benzylpyridinium bromide, *N*-methylpyridinium chloride, *N*-ethylpyridinium chloride, *N*-(n-propyl)pyridinium chloride, *N*-benzylpyridinium chloride, *N, N'*-ethyldipyridinium bromide have been reported [90]. However, the investigations into whether if these compounds can form ambient temperature molten salts with $AlCl_3$ have not performed.

It is noteworthy that in addition to $AlCl_3$, some anhydrous metal chloride salts such as AgCl, CuCl, LiCl, $CdCl_2$, $CuCl_2$, $SnCl_2$, $ZnCl_2$, $LaCl_3$, YCl_3, $SnCl_4$ and $TiCl_4$. produced ionic liquids with MEIC at or near room temperature for at least some compositions, based on the following reaction [124]:

$$mCl^- + MCl_n \rightleftharpoons MCl_{n+m}^{m-} \qquad (1.3.5)$$

Moreover, literature calculations [122] have indicated that quaternary ammonium species were expected to have superior electrochemical stabilities, *i.e.*, they were less easily reduced as compared to BP^+ and MEI^+ ions. Thus, molten salts made from quaternary ammonium halides and $AlCl_3$ would be expected to have increased stabilities. However, a quaternary ammonium salt having alkyl groups for all four substituents did not form a room temperature melts with $AlCl_3$ unless the alkyl groups were such long chains that the melting

points of the onium melts were depressed to near room temperature by entropic effects [132]. But in the case of long-chain alkyl substituents, the viscosities of the melts would increase and the ion mobilities would decrease, resulting in such low conductivities of the melts as to render them useless for most electrochemical applications.

On the other hand, the aryl groups contributed to lowering the melting point by increasing the interaction between the cation and the chloroaluminate anions [120]. It was considered that π electrons on the aryl group might interact with the polarisable chloroaluminate anions to form solutions of high salt concentration. Besides this, the large size of the π electron cloud in the onium salts could make the interaction completely delocalised, so that the entropy of the melt was considerably enhanced over the separated solids, resulting in a lower melting point. Also, the formation of the large chloroaluminate anions would lower the lattice energy of the crystalline salt, serving to drive the melting temperature to lower values.

In addition to the quaternary ammonium salts, those aralkyl quaternary salts containing sulphur and phosphorus substituted for nitrogen were also investigated [132]. A family of commercially available, fully substituted quaternary ammonium salts were found suitable for forming low-temperature melts. Besides TMPAC, methyldiphenylsulfonium tetrafluoroborate, trimethylphenyl phosphonium iodide and ethyldiphenylsulfonium tetrafluoroborate with AlCl3 at 2:1 mole ratio can produce ambient temperature melts [132].

According to the above results, as an extension of **Reactions 7.2.1** and **1.3.5**, a general reaction for producing low (< 100°C) or ambient temperature molten salts was proposed in this thesis:

$$mR^+X^- + MX_n \rightleftharpoons MX_{n+m}^{m-} + mR^+ \qquad (7.2.2)$$

where X^- is Cl^-, Br^-, I^- or BF_4^- anions; MX_n are metal halides; R^+ are:

i. quaternary or ternary onium cations:

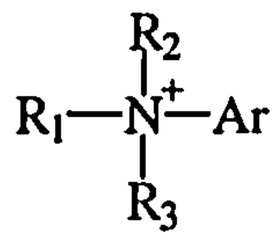

(N is N, S or P atom; R_1, R_2 and R_3 are short-chain alkyl groups, respectively; Ar is an aryl group, phenyl or benzyl);

ii. heterocyclic nitrogen onium cations whose structures and hetero conjugations are similar to BP^+ and MEI^+ ions, or the derivatives of BP^+ and MEI^+ ions.

The onium salts reported for case (ii) mainly contained the following three structures:

a. the pyridinium type, *e.g.*, BP^+ ion,

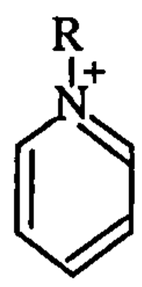

b. the imidazolium type, *e.g.*, MEI^+ ion,

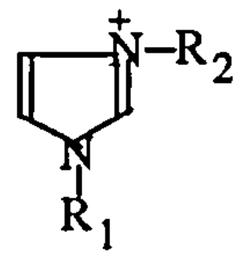

c. the triazolium type, *e.g.*, DMT^+ (1,4-dimethyl-1,2,4-triazolium) ion [232],

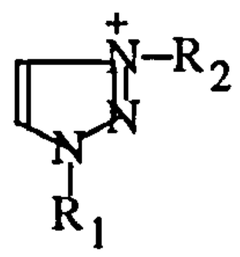

d. the pyrazolium type, *e.g.*, $DMFP^+$ (1,2-dimethyl-4-fluoro pyrazolium) ion [233],

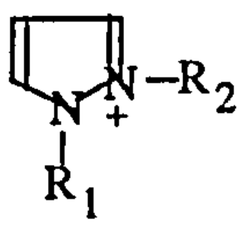

As have been noted before, it is well known that a considerable drawback of ambient ionic liquids concerns the need to protect rigorously the ionic liquids from moisture and other oxide impurities and the tendency of many substrates to react with halometallates. Use of ambient temperature ionic liquids has therefore thus far been limited to a narrow range of organic substrates, typically those that react desirably with Lewis acids. In contrast, there are a plethora of higher melting salts, typically based upon halides, halometallates and more inert anions such as nitrite, sulphate and carbonate, that have been used as electrolytes [234]. It could be expected that the inertness and facile handling capability of some of the higher melting salts became feasible under ambient conditions, then the possibilities for applications of ionic liquid media would become greatly enhanced.

It is exciting that air and water stable low melting salts based upon MEI^+ cations have greatly progressed, recently. Wilkes and Zaworotko [235] found two salts, $MEI^+BF_4^-$ and $MEI^+CH_3COO^-$, without $AlCl_3$, were liquids with m.p. 15°C and -45°C, respectively; m.p. of three other salts, $MEI^+NO_3^-$, $MEI^+NO_2^-$ and $[MEI^+]_2SO_4^{2-}\cdot H_2O$, were 38°C, 55°C and 70°C. With the exception of $[MEI^+]_2SO_4^{2-}\cdot H_2O$ all salts were hygroscopic but no special precautions were required during synthesis as they may be dried conveniently in a vacuum oven at 80°C. This was in contrast to higher melting point metal based salts which can form thermodynamically stable hydrates that were much more difficult to dehydrate [236].

More recently, a similar low-temperature molten salt $MEI^+PF_6^-$, m.p. 58-60°C, has been reported [237]. It also had the desirable property of being fully air stable and may be useful as an electrolyte for operation at moderately elevated temperatures. Significantly, the crystal structure of this salt consisted of interionic interactions dominated by cation-anion coulombic forces with minimal hydrogen bonding. Due to similar to the structures of $MEI^+AlCl_4^-$,

$MEI^+BF_4^-$ ions, it was considered to serve as a model for MEI^+ type room temperature molten salts containing weakly complexing anions.

By analogy with the above salts, it is reasonable to expect that some novel air and water stable low or ambient temperature molten salts could be made by the reactions between R^+X^- in Reaction 7.2.2 and the noted inert anions such as nitrite, sulphate and carbonate.

7.2.3 Future Work

In accordance with the problems encountered in the experiments and the general reaction proposed, it is expected that the future work should be carried out in the following aspects:

1. the further study of the mechanistic investigation of the electrode processes by using a combination of multi-techniques as noted in **Sec. 7.2.1.**
2. the investigation of various additives to minimise passivation and corrosion effects, removing water and oxygen contents in the melts, decreasing viscosities and increasing conductivities of the melts.
3. the derivation of mathematical models suitable for the exact explanation of the deposition processes involving nucleation.
4. the search for novel ambient temperature molten salt systems with the wider electrochemical windows and adjustable Lewis acidities, more chemical, water and air stabilities, low or non corrosivities and toxicities, lower viscosities and higher conductivities.
5. the development of industrial Al and Al alloys electroplating technological processes with operation at ambient conditions.

To sum up, through the investigation of the electrodeposition of aluminium from room temperature molten salts 2:1 $AlCl_3$-TMPAC and the proposed general reaction, it can be prophesised that not only the $AlCl_3$-TMPAC system but also more novel ambient temperature molten salts will be promising industrial baths for the electroplating of aluminium and its alloys. Moreover,

these systems will also be expected to find use in other fields of electrochemistry.

REFERENCES

1. H. Lehmkuhl, K. Mehler and U. Landau, *Adv. Electrochem. Sci. Eng.*, **3,** 163 (1994).
2. A. R. Brukin "*Productionof Aluminium and Alumina, Critical Reports in Applied Chemistry*", Vol, **20,** Wiley, Chichester, UK, (1987).
3. A. S. Russell, *Proc. 7th Int. Light Metals, Congress, Aluminium-Verlag,* , p. 40, Disselgorf, (1981).
4. L. L. Sheir, *Corrosion*, Vol. **2,** Butterworth, London, (1976).
5. M. Galova, *Surface Technology*, **11,** 357 (1980).
6. V. A. Plotnikov, *J. Russ. Phys. Chem. Soc.*, **31,** 1020 (1899).
7. M. W. M. Great, *J. Electrochem. Soc.*, **132,** (5), 1308 (1985).
8. T. Garai, *Mater. Chem. Phys.* **8,** 399 (1983).
9. S. Simanavicius, *Chemija,* **178,** 3 (1990).
10. D. E. Couch and A. Brenner, *J. Electrochem. Soc.*, **99,** 234 (1952).
11. A. Brenner and D. E. Couch, *U. S. Patent*, 2,651,608, (1953).
12. A. Brenner, in *Advances in Electrochemistry and Electrochemical Engineering* (Edited by C.W. Tobias), Vol. **5,** p. 217, Interscience, New York, (1967).
13. A. Brenner, *J. Electrochem. Soc.*, **106,** 148 (1959).
14. D. E. Couch and A. Brenner, *J. Electrochem. Soc.*, **103,** 657 (1956).
15. F. A. Clay, W. B. Harding and C. J. Stimetz, *Plating*, **56,** 1027 (1969).
16. W. C. Schickner, *Steel*, **133,** 125 (1953).
17. J. Elze, G. Lange and D. Mayer, *Metalwiss. Techn.*, **13,** 541 (1959).
18. F. J. Schmidt and I. J. Hess, *Plating*, **53,** 229 (1966).
19. D. E. Couch and A. Brenner, *J. Electrochem. Soc.*, **103,** 657 (1956).
20. R. J. Roethlein, *J. Electrochem. Soc.*, **117,** 715 (1970).
21. A. G. Buschov and C. H. Esola, *Plating*, **55,** 931 (1968).
22. A. Levinskas and J. Sinius, *C. A.*, **72,** 62161y (1970).
23. J. Hess and J. F. Betz, *Metal Finish.*, **69,** 38 (1971).
24. A. Levinskas, *Usp. Khim.*, **44,** 1236 (1975).
25. N. Ishibashi and M. Yoshio, *Electrochim. Acta,* **17,** 1343 (1972).
26. M. Yoshio and N. Ishibashii, *J. Appl. Elecetrochem.*, **3,** 321 (1973).
27. H. J. Eckert and H. Kolling, *Wiss. Z. Tech. Univ. Dresden.*, **24,** 19 (1975).
28. T. Kurata, R. Kawabata K. Ktayama and E. Yakishima, *Jpn. Pat.*, 73 44,608 (1973).
29. T. Kurata, R. Kawabata K. Ktayama and E. Yakishima, *Jpn. Pat.*, 73 44,609 (1973).
30. T. Kurata, R. Kawabata K. Ktayama and E. Yakishima, *Jpn. Pat.*, 73 00,018 (1974).
31. M. Yoshio, *Mat. Finish.*, **7,** 33 (1987).
32. S. P. Sidelnikova V. N. Sherstkina and A. N. Jakubetz, *Izv. Akad. Nauk Mold. SSR, Ser. Fiz.-Tekh. Mat. Nauk,* **1,** 69 (1979).

33. W. Altgeld, *Metalloberflache*, **40**, 253 (1986).
34. E. Eckert, *Dechema-Monographien*, Vol. **125**, p. 425, VCH Verlagsgesellschaft, Winheim (1992).
35. H. C. Brown, W. J. Wallance, *J.Am.Chem.Soc.*, **75**, 6265 (1953).
36. D. D. Eley and P. J. King, *J. Chem. Soc.*, 2517 (1952).
37. E. Peled and E. Gileadi, *J. Electochem. Soc.*, **123**, 15 (1976).
38. L. E. Simanavicius and P. P. Dobrovoskis, *Issled. Obe. Electroosazhd. Met.*, **2**, 192 (1971).
39. L. E. Simanavicius and P. P. Dobrovoskis, *USSR Pat.*, **382**,761 (1972).
40. E. Peled and E. Gileadi, *Plating*, **62**, 342 (1975).
41. C. A. Capuano and W. G. Davenport, *J. Electrochem. Soc.*, **118**, 1688 (1971).
42. C. A. Capuano and W. G. Davenport, *Plating*, **60**, 251 (1973).
43. W. G. Davenport and C. A. Capuano, in *Proc. Richardson Conf. on the Physical Chemistry of Process Metallurgy*, (Edited by H. E. Jeff and R.J. Tait), p. 77, Institution of Mining and Metallurgy, London, (1973).
44. C. A. Capuano and W. G. Davenport, *Can. Pat.*, 4375 (1971).
45. L. E. Simanavicius and A. M. Levinskiene, *Elektrokimiya*, **2**, 353 (1966).
46. L. E. Simanavicius and A. P. Karpavicius, *Issled. Obl. Elektroosazhd. Met.*, **1**, 164 (1968).
47. L. E. Simanavicius and A. P. Karpavicius, *Nauchn. Tr. Vyssh. Uchebn. Zaved. Lit. SSR, B*, **4**, 139 (1970).
48. L. E. Simanavicius and A. M. Levinskiene, *Tr. Akad. Nauk Litov. SSR, B*, **4**, 39 (1966).
49. E. Boker, *Proc. 29th Meet. ISE*, MTA Kozponti Kemiai Kutato Intezet, p. 1182, Budapest, (1978).
50. V. A. Kazakov and V. N. Titova and N. V. Petrova, *Elektrokhimija*, **12**, 576 (1976).
51. V. E. Larchenko V. A. Kazakov, V. N. Titova and V. F. Chuvajev, *Elektrokhimija*, **14**, 588 (1978).
52. H. Lehmkuhl, *Dissertation*, Rheinisch-Westfalische Tehnische Hochschule, Aachen (1954).
53. K. Ziegler, H. Lehmkuhl, *C. A.*, **52**, 19619d (1958).
54. K. Ziegler, H. Lehmkuhl, *Angew. Chem.*, **67**, 424 (1955).
55. K. Ziegler, H. Lehmkuhl, *Z. Anorg. Allg. Chem.*, **283**, 414 (1956).
56. S. Birkle, *Metalloberflache*, **40**, 249 (1986).
57. U. Landau, *Jahrbuch Oberflachentechnik*, **44**, 126 (1988).
58. W. D. Hannibal, G. Ibe, H. Pfunde, W. Reuter, G. Winkhaus, *Metall.* **27**, 203 (1973).
59. T. Kusel, R. Sudholter, *Metall.*, **42**, 812, (1988).
60. H. Lehmkuhl, K. Mehler, unpublished results, (1986).
61. J. P. Pereira-Ramos, *Dessertation*, University of Paris, 12 (1988).
62. T. R. Griffiths, *J. Chem. Soc., Chem. Comm.*, 1222 (1967).
63. J. Hennion and J. Nicole, *J. Bull. Soc. Chim. Fr.*, 426 (1978).

64. J. P. Pereira-Ramos, R. Messina and J. Perichon, *J. Electrochem. Chem.*, **209**, 283 (1986).
65. L. Legrand, A. Tranchant and R. Messina, *Electrochim. Acta*, **39**, 1427 (1994).
66. L. Legrand, A. Tranchant and R. Messina, *J. Electrochem. Soc.*, **141**, 378(1994).
67. L. Legrand, A. Tranchant and R. Messina, and Lautie, *Inorg. Chem.*, **35**, 1310 (1996).
68. J. W. Fung and G. Mamantov, in *Advances in Molten Salt Chemistry,* (Edited by J. Braunstein, G. Mamantov, and G. P. Smith), Vol. **2**, p. 199-254, Plenum, New York, (1973).
69. J. W. Fung and G. Mamantov, in *Advances in Molten Salt Chemistry,* (Edited by J. W. Fung and G. Mamantov, in *Wilson's Comprehensive Analytical Chemistry,* (Edited by G. Svehla), Vol. **3**, p. 305-370, Elsevier, Amsterdam, (1975).
70. A. Plambeck, in *Encyclopedia of Electrochemistry of the Elements,* (Edited by A. J. Bard), Vol. **10**, Dekker, New York, (1976).
71. D. G. Lovering and R. J. Gale, eds., *Molten Salt Techniques*, Vol. **1**, Plenum, New York, (1983).
72. D. G. Lovering and R. J. Gale, eds., *Molten Salt Techniques*, Vol. **2**, Plenum, New York, (1984).
73. D. G. Lovering and R. J. Gale, eds., *Molten Salt Techniques*, Vol. **3**, Plenum, New York, (1987).
74. M. Inman and D. G. Lovering, in *Comprehensive Treatise of Electrochemistry,* (Edited by B. E. Conway, J. O. M. Bockris, E. Yeager, S. U. M. Khan, and R. E. White), Vol. **7**, p. 593-640, Plenum, New York, (1983).
75. J. Robinson, in *Electrochemistry,* (Edited by D. Pletcher), Vol. **8**, Spec. Period. Rep., p. 54-80, Royal Society of Chemistry, London, (1983).
76. G. Mamanov and R. A. Osteryoung, in *Characterization of Solutes and nonaqueous Solvents*, (Edited by G. Mamanov), p. 223-249, Plenum, New York, (1978).
77. J. Braustein, G. Mamantov and G. P. Smith, eds., in *Advances in Molten Salt Chemistry,* Vol. **3**, Plenum, New York, (1975).
78. G. Mamantov, J. Braustein, eds. in *Advances in Molten Salt Chemistry,* Vol. **4**, Plenum, New York, (1981).
79. G. Mamantov, in *Advances in Molten Salt Chemistry,* Vol. **5**, Elsevier, Amsterdam, (1983).
80. G. Mamantov, C. B. Mamantov, J. Braunstein, in *Advances in Molten Salt Chemistry,* Vol. **6**, Elsevier, Amsterdam, (1987).
81. P. Pemsler, J. Braustein and K. Nobe, D. R. Morris and N. E. Richards, eds., *Proceedings of the International Symposium on Molten Salts*, Electrochem. Soc., Princeton, New Jersey, (1976).
82. J. Braustein, J. R. Selman, eds., *Proceedings of the Second International Symposium on Molten Salts*, Electrochem. Soc., Princeton, New Jersey, (1981).

83. G. Mamantov, M. Blander, and G. P. Smith, eds., *Proceedings of the Third International Symposium on Molten Salts*, Electrochem. Soc., Princeton, New Jersey, (1983).
84. J. Blander, D. S. Newman,G. Mamantov, eds., *Proceedings of the Fourth International Symposium on Molten Salts*, Electrochem. Soc., Princeton, New Jersey, (1984).
85. M. -L. Saboungi, D. S. Newman, K. Johnson, and M. Inman, eds., *Proceedings of the Fifth International Symposium on Molten Salts*, Electrochem. Soc., Princeton, New Jersey, (1986).
86. G. Mamantov, M. Blander, C. L. Hussey, C. B. Mamantov, M. -L. Saboungi, and J. S. Wilkes, eds., *Proceedings of the Sixth International Symposium on Molten Salts*, Electrochem. Soc., Princeton, New Jersey, (1987).
87. G. Mamantov, and R. Marassi, eds. in *Molten Salt Chemistry--An Introduction and Selected Applications*, Reidel, Dordredcht, Holland, (1987).
88. R. J. Gale, and R. A. Osteryoung, in *Molten Salt Techniques* (Edited by D. G. Lovering and R. J. Gale), Vol. **1**, Chapter **3**, Plenum, New York, (1984).
89. L. Legrand, A. Tranchant, R. Messina and A. Lautie, *J. Electrochem. Soc.*, **141**, 378 (1994).
90. C. L. Hussey, in *Advances in Molten Salt Chemistry,* (Edited by G. Mamantov and C. B. Mamantov), Vol. **5**, P. 185, Elsevier, Amsterbam, (1983).
91. H. Stegemann, A. Rohde, A. Reiche, A. Schnittke and H. Fullbier, *Electrochimi. Acta*, **37**, 379 (1992).
92. F. H. Hurley, *U. S. Pat.*, 2,446331 (1948).
93. W. W. Porterfield and J. T. Yoke, *Advances in Chemistry Series*, No. **150**, Am. Chem. Soc., Washington D.C. (1976).
94. H. Stegemann, A. Rohde, A. Reiche, A. Schnittke and H. Fullbier, *Electrochimi. Acta*, **37**, 379 (1992).
95. G. E. McManis, A.N. Fletcher, D. E. Bliss and M. H. Miles, *J. Electroanal. Chem.*, **190**, 171 (1985).
96. C. L. Hussey, *Pure & Appl. Chem.*, **60**, 1763 (1988).
97. D. B. Keyes, T. E. Phipps and W. Klabunde, *U. S. Pat.*, 1,911122 (1933).
98. D. B. Keyes and S. Swann, *U. S. Pat.*, 1,939397 (1933).
99. D. B. Keyes, S. Swann, W. Klabunde and S. T. Schiktanz, *Ind. Eng. Chem.*, **20**, 1068 (1928).
100. F. H. Hurley and T. P. Wier, *U. S. Pat.*, 2,446349 (1948).
101. T. P. Wier, *U. S. Pat.*, 2,446350 (1948).
102. F. H. Hurley and T. P. Wier, *J. Electrochem. Soc.*, **98**, 203 (1951).
103. F. H. Hurley and T. P. Wier, *J. Electrochem. Soc.*, **98**, 207 (1951).
104. W. H. Safranek, W. C. Schickner and C. L. Fraust, *J. Electrochem. Soc.*, **99**, 53 (1952).
105. W. H. Safranek, W. C. Schickner and C. L. Fraust, *U. S. Pat.*, 2,692850 (1954).
106. W. C. Schickner, *U. S. Pat.*, 2,728718 (1955).
107. W. C. Schickner, *U. S. Pat.*, 2,934478 (1960).

108. W. H. Safranek, W. C. Schickner and C. L. Fraust, *J. Electrochem. Soc.*, **99**, 53 (1952).
109. L. Simanavicius and P. Dobrovolskis, *C. A.*, **78**, 23137z (1973).
110. L. Simanavicius and P. Dobrovolskis, *C. A.*, **78**, 105271c (1973).
111. L. Simanavicius and P. Dobrovolskis, *C. A.*, **78**, 91702e (1973).
112. L. Simanavicius and A. Stakenas, *C. A.*, **78**, 91701d (1973).
113. P. Silvestroni, and F. Rallo, *Ann. Chim., (Roma)*, **64**, 781 (1974).
114. E. Peled and E. Gileadi, *J. Electrochem. Soc.*, **123**, 15 (1976).
115. L. Bokor, *ISE* 29th *Meeting*, p. 1182, Budapest , (1978).
116. R. A. Osteryoung and J. Robinson, *J. Am. Chem. Soc.*, **101**, 323 (1979).
117. R. A. Osteryoung and J. Robinson, *J. Am. Chem. Soc.*, **102**, 4415 (1980).
118. R. J. Gale and R. A. Osteryoung, *Inorg. Chem.*, **18**, 1603 (1979).
119. R. J. Gale and R. A. Osteryoung, *J. Electrochem. Soc.*, **127**, 2167 (1980).
120. H. L. Chum and R. A. Osteryoung, in *Ionic Liquids*, (Edited by M. Inman and D.G. Lovering), Plenum, New York, (1981).
121. J. Robinson and R. A. Osteryoung, *J. Electrochem. Soc.*, **127**, 122 (1980).
122. J. S. Wilkes and C. L. Hussey, in *The Frank J. Seiler Research Laboratory Technical Report*, FJSRL-TR-820002, Jan., (1982).
123. J. S. Wilkes, J. A. Leviski, C. L. Hussey and M. Druelinger, *158th Meeting Electrochem. Soc., Extended Abstr.*, no. 648, p. 1622.
124. T. B. Scheffler and M. S. Thomson, in *Proc. 8th Inter. Symp. on Molten Salts*, (Edited by M. -L. Sabouugi, K. Johnson, D. S. Newman), p. 281, Electrochem. Soc. Inc., Pennington, New Jersey, (1992).
125. R. A. Osteryoung, in *Molten Salt Chemistry*, (Edited by G. Mamantov and R. Marassi), p.329, D. Reidel Publishing, Holland, (1987).
126. S. Takahashi, I. Saeki, I. Kazuhiko and M. Shoichiro, *177th Meeting of the Electrochemical Society, Extended Abstracts*, Abstrac No. 889, Montreal, Quebec, Canada, May 6-11, (1990).
127. J. J Auborn and Y. L. Barberio, *J. Electrochem. Soc.*, **132**, 598 (1985).
128. R. T. Carlin, W. Crawford and M. Bersch, *J. Electrochem. Soc.*, **139**, 2720 (1992).
129. S. Takahashi, I. Kazuhiko and M. Shoichiro, in *Molten Salts*, (Edited by C. L. Hussey, S. N. Flengas, J. S. Wilkes and Y. Ito), Pv **90-17**, p. 661, Electrochem. Soc. Softbound Proc. Series, Pennington, New Jersey, (1990).
130. S. Takahashi, I. Seaki, I. Kazuhiko and M. Shoichiro, Abstract No. **889**, p. 1254, *Electrochemical Society Extended Abstracts*, Montreal, Quebec, Canada, May 6- 11, (1990).
131. R. Moy and F. M. Donahue, *Electrochim. Acta*, **33**, 721 (1988).
132. S. D. Jones and G. E. Blomgren, *J. Electrochem. Soc.*, **136**, 424 (1989).
133. R. Moy and F. P. Emmenegger, *Electrochim. Acta*, **37**, 1061 (1992).
134. N. Papageorgiou and F. P. Emmenegger, *Electrochim. Acta*, **38**, 245 (1993).
135. R. T. Carlin and R. A. Osteryoung, *J. Electrochem. Soc.*, **136**, 1409 (1989).
136. P. K. Lai and M. Skyllas-Kazacos, *Electrochim. Acta*, **32**, 1443 (1987).
137. V. A. Plotikov, *J. Russ. Phys. Chem. Soc.*, **34**, 466 (1902).

138. W. H. Safrannek, W. C. Schckner and C. L. Fraust, *J. Electrochem. Soc.*, **99**, 53 (1952).
139. S. Birkle, *Metalloberflache.*, **40**, 249 (1986).
140. D. J. Levy, *Plat. Surface Finish.*, **68**, 26 (1981).
141. G. Pforr, H. Meger, W. Goesele, H. Stark, *Ger. Offen De.*, 3,620,023.
142. B. Gilbert, G. Mamantov, and K. W. Fung, *Inorg Chem.*, **14**, 1802 (1975).
143. G. Ting, K. W. Fung, and G. Mamantov, *J. Electrochem. Soc.*, **123**, 634 (1976).
144. P. Rolland, and G. Mamantov, *J. Electrochem. Soc.*, **123**, 1299 (1976).
145. G. J. Hills, D. J. Schiffrin, and J. Thompson, *Electrochim. Acta*, **19**, 657 (1974).
146. G. J. Hills, D. J. Schiffrin, and J. Thompson, *Electrochim. Acta.*, **19**, 671 (1974).
147. G. J. Hills, D. J. Schiffrin, and J. Thompson, *J. Electrochem. Soc.*, **120**, 157 (1973).
148. B. R. Scharifker and G. Hill, *Electrochim. Acta*, **28**, 879 (1983).
149. B. R. Scharifker, in *Electrochemistry in Transition*, (Edited by O. J. Murphy, S. Srinivasan, and B.E. Conwey), Plenum Press, New York (1992).
150. W. J. McTgart, *Polishhage Electolytique et Chimique des Metaux au Laboratorie et dans I'Industrie*, Dunod, Paris, (1960).
151. A. J. Bard and L. R. Faukner, *Electrochemical Methods: Fundamentals and Applications*, p. 31, John wiley & Sons, Inc., (1980).
152. R. Greef, R. Peat, L. M. Peter, D. Pletcher and J. Robinson, *Instrumental Methods in Electrochemistry*, Southampton Electrochemistry Group, p. 283, Ellis Horwood Ltd. (1985).
153. L. H. L. Miaw, P. A. Boudreau, M. A. Pichler and S. P. Perone, *Anal. Chem.*, **48**, 1988(1978).
154. R. Greef, R. Peat, L. M. Peter, D. Pletcher and J. Robinson, *Instrumental Methods in Electrochemistry*, Southampton Electrochemistry Group, p. 283, Ellis Horwood Ltd. (1985).
155. J. H. Christie, G. Lauer and R. A. Osteryoung, *J. Electroanal. Chem.*, **7**, 60 (1964).
156. J. H. Christie, G. Lauer, R. A. Osteryoung and F. C. Anson, *Anal. Chem.*, **35**, 1979 (1963),
157. J. C. Imbeaux and J. M. Saveant, *J. Electroanal. Chem.*, **44**, 1969(1973).
158. F. Ammar and J. M. Saveant, *J. Electroanal. Chem.*, **47**, 215(1973).
159. L. Nadjo, J. M. Saveant and D. Tessier, *J. Electroanal. Chem.*, **52**, 403 (1974).
160. J. M. Saveant and D. Tessier, *J. Electroanal. Chem.*, **61**, 251 (1975).
161. K. B. Oldham, *Anal. Chem.*, **44**, 196 (1972).
162. J. M. Saveant and D. Tessier, *J. Electroanal. Chem.*, **65**, 57 (1975).
163. K. B. Oldham and J. M. Saveant, *J. Electroanal. Chem.*, **26**, 331 (1970)
164. A. J. Bard and L. R. Faukner, *Electrochemical Methods: Fundamentals and Applications*, p. 236, John wiley & Sons, Inc., (1980).
165. J. M. Saveant and D. Tessier, *J. Electroanal. Chem.*, **65**, 57 (1975).
166. K. B. Oldham and J. M. Saveant, *J. Electroanal. Chem.*, **26**, 331 (1970)
167. J. C. Imbeaux and J. M. Saveant, *J. Electroanal. Chem.*, **44**, 1969(1973).

168. K. B. Oldham and J. M. Saveant, *J. Electroanal. Chem.*, **26**, 331 (1970)
169. K. B. Oldham, Anal. Chem., **44**, 196 (1972).
170. A. J. Bard and L. R. Faukner, *Electrochemical Methods: Fundamentals and Applications*, p. 30, 160, John wiley & Sons, Inc., (1980).
171. F. Ammar and J. M. Saveant, *J. Electroanal. Chem.*, **47**, 215(1973).
172. P. K. Lai and M. Skyllas-Kazacos, *J. Electroanal. Chem.*, **248**,431 (1988).
173. J. Robinson, R. A. Osteryoung, *J. Electrochem. Soc.*, **127**, 122 (1980).
174. R. E. Noftle and D. Pletcher, *J. Electroanal. Chem.*, **227**, 229 (1987).
175. A. J. Bard and L. R. Faukner, *Electrochemical Methods: Fundamentals and Applications*, p. 258, John wiley & Sons, Inc., (1980).
176. T. Berzins and P. Delahay, *J. Am. Chem. Soc.*, **75**, 555 (1955).
177. D. J. Schiffrin, *J. Electroanal. Chem.*, **201**, 199 (1986).
178. B. R. Sundheim in *Fused Salts*, B.R. Sundheim, Ed., p. 165, McGraw-Hill, New York, N.Y., (1964).
179. T. Berzins and P. Delahay, *J. Am. Chem. Soc.*, **75**, 555 (1953).
180. Q.-X. Quin and M. Skiyllas-Kazacos, *J. Electroanal. Chem.*, **168**, 193 (1984).
181. R. J. Gale and R. A. Osteryoung, *J. Eelctrochem. Soc.*, **121**, 983 (1974).
182. Y. J. Zhang, A. Bjorgum, U. Erison, R. Tunold, and R. Odegard, *J. Electroanal. Chem.*, **210**, 127 (1986).
183. M. Hansen, *Constitution of Binary Alloys*, McGra- Hill, New York, (1958).
184. Z. Zstakhov, T. Finnovisky, and G. Teplitskaya, *Electrokhimiyal. Chem.*, **13**, 253 (1965).
185. Q. Li, H. A. Hjuler, R. W. Beng and N. J. Bjerrum, *J. Electrochem. Soc.*, **138**, 763 (1991).
186. Z. Zstakhov, T. Finnovisky, and G. Teplitskaya, *Electrokhimiyal. Chem.*, **13**, 253 (1965).
187. Y. Chryssoulakis, J. -C. Poigent and G. Manoli, *J. Appl. Electrochem.*, **17**, 857 (1987).
188. T. P. Moffat, *J. Electrochem. Soc.*, **141**, 3059 (1994).
189. P. M. Rigano, C. Mayer, and T. Chierchie, *J. Electroanal. Chem.*, **248**, 219(1988).
190. P. Rolland and G. Mamantov, *J. Electrochem. Soc.*, **123**, 1299 (1976).
191. P. Allongue, and E. Souteyrand, J. Electroanal. Chem., **286**,217, (1990).
192. R. G.Barradas and A.Q.Contractor, *J. Electroanal, Chem.*, **138**, 425 (1982).
193. J. Zeldvich, *J. Expxtl. Theroet. Phys.(U.S.S.R.)*, **12**, 525 (1942).
194. J. C.Fisher, J. H. Holloman, and D. Turnbull, *J. Appl. Phys.*, **19**, 775 (1948).
195. A. Kantrowwitz, *J. Chem. phys.*, **19**, 1907 (1951).
196. F. C. Collins, *Z. Elektronchem.*, **59**, 404 (1955).
197. H. L. Frish, *J. Chem. Phys.*, **27**, 90 (1957).
198. W. G. Courtney, *J. Chem. Phys.*, **36**, 2009 (1962).
199. D. Kaishchiev, *Surface. Sci.*, **14**, 209 (1969).
200. R. Kaischev, and B. Mutaftschiev, *Z. Phys. Chem.*, **204**, 334 (1955).
201. E. Peled and E. Gileadi, *J. Electrochem. Soc.*, **123**, 15 (1976).

202. V. Gutmann, *Co-ordination Chemistry in Non-Aqueous Solutions*, Springer, Wien (1968).
203. V. Gutmann, *The Donor-Acceptor Approach To Molecular Interactions*, Plenum Press, New York (1978).
204. T. A. Zawodzinski and R. A. Osteryong, *Inorg. Chem.*, **28**, 1710 (1989).
205. J. A. Boon, S. W. Lander, J. A. Levisky, J. L Pflug, L. M. Skrynecki-Cook and J. S. Wilkes, *Extended Abstracts, Electrochemical Society Fell Meting*, Vol. **87-2**, p. 2044, Honolulu, (1987).
206. M. Lipsztajin and R. A. Osteryoung, *J. Electrochem. Soc.*, **132**, 1126 (1985).
207. J. S. Wilkes, C. L. Hussey and J. R. Sanders, *Polyhedron*, **5**, 1567 (1986).
208. A. A. Fannin, L. A. King, J. A. Levisky and J. S. Wilkes, *J. Phys. Chem.*, **88**, 2609 (1984).
209. M. Seruge and M. Metikos-Hukovic, *J. Electranal. Chem.*, **334**, 223 (1992).
210. A. J. Calndra, N. R. de Tacconi, R. Pereiro and A. J. Arvia, *Electrochim. Acta*, **19**, 901 (1974).
211. W. J. Muller, *Trans. Faraday Soc.*, **27**, 737 (1971).
212. D. D. MacDonald, *Transient Techniques in Electrochemistry*, Plenum Press, p. 296, New York, (1977).
213. D. M. Kolb, in *Advances in Electrochemistry and Electrochemical Engineering*, Vol. **11**, (Edited by H. Gerischer and C. W. Tobias), Wiley-Interscience, New York, (1978).
214. G. Staikov, K. Juttner, W. J. Loorenz and E. Budevski, *Electrochim. Acta*, **39**, 1019 (1994).
215. J. Horkans, I-C. H. Chang, P. C. Andriacos and H. Deligianni, *J. Eletrochem. Soc.*, **142**, 2244 (1995).
216. D. Landolt, *Electrochim. Acta*, **39**, 1075 (1994).
217. R. J. Gale and R. A. Osteryoung, *Inorg. Chem.*, **18**, 2723 (1979).
218. W. R. Pitner, C. L. Hussey and G. R. Stafford, *J. Electrochem. Soc.*, **143** , 130 (1996).
219. C. L. Hussey, *Chemistry of Nonaqueous Solvents*, (Edited by a. Popov and G. Mamantov), Chap. **4**, VCH Publishers, New York, (1996).
220. L. Herman and W. D'Olieslager, in *Proceedings of 9th International Symposium on Molten Salts*, (Edited by C. L .Hussey, D. S. Newman, G. Mamantov and Y. Ito), PV **94-13**, p. 441, Electrochem. Soc. Proc. Series, Pennington, New Jersey, (1994).
221. W. R. Piter and C. L. Hussey, in *Molten Salts*, (Edited by C. L. Hussey, D. S. Newman, G. Mamantov and Y. Ito), PV **94-13**, p. 400-414, The Electrochemical Society Proceedings Series, Pennington, NJ (1994).
222. A. Brenner, *Electrodeposition of Alloys*, Vol. **1**, Academic Press, Inc., New York (1963).
223. K. M. Gorbunova and Yu. Polukarov, in *Advances in Electrochemistry and Electrochemical Engineering*, Vol. **5**, Interscience, New York, (1967).
224. B. Gibert and R. A. Osteryoung, *J. Am. Chem. Soc.*, **100**, 2725 (1978).

225. H. Bort, K. Juttner, W. J. Lorenz, and G. Staikov, *Electrochim. Acta*, **28**, 993 (1983).
226. M. P. R. Panicker, M. Knaster, and F. A. Kroger, *J. Electrochem. Soc.*, **125**, 566 (1983).
227. C. R. Boston and G. P. Smith, *J. Phys. Chem.*, **62**, 409 (1958).
228. D. M. Gruem and R. L. McBeth, *J. Phys. Chem.*, **63**, 393 (1959).
229. B. R. Sundheil and G. Harrington, *J. Chem. Phys.*, **31**, 700 (1959).
232. Vestrgard, N. J. Bjerrum, I. Petrushina, H. A. Hjuler, R. W. Berg, and M. Begtrup, *J. Electrochem. Soc.*, **140**, 3208 (1993).
233. Caja, A. A. Gakh, T. D. J. Dunstan, J. L. Adcock and G. Mamantov, *Proceedings of the nineth International Symposium on Molten Salts*, (Edited by G. Mamantov, M. Blander, C. L. Hussey, C. B. Mamantov, M. -L. Saboungi, and J. S. Wilkes), p. 752, Electrochem. Soc., Pennington, New Jersey, (1994).
234. M.Chemla and D. Devilliers, eds, *Molten Salt Chemistry and Technology*, Material Science Forum, Vols. 73-75, Trans Tech Publications, Switzerland, (1991).
235. S. Wilkes and M. J. Zaworotko, *J. Chem. Soc., Chem, Commun.*, 965 (1992).
236. H. White, in *Ionic Liquids*, (Edited by M. Inman and D.G. Lovering), Plenum, New York, (1981).
237. Fuller, R. T. Carlin, H. C. De Long and D. Hwaorth, *J. Chem. Soc., Chem, Commun.*, 299 (1994).

PUBLICATIONS

1. Yuguang Zhao and T. J. VanderNoot, "**Electrodeposition of aluminium from nonaqueous electrolytic systems and room temperature molten salts**", *Electrochim. Acta*, **42(1)**, 3 (1996).

2. Yuguang Zhao and T. J. VanderNoot, "**Electrodeposition of aluminium from room temperature molten salts 2:1 $AlCl_3$-TMPAC**", *Electrochim. Acta*, **42(11)**, 1639 (1997).

BIBL. LONDIN. UNIV